UNIVERSITAT DE BARCELONA

Identification of deubiquitinating enzyme genes relevant for the regulation of retina-specific genes

Mariona Esquerdo Barragan

Identification of deubiquitinating enzyme genes relevant for the regulation of retina-specific genes.

Memòria presentada per
Mariona Esquerdo Barragan

Per optar al grau de
Doctora per la Universitat de Barcelona

Tesi realitzada sota la direcció de la **Dra. Gemma Marfany i Nadal** al
Departament de Genètica, Microbiologia i Estadística,

Universitat de Barcelona,

Programa de Genètica (H0Q03)

Dra. Gemma Marfany i Nadal **Mariona Esquerdo Barragan**

A Barcelona, 2 de març de 2017

Als meus avis

Table of content

List of abbreviations

661w	Precursor of cones stable cell line
AD	Alzheimer Disease
AON	Antisense Oligonucleotide
AS	Antisense riboprobe
cDNA	Complementary DNA
ChIP	Chromatine Immunoprecipitation
CNS	Central Nervous System
CoIP	Co-Immunoprecipitation
CRX	Cone-rod homeobox protein
DAPI	4',6-diamidino-2-phenilindole
DUB	Deubiquitinating enzyme
E#	Embryonic day #
ELM	External limiting membrane
ESE	Exonic Splicing Enhancer
Fwk #	Foetal week #
GAPDH	Glyceraldehyde-3-phosphate dehydrogenase
GCL	Ganglion cell layer
GFP	Green Fluorescent Protein
GNAT	G Protein Subunit Alpha Transducin 1
HEK293	Human Embryonic Kidney stable cell line
IHC	Immunohistochemistry
ILM	Internal limiting membrane
INL	Inner nuclear layer
IP	Immunoprecipitation
IPL	Inner plexiform layer
IS	Photoreceptor inner segments
ISH	*In situ* hybridization
JAMM	JAB1/MPN/MOV34 proteases
K	Lysin
KD	Knockdown

KO	Knockout
L opsin	Long wavelength (red) sensitive opsin
Lys	Lysin
M opsin	Medium wavelength (green) sensitive opsin
MINDY	Motif Interacting with Ub containing Novel DUB family
MIO-M1	Human Müller stable cell line
MJD	Machado-Joseph Disease proteases
mRNA	Messenger RNA
NFκB	Nuclear Factor Kappa B Subunit 1
NR2E3	Nuclear Receptor Subfamily 2 Group E Member 3
NRL	Neural retina leucine zipper protein
ONL	Outer nuclear layer
OPL	Outer plexiform layer
OS	Photoreceptor outer segment
OTU	Ovarian tumor proteases
OTX2	Orthodenticle homeobox 2 protein
P#	Postnatal day #
PAX6	Pair box protein
PD	Parkinson Disease
PhR	Photoreceptor cells
RHO	Rhodopsin
RNA seq	RNA sequencing
RORβ	RAR Related Orphan Receptor β
RP	Retinitis Pigmentosa
RPC	Retinal progenitor cell
RPE	Retinal pigmented epithelium
RT qPCR	Real time quantitative PCR
S	Sense Riboprobe
S opsin	Short wavelength (blue) sensitive opsin
shRNA	Short hairpin RNA
siRNA	Small interfering RNA
SNP	Single-nucleotide polymorphism
SUMO	Small Ubiquitin-like Modifier
TF	Transcription factor

TGFβ	Transforming Growth Factor Beta
TRβ2	Thyroid hormone receptor β2
Ub	Ubiquitin
UbL	Ubiquitin-Like proteins
UCH	Ubiquitin COOH-terminal hydrolases
USP	Ubiquitin specific proteases
WB	Western Blot immunodetection
WT	Wild Type
Y-79	Human retinoblastoma stable cell line

Introduction

1. THE RETINA

1.1. STRUCTURE AND FUNCTION

In humans, most of the higher neuronal functions, like behaviour, learning, memory and emotions are driven by or are dependent on vision. In fact, vision is the most developed sense in human beings and almost 30% of the brain's input information is originated in the retina[1].

The retina is the part of the eye responsible for capturing light stimuli from our surroundings. It is a neuronal tissue located at the posterior part of the eye, which captures light photons, converts the luminic energy into electrochemical stimuli, and finally sends visual information to the brain where it is integrated. Vertebrate retina is formed by seven neuronal cell types organized in six precise functional and structural layers (Figure 1). The main function of the retina, the phototransduction, is mainly carried out by two types of photoreceptor cells (PhR), cones and rods (see below). The retinal pigmented epithelium (RPE) is found in the most posterior part of the eye, and it is formed by a monolayer of pigmented cells that are responsible for: 1) phagocyting the old and unstructured distal discs of the photoreceptors, and 2) protecting and nursing photoreceptor cells.

The rest of the retina is composed of different finely interconnected neuronal types. Below the RPE the retina is structured in three nuclear layers (NL) with two intercalated plexiform layers (PL). The nuclear layers are: the outer nuclear layer (ONL), formed by the photoreceptor nuclei; the inner nuclear layer (INL), where nuclei of bipolar, horizontal, amacrine, Müller glial and interplexiform cells are located; and the ganglion cell layer (GCL), with the ganglion cell nuclei and somas. The two plexiform layers are the

outer plexiform layer (OPL) (between the ONL and the INL), which is the layer where photoreceptors synapse with horizontal and bipolar cells; and the inner plexiform layer (IPL) (between INL and GCL), where ganglion cells synapse with bipolar and amacrine cells. Phototransduction takes place right below the RPE, within the membranous discoid outer segments (OS) of photoreceptors.

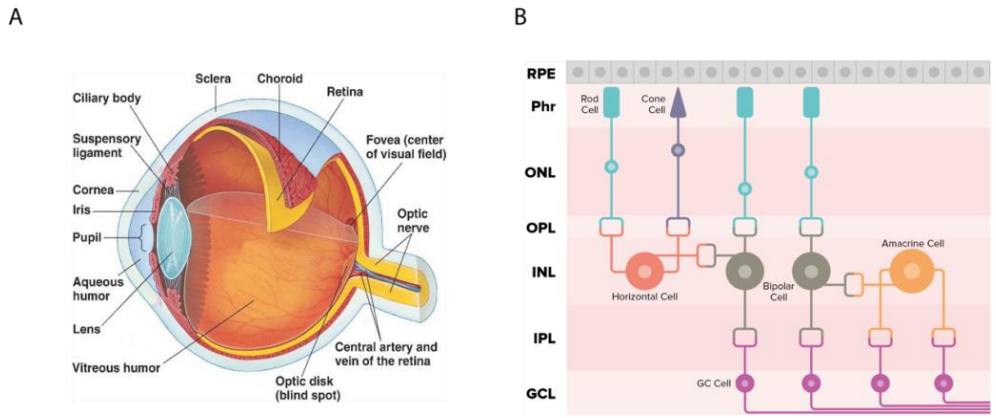

Figure 1. A. Human eye structure. Note that in humans there is a high cone density area, named fovea (upper right hand of the image), which is not present in mice. (Google Images). **B. Retina structure**. **RPE**: Retinal Pigmented Epithelium, **PhR**: Photoreceptor, **ONL**: Outer Nuclear Layer, **OPL**: Outer Plexiform Layer, **INL**: Inner Nuclear Layer, **IPL**: Inner Plexiform Layer and **GCL**: Ganglion Cell Layer. (Blanco, A.; 2016).

The vision process starts with light entering the eye and passing through all the retinal layers, from the GCL to eventually find the outer segments of photoreceptors. The photosensitive pigment (opsin) of these segments is the responsible for the phototransduction process, thereby converting light stimuli into electrochemical stimuli. This electric pulse will then be sent from the PhR to the bipolar cells and finally, to the ganglion cells. The axons of

these ganglion cells converge to form the optic nerve, which will directly send the electrical information to the visual cortex, thus allowing the brain to create and perceive an image.

In this visual process, horizontal cells synapse to photoreceptors and bipolar cells to increase the image quality; while amacrine cells interconnect bipolar cells to control the information flow. In addition, there is another information flow that travels backwards, from the ganglion cells to the photoreceptors, which is carried out by the interplexiform cells.

1.2. FORMATION AND DEVELOPMENT

The development of the vertebrate retina is initiated from an outgrowth of the neural tube that generates two symmetric protrusions called optic vesicles. The furthest end of these vesicles invaginates and generates a double layered cup-shaped structure, serving as the basic structure from which the different layers of the retina are built up. The outer wall, closer to the ventricular surface (named external laminar membrane, ELM), becomes the retinal pigmented epithelium (RPE); while the inner wall, closer to the vitreal surface, is formed transiently by a pseudoestratified epithelium (the internal limiting membrane, ILM) that thickens and differentiates into the neural retina[2] (Figure 2).

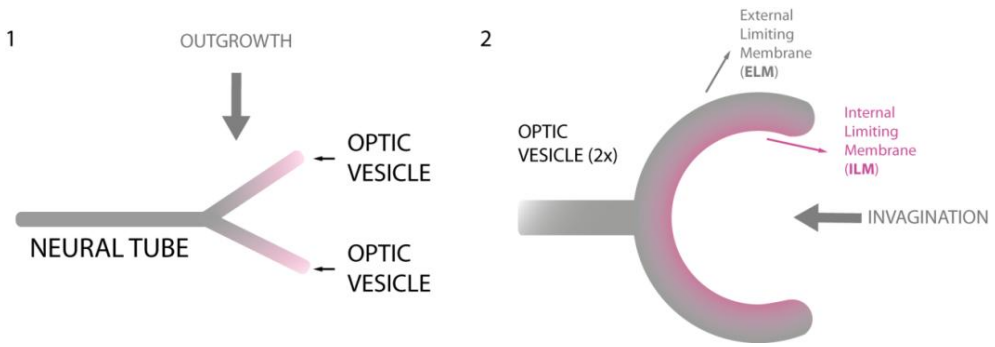

Figure 2. Formation of the optical vesicles from the neural tube during vertebrate retinal development. The neural tube undergoes an overgrowth that creates two protrusions, called the optic vesicles. Each of these vesicles will invaginate, thus generating a double layered cup-shaped structure. These optical cups are the basic structure where the whole retina is built on. (Esquerdo, M.; 2017)

Once the optical vesicle has been generated, two major steps must occur in order to build up the final stratification of the retina: 1) the generation and establishment of cohorts of retinal progenitors; and 2) the fate determination and migration of these progenitors to their final destiny[2,3] (Figure 3).

Therefore, after the generation of the optic vesicle, several cell divisions occur, leading to the generation of cohorts of retinal precursors. During this process, precursor cells generate cytoplasmic processes that connect with both the external and internal limiting membranes (ELM and ILM). These cells undertake several displacements until they settle in the ELM, generating non-replicative cohorts of post-mitotic retinal progenitors[2].

Subsequently, post-mitotic retinal progenitors differentiate into the seven retinal cell types and migrate to form a stratified and functional neural retina. The migration progression has not been precisely defined, but the most accepted scenario is what is called the *perikaryal translocation*. In this process,

post-mitotic cells settled close to the RPE (or ELM) extend a cytoplasmic process and translocate their nuclei towards the IML. During translocation of the nuclei, cells maintain cytoplasmic contact with the two limiting layers of the optic vesicle and they lose contact with the external laminar membrane only when they arrive at their final position in the retina, where post-mitotic progenitors readily differentiate into a particular cell type[2,3] (Figure 3).

The first cells to become post-mitotic and establish a differentiated layer are the ganglion cells, which form the ganglion cell layer (GCL). Subsequently, horizontal and amacrine cells differentiate; and synapses between amacrine and ganglion cells are formed, generating the inner plexiform layer (IPL). Later on, photoreceptors differentiate as well as bipolar and Müller cells, creating the inner nuclear layer (INL) and starting to form the first synapses of the outer plexiform layer (OPL). At the final stages of retinal development, rods are differentiated and the functional outer segments of PhR are formed[2,3].

Therefore, retinal layers are created through a strictly ordered process, starting from the differentiation of the basal GCL upon which the rest of the layers are built. The differentiation of each cell type occurs sequentially; hence, the signals emitted by each differentiating cell type promote the differentiation of the following cell type while self-inhibiting further differentiation of their own layer. Eventually, retinal cell layers are established that allow the capture, **Figure 7** integration and transmission of light stimuli from the retina to the brain.

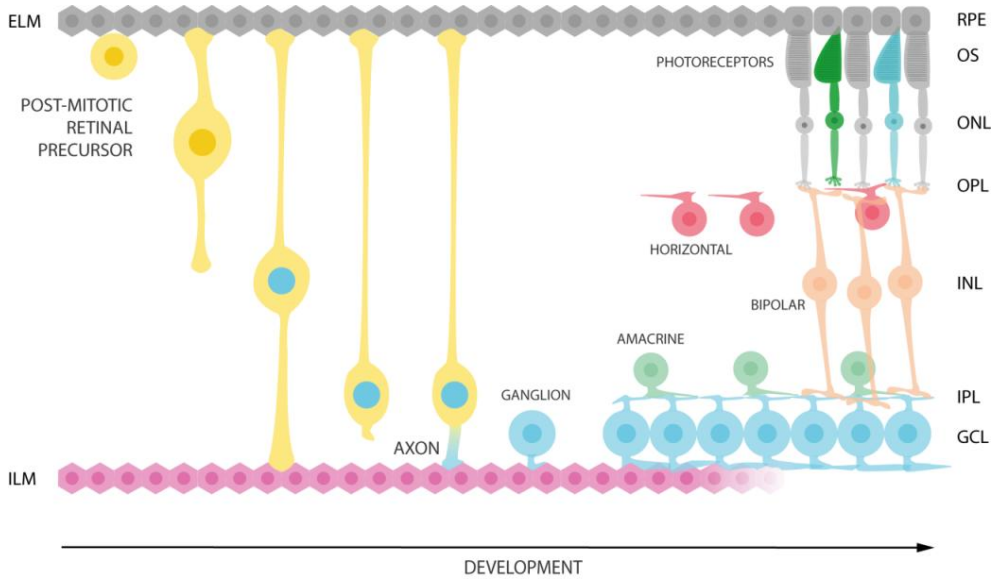

Figure 3. Perikaryal translocation process of retinal precursors. Post-mitotic retinal precursors differentiate to all cell types of the retina by projecting the cytoplasm to the internal laminar membrane (ILM) and translocating the nucleus to their final position. Then, the cytoplasmic projection retracts from the external laminar membrane (ELM) and axons are generated. The first cells to differentiate are ganglion cells, followed by amacrine and horizontal cells. Finally, bipolar cells and photoreceptors differentiate and mature. RPE: Retinal Pigmented Epithelium, **OS**: photoreceptor Outer Segment, **ONL**: outer nuclear layer, **OPL**: Outer Plexiform Layer, **INL**: Inner Nuclear Layer, **IPL**: Inner Plexiform Layer, **GCL**: Ganglion Cell Layer. **ELM**: External Laminar Membrane, **ILM**: Inner Laminar Membrane. (Esquerdo, M.; 2017)

1.3. PHOTORECEPTOR CELLS

1.3.1. MORPHOLOGY AND FUNCTION

Photoreceptors are the cells responsible for capturing light stimuli and transducing it into an electrochemical signal. They are extremely specialized cells with a distinctive morphology and can be subdivided into two types: cones and rods. Cones are responsible for visual acuity and colour

perception in photopic conditions; while rods are sensitive in dim light conditions and are responsible for scotopic vision (Figure 4).

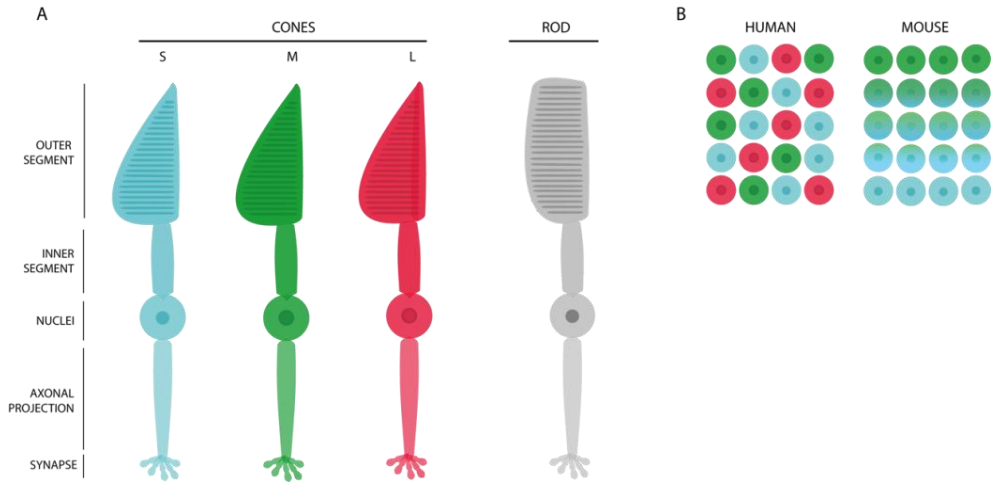

Figure 4. Photoreceptor morphology and distribution in human and mouse retina. In mammals, there are two kinds of photoreceptors (**PhR**): cones and rods. Humans present three types of cones, which are excited by three different wavelength photons (short, **S**; medium, **M**; and long, **L**) and are distributed in a mosaic-like pattern. In mice, instead, there are only S and M cones, distributed in an opposed gradient throughout the retina. (Esquerdo, M.; 2017)

Both cell types show a polarized morphology, and display outer (OS) and inner segments (IS) and a synaptic region, besides the nucleus, which is surrounded by a reduced cytoplasm region. The axon projects and synapses with the bipolar and horizontal cells. The inner segment is highly enriched in mitochondria and other organelles, and it is where cellular metabolic processes take place. On the other hand, the outer segment, which intimately contacts the RPE, is formed by a series of stacked membranous discs that contain the photopigments or opsins. In cones, these discs are attached to the inner part of the plasma membrane, contrary to what occurs in rods,

where discs are unattached. The discs are generated from the lower part of OS and grow up to the apical part, where will be recycled and phagocyted by the RPE.

The main morphological and functional differences between PhR cells reside in the OS. Morphologically, cones owe its name to the cone-like morphology of their OS; whereas rods, to their straight rod-like shape. Physiologically, the difference between cones and rods resides in their different photopigments or opsins. Rods express rhodopsin as the only photopigment: it is the most abundant protein in rods, accounting for the 95 % of the total proteins in the OS; and it is capable of capturing even single light quanta. However, opsin diversity in cones is wider, both within an individual and among different species. In humans, there are three types of cones, containing one of three possible types of opsins: S, M and L opsin – sensitive to short (blue), medium (green) and long (red) light wavelengths, respectively. They are distributed in a mosaic-like pattern throughout the retina. In mice, the only opsins present are the S and M opsins. These two opsins are expressed within the same cell although their amount is distributed in opposing gradients throughout the retina[4]. In diurnal primates, the L opsin gene generated from the duplication of the ancestral M opsin gene located at the X chromosome.

Concerning the vision process, both rods and cones synapse in the OPL with bipolar cells, which transfer their impulses to the ganglion cells. If the image thus generated were to be sent to the brain, the visual perception would be rather fuzzy and imprecise; to produce a neater and accurate image, horizontal cells capture stimuli from several cones at a time and send the information to the ganglion cells.

Around 70% of retinal cells are photoreceptors, but both in human and in mouse, rods outnumber cones in 18-20:1 and 30:1 proportions[5,6], respectively. The difference between species is due to the fact that mice are nocturnal animals, which require a larger number of rods since they provide night-vision. Humans, as diurnal primates, not only have more cones throughout the retina but they also show a unique rich-cone region called fovea, which is located in the centre of the retina and provides higher visual acuity.

1.3.2. DEVELOPMENT

The development of photoreceptor cells follows a tightly controlled genetic program in which a multipotent retinal progenitor cell (RPC) undergoes first a process of fate determination and later on commits into differentiation of a specific photoreceptor type. The very same RPC can become either a rod or a cone, and this fate decision is regulated through an intricate genetic network. The timeframe for this fate determination varies among species: for instance, in humans the S opsin mRNA is detected at foetal week 12 (Fwk 12), while expression of rhodopsin, M and L opsins appear by Fwk 15[7]. On the other hand, murine cones start to differentiate by embryonic day 11 (E11), and the S opsin is expressed at later embryonic stages whereas M opsin expression is not detected until postnatal day 6 (P6). The genesis of rods peaks at P2, close to the time of rhodopsin transcription[8,9]. Several developmental traits are shared between both species: opsin expression increases with time; the outer segments grow towards the RPE and axons grow towards bipolar and horizontal neurons for synapsing.

During development, RPC multipotency and proliferation is maintained by the expression of several transcription factors (TF), such as paired box

protein PAX6, retinal homeobox RX1, SIX3, SIX6, LIM-homeobox protein LHX2, visual system homeobox 2 (VSX2), HES1 and Notch1. RPCs will divide and produce either more multipotent progenitors, or progenitors that will be restricted in competence. These cells can then become lineage specific, e.g. photoreceptor precursors. The transcription factor OTX2 together with undetermined signals controls the formation of early photoreceptors. At the same time, the cone-rod homeobox protein CRX and the nuclear receptor RORβ are also expressed and elicit the cell default pathway, which is to become an early S cone. Thyroid hormone receptor β2 (TRβ2) expression will decide between M opsin or S opsin identity. However, the determination of a rod fate from the early S cone requires the action and fine regulation of additional factors. In particular, NRL binds several promoters, including that of the photoreceptor specific nuclear receptor gene (NR2E3), which also induces and consolidates the rod cell state by both, activating rod-specific genes, such as rhodopsin (*RHO*) and *GNAT*, and suppressing cone specific genes[1] (Figure 5).

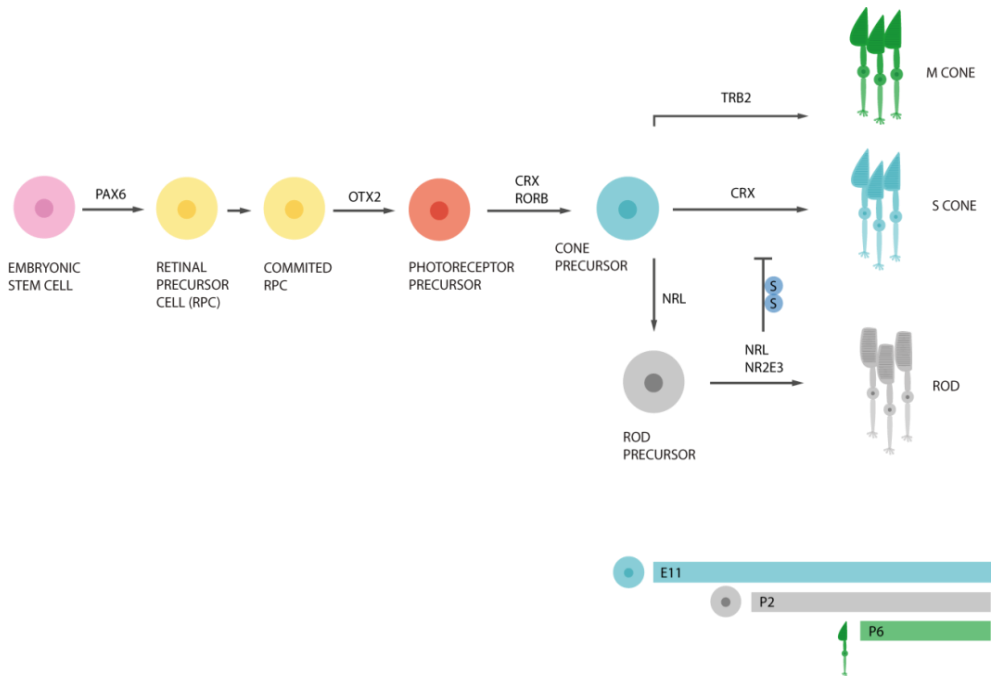

Figure 5. Murine photoreceptor development. From an embryonic stem cell, several transcription factors at specific developmental times are required to determine the photoreceptor cell fate, and for retinal precursor cells to eventually become fully mature photoreceptors. PAX6, CRX, NRL and NR2E3 are considered the key regulators of retinal development and differentiation. (Esquerdo, M.; 2017)

Other transcription factors participating in cone development and maintenance are the retinoid X receptor-γ (RXRγ), COUP transcription factor 1 (COUP-TF1 or NR2F1) and neurodiferentiation factor 1 (NEUROD1). While achaete-scute homologue 1 (ASCL1 or MASH1) and PIAS3 also participate in the rod state acquisition[1].

In mouse, CRX knockouts (KO) fail to produce cells expressing opsins, which eventually leads to retinal degeneration. Concerning NRL, mutations in this gene have been reported to cause rod absence and S-cone syndrome,

characterized by an excess of cones in the retina. Finally, NR2E3 mutant mice show rod-like photoreceptors that express cone-specific genes.

In humans, mutations in *Crx* have been described as causative of several retinopathies, including, cone-rod dystrophy[10], Leber congenital amaurosis (LCA)[11] and retinitis pigmentosa[12]. Moreover, *Nrl* and *Nr2e3* has also been related to human enhanced S-cone syndrome[13,14] and retinitis pigmentosa[15,16]. All these diseases cause a degeneration in cones and rods, which at first lead to tunnel-like vision and finally to a complete blindness.

2. UBIQUITIN AND UBIQUITINATION

Ubiquitin (Ub) is a 76 amino acid (8kDa) peptide extremely conserved among eukaryotic cells: only three amino acids differ between the yeast to the human proteins. The three dimensional structure shows an α-helix surrounded by five β-sheets (Figure 6)[17]. Ubiquitination is the reversible post-translational conjugation of a ubiquitin peptide to the lysine (Lys, K) residues of target substrate proteins through an isopeptidic bond. The number of conjugated Ubs and the lysines within the Ub molecules used to build chains will determine the fate and function of the modified protein. In fact, this post-translational modification changes the interaction interfaces between proteins, thus providing changes in protein recognition and binding affinities[18].

Protein post-translational modifications are regulatory mechanisms that cells use in response to intra- and extracellular signals. These signals modulate a panoply of conjugating enzymes that modify proteins post-translationally by the conjugation of a small functional group or peptide. The consequences of these modifications are very diverse, but they all present a common feature: they shift protein fate, localization or function. Besides, in the case of covalent protein modifications, such as ubiquitination, these regulatory mechanisms are reversible and dynamic.

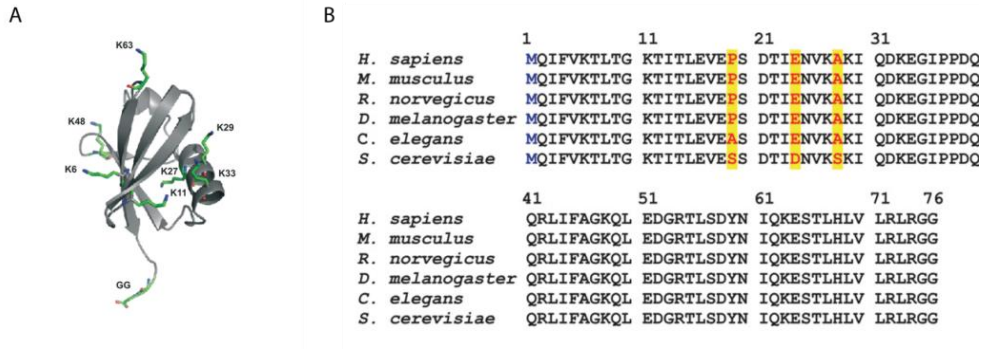

Figure 6. Ubiquitin structure and sequence conservation. A. Tridimensional structure of the human ubiquitin molecule. **B.** Protein sequence alignment of ubiquitin from different species.

Ubiquitination relies on the formation of an isopeptidic bond between the C-terminal glycin (Gly, G) of the ubiquitin molecule and the ε-amino group of a lysine in the substrate protein. This substrate can be any protein in the cell, including other ubiquitin molecules, which will thereby generate ubiquitin polymers (also called ubiquitin chains). Furthermore, other type of unions have been observed, such as the attachment of a Ub moiety to the N-terminal part of the protein instead to a inner Lys, known as the "N-end rule"[19], or to a cysteine (Cys, C) via a thioester bond[20]. Ubiquitination always necessarily initiates through the activation of the ubiquitin molecule by an activator enzyme E1, which will then transfer the active ubiquitin to the conjugating enzyme E2. This E2-ubiquitin complex is able to interact with an E3 ligase, responsible for the eventual conjugation of the Ub molecule to the substrate protein.

In mammals, only two E1 and around thirty E2 ligases have been described, in contrast to the approximately 600 E3 ligases identified. This remarkably large number of E3 ligases can be explained by their high substrate

specificity: E3 Ub ligases are the enzymes responsible for substrate recognition. Finally, as aforementioned, this is a highly dynamic process and thus, cells also deploy a group of deubiquitinating enzymes (DUBs), responsible for detaching ubiquitin from its substrates (Figure 7).

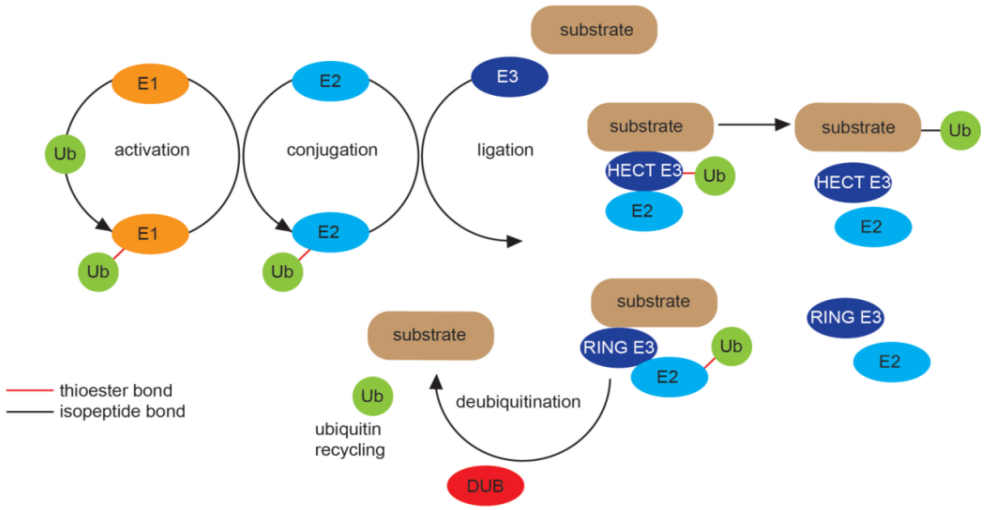

Figure 7. Ubiquitin cycle[21]**.** The binding of a ubiquitin molecule to its substrate protein occurs in three steps – activation, conjugation and ligation - carried out by E1, E2 and E3 ligases, respectively. The ubiquitin moiety is finally conjugated through an isopeptidic bond. Ubiquitination is a dynamic and reversible process that relies on deubiquitinating enzymes (DUB) to cleave off ubiquitin from substrates.

Concerning evolution, ubiquitination is a well established and conserved cellular process common to all eukaryotes; it is even present in archaeal groups although not in eubacteria. *In silico* research has revealed that the ubiquitin system has greatly expanded and diversified through evolution, in terms of gene innovation and domain architecture[22], thus supporting the concept that higher organism complexity comes along with a higher need of a more tight and fine regulation of ubiquitination.

2.1. UBIQUITIN CHAINS STRUCTURE AND FUNCTION

Conjugation of ubiquitin onto a substrate protein can be performed as a modification with either single Ub moieties (mono- and multi-monoubiquitination), or with Ub polymers (polyubiquitination). In any case, this process is never performed randomly by E3 ligases, but rather it is a tightly regulated mechanism that will alter protein fate and function. Generally, monoubiquitination is involved in signalling, endocytosis and DNA repair, while multiple monoubiquitination is implicated in signalling and endocytosis, and polyubiquitination is involved in a variety of cell processes, as described below (Figure 8).

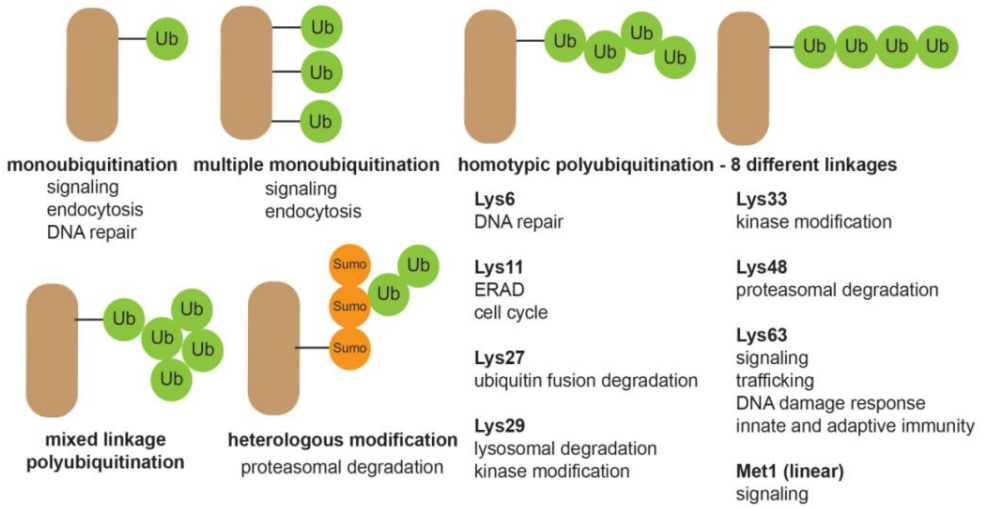

Figure 8. Different cellular roles of ubiquitin modifications[21]. Ubiquitin moieties can bind to their substrates in single or multiple points, depending on the availability of lysines. Besides, ubiquitin chains can be built using one or several internal ubiquitin lysines, which generates different chain structures and topologies. Ubiquitination changes the substrate interface for protein-protein interaction, which changes recognition and recruitment to different protein complexes and so does the substrate protein activity or cell fate.

Ubiquitin chains can be assembled by the conjugation of two or more ubiquitin molecules through one of their lysine residues: K6, K11, K27, K29, K33, K48 and K63; or to the N-terminal methionine residue (M1). These Ub polymers can contain bonds to either a single type of lysine–homotypic chains, or to different lysines –heterotypic chains[23]. Furthermore, the same ubiquitin can be ubiquitinated at two different sites, creating branches[24], or be posttranslationally modified by acetylation or phosphorylation[23].

The Ub chains build upon K48 and K63 have been extensively shown to be the main proteasomal degradation signal[25]. Thus, proteins post-translationally modified with these ubiquitin chains will be targeted to the proteasome, where they will be degraded, constituting the proteolytic ubiquitin pathway. It is well known that tetra-ubiquitin K48 chains increase the affinity for proteasome up to a 100x fold, in comparison to di-ubiquitin chains[25].

The non-proteolytic ubiquitin pathway involves monoubiquitination or the rest of polyubiquitin chains, and the effect they have on their substrates is very diverse. Heterotypic K11 polymers widely increase when the metazoan anaphase-promoting complex (APC/C) is expressed, which ubiquitinates substrates to activate proteasomal degradation and mitotic exit, thus strongly indicating these types of chains are involved in cell cycle control[23]. On the other hand, K27 chains have been linked to DNA damage response, as they are the most abundant type of ubiquitin polymers on chromatin and histones H2. These ubiquitination events at the damage site is one of the signals that activate the DNA Damage Response (DDR)[23,26]. They have also been involved in interferon/NFκB innate immune response[23]. Also, K33 chains are implicated in protein trafficking through microtubules; while K6 polymers might be involved in mitochondrial quality control and UV DNA

damage, but their specific function remains to be elucidated[23]. Finally, M1 ubiquitination has been related to NFκB signalling[23]

2.2. DEUBIQUITINATING ENZYMES

Ubiquitination is a reversible cell process and thus, besides the large number of Ub ligases, cells also deploy a significant number of Ub deconjugating enzymes, named deubiquitinating enzymes (DUBs). DUBs are responsible for hydrolizing and editing ubiquitin bonds and thus, recovering Ub moieties to maintain the intracellular pool; but most importantly, for making ubiquitination a dynamic and reversible regulatory mechanism. DUBs: 1) process the ubiquitin precursor that has been transcribed from several genes as fusion proteins; 2) deubiquitinate substrate and rescue them from protein degradation; and finally 3) recycle Ub molecules from proteins targeted to proteasomal degradation[27]. DUBs play important roles in cellular processes and disease; however and despite its evident importance in the organism, data on their mode of regulation and substrate specificity is still scarce[28].

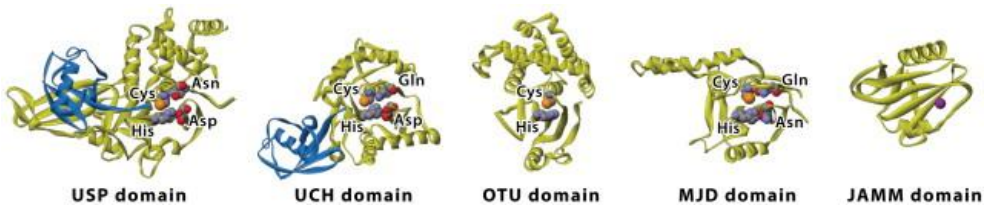

Figure 9. Three dimensional structures of the five deubiquitinating enzyme families[28].

2.2.1. DUB FAMILIES

There are 95 putative deubiquitinating enzymes described in the human genome, but only around 80 have been demonstrated to display deubiquitinating activity, similarly to what has been observed in the mouse genome. The large number of DUB genes might well be explained by their high substrate specificity, since so far no overlapping functions have been described, at least in humans. DUBs can be divided into 5 major families depending on their catalytic domain architecture: i) ubiquitin specific proteases (USP), ii) ubiquitin COOH-terminal hydrolases (UCH), iii) ovarian tumour proteases (OTU), iv) Machado-Joseph Disease proteases (MJD) and v) JAB1/MPN/MOV34 (JAMM) proteases. Most families are cysteine proteases, whose enzymatic activity resides on the thiol group of a central cysteine, Cys, C, and two adjacent residues (a histidine, His, H; and an aspartate, Asp, A, or an asparagine, Asn, N) in their catalytic site[28,29]. Only the JAMM family are Zn^{2+} metalloproteases, in which a triad of His, Asp and Ser residues coordinate the catalytic Zn2+[29] (Figure 9 and Table 1).

Table 1. List of deubiquitinating enzyme genes annotated in the human genome, classified per family.

USP			
USP 1	USP 2	USP 3	USP 4
USP 5	USP 6	USP 7	USP 8
USP 9X	USP 9Y	USP 10	USP 11
USP 12	USP 13	USP 14	USP 16
USP 17	USP 18	USP 19	USP 20
USP 21	USP 22	USP 24	USP 25
USP 26	USP 27	USP 28	USP 29
USP 30	USP 31	USP 32	USP 33
USP 34	USP 35	USP 36	USP 37
USP 38	USP 39	USP 40	USP 42
USP 43	USP 44	USP 45	USP 46
USP 47	USP 48	USP 49	USP 50
USP 51	USP 52	USP 53	USP 54
CYLD			

JAMM			
AMSH	AMSH-LIKE	BRCC36	CSN5
EIF3H	JAMM2	JAMM3	MYSM1
POH1	PRPF8	PSMD7	

MJD			
ATX	JOSD1	JOSD2	JOSD3

OTU			
OTU B1	OTU B2	OTU D1	OTU D3
OTU D4	OTU D5	OTU D6a	OTU D6b
OTU D7a	OTU D7b	PARPF11	TNFAIP3
VCPIP1	YOD1	ZRANB1	

UCH			
BAP1	UCH-L1	UCH-L3	UCH-L5

2.2.1.1. UCH FAMILY

The first DUB family to be structurally characterized was the UCHs. This family is formed by four proteins that contain a 230 amino acid catalytic core that share close homology and usually deubiquitinate small proteins (20-40 amino acids)[30]. The substrate specificity is limited by the three dimensional structure of the catalytic core: ubiquitinated peptides cannot be larger than 20-40 amino acids, as they have to pass through a confined loop that sits directly over the active site[29]. Furthermore, neither UCH-L1, nor UCH-L3

can cleave K48 or K63 Ub polymers, and therefore their function is highly specific[27]. They play an important role in the processing of new Ub free monomers from ubiquitin precursors and in the recycling of Ub moieties from already lysed or wrongly modified substrates.

UCH-L1 is one of the most abundant proteins in the brain, making up to 1-2% of the total protein. Not surprisingly, mutations in UCH-L1, both gain or loss of function, are directly related with neurodegenerative disorders, such as Parkinson's (PD) and Alzheimer's (AD) diseases[29]. Moreover, aberrant expression of this gene has been observed in several types of cancer and associated with cell invasion and chemotherapy resistance[29].

Another member of this family is BAP1, a protein that is basically confined in the nucleus. It has been related to several types of cancer and it described to participate in the regulation of several transcription factors[29].

2. 2.1.2. OTU FAMILY

Makarova et al. (2000)[31] identified amino acid sequence similitude and evolutionarily conservation between the gene responsible for ovarian development in *Drosophila melanogaster*, *otu*, and a cysteine protease present in some viruses and in *Chlamydea pneumoniae*, thus proposing OTU as a new deubiquitinating enzyme family. Despite basal structural conservation, phylogenetically, the 15 OTU members can be divided into three subgroups: the Otubains, OTUB1 and OTUB2; the A20-like OTUs, including A20 (also known as TNFAIP3), VCPIP1, OTUD7B and ZRANB1; and the classical OTUs[27]. Besides, OTU members show different Ub chain specificity[29]. Concerning the structure of the catalytic site, it is worth mentioning that it differs from the rest of the cysteine proteases, as the canonical catalytic triad

of the DUBs is incomplete in OTUs, creating a hole in the catalytic core that is stabilized by hydrogen bonds[28].

So far, research on OTU proteins has mainly been focused on A20 (TNFAIP3). Previous studies have demonstrated that this protein regulates the duration and intensity of NFκB (Nuclear Factor Kappa B Subunit 1) signalling during proinflammatory processes. Not surprisingly, germ-line single-nucleotide polymorphisms (SNPs) in humans have been linked to inflammatory conditions such as lupus erythematosus, rheumatoid arthritis and Chron's disease[29]. On the other hand, OTUB1, involved in DNA double strand break repair and one of the most highly expressed DUBs in cells[29] has also attracted some attention. OTUB1 has been shown to regulate the activity and stability of p53, increasing apoptosis and inhibiting proliferation[32]. However, both the ubiquitous expression and the functional role on double strand breaks, suggest an alternative function independent of the deubiquitinating activity. Finally, ZRANB1 (also known as TRABID) is involved in the regulation of the Wnt canonical pathway during development by promoting WNT[33]-dependent transcription.

2.2.1.3. MJD FAMILY

Machado-Josephine Disease (MJD) is the most common type of spinocerebellar ataxia worldwide. It is caused by CAG (triplet encoding Glutamine, Gln, Q) expansion in the ataxin 3 gene, *ATXN3*, which causes the formation of protein aggregates once a threshold in the number of polyQ repeats has been reached[29]. Some experimental evidence indicates that ATXN3 plays a role in transcription regulation or even in DNA repair[34], but it is not clear whether it is related to its deubiquitinating activity[28].

In vitro experiments confirm the deubiquitinating activity of ATXN3, but protease activity for the other three family members has not been described so far[28].

2.2.1.4. JAMM FAMILY

The JAMM family in the human genome is constituted by 12 Zn^{2+} metalloproteases containing a JAB1/MPN/MOV34 motif. Generally, they participate of larger protein complexes such as the proteasome (POH1), COP9 signalosome (CSN5) or the endocytic ESCRT (endosomal sorting complex required for transport) machinery (AMSH). However, they are involved in other cellular processes such as DNA repair (BRCC36) and the epigenetic switch in B-cell development (MYSM1). Most of them, e.g. AMSH, AMSH-L, BRCC36 or POH1, show strong preference for K63 polyubiquitin chains. Nonetheless, there are some functional differences worth noting: POH1, a constitutive proteasomal component, cleaves in block whole Ub polymers from the proximal end to the substrate, whereas MYSM1 cleaves off monoubiquitin[29].

Concerning the catalytic site, the JAMM motif is a highly conserved domain throughout evolution, including prokaryotes. However, proteins of this family in bacteria do not display Ub or Ub-like cleavage activity, which suggests that JAMM proteases might have evolved to process different types of protein conjugation[28].

2.2.1.5. USP FAMILY

USPs constitute the largest DUB family, with more than 50 DUB encoding genes in the human genome. The number of USP members has greatly

expanded during evolution, conferring the family specialization and *de novo* functions. The USP catalytic core contains two short motifs, the cysteine (Cys, C) and histidine (His, H) boxes, that combined span 300 to 800 amino acids[28]. Note that some members of the USP family lack part of the catalytic triad, as observed in the OTUs: for instance, the stabilizing Asp of the catalytic triad is missing in USP30 and USP16. There is a special case, USP39, which lacks the Cys or the His residues in the catalytic core, which strongly indicates that USP39 is no longer a deubiquitinase. However, this DUB plays a role in spliceosomal maturation, as well as other DUBs, which led researchers to speculate whether these members display ubiquitin binding but no protease capacity[28].

The functional roles of USPs are as wide as the family itself, ranging from histone deubiquitination (USP16) to the control of tumour suppression gene levels (p53, FOXO4 or PTEN among others), as is the case of USP7. Knockout USP7 -/- mice suffer embryonic lethality, in part due to permanent p53 activation[29]. Other USPs have been linked to the regulation of DNA metabolism pathways: e.g. USP1 regulates the DNA cross-link repair genes complementation group D2 (FANCD2) and proliferating cell nuclear antigen (PCNA) in Fanconi anemia. Besides, it has also been related with osteosarcoma cancer when depleted in mouse and human[29]. In the case of USP14, together with UCHL5 (not present in yeast), they are reversibly associated to the proteasomal machinery and deubiquitinate proteins that are committed to degradation.

Several USPs influence otherwise cell physiology through the control of receptors and channels and their regulatory cascade. In fact, the closely related USP4, USP11, USP15 and USP19 have been linked to the regulation

of the signalling events triggered by TGFβ (Transforming Growth Factor Beta) and NFκB, an been involved in the MAP kinase pathway and β-catenin stability.

The above related structural and functional differences within the whole set of deubiquitinating enzymes highlight that, despite the large number of DUBs present in the human genome and their a priori similar function, high substrate and functional specificity must prevail within these gene families.

2.2 1.6. MINDY FAMILY

This novel family was reported for the first time in July 2016. Motif Interacting with Ub containing Novel DUB family (MINDY)[35] is an evolutionary conserved cysteine (thiol proteases) DUB family which selectively cleaves K48 polyubiquitin chains, that is, the poly Ub tag that targets substrates to proteasomal degradation. Rehman et al. described the catalytic activity to be encoded by a previously unnanotated domain which displays a distinct crystal structure (Figure 10). Nonetheless, a single unique protein has been described in the family. MINDY-1 is a DUB enzyme whose catalytic active site shows a preference for hydrolizing long ubiquitin chains from the distal end.

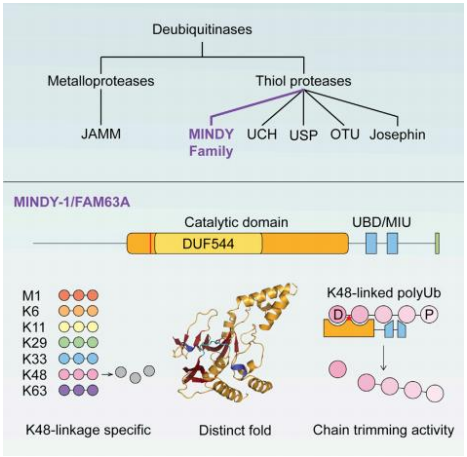

Figure 10. MINDY, a novel DUB cystein protease. The MINDY family is characterized by a cysteine catalytic domain, a distinct three dimensional fold, and a preference for trimming long K48 polyubiquitin chains[35].

Note that almost all the experiments in this Thesis were performed prior to the description of this very novel family and thus, the unique member of the MINDY family does not appear in any of them (neither in most of the most acclaimed reviews of the field).

2.2.2. PHYSIOLOGICAL RELEVANCE OF DUBS

As previously seen, the whole panoply of DUBs presents a high level of substrate specificity, which implies their involvement in a great variety of cellular processes. Thus, their dysfunction can vastly affect cell physiology and metabolism. In fact, several mutations in DUBs have been described as the genetic cause of human diseases ranging from cancer and neuropathies to autoimmunity.

One of these cases is BAP1 (breast cancer early-onset 1-associated protein 1), which associates with the potent tumour suppressor BRCA1, and

interacts with transcriptional machinery proteins. Mutations in this gene have been strongly correlated with predisposition to several types of cancer. BAP1 recruits polycomb proteins to control the expression of selected target genes, generating a self-regulating complex controlled by deubiquitination[36]. Thus, when mutated, it produces the misregulation of the target genes leading to a potential cancer. Other DUBs instead, stabilize oncogenes or tumour suppressors, e.g. USP7, ATX3, JOSD1 (PTEN); USP7, USP10, OTUB1 (p53); USP7, USP2a (MDM2); USP28 (MYC); or USP9X (MCL1)[36]; making them potential cancer-causing genes.

Concerning neuropathies, the aforementioned member of the MJD family, ATXN3, has been described as the causative gene of the most common type of autosomal dominant inherited ataxia. Polyglutamine repeats expansion on the gene leads to ATXN3 aggregation, as well as to dysfunctional association to other proteins and DNA. Despite the exact molecular contribution to disease is still unclear, it has been argued[36] that these clumps might produce: 1) functional depletion of ATXN3, 2) retention of target proteins and consequent functional incapacity, and 3) toxic accumulation of polyubiquitinated proteins within the cell.

Mutations in *AMSH* have also been related to another neuropathy, microcephaly-capillary malformation syndrome (MIC-CAP); in this case, however, the disease is due to the incapacity of AMSH to deubiquitinate, and thus regulate, RAS-MAPK and PI3K pathway[36].

It is worth mentioning that both A20 (also known as TNFAIP3) and CYLD, when mutated, cause a down regulation of NFκB singling pathway. Nevertheless, the first causes autoimmunity and lymphomas; while the second has been described as the driving cause of several types of cancer,

including melanoma, breast and prostate cancer. This striking differences might be partly due to the chain specificity of each of the enzymes[36]: *in vitro* studies have shown that A20 prefers K48 and K11 chains over K63 chains; while CYLD prefers K63 polyubiquitin chains.

Overall, DUB protein specificity is vast enough as to participate in a wide range of human diseases and syndromes. And despite they have a common deubiquinating activity, the molecular bases for each of these diseases are also very diverse and might imply: 1) non-processing of ubiquitin precursors, which leads to a lack of free ubiquitin molecules and a disruption of the whole ubiquitin cycle; 2) rescue of a protein that should be degraded, thus increasing its nocive effects; 3) hyper-degradation of proteins; 4) mis-functioning of the proteasomal machinery and a consequent accumulation of malfunctioning proteins; or 5) disruption of the regulation of DNA binding complexes regulation and a further disruption in transcriptional regulation.

2.3. UBIQUITIN-LIKE MOLECULES: SUMO

Ubiquitin is merely the best well-known representative member of a much larger group of other small peptides (from 40 to 100 amino acids) that can be also post-translationally conjugated to substrate proteins. All the members in this group, called Ubiquitin-Like proteins (UbL), maintain an evolutionarily preserved structural folding, named the *Ub folding*, and an extremely similar hierarchical conjugation system based on E1-E2-E3 enzymes[37] (Table 2, adapted from[38]).

Table 2. List of ubiquitin-like proteins.

Modifier	Amino acid identity with Ub (%)	E1	E2	Comments
Ubiquitin (Ub)	100	Uba1 & Uba6	many	Multiple genes encode ubiquitin precursors
Rub1/NEDD8	55	Uba3-Ula1	Ubc12	Substrates: cullins, p53
Smt3/SUMO1–3	18	Uba2-Aos1	Ubc9	Vertebrates have 3–4 ***SUMO*** genes
Atg12	ND[c]	Atg7	Atg10	~20% identical to Atg8
Atg8	ND	Atg7	Atg3	3 known human isoforms; β-grasp fold
Urm1	ND	Uba4	–	Related to MoaD, ThiS; β-grasp fold
ISG15	32/37[b]	Ube1L	UbcH8	Induced by type I interferons
UFM1	ND	Uba5	Ufc1	β-grasp fold
FUBI/MNSFβ	38	–	–	Derived from ribosomal protein precursor
FAT10	32/40[b]	Uba6	–	Substrates unknown; β-grasp fold

One of the most studied UbLs is the Small Ubiquitin-like Modifier (SUMO). SUMO proteins can be found in all evolutionary eukaryotic clades, from protozoans to metazoans. Considering mammals, four SUMO paralogs have been described: SUMO 1, SUMO 2, SUMO 3 and SUMO 4. SUMO 1 is a small 11kDa protein that only shares 47% identity with SUMO 2 and 3, which between them only differ by three N-terminal residues. The high similarity peptide sequence between SUMO 2 and 3 explains why they are often referred as a single group, SUMO2/3. Concerning SUMO 4, it was first annotated *in silico* from human genome DNA sequences, as it shares

87% amino acid similarity with SUMO2. However, no evidences have been reported so far to support actual functionality[39,40].

SUMO conjugation is, similarly to ubiquitination, a dynamic and reversible ATP-dependent process, in which E1, E2 and E3 ligases coordinate to bind a SUMO moiety to its substrate protein (Figure 11, Table 3). There are only two activating E1 enzymes, SAE1 (SUMO-activating enzyme E1) and SAE2 (only present in mammals), that act as a dimer and will transfer the activated SUMO molecule to the only known E2 conjugating enzyme, UBC9 (ubiquitin-conjugating 9). UBC9 recognizes in the protein substrate the consensus ψKxD/E (where ψ is a large hydrophobic residue) sequence, which is considered a SUMOylation motif. Despite UBC9 can recognize the protein on its own, there are a set of E3 ligases, such as PIAS 1-4 (Protein inhibitor of activated STAT; Signal Transducer and Activator of Transcription), which will serve as scaffold for the UBC9-SUMO and the final substrate[41]. In addition, other proteins have been reported to work as SUMO E3 ligases: MUL1 (mitochondrial E3 ubiquitin ligase 1), MMS21 and TOPORS (topoisomerase I-binding, arginine/serine-rich), the latter being the first dual ubiquitin and SUMO ligase ever reported. On the other hand, HDAC4 (histone deacetylase 4), HDAC7, TLS (translocated in liposarcoma) and TRAF7 (tumour-necrosis-factor-associated protein 7) also serve as scaffold for SUMOylation. None of the aforementioned ligases display any active E3 ligase activity *per se*[41].

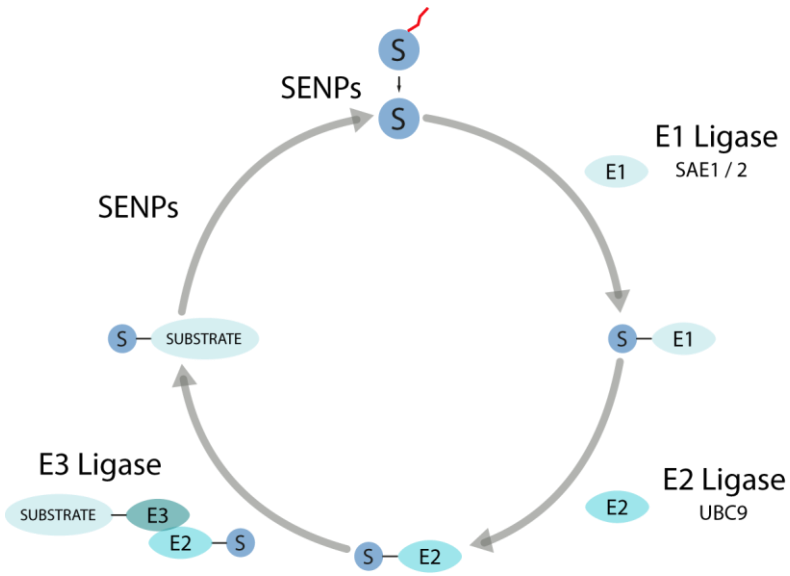

Figure 11. SUMO cycle. SUMO-specific proteases (SENPs) are responsible for activating the precursor SUMO moieties. Once activated, the E1 ligases SAE1 and SAE2 will transfer the SUMO molecule to the E2 ligase UBC9. The complex UBC9-SUMO will bind a second complex constituted by a substrate protein and an E3 ligase. This E3 ligase will then transfer the SUMO moiety to its substrate. As it is a reversible and dynamic cycle, SENP proteases can deconjugate SUMO from its protein substrate, similarly to deubiquitinating enzymes with ubiquitin. (Esquerdo, M.; 2017)

SUMOylation is reversible thanks to the presence of deSUMOylating enzymes, SENP (sentrin/SUMO-specific protease) proteases. In contrast with the large amount of deubiquitinating enzymes, there are only six different SENPs in mammals, SENP 1-3 and SENP 5-7, which differ by their specificity and subcellular localization: SENP 1/2 are responsible for SUMO maturation as well as the deconjugation of SUMO 1, 2 and 3. All SENPs are preferentially located within the nucleus, but while SENP 1, 6 and 7 are mainly found in the nucleoplasm, SENP 2 is located in the nuclear pore, and SENP 3 and 5 are enriched in the nucleoli[42].

Table 3. SUMO pathway genes.

SUBSTRATES	E3 LIGASES		PROTEASES
SUMO1	PIAS1	HDAC7	DESI1
SUMO2	PIAS2	MUL1	DESI2
SUMO3	PIAS3	RASD2	SENP1
E1 LIGASES	PIAS4	TOPORS	SENP2
SAE1	RANBP2	TLS	SENP3
SAE2	CBX4	TRAF-7	SENP5
E2 LIGASE	MMS21	EGR2	SENP6
UBC9	HDAC4		SENP7

Similarly to Ub, the SUMO pathway genes are involved in cell cycle progression, DNA damage repair, cellular transport and transcription factor regulation[43]. Furthermore, it has been observed that SUMO can synergize, antagonize or cooperate with ubiquitin and other posttranslational modifications to more precisely regulate cellular processes[42,43].

3. UBIQUITIN AND SUMO IN PHOTORECEPTOR DEVELOPMENT

Photoreceptors are highly specialized cellular types, which differ both structurally and functionally, but that develop from the same photoreceptor progenitor precursor. Therefore, there must be a fine and tight genetic control to successfully achieve a properly structured and functional retina.

Gene expression regulation by photoreceptor-specific transcription factors has been amply described[1,44,45]; however, it is not their bare action that determines photoreceptor fate, since SUMO conjugation –and possibly other post-translational modifications– of TFs play a key role in this process[46]. As mentioned, during photoreceptor commitment NR2E3 activates rod specific genes; however, when this TF is post-translationally modified by SUMO, NR2E3 recruits an alternative protein complex that will instead silence cone-specific genes. In fact, mutations in the human gene that interfere with this process cause S-cone syndrome, a retinal dystrophy with an excess of cone-like photoreceptor cells. Similarly the rod specific TF, NRL, is also SUMOylated, leading to a finer regulation of rod specific genes [47] (Figure 12, adapted from [46]).

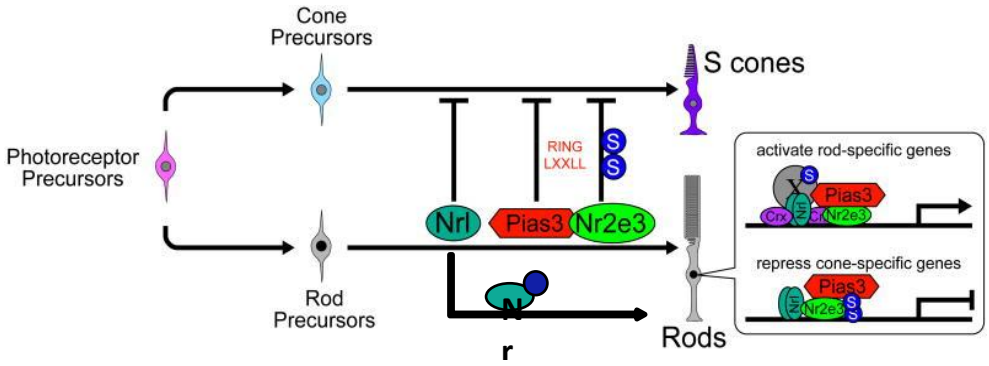

Figure 12. Involvement of SUMOylation in photoreceptor cell fate. The retinal transcription factor NR2E3 promotes the activation of rod-specific genes. However, SUMOylation of this TF leads to the silencing of cone-specific genes. In addition, the rod-specific transcription factor NRL inhibits cone-specific genes, but when SUMOylated, it activates rod-specific genes.

Other examples illustrate Ub cycle genes participating in retinal development and retinal disease: mutations in ubiquitin pathway genes, such as the E3 ligases TOPORS[48–50] and KLHL7[51,52] are causative of the most prevalent retinal hereditary dystrophy, retinitis pigmentosa (RP)[48–50]. Moreover, protein homeostasis via the ubiquitin-proteasome system is also relevant to other retinal diseases, as altered protein degradation has been associated to Stargardt's disease, age-related macular degeneration, glaucoma, diabetic retinopathy and retinal inflammation (reviewed in[53]). Thus, given the clear implication of ubiquitin and SUMO pathway genes in retinal processes, it might well be that deubiquitinating enzyme genes are also involved in retinal development.

In mammals, several comprehensive surveys of DUBs have been reported resulting in: *in silico* inventories of the DUBs in the human genome[27,28]; identification of protein interactors by cell-based proteomics analysis[54];

studies of subcellular localization[55]; functional involvement in maintaining genome integrity[56]. A recent review reported the expression levels of DUBs in human organs and the disease phenotypes associated to DUB mutations in humans and animal models[29]. Despite their importance, detailed expression and functional analysis for most DUBs on particular tissues or organs, such as the retina, is still missing. For these reasons, this work is intended as a study of deubiquitinating enzymes in the retina and their possible role in photoreceptor development and homeostasis.

Objectives

1. Analysis of the involvement of deubiquitinating enzymes (DUBs) in the mouse retina:

I. Description of the **expression pattern** of all **DUBs in the mouse retina**, analyzing mRNA expression and pattern of expression via real time RT-qPCR and *in situ* hybridization.

II. Determination of the **protein localization** of a set of DUB enzymes in the adult mouse retina via fluorescent immunohistochemistry.

III. **Sequence and functional conservation analysis** of DUBs through phylogenetic and phenotypic studies.

IV. **Transcriptomic analysis** of DUBs' mRNA expression in the retina during development, considering wild type mouse retinas; CRX and NRL knockout mouse retinas; flow sorted rods and cones; and human retina.

V. **Preliminary analysis of the functional role of selected DUBs** in mouse retinal development via *in vivo* gene knockdown.

2. Devising an in-vivo cell system to study the role of DUB enzymes on the regulation of retinal promoters:

I. Establishing **a cell culture system** to study the behaviour of DUBs upon retinal promoters.

II. **Knockdown of DUB genes in the established cell culture system** via shRNA and siRNA silencing techniques.

3. Identification of CRX post-translational modifications, particularly ubiquitination.

Materials and methods

BACTERIAL TRANSFORMATION AND CULTURE

For bacterial transformation, competent DH5α Escherichia coli strain were heat shocked at 42°C for 90 seconds, kept in ice for 2 min, grown at 37°C for 1h in LB medium and plated in LB-agar plates with either ampicillin or kanamycin (according to the resistance provided by the transformed plasmid). LB plates were with transformed bacteria were incubated overnight (O/N) at 37°C.

For constructs made in pGEM-T vector, colony colour selection was performed adding to LB-agar plates with transformed bacteria 1:1 IPTG:X-Gal reagents. White colonies contained pGEM-T with a DNA inserted, while blue colonies contained religated pGEM-T.

GENE EXPRESSION CONSTRUCTS

The promoters of the retinal specific genes: S opsin, M opsin, Rhodopsin and GNAT were cloned upstream the luciferase gene in the *pGL3-Promoter Vector*. Thus, if a transcription factor bound the promoter, the changes in the luciferase gene expression could be easily quantified by the changes in luciferase activity as measured in a luminometre. The human CRX, NRL, NR1D1 and NR2E3 transcription factors were cloned in the pcDNA3 vector containing Xpress epitope. The DNA fragments containing the human Rhodopsin, human M opsin and mouse GNAT promoters, as well as the transcription factor (TF) constructs were provided by Dr. Pomares (a former member of our group).

For *in situ* hybridization, 400-700 bp cDNA sequences of each analyzed DUB were cloned into a pGEM-T Easy Vector (Promega) to obtain the riboprobes.

MAMMALIAN CELL CULTURE

The mouse cell line 661W (precursor of cones) was cultured in DMEM 4.5 g/L glucose, 1.1 g/L sodium pyruvate (Invitrogen) medium, supplemented with 0.3 g/L glutamine, β-mercaptoethanol (40 μL/L) (Invitrogen). RGC5 cells (rat transformed ganglion cell line) were cultured in 4.5 g/L glucose, 1.1 g/L sodium pyruvate (Invitrogen) DMEM medium, supplemented with 0.3 g/L glutamine, 1 g/L D-glucose. Human retinoblastoma Y-79 was cultured in DMEM with 25mM HEPES (Invitrogen). HEK293 (Human Embryonic Kidney), HEK293T (Human Embryonic Kidney transformed with SV40 virus T antigen) and Mio-M1 (human Müller cells) were cultured in DMEM with L-glucose (ATCC). All culture media were further supplemented with 10% Foetal Bovine Serum (FBS; Invitrogen) and 1% Penicillin-Streptomycin (PenStrep, Invitrogen). Cells were kept at 37°C and 5% CO_2.

TRANSFECTION IN CELL CULTURES

HEK293T, 661W, RGC5 and Y-79 cells were transfected with *Lipofectamine 2000* (Invitrogen) following the manufacturer's instructions. HEK 293 cells were transfected with *Lipotransfectine* (Niborlab) following the manufacturer's instructions, using a ratio of DNA:Lipotransfectine of 1:3. The efficiency of different liposomal systems was tested on HEK293T cells by transfecting a control GFP construct, and checking GFP expression at 28 h, 50 h and 72 h post-transfection. *TransIT-Neural* (Mirus), *TransIT-293 Transfection Reagent* (Mirus), *FuGENE HD Transfection Reagent* (Roche), *TransFast Transfection*

Reagent (Promega) and *Metafectene Pro* (Biontex) were used following the manufacturer's instructions. The appropriate amount of CRX and S opsin promoter was tested using different relative amounts, as referred in Table 4.

Table 4. Tested amounts of the S opsin promoter and CRX expression vectors

µg of S opsin promoter	µg of CRX
0,05	0,2
0,2	0,2
0,3	0,1
0,4	0,4
0,4	0,1
0,6	0,1
0,6	0,075
0,8	0,05
0,8	0,1
1	0,1
2	0,1
3	0,1

shRNA SILENCING

HEK293 cells were transfected with 145 ng of S opsin-Luciferase construct (reporter gene), 25 ng of β-galactosidase construct (for transfection normalization), 240 ng of CRX construct (transcription factor) and a total of 750 ng of shRNA (for assaying the effects of the each analyzed DUB knockdown) per condition in 48 well plates. Three different constructs of shRNA were used per each silenced gene. *Lipotransfectine* (Niborlab) was used in a 1:3 ratio of DNA:Lipotransfectin according to the manufacturer's instructions, and cell lysates were collected 72h post-transfection. The list of

genes silenced with shRNA is shown in Table 5. Deconvolution of the three shRNA from selected genes was performed under the same conditions, using 750 ng of each shRNA construct.

Table 5. List of selected genes silenced with shRNA.

shRNA		
SUMO		**DUBs**
SUMO-1	Rasd2	JOSD2
SUMO-2	TOPORS	ATXN3
SUMO-3	TLS	BAP1
SAE1	TRAF-7	STAMPB
SAE2	DESI1	USP9X
Ubc9	DESI2	USP25
PIAS1	SENP1	USP45
PIAS3	SENP2	USP54
PIAS2	SENP3	UCHL1
PIAS4	SENP5	UCHL3
RANBP2	SENP6	USP12
CBX4	SENP7	USP11
Mms21	SENP8	TNFAIP3
HDAC4	USPL1	USP47
HDAC7A		PRPF8
Mul1		OtuD7b

siRNA SILENCING

HEK293 cells were transfected with 150 ng of S opsin-Luciferase construct (reporter gene), 25 ng of β-galactosidase construct (for transfection normalization), 250 ng of CRX construct (transcription factor) and a total of 5 μM of siRNA (for assaying the effects of the each analyzed DUB knockdown) per condition in 48 well plates. Two different constructs of siRNA were used per each silenced gene. *Lipotransfectine* (Niborlab) was used in a 1:3 ratio of DNA:Lipotransfectin according to the manufacturer's

instructions, and cell lysates were collected 48h post-transfection. The list of genes silenced with siRNA is shown in Table 6. Deconvolution of the three siRNA from selected genes was performed under the same conditions, using 750 ng of each siRNA.

Table 6. List of selected genes silenced with siRNA

siRNA		
DUB genes		
USP 1	USP 13	USP 31
USP 2	USP 14	USP 32
USP 3	USP 15	USP 33
USP 4	USP 16	USP 34
USP 5	USP 18	USP 36
USP 6	USP 19	USP 37
USP 7	USP 20	USP 42
USP 8	USP 22	USP 44
USP 9	USP 24	USP 46
USP 10	USP 25	USP 47
USP 11	USP 29	CYLD
USP 12	USP 30	

LUCIFERASE ASSAY

To assess the activity of the S opsin-Luciferase promoter, a luciferase assay was performed to measure luciferase activity. Cells were lysed using the Reporter Lysis Buffer (Promega), frozen at -80°C and centrifuged to discard cellular debris for 2 min at 12000 g. Luciferase activity was measured after 5 min of reaction with ONE-Glo Luciferase Assay System (Promega). Reads were performed in the Modulus Microplate Multimode Reader (Turner Biosystems) luminometer. Results were normalized with values obtained from β-galactosidase reaction, expressed from the cotransfected pCMV- β-

gal vector, measured with Beta-Glo Assay System (Promega), following the manufacturer's instructions.

ETHICS STATEMENT FOR ANIMAL PROCEDURES

All procedures in mice were performed according to the ARVO statement for the use of animals in ophthalmic and vision research, as well as the regulations of the Animal Care facilities at the Universitat de Barcelona. The protocols and detailed procedures were evaluated and approved by the Animal Research Ethics Committee (CEEA) of the Universitat de Barcelona (our institution), and were submitted and also approved by the Generalitat de Catalunya (local Government), with the official permit numbers DAAM 6562 and 7185.

ANIMAL HANDLING, TISSUE DISSECTION AND PREPARATION OF SAMPLES

Murine retina samples and eye slides were obtained from 2 month-old C57BL/6J (wild-type) and CD-1 (albino) animals. Animals were euthanized by cervical dislocation. Some retinas were dissected and immediately frozen in liquid nitrogen, while the rest were fixed in 4% paraformaldehyde (PFA) for 2 h at room temperature (RT), washed, cryoprotected overnight in acrylamide at 4°C, embedded in O.C.T. (Tissue-Tek, Sakura Finetech, Torrance, CA), frozen in liquid nitrogen and sectioned at -20°C.

RNA EXTRACTION AND cDNA SYNTHESIS

For each sample, retinas from three different animals were pooled. Therefore, up to 9 animals in three independent replicates were analysed. Retinas were homogenized using a Polytron PT 1200 E homogenizer

(Kinematica, AG, Lucerne, Switzerland). Total RNA was extracted using the High Pure RNA Tissue Kit (Roche Diagnostics, Indianapolis, IN) following the manufacturer's instructions with minor modifications (increasing the incubation time with DNase I). Reverse transcription reactions were carried out using the qScript cDNA Synthesis Kit (Quanta Biosciences) following the manufacturer's protocol.

REAL TIME qPCR

Quantitative reverse transcription PCR was performed using the LightCycler® 480 SYBR Green I Master Mix (Roche Applied Science) and a LightCycler® 480 Multiwell Plate 384. The final reaction volume was 10 µl. Raw data was analysed with the LightCycler® 480 software using the Advanced Relative Quantification method. *Gapdh* expression was used to normalize the levels of expression. *Rho* and *Cerkl* were considered as reference genes with high and low levels of expression, respectively, in the mouse retina. Three independent sample replicates were analysed for each gene. Primers used for the Real Time qPCR are listed in Table 7 and in Table 8.

Table 7. Primer list used for performing RT qPCR in human- and mouse-derived cell lines.

Human			*Mouse*		
GAPDH	Fw	ctcaagggcatcctggctac	***GAPDH***	Fw	agactgaacggaagctcac
	Rv	agcgtcaaaggtggaggagtg		Rv	tactccttggaggccatgtagg
RHO	Fw	tcgactactacacgctcaagc	***Rho***	Fw	gcccttctccaacgtcacag
	Rv	gaagacgagctgcccatagg		Rv	gcagcttcttgtgctgtacgg
M opsin	Fw	catagccatggcccagcagt	***M opsin***	Fw	tcttgtggtcgttgcatctgtc
	Rv	agttgctgttggtgtaggtga		Rv	agtggatggcgcagcttctt
S opsin	Fw	gtgggcctcagtaccacat	***S opsin***	Fw	gcgggagatgtcaggagagg
	Rv	cagtgtggccaccagcac		Rv	caggagcaaggtggtactgagg
GNAT	Fw	gacctggagcgcctggtaac	***Gnat***	Fw	tgcctaccctgtccctttgc
	Rv	cgatgatgccagtggtcttga		Rv	tccagctctctggagtgcttct
CRX	Fw	caactggaggagctggagg	***Crx***	Fw	ccaccgtgtccatttggagt
	Rv	tgaaccctggactcaggcag		Rv	agagggcccagaagccacta
NRL	Fw	ccgttcagagcaccttgtgg	***Nrl***	Fw	ggtgcctccttcacccacct
	Rv	cgatgcagagaaccgtgcag		Rv	gggtggccagccaatatagc
NR1D1	Fw	agacttcacccacccagcac	***Nr1d1***	Fw	actccacatccacctctgg
	Rv	aggcgtcagctgttgtggaa		Rv	ggaactgagagaagcccacca
NR2E3	Fw	ccagcaatgaccctgagttcc	***Nr2e3***	Fw	gccttggccagtgcagagac
	Rv	ccgaggtctcatggatgctg		Rv	Gccttcaggcaggcaaactc

IN SITU HYBRIDIZATION

For *in situ* hybridization (ISH), 16-18µm sections were recovered on commercial Superfrost Plus glass slides (Electron Microscopy Sciences, Hatfield, PA), dried 1 h at RT, rinsed three times for 10 min with phosphate-

buffered saline (PBS), treated with 2 μg/ml proteinase K for 15 min at 37°C, washed twice for 5 min with PBS, and fixed with 4% PFA. Acetylation with 0.1 M triethanolamine-HCl (pH 8.0) containing first 0.25%, and then 0.5% acetic anhydride, was performed for 5 min each. Hybridization was carried out overnight at 55°C with digoxigenin-labelled riboprobes (2 μg/ml) in 50% formamide, 1 x Denhardt's solution, 10% dextran-sulfate, 0.9 M NaCl, 100 mMTris-HCl (pH 8.0), 5 mM EDTA (pH 8.0), 10 mM NaH_2PO_4, and 1 mg/ml yeast tRNA. For each gene, cDNA fragments generated by RT-PCR of approximately 400-700bp were subcloned into the pGEM-T® Easy Vector (Promega) and sense and antisense riboprobes were generated from the flanking T7 RNApol promoter. The name and sequence of all the primers used for RT qPCR and *in situ* hybridization are listed in Table 8.

After hybridization, slides were washed in 2x SSC for 20 min at 55°C, equilibrated in NTE (0.5 M NaCl, 10 mM Tris-HCl pH 8.0, 5 mM EDTA) at 37°C, and then treated with 10 μg/ml RNase A in NTE at 37°C for 30 min. Subsequently, the sections were washed at 37°C in NTE for 15 min, twice in 2x SSC and 0.2x SSC for 15 min each, equilibrated in Buffer 1 (100 mM Tris-HCl pH 7.5, 150 mM NaCl), and blocked in Blocking Buffer (1% BSA and 0.1% Triton X-100 in buffer 1) for 1 h at RT. An anti-digoxigenin-AP conjugate antibody (1:1000; Roche Diagnostics, Indianapolis, IN) in Blocking Buffer was incubated overnight at 4°C. Sections were then washed twice in Buffer 1 for 15 min, once in Buffer 2 (100 mM Tris-HCl pH 9.5, 150 mM NaCl), and once in Buffer 2 supplemented with 50 mM $MgCl_2$ (5 min each) prior to adding the BM Purple AP Substrate (Roche Diagnostics, Indianapolis, IN). For each gene, antisense and sense ISH staining reactions were processed in parallel. The reaction was stopped in 1x PBS. Sections were cover-slipped with Fluoprep (Biomérieux, France) and photographed

using a Leica DFC Camera connected to a Leica DM IL optic microscope (Leica Microsystems, Germany).

Table 8. DUB genes primer list used for RT qPCR and for *in situ* hybridization

	Real Time qPCR			*In Situ Hybridization*		
Family	**Gene**	**Orientation**	**Sequence (5'-3')**	**Gene**	**Orientation**	**Sequence (5'-3')**
	Gapdh*	Fw	tgacaatgaatacggctacagcaa			
		Rv	tactccttggaggccatgtagg			
	Rho	Fw	gcccttctccaacgtcacag	***Rho****	Fw	gcccttctccaacgtcacag
		Rv	gcagcttcttgtgctgtacgg		Rv	gcagcttcttgtgctgtacgg
JAMM	***Amsh***	Fw	attgttcaagagttcgggaagg	***Amsh***	Fw	caccgagactacaaatcagctatc
		Rv	gggggccacatctacacaagg		Rv	gggggccacatctacacaagg
	Amsh-L	Fw	gctgctatgcctgaccatacaga	***Amsh-L***	Fw	gagaacccagaggcccggacta
		Rv	gacctgaagtaacggcgtggggtg		Rv	gacctgaagtaacggcgtggggtg
	Brcc36	Fw	gcggcgttctgacaagagaaagg	***Brcc36***	Fw	aacacaaagactggccgggta
		Rv	ataccagccaacaactctcatggg		Rv	cgatgcaggaaccaaagcag
	Csn5	Fw	ttccgggagtggtatggcccag	***Csn5***	Fw	ttccgggagtggtatggcccag
		Rv	cgccgccaggatttctttcttgttg		Rv	gtgtactaacatcaatcccggag
	Eif3h	Fw	catgtttgaagaagtgccgattg	***Eif3h***	Fw	NP
		Rv	gtgcttatccgccacagctgac		Rv	NP
	Jamm2	Fw	cctgcctgaatgctgtaaagattg	***Jamm2***	Fw	cctgcctgaatgctgtaaagattg
		Rv	agtaagatggctgccagaattctgt		Rv	tcctctcttacttctcctctgtg
	Jamm3	Fw	cctgttcctcgaggcctgt	***Jamm3***	Fw	tccatggcagctcccgagtct
		Rv	tcaatgtcctgcaagcaaggagggta		Rv	ctcctccaacagcagttcttcc
	Mysm1	Fw	tgtctctgctctgtgccaactg	***Mysm1***	Fw	NP
		Rv	cacctctcctgctgagaaacca		Rv	NP
	Poh1	Fw	acatgtggatgtcttatgacttca	***Poh1***	Fw	caatgctaatatgatggtcttgg
		Rv	gcgccactgacagctctctacgt		Rv	gccactgacagctctctacg
	Prpf8	Fw	gcgtggaattacccctctgc	***Prpf8***	Fw	NP
		Rv	cacccgctgcttcgttactg		Rv	NP
	Psmd7	Fw		***Psmd7***	Fw	NP
		Rv		***Amsh***	Rv	NP
MJD	***Atxn***	Fw	gccctgtggagctatcctcaat	***Atxn***	Fw	gccctgtggagctatcctcaat
		Rv	actccccttctgccattctc		Rv	gagggcactctgctctttcaga
	Josd1	Fw	ccatggtctctgcaggtctga	***Josd1***	Fw	ccatagtttgggacagagttggg
		Rv	tgctcaggattaacatgcaagc		Rv	tgctcaggattaacatgcaagc
	Josd2	Fw	gtgcgaggtgctattggtggt	***Josd2***	Fw	gccgacgaaatctgcaagag
		Rv	gcagcagatcagcttgtgttca		Rv	gcagcagatcagcttgtgttca

	Josd3	Fw	gaacaccaccttaaggaatgcttg	***Josd3***	Fw	ggcatcggatagagctggagat
		Rv	gtatttgtgcctccgactgtca		Rv	gtatttgtgcctccgactgtca
OTU	***Otub1***	Fw	agcaggtggacaagcagacctc	***Otub1***	Fw	agcaggtggacaagcagacctc
		Rv	cagtcgcaggtagaccacaagg		Rv	cctctgtacatgtctagcgcc
	Otub2	Fw	gccacttaccttgccttgctgc	***Otub2***	Fw	acattctatccattcttcgggatca
		Rv	acagggtggtcccatggttatc		Rv	agaagtcagctcggttcctgatg
	Otud1	Fw	catggggcagatgctgaatgtg	***Otud1***	Fw	agaagctagccctgtacctgg
		Rv	ggcccagatagtggatcatgg		Rv	ggcccagatagtggatcatgg
	Otud3	Fw	gatgcggaggagaaccatga	***Otud3***	Fw	tccacatcgcctaccgctac
		Rv	tgccttcatttctgccctga		Rv	tgccttcatttctgccctga
	Otud4	Fw	cctgttcccgtgtatcctcaga	***Otud4***	Fw	cctgttcccgtgtatcctcaga
		Rv	catcggtgcaaggacagtcac		Rv	tccaaaggcaaatccaattctcc
	Otud5	Fw	ctgagcaccctgaactgcat	***Otud5***	Fw	gcctaccgtcatttaagccagg
		Rv	tgaaggaggtttggcaagagcta		Rv	tgaaggaggtttggcaagagcta
	Otud6a	Fw	cgagatggagcagaggcacaa	***Otud6a***	Fw	NP
		Rv	gctgtaaccgaatccacactgc		Rv	NP
	Otud6b	Fw	ccgggaagaaaggatagcagagg	***Otud6b***	Fw	NP
		Rv	ggctgccaatatttgagcaagtt		Rv	NP
	Otud7a	Fw	tctgacggattcggaacacaag	***Otud7a***	Fw	cttgcacagccagagtctcc
		Rv	tggctaaccgggcattgtcg		Rv	ggcgacgctcccgacgc
	Otud7b	Fw	atgatccagcgttaccttgcag	***Otud7b***	Fw	gggcctgatgcacagcaagg
		Rv	ccctccattcatgatcttcctc		Rv	ccctccattcatgatcttcctc
	Parp11	Fw	tgctatccccatccagctttg	***Parp11***	Fw	NP
		Rv	tgcttcccaatttgagtgactg		Rv	NP
	Tnfaip3	Fw	ataatggattctgtgagcgttgc	***Tnfaip3***	Fw	tttgagcttgttcagcacgaatac
		Rv	gaaggcaggcttggcactttc		Rv	gaaggcaggcttggcactttc
	Vcpip1	Fw	atggggtgtgcctcaggaccttatt	***Vcip1***	Fw	gaaacgaagggaccgaagaatc
		Rv	ctgcaaacttctgtctcctccaa		Rv	tgctgctgaaagtgctgctta
	Yod1	Fw	cagcgtaacttccctgatccaga	***Yod1***	Fw	gaaggaccgaggccgagtc
		Rv	cttcatcagctaattccagtgcttg		Rv	cgggtagccaacgaggattc
	Zranb1	Fw	tcccagacctaataacattgaagca	***Zranb1***	Fw	ggtggaagtagtcctttgatatg
		Rv	ctccatcgagctctgtcttgctc		Rv	ctccatcgagctctgtcttgctc
UCH	***Bap1***	Fw	tcctgggagtgggagtgacat	***Bap1***	Fw	ctgcttcctgagcattgaggag
		Rv	ctgcttcctgagcattgaggag		Rv	gctgtgactcttgagatttgtg
	Uch-l1	Fw	gattaaccccgagatgctgaac	***Uch-l1***	Fw	cgcttcgccgacgtgctagg
		Rv	ggatggcactgagcccagag		Rv	gcccatcgagctcgtacaga
	Uch-l3	Fw	tatgcgcgcagtgttactcctctt	***Uch-l3***	Fw	tatgcgcgcagtgttactcctctt
		Rv	tcgttccacaggcattgctgat		Rv	ggcatcctctaacaacgtctcatc
	Uch-l5	Fw	agatgtgattcgacaagtgcacaa	***Uch-l5***	Fw	ggggtcttcaccgagctcat
		Rv	agatgtgattcgacaagtgcacaa		Rv	agatgtgattcgacaagtgcacaa

USP	***Usp1***	Fw	ggacaccattcaccgacaatag	***Usp1***	Fw	NP
		Rv	aacgcctgtttggtcactggat		Rv	NP
	Usp2	Fw	acctgaagcgattctcagaatc	***Usp2***	Fw	gatggtctccacaatgaggtg
		Rv	ctctcaagtccaggtctctta		Rv	ctctcaagtccaggtctctta
	Usp3	Fw	ccgctggttccatttcaatgac	***Usp3***	Fw	NP
		Rv	ctggcctgacgctccacataa		Rv	NP
	Usp4	Fw	tggtgaggacgatcagggaga	***Usp4***	Fw	NP
		Rv	aggagttcacgaggctgaagg		Rv	NP
	Usp5	Fw	cacccatgctggacgaatccg	***Usp5***	Fw	cggatgagcccaaaggtagcct
		Rv	gccccgctgtttcccgtatag		Rv	gccccgctgtttcccgtatag
	Usp6	Fw	cggaagtatctggagctgagc	***Usp6***	Fw	NP
		Rv	cagtccatctttcggcccttc		Rv	NP
	Usp7	Fw	gatgatgacgtggtatccaggtg	***Usp7***	Fw	NP
		Rv	catataggcatttgtgcagtgtc		Rv	NP
	Usp8	Fw	caacgagcacctggatgacc	***Usp8***	Fw	tatttggaggatcaggaccagc
		Rv	acgatgatggactcgttgagc		Rv	acgatgatggactcgttgagc
	Usp9X	Fw	ttaaaaggaaatggacctgggc	***Usp9X***	Fw	tcaagaatgcagtcttcgatca
		Rv	gctttgcactggaggagacc		Rv	gctttgcactggaggagacc
	Usp9Y	Fw	gtggacttgggctatggaatgg	***Usp9Y***	Fw	NP
		Rv	gtactggaggagaccagttgc		Rv	NP
	Usp10	Fw	atgcccaggacttgtgacagc	***Usp10***	Fw	NP
		Rv	cctggcatcgcctcctagtg		Rv	NP
	Usp11	Fw	gcctggcagaaccataaacgac	***Usp11***	Fw	NP
		Rv	cattgccacaatcagggcacac		Rv	NP
	Usp12	Fw	accagcttcaccggtacacga	***Usp12***	Fw	NP
		Rv	ctgtcagggttggtcgcatct		Rv	NP
	Usp13	Fw	cactggactggatcttcagcc	***Usp13***	Fw	tgatgaaccagttgatagaccc
		Rv	gcctcagacacgatgttggca		Rv	gcctcagacacgatgttggca
	Usp14	Fw	atggaattgccatgtggattgac	***Usp14***	Fw	NP
		Rv	gggcatctttgagttcaggcac		Rv	NP
	Usp15	Fw	cgcgcagtcacttaaggagca	***Usp15***	Fw	NP
		Rv	ccatcagtgtgtaccagctgac		Rv	NP
	Usp16	Fw	agcacttgcgggagaagtgga	***Usp16***	Fw	NP
		Rv	ggccatccaaatccttctggtta		Rv	NP
	Usp17L8	Fw	ctgccaatgacaagcccagtc	***Usp17L8***	Fw	NP
		Rv	cagggctgcattcaggtagca		Rv	NP
	Usp18	Fw	acgcaggagtccctgatttgc	***Usp18***	Fw	NP
		Rv	cagaggctttgcgtccttatcaa		Rv	NP
	Usp19	Fw	cctggctctggtgtggcgga	***Usp19***	Fw	NP
		Rv	cagcagagcctggatcttcagc		Rv	NP

Usp20	Fw	cggcatgaggtgatgtactcct	***Usp20***	Fw	tggctggccttcatcgtgg
	Rv	cagggacgtgcactccttgg		Rv	cagggacgtgcactccttgg
Usp21	Fw	ccgagtgggagccaagatacc	***Usp21***	Fw	NP
	Rv	cctgggaggcaaaggtcgtaa		Rv	NP
Usp22	Fw	tctaccccattctggcccttg	***Usp22***	Fw	NP
	Rv	ttcgcaggcagtctgtgagag		Rv	NP
Usp24	Fw	gtgtgcccagacaggatgctc	***Usp24***	Fw	NP
	Rv	ggttctcctcccactcctgg		Rv	NP
Usp25	Fw	agagcagccatcaagaagtgac	***Usp25***	Fw	ccaccgggagagccggtggat
	Rv	atcttcaagatcatgtgacgcct		Rv	atcttcaagatcatgtgacgcct
Usp26	Fw	cgcaaggtggatccaacaaagt	***Usp26***	Fw	NP
	Rv	tagtggcctccattgggactg		Rv	NP
Usp27X	Fw	tctggacttgcctggctcttg	***Usp27X***	Fw	NP
	Rv	agtggtgatgcctgggatgtg		Rv	NP
Usp28	Fw	catgaggagtactccaggctct	***Usp28***	Fw	catgaggagtactccaggctct
	Rv	catgctgaaggcgagggtcac		Rv	acaccaggtaggacaatgcttc
Usp29	Fw	ccagcgcagaagtgaacaagg	***Usp29***	Fw	NP
	Rv	ttctctgctttgccgcctctg		Rv	NP
Usp30	Fw	ctgccacagtgcctctgcat	***Usp30***	Fw	actggaagtctcagcaccct
	Rv	aactgcacgtgctcgtgcc		Rv	aactgcacgtgctcgtgcc
Usp31	Fw	ctgacagagccagcgtcacct	***Usp31***	Fw	NP
	Rv	acgtgcttgccatccactctg		Rv	NP
Usp32	Fw	caccgactctgcctacattctt	***Usp32***	Fw	NP
	Rv	ctcgtgtccgccatcttcttg		Rv	NP
Usp33	Fw	tcctccgacctccagttgttc	***Usp33***	Fw	NP
	Rv	gtgtcctcagaactacaaagagc		Rv	NP
Usp34	Fw	atggcaggtttgacgactgt	***Usp34***	Fw	tgacgaaggagcaactcctgt
	Rv	tcggattcatcttcagctagtg		Rv	tcggattcatcttcagctagtg
Usp35	Fw	catggtggcctctctggtcaa	***Usp35***	Fw	NP
	Rv	agcccgggaaccgaaacacc		Rv	NP
Usp36	Fw	gcatcgacacgctcctccca	***Usp36***	Fw	gcatcgacacgctcctccca
	Rv	gcaccctcaccctccgagc		Rv	ctcttcatcctgctgtggctc
Usp37	Fw	agaggtgctggcagctgtgtt	***Usp37***	Fw	NP
	Rv	gtgtccggactgctggttgg		Rv	NP
Usp38	Fw	cagcttcgttacccagtgctca	***Usp38***	Fw	NP
	Rv	gacaaaggcagctgttgctgga		Rv	NP
Usp39	Fw	caagccgtccacaagaacacc	***Usp39***	Fw	NP
	Rv	tgatgaagcacgtggatcctg		Rv	NP
Usp40	Fw	ctgaggacacagctacgcatc	***Usp40***	Fw	NP
	Rv	tcaaggagccagcagtccatc		Rv	NP

Usp41	Fw		***Usp41***	Fw	NP
	Rv			Rv	NP
Usp42	Fw	acaacgtcgacttcccccagt	***Usp42***	Fw	NP
	Rv	tctgaggactcggccccatag		Rv	NP
Usp43	Fw	gactcgggagcctcaacaaca	***Usp43***	Fw	NP
	Rv	tggtgaagacaggagagtcgg		Rv	NP
Usp44	Fw	gagcccagttccccgtacag	***Usp44***	Fw	NP
	Rv	agcatggcaaacggtgagacc		Rv	NP
Usp45	Fw	agcctcactgacggcagcg	***Usp45***	Fw	agcctcactgacggcagcg
	Rv	aggctgcttggaagcgatc		Rv	gacaggactggactgagcat
Usp46	Fw	accgggtggtcttccctctg	***Usp46***	Fw	NP
	Rv	aacgaccacagcaaccaggtc		Rv	NP
Usp47	Fw	gtccatgtcacagcttgccatc	***Usp47***	Fw	gagagtacagagttaaagtgtgcc
	Rv	gctttccaacacaagctcctgg		Rv	gctttccaacacaagctcctgg
Usp48	Fw	gcagcagcaggatgcacaaga	***Usp48***	Fw	NP
	Rv	ctgctgcacaacattccgaaca		Rv	NP
Usp49	Fw	caggagcctggagctcattca	***Usp49***	Fw	NP
	Rv	cccacttcccagaccacatga		Rv	NP
Usp50	Fw	actttggagatctggatggtgg	***Usp50***	Fw	NP
	Rv	tcactgactcgggtgtcatcaa		Rv	NP
Usp51	Fw	gacctgggtagcagtgccaaa	***Usp51***	Fw	NP
	Rv	gaaagcaggccacaatcggtaa		Rv	NP
Usp52	Fw	cggaagtatctggagctgagc	***Usp52***	Fw	NP
	Rv	cagtccatctttcggcccttc		Rv	NP
Usp53	Fw	ggagtccatgcatgacccagg	***Usp53***	Fw	tgaacaactggacgggtagctg
	Rv	tgaacaactggacgggtagctg		Rv	catctgtgagaactgctgggct
Usp54	Fw	cacgtgcaacctgcctagaa	***Usp54***	Fw	gaagagagcactgtcgctgg
	Rv	tccagttcagaggtctcctgc		Rv	tccagttcagaggtctcctgc
Cyld	Fw	tcccaggcagtgccgcatc	***Cyld***	Fw	tcccaggcagtgccgcatc
	Rv	tgcttgatcttcccagctgag		Rv	gaatgttgaagccattctgacc

FLUORESCENT IMMUNOHISTOCHEMISTRY

For retina immunofluorescence, 16 µm sections were recovered on commercial Superfrost Plus glass slides (Electron Microscopy Sciences, Hatfield, PA), dried 30-45 min at RT, washed 10 min with PBS and blocked for 1 h with Blocking Buffer (2% Sheep Serum and 0.3% Triton X-100, in

PBS 1x). Primary antibodies were incubated overnight at 4°C with Blocking Buffer. After incubation, slides were washed with PBS (3 x 10 min) and treated with DAPI (Roche Diagnostics, Indianapolis, IN) (1:300) and with secondary antibodies conjugated to either Alexa Fluor 488 or 561 (Life Technologies, Grand Island, NY) (1:300) in a 1x PBS solution. After secondary antibody incubation slides were washed again in PBS (3 x 10 min). Sections were mounted in Fluoprep and analyzed by confocal microscope (SP2, Leica Microsystems). Primary antibodies and dilutions used were:

Table 9. List of primary antibodies used for immunohistochemistry.

Dilution	Host	Protein	Manufacturer
1:50	Rabbit	ATXN3	in house, kind gift from Dr. S. Todi
1:20	Rabbit	BAP1	Biorbyt (orb33784)
1:300	-	DAPI	Roche (70237122)
01:50	Rabbit	JOSD2	Aviva Systems Biology (OAAB00616)
1:50	Rabbit	JOSD2	Origene (TA337367)
1:50	Rabbit	JOSD3	
1:100	Rabbit	OTUD4	Abcam (ab106368)
1:50	Rabbit	OTUD7B	ProteinTech (16605-1-AP)
1:50	-	PNA	Life Technologies (L32460)
1:100	Rabbit	PRPF8	Abcam (ab79237)
1:500	Mouse	Rhodopsin	Abcam (ab5417)
1:100	Rabbit	TNFAIP3	Abcam (ab74037)
1:100	Rabbit	UCHL3	Abcam (ab126703)
1:100	Rabbit	USP13	Abcam (ab109264)
1:100	Rabbit	USP16	Abcam (ab135509)
1:100	Rabbit	USP22	Abcam (ab4812)
1:300	Rabbit	USP25	in house
1:250	Rabbit	USP28	ABGEN (AP2152b)
1:50	Rabbit	USP46	ProteinTech (13502-1-AP)
1:20	Rabbit	USP48	Abcam (ab72226)
1:100	Rabbit	USP9X	Abcam (ab19879)
1:3000	Mouse	β3-Tubulin	Sigma Aldrich

PNA (Life Technologies, L32460) was used to label cone photoreceptors; and DAPI to counter-stain DNA. Antibodies against: AMSH (Biorbyt orb101007), JAB1 (Abcam ab12323), OTUB1 (Abcam ab76648), OTUD1 (Abcam ab122481), POH1 (Abcam ab8040), USP5 (Abcam ab154170) and USP45 (Novusbio H00085015) did not produce reproducible and consistent results and are thus not included.

PROTEIN IMMUNODETECTION BY WESTERN BLOT

Retinas were homogenized in RIPA buffer, containing deoxycolate 0.25% w/v, NP40 1% v/v, Tris pH 7.5 1 M, EDTA 500 mM, NaCl 5 M with addition of a cocktail of protease inhibitors (Complete Mini, Roche). Though occasionally cultured cells were also recovered with RIPA, generally they were directly lysed with 1x Protein Loading Buffer (120 mM Tris-HCl pH 6.8, 4% SDS, 20% Glycerol, 0,2% Bromophenol Blue in MiliQ Water). Protein lysates were boiled 5 min at 95°C and loaded on 10% or 12.5% SDS-PAGE gels, transferred onto PVDF (polyvinylidene fluoride) membranes and blocked with 10% skimmed milk in PBST for 1 h. Only when using the GAPDH antibody the blocking solution was 5% BSA (Bovine Serum Albumin). Membranes were incubated overnight 4°C, washed three times 10 min in PBST, incubated 1h at RT with the corresponding secondary antibodies and washed again three times 10 min in PBST. Chemiluminiscene signal was revealed using a LAS-4000 mini (Fujifilm). Primary antibodies and dilutions were as follows: 1:500 Mouse CRX (Abnova H00001406-M02), 1:1000 Mouse GAPDH (Abcam ab9484), 1:1000 Rabbit GFP (SantaCruz), 1:1000 Mouse HA (Covance), 1:1000 Mouse Nr2e3 (Abcam ab41922), 1:1000 Rabbit PIAS3 (Abcam ab58406), 1:2000 Mouse Tubulin (Sigma

Aldrich T5168), 1:1000 Mouse Xpress (ThermoFisher R910-25). The ImageJ software (http://imagej.nih.gov/ij/) was used for quantification.

IMMUNOPRECIPITATION

Both cells and retinas were lysed with RIPA Buffer (for composition, see above), sonicated and centrifuged for 10 min at 13000 rpm at 4°C. Fifty microliters of protein lysate was kept as the input protein control (INPUT from now on), and the rest of supernatant was separated from the debris and incubated with 4 μg of antibody, end-over-end overnight at 4°C. Protein-antibody complexes were captured using Sepharose-Potein G (Invitrogen) and incubated for 4 h at RT. The mix was centrifuged 30 seconds at 3000 rpm at 4°C, and the supernatant was kept as the bead efficiency control. The pellet containing the beads attached to the antibody was washed three times with PBS and centrifuged 30 seconds at 3000 rpm at 4°C between each washing step. The elution from the bead-antibody complex to recover the immunoprecipitated proteins was performed by adding 2x Protein Loading Buffer and boiling the samples for 5 min at 95°C. The protein lysate was then loaded into a SDS-Page gel to perform immunoblotting.

In protein samples that were further processed for Mass Spectrometry, precipitation with urea was used for protein elution: bead-antibody complexes were washed with pre-urea buffer (50 mM Tris HCl pH 8.5, 1 mM EGTA, 75 mM KCl), centrifuged 30 min at 3000 rpm. After discarding the supernatant, samples were incubated 30 min end-over-end in urea elution buffer (7 M urea, 20 mM Tris-HCl pH 7.5 and 100 mM NaCl), centrifuged 30 seconds at 3000 rpm, and the supernatant containing eluted proteins was electrophoresed in a 12,5% Tris-HCl SDS-page gel.

MASS SPECTROMETRY

Mass spectrometry was performed at the CCiT UB Proteomic Platform (Barcelona Science Park). The sample was digested in-gel with trypsin as follows: The gel band was washed with ammonium bicarbonate (25mM NH4HCO3) and acetonitrile (ACN). The sample was reduced (DTT 10mM; 30 min, 56o and alkylated (iodoacetamide 55mM; 21oC, 30 min, in the dark). Subsequently, the sample was digested with trypsin (Sequence grade modified Trypsin, Promega; 37o peptide mixture was extracted from the gel matrix with 10% formic acid (FA) and ACN, and dried on a SpeedVac vacuum system. The dried-down peptide mixture was analyzed in a nanoAcquity liquid chromatographer (Waters) coupled to a LTQ-Orbitrap Velos (Thermo Scientific) mass spectrometer. Tryptic peptides were resuspended in 1% FA solution and an aliquot was injected for chromatographic separation. Peptides were trapped on a Symmetry C18TM trap column (5 µm 180 µm x 20 mm; Waters), and were separated using a C18 reverse phase capillary column (75 µm Øi, 25 cm, nanoAcquity, 1.7 µm BEH column; Waters). The gradient used for the elution of the peptides was 1% to 40% B in 25 min, followed by gradient from 40% to 60% in 5 min (A: 0.1% FA; B: 100% ACN, 0.1% FA), with a 250 nL/min flow rate.

Eluted peptides were subjected to electrospray ionization in an emitter needle (PicoTipTM, New Objective) with an applied voltage of 2000 V. Peptide masses (m/z 300-1700) were analyzed in data dependent mode where a full Scan MS was acquired in the Orbitrap with a resolution of 60,000 FWHM at 400m/z. Up to the 10 most abundant peptides (minimum intensity of 500 counts) were selected from each MS scan and then fragmented in the linear ion trap using CID (38% normalized collision

energy) with helium as the collision gas. Multistage activation was enabled in order to favour the detection of phosphopeptides. The scan time settings were: Full MS: 250 ms (1 microscan) and MSn: 120 ms. Generated .raw data files were collected with Thermo Xcalibur (v.2.2). Searches were performed by Sequest HT search engine against the Uniprot Swissprot Human database (v. March 2015) using Thermo Proteome Discover (v.1.4.1.14.) To improve the sensitivity of the database search, Percolator (semi-supervised learning machine) was used in order to discriminate correct from incorrect peptide spectrum matches. The PhosphoRS node was used to provide a confidence measure for the localization of phosphorylation in the peptide sequences identified with this modification.

PHYLOGENETIC ANALYSES

Phylogenetic analyses were performed in collaboration with Xavier Bové-Grau and Dr. Iñaki Ruiz-Trillo at Institut de Biologia Evolutiva (CSIC-Universitat Pompeu Fabra). Protein sequences from each enzyme group were queried against complete genome sequences of 14 animal taxa (*Homo sapiens, Mus musculus, Danio rerio, Petromyzon marinus, Branchiostoma floridae, Saccoglossus kowalevskii, Strongylocentrotus purpuratus, Drosophila melanogaster, Daphnia pulex, Caenorhabditis elegans, Lottia gigantea, Capitella teleta, Nematostella vectensis* and *Acropora digitifera*) using the HMMER 3.1 algorithm. For each analyzed enzyme family (USP, UCH, OTU, MJD and JAMM) we searched all proteins containing the Hidden Markov motifs of their catalytic region as defined in Pfam (UCH/UCH_1, Peptidase_C12, OTU/Peptidase_C65, Josephin and JAB domains, respectively). Protein domain architectures of each retrieved protein were then computed using Pfamscan 1.5 and Pfam 27 database[57] of protein domains.

We aligned the catalytic region of each enzyme family using Mafft 7 L-INS-i [58](optimized for local sequence homology), and inspected each alignment matrix manually. The most suitable evolutionary model for the analyses, selected with ProtTest 3.4[59], was LG+ Γ. We used RaxML 8.1.1 [60] to infer Maximum Likelihood trees of each family, with 100 bootstrap replicates as statistical supports. Complete sequences, alignments and phylogenies are provided in the Annex I, Supporting Information (S1-S3 Files). Manual inspection of the trees allowed us to identify subfamilies, named after their human orthologs, based on their bootstrap support and conservation of protein domain architectures.

TRANSCRIPTOMICS DATABASE SEARCH

For direct comparison of disparate RNA-sequencing (RNA-seq) datasets used for expression analysis of DUB genes all data was analyzed with a single analysis pipeline1. Datasets included in the analysis were mouse retinal development (Brooks, *et. al*, Manuscript in Preparation), Nrl and Crx KO mouse retina[61], flow sorted rod and S-like cone photoreceptors8, extra-ocular mouse tissue[62], and human foetal retina (Hoshino, et. al, Manuscript in Preparation). Transcript level FPKM values were averaged and log 2 transformed prior to hierarchical clustering using Euclidean distance and Ward's method. Heatmaps of clustered data were generated using the heatmap.2 function in the gplots package in the R environment [www.r-project.org].

IN VIVO DNA ELECTROPORATION IN MOUSE RETINAS

In vivo DNA electroporation in the mouse retina (technique developed by C. Cepko´s laboratory)[63] was performed following Dr. Ana Méndez and Dr.

Santiago López-Begines instructions and small modifications. This technique allows transient expression or silencing of a gene of interest into retinal cells.

Either siRNA (small interfering RNA) against USP48, or shRNAs (short hairpin RNA) against JOSD1 and USP46 were separately used to perform specific DUB silencing in mice retinas. A DNA solution (6 μg/μl) in PBS and fast green 0,1% dye was prepared by mixing the siRNA or shRNA of interest at a molar ratio of 2:1. The plasmid encoding EGFP was added to easily identify the injection area for analysis 10 or 21 days later. For *in vivo* DNA electroporation, new born mouse pups at postnatal day 1 are anesthetized by immersion in ice for 4 min, an opening is performed with a scalpel following the natural line of the eyelid, after cleaning the zone with povidone-iodine solution. A small incision is then performed on the sclera, with a 30-gauge needle. For DNA injection, customized capillary glass pipettes were used [(#300048. Harvard Apparatus), pulled in a Puller P-97 from Sutter Instruments according to the following parameters: heat=650, Pull=60, Velocity=60, Time=200)]. The capillary glass pipettes were attached to a nanoinjector (Drummond Nanoject) and were managed by a micromanipulator. After inserting the glass pipette in the eye, and carefully micromanipulating it to reach the subretinal space (reached when the pipette meets the resistance of the back of the eye upon touching the choroid), approximately 0,5-1 μl of circular naked DNA were delivered. After DNA injection, tweezer-type electrodes briefly soaked in PBS were placed to softly hold the heads of the pups placing the positive electrode of the tweezer over the injected eye, and five square pulses of 80 V of 50-ms duration with 950-ms intervals were applied by using a pulse generator (CUY21, Nepagene). Pups were left to recover over a thermal blanket until the end of procedure, returned to their cage and raised in normal conditions. Mice were processed

at postnatal day 10 or 21, retinas were dissected and processed for IHC and western blotting.

Results

CHAPTER 1. DEUBIQUITINATING ENZYMES IN THE MOUSE RETINA

NOTE: Most of the data presented in Section 1 and 2 of the present chapter have been published in the referred PloS One article below (see Annex I).

TITLE

"Expression atlas of the deubiquitinating enzymes in the adult mouse retina, their evolutionary diversification and phenotypic roles."

AUTHORS

Mariona Esquerdo, Xavier Grau-Bové, Alejandro Garanto, Vasileios Toulis, Sílvia Garcia-Monclús, Erica Millo, Mª José López-Iniesta, Víctor Abad-Morales, Iñaki Ruiz-Trillo, Gemma Marfany

REFERENCE

PLoS One. 2016 Mar 2;11(3):e0150364. doi: 10.1371/journal.pone.0150364. eCollection 2016.

1. EXPRESSION PATTERN OF DUBS IN THE MOUSE RETINA

Ubiquitin has been amply shown to play a major role in regulating several cellular processes[23,26,64], including cell differentiation[37]. Moreover, many studies on the function of ubiquitin E3 ligases in a wide variety of research fields have been reported. Nonetheless, their counter-partners in the ubiquitination cycle, the Deubiquitinating enzymes (DUBs), have been the focus of attention in research only in the last few years.

Concerning the retina, several studies pointed to the importance of ubiquitin and ubiquitin-like cycle enzymes in retinal development[46,47,50,65], but little is known about the roles DUBs might play in this intricate regulatory network. For this reason, the first aim of the present work was to define the expression levels and tissular localization of these genes in the adult mouse retina in order to establish a reference framework to elucidate the possible role of specific DUBs in retinal development and disease.

It was important to determine the expression state of the DUBs in the mouse retina since it had not been previously reported. Thus, real time quantitative PCR (RT qPCR), *in situ* hybridization and fluorescent immunohistochemistry studies in adult mouse retinas were designed and performed, so that a map of mRNA and protein expression and localization in the mammalian retina was drawn.

These analyses allowed defining an expression framework for deubiquitinating enzyme genes in the mouse retina.

1.1. mRNA EXPRESSION LEVELS

A quantitative real time PCR (RT qPCR) was performed on mouse neuroretinas to assess the mRNA expression levels of all DUBs. The

complete DUB list (87 genes) of the mouse genome including members of the five aforementioned families (namely, 11 JAMM, 4 MJD, 15 OTU, 4 UCH, and 53 USP genes) were analyzed, together with two reference genes, *Rhodopsin* and *Cerkl*, previously reported of being expressed at high and low levels in the mouse retina, respectively [66]. The expression levels were normalized to *Gapdh* expression.

The relative expression levels are shown in Figure 13 as the mean and standard deviation of the Z-score, which was calculated for the whole set of genes for direct comparison among them and between different samples. An arbitrary Z-score of zero corresponds to the mean value of expression for all the DUBs analyzed in the retina. Thus, genes with positive values have an expression above the mean, whereas genes with negative values show less expression than the mean (e.g. most USP genes).

The results showed that *Prpf8* was the highest expressed gene from the JAMM subfamily, followed by *Eif3h* and *Psmd7*. Both *Atxn3* and *Josd2* rendered the highest expression levels within the MJD subfamily. Concerning the OTU subfamily, *Otub1* and *Tnfaip3* produced the higher expression levels, followed by *Otud7b*, *Vcpip1*, *Otud4* and *Otud5*; whereas the levels of *Otud6a* were considered as negligible. *Uchl1* was the most highly expressed gene from the UCH family (and also with respect to all DUB genes), while *Uchl3* and *Uchl5* are lowly expressed in the retina. Finally, the genes from the large USP subfamily showed the lowest level of expression among all the DUB genes. Some USPs (20%) were highly expressed and showed positive Z-scores (*Usp5*, *Usp6*, *Usp10*, *Usp12*, *Usp19*, *Usp21*, *Usp22*, *Usp33*, *Usp47* and *Usp52)* whereas 25% of the USPs showed lower levels

than the mean (*Usp8*, *Usp9Y*, *Usp17*, *Usp18*, *Usp26*, *Usp27*, *Usp29*, *Usp35, Usp43*, *Usp44*, *Usp45*,*Usp50*, and *Usp51*) (Figure 13).

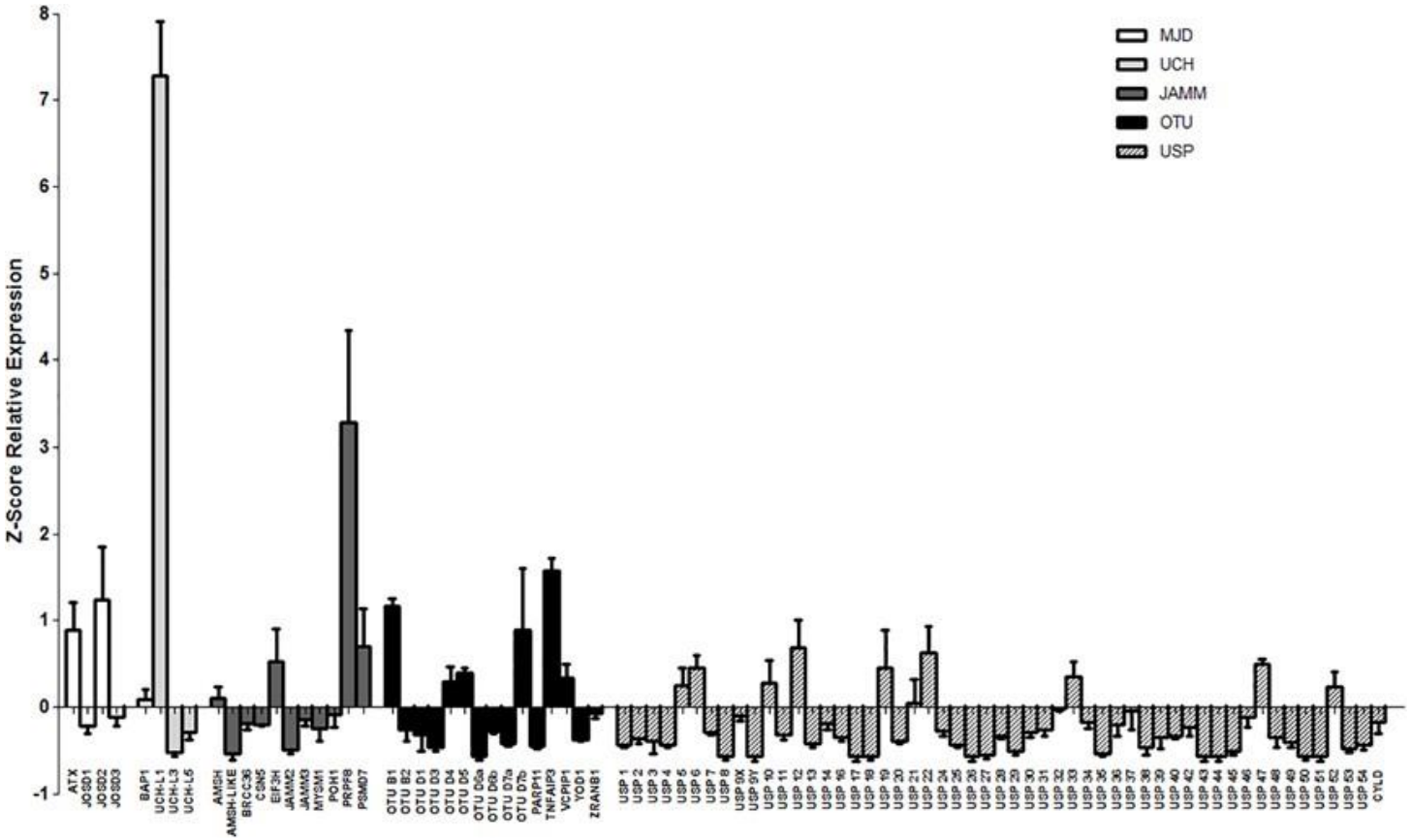
MJD
UCH
JAMM
OTU
USP
Z-Score Relative Expression
8
7
6
5
4
3
2
1
0
-1
ATX
JOSD1
JOSD2
JOSD3
BAP1
UCH-L1
UCH-L3
UCH-L5
AMSH
AMSH-LIKE
BRCC36
CSN5
EIF3H
JAMM2
JAMM3
MYSM1
POH1
PRPF8
PSMD7
OTU B1
OTU B2
OTU D1
OTU D3
OTU D4
OTU D5
OTU D6a
OTU D6b
OTU D7a
OTU D7b
PARP11
TNFAIP3
VCPIP1
YOD1
ZRANB1
USP 1
USP 2
USP 3
USP 4
USP 5
USP 6
USP 7
USP 8
USP 9X
USP 9Y
USP 10
USP 11
USP 12
USP 13
USP 14
USP 15
USP 17
USP 18
USP 19
USP 20
USP 21
USP 22
USP 24
USP 25
USP 26
USP 27
USP 28
USP 29
USP 30
USP 31
USP 32
USP 33
USP 34
USP 36
USP 37
USP 38
USP 39
USP 40
USP 42
USP 43
USP 44
USP 45
USP 46
USP 47
USP 48
USP 49
USP 50
USP 51
USP 52
USP 53
USP 54
CYLD

Figure 13. Relative expression levels of the five DUB subfamilies. Gene expression values are the average of three independent samples (each measured in three replicates). Besides, each sample contained the retinas from three individuals. The expression levels are obtained as a ratio with GAPDH expression levels (used for normalization) per 10^4. The Z-Score has been calculated for the whole set of genes per each sample, and mean and standard deviation was obtained so that the results can be directly compared among them. In this graph, 0 is the mean value of gene expression for the whole set of genes (87 in total) in each sample; negative values indicate genes expressed below the global average, and positive values, when genes are more highly expressed. **JAMM**: Jab1/Mpn/Mov34 motif proteases; **MJD**: Machado-Joseph disease protein domain proteases; **UCH**: ubiquitin c-terminal hydrolases; **OTU**: ovarian tumour proteases; **USP**: ubiquitin-specific proteases.

1.2. mRNA LOCALIZATION

Once the expression levels of all the DUB family members were assessed, we characterized and compared their expression pattern within the different layers of the mouse retina. Given the high number of genes to be analyzed and the fact that antibodies for all the proteins are not always available or reliable, gene expression by mRNA localization using *in situ* hybridization (ISH) was performed for most of the genes. Later on, protein localization of selected DUB members was assessed by fluorescent immunohistochemistry.

For ISH, antisense (AS) riboprobes against a large group of DUBs were used on mouse retinal cryosections (Figure **14**). As negative controls, the corresponding sense riboprobes (S) of each gene were generated and hybridized in parallel using the same conditions (see Annex I S1 Fig). The staining time was adjusted for each set of antisense/sense riboprobes, so that a maximum signal was obtained in the antisense retinal sections with minimum background in the sense control counterparts (for instance, *Prpf8* and *Tnfaip3 in situ* stained in much less time than *Uchl5, Usp8* and *Usp18,*

which required half a day). *Rhodopsin* was used as a positive control because of the reported high expression in the retina and its well-known localization in the inner segment of the photoreceptors.

Notice that the large USP subfamily contains 57 members in the mouse genome. However, only a set of genes was considered for ISH. Representative ISH results are displayed in Figure **14**. Our selection criteria included genes with relevant ocular phenotypes previously described in systematic knockdown analyses of DUBs in *Drosophila* [67] and zebrafish [68].

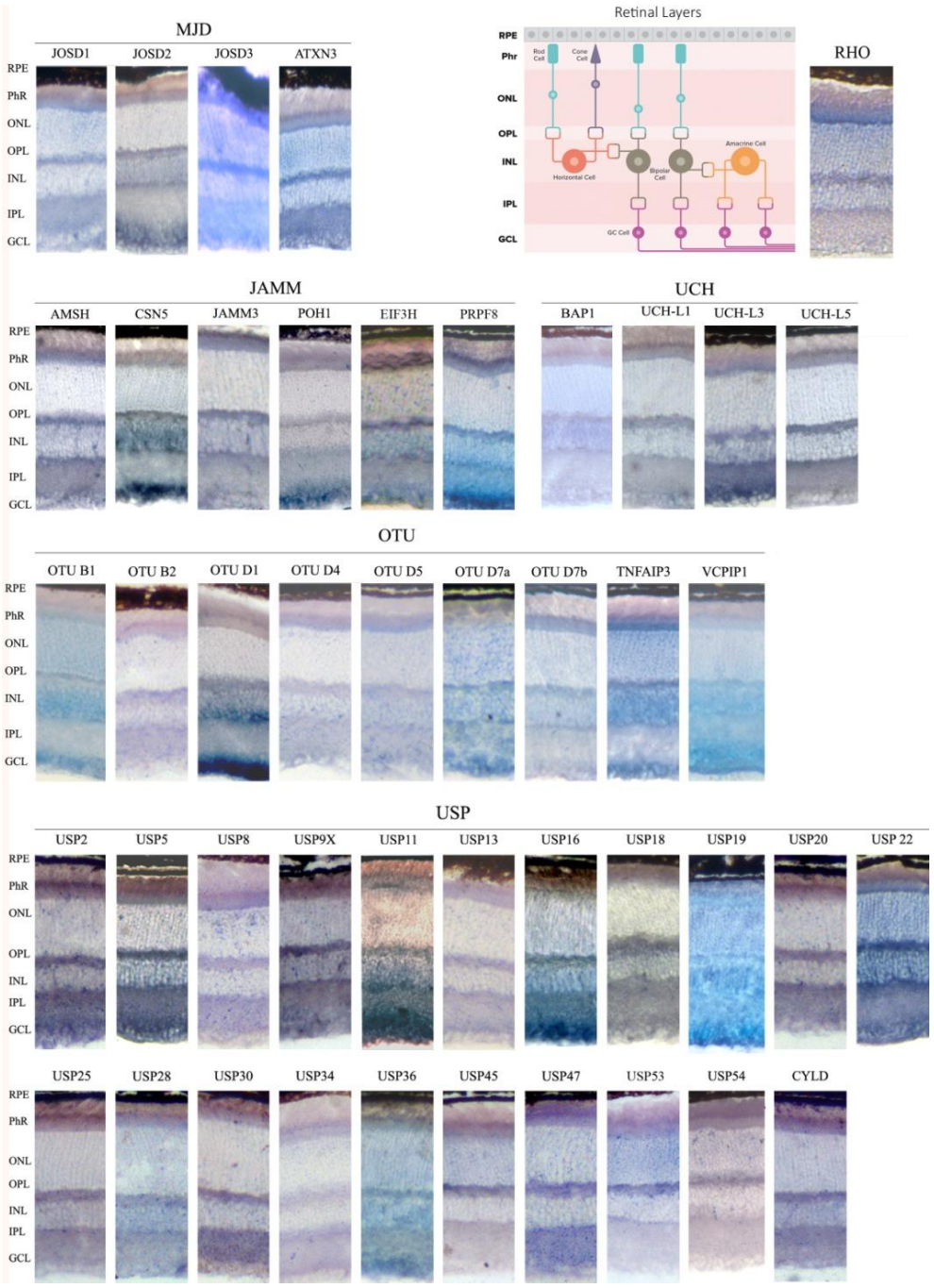
MJD
JOSD1
JOSD2
JOSD3
ATXN3
RPE
PhR
ONL
OPL
INL
IPL
GCL
Retinal Layers
Rod Cell
Cone Cell
Horizontal Cell
Bipolar Cell
Amacrine Cell
GC Cell
RHO
JAMM
AMSH
CSN5
JAMM3
POH1
EIF3H
PRPF8
UCH
BAP1
UCH-L1
UCH-L3
UCH-L5
OTU
OTU B1
OTU B2
OTU D1
OTU D4
OTU D5
OTU D7a
OTU D7b
TNFAIP3
VCPIP1
USP
USP2
USP5
USP8
USP9X
USP11
USP13
USP16
USP18
USP19
USP20
USP 22
USP25
USP28
USP30
USP34
USP36
USP45
USP47
USP53
USP54
CYLD

Figure 14. *In situ* hybridization of genes encoding DUB enzymes on retinal cryosections. Sections from wild-type C57BL/6J mouse retinas were hybridized using digoxigenin-labelled antisense riboprobes. Their corresponding sense riboprobes (negative controls) stained for the same length of time (lower panels in each row) are in the Annex I, S1 Fig. The antisense *rhodopsin* probe, which strongly labels the inner photoreceptor segment, was used as a positive control for the assay. RPE- retinal pigmented epithelium; PHR- photoreceptor cell layer; ONL- outer nuclear layer; OPL- Outer plexiform layer; INL- inner nuclear layer, IPL- inner plexiform layer; GCL- ganglion cell layer.

Most DUBs are ubiquitously expressed throughout the layers of the murine retina, which would be compatible with a general role in the neuronal cell metabolism and regulation and thus, not restricted to particular retinal neurons. Nonetheless, specific patterns of expression were detected for particular DUBs. For instance, a strong hybridization signal in the plexiform layers was observed for *Uchl3*, *Uchl5*, *Usp2*, *Usp9X*, including in some cases the inner segment of the photoreceptor layer, as detected for *Amsh*, *Josd3*, *Atxn3* and *Usp47*. Some DUBs appear to be highly expressed in the GCL (*Csn5*, *Poh1*, *Prpf8*, *Josd2*, *Otud1*, *Vcpip1*, *Usp11, Usp5* and *Usp19*) in contrast to the pattern generated by *Usp8*, *Usp13*, *Usp30*, *Usp45* and *Usp54*, which yielded virtually no mRNA localization signal in the ganglion cells.

Several DUB genes of the USP family (*Usp5*, *Usp13*, *Usp19* and *Usp34*) were previously reported to be differentially expressed in the Retinal Pigmented Epithelium (RPE) by transcriptome analysis [69]. To assess their specific pattern of expression, and given that pigmented cells mask positive hybridization signals, ISH on albino retinas from CD-1 mice was performed (Annex I, S2 Fig), by another member of the group (M. J. López-Iniesta). Although these four genes are expressed in this non-neuronal layer, their

expression is not restricted to the RPE. In fact, *Usp5* and *Usp19* are very highly expressed throughout the retina (Figure **14**). Comparison of the retinal expression pattern for these four genes did not show any detectable difference between C57BL/6J (wild-type black) and CD-1 (albino) mice strains.

Several genes, namely *Amsh-like*, *Brcc36*, *Jamm2, Mysm1* and *Psmd7* (JAMM group) and *Otud3*, *Yod1*, *Zranb1* (OTU group), did not render reproducible and reliable ISHs, even though several riboprobes spanning different gene regions were used. In most cases (e.g. *Amsh-like*, *Brcc36, Jamm2*, *Mysm1*, and *Otud3*) very low levels of expression were obtained and the signal was too faint to be distinguished from the negative control (sense riboprobe), or the sense and antisense riboprobes both produced signals of similar intensity. The ISH results of these genes are not presented in the present work.

Taking the ISH results together, an atlas of expression for DUBs in the retina of adult mouse was drawn. In general, all analyzed genes except *Otud1* are expressed in the photoreceptors, and their mRNAs are localized in a wide range of intensities in the inner segment (perinuclearly) and the outer plexiform layer. Among layers, the GCL showed the most different pattern of gene expression. Notably, some DUBs, such as *Usp45*, *Usp53* and *Usp54*, are only detected in photoreceptors (PhR -inner segments, ONL (photoreceptor nuclei and perinuclei) and OPL (photoreceptor synapsis), whereas nearly no hybridization could be detected in the rest of retinal layers, which would suggest specific roles for these DUBs in this highly specialized photosensitive cells.

Table 10. Schematic representation of *in situ* hybridization signal on different retinal layers of analyzed dub genes in the mouse retina.

Family	Gene	PhR	ONL	OPL	INL	IPL	GCL
JAMM	JAMM3						
	AMSH						
	PRPF8						
	EIF3H						
	CSN5						
	POH1						
	AMSH- like						
MJD	ATX3						
	JOSD3						
	JOSD1						
	JOSD2						
OTU	TNFAIP3						
	OTUD7b						
	OTUB2						
	OTUD7a						
	VCPIP1						
	OTUB1						
	OTUD5						
	ZRANB1						
	OTUD4						
	OTUD1						
UCH	UCH-L3						
	UCH-L5						
	BAP1						
	UCH-L1						
USP	USP47						
	CYLD						
	[USPL2]						
	USP8						
	USP30						

Family	Gene	PhR	ONL	OPL	INL	IPL	GCL
USP	USP2						
	USP19						
	USP20						
	USP5						
	USP22						
	USP36						
	USP9X						
	USP54						
	USP53						
	USP45						
	USP18						
	USP28						
	USP13						
	USP25						
	USP34						

PhR- Photoreceptors; **ONL**- Outer Nuclear Layer; **OPL**- Outer Plexiform Layer; **INL**- Inner Nuclear Layer; **IPL**- Inner Plexiform Layer; and **GCL**- Ganglion Cell Layer.

1.3. PROTEIN LOCALIZATION

These ISH results prompted us to confirm and more accurately define protein localization by fluorescent immunohistochemistry of a group of selected DUBs. Of note, due to very specialized morphology of photoreceptors, the mRNA localization might be different to where the encoded proteins are localized and exert their function (e.g. the mRNA of rhodopsin is localized in the ribosome-rich photoreceptor inner segment whereas the protein is highly abundant in the membranous disks of the outer segment).

The criteria of DUB selection for immunohistochemistry detection were based on: 1) interesting ISH pattern, 2) relevance for eye phenotype in

animal models, 3) putative functional diversification in phylogenetically closely related enzymes (see next section), and 4) antibody commercial availability and affinity. Twenty one DUBs were selected (gene list is detailed in the Material and Methods), but unfortunately, only 14 immunodetections rendered a reproducible and reliable signal (Figure **15** and Annex I, S3 Fig).

Overall, immunodetection confirms the ISH results since protein is detected in the same retinal cell layers (Figure **15**). Besides, comparing RT qPCR to ISH and immunohistochemistry results, high levels of retinal expression correlated with a ubiquitous expression pattern. On the other hand, some particular protein locations are worth mentioning as indicative of distinct functions in specific cellular compartments. OTUD4 is highly detected in the axonal processes of bipolar and other retinal cells, supporting its involvement in neurodegeneration in human [70]. USP25 is mainly detected in the inner plexiform and ganglion cell layer. USP9X and TNFAIP3 are particularly detected (but not exclusively) at the outer photoreceptor segment. Besides, USP22 is localized in the nucleus of ganglion cells, and perinuclearly in the rest of retinal neuronal somas. For details, merge and separate immunodetection images are in Annex I, S3 Fig. Overall, immunodetection is much more indicative of protein functional localization but appears to be less successful than ISH in complex tissues.

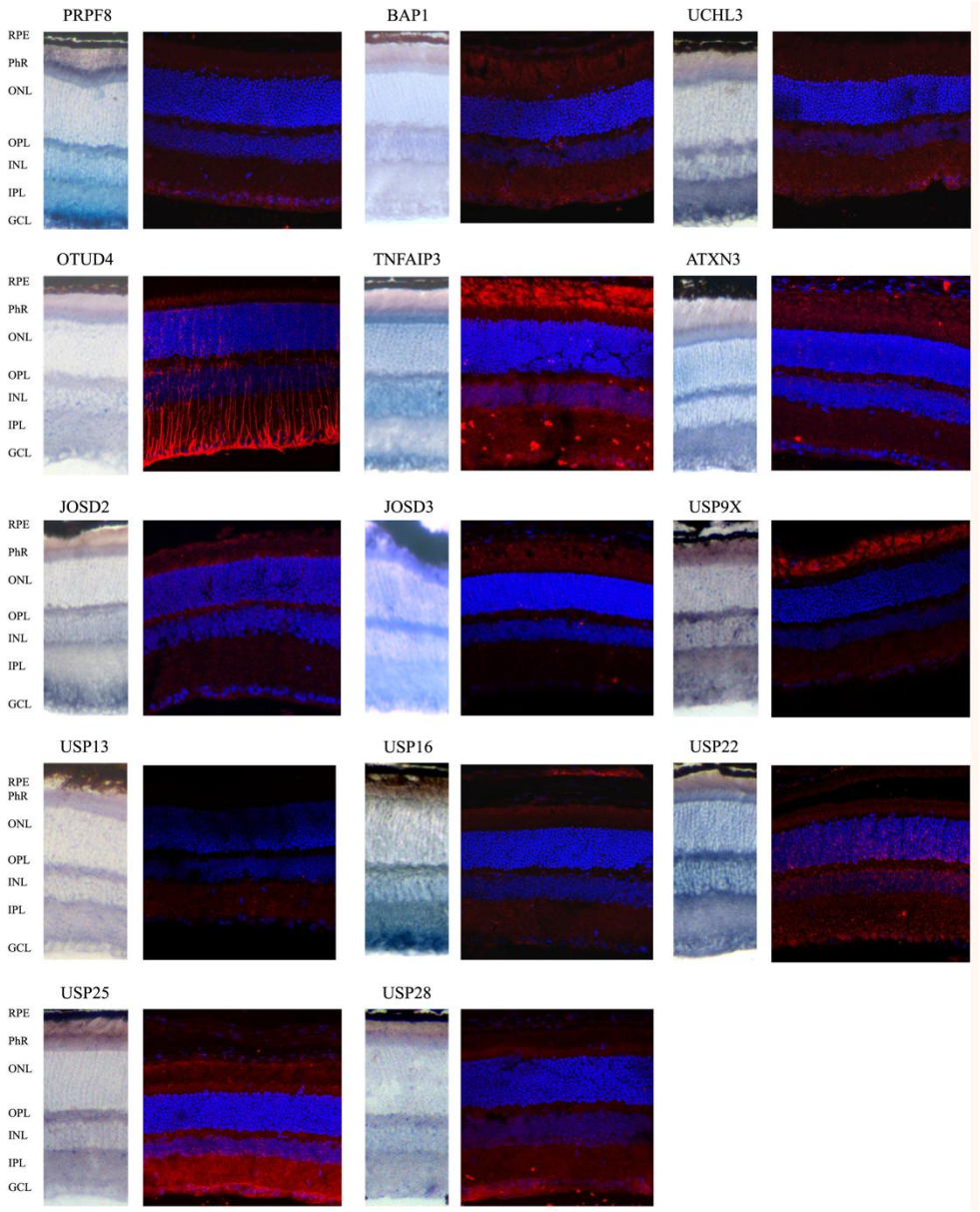
PRPF8
BAP1
UCHL3
OTUD4
TNFAIP3
ATXN3
JOSD2
JOSD3
USP9X
USP13
USP16
USP22
USP25
USP28
RPE
PhR
ONL
OPL
INL
IPL
GCL

Figure 15. Comparison of mRNA and protein immunodetection of selected DUBs in mouse retinal cryosections. Most analyzed genes rendered a consistent expression pattern when comparing mRNA and protein localization in the wild type mouse retina. The merged immunohistochemistry figures show immunodetection of **DUBs** in red, and nuclei counter-staining with **DAPI** (in blue). Details in S3 Fig. **RPE**- Retinal Pigmented Epithelium **PhR**- Photoreceptors; **ONL**- Outer Nuclear Layer; **OPL**- Outer Plexiform Layer; **INL**- Inner Nuclear Layer; **IPL**- Inner Plexiform Layer; and **GCL**- Ganglion Cell Layer.

2. SEQUENCE AND FUNCTIONAL CONSERVATION OF DUBS THROUGH PHYLOGENY

Recent analyses have shown that the Ubiquitin signalling system predates the eukaryotic origin, since the core components of the pathway are present in *Archaea*. Moreover, early-branching unicellular eukaryotes already display the full set of Ub ligase and DUB families[22]. A massive expansion of ligases and proteases involved innovation and incorporation of new protein domains, particularly at the origin of multicellularity and associated with the diversity of proteins and protein roles in different cell types. We aimed to provide a comprehensive picture of the DUBs during the diversification of metazoans, related to the retinal and neuronal function.

2.1. PHYLOGENETIC ANALYSIS

Completely sequenced genomes from 14 species (from cnidarians to vertebrates) were queried with the catalytic region of each enzyme family (as defined in Pfam) in search of orthologs. This work was performed in collaboration with Dr. Iñaki Ruiz-Trill and Xavier Grau Bové at the Institut de Biologia Evolutiva (CSIC – Pompeu Fabra). Phylogenetic trees were generated using the retrieved sequences, and the statistical support for each

node is also indicated (Figure 16 A, B, C, D and E). For the sake of clarity, protein nomenclature is according to human DUBs. Highly similar sequences that expanded recently (during the pre-vertebrate/vertebrate expansion) and clustered together appear collapsed.

The presence of an identified ortholog in each species/clade is represented with a black dot. Vertebrate species that present all the paralogs in a collapsed branch are circled in black. White dots mark the presence of homologs that could not be confidently assigned to a characterized DUB type, either because they are sister-group to various known DUB paralogs (and therefore represent the pre-duplication homolog), or because statistical support is too low to confidently cluster them with a specific ortholog. Question marks represent statistically supported clades that cannot be assigned to any known DUB (or group of paralogous DUBs).

Protein motifs (as defined in Pfam) including the catalytic domain are drawn next to each branch to illustrate the diversity/conservation in protein architecture within each family. For detailed and complete phylogenetic trees, see Annex I, S3 File.

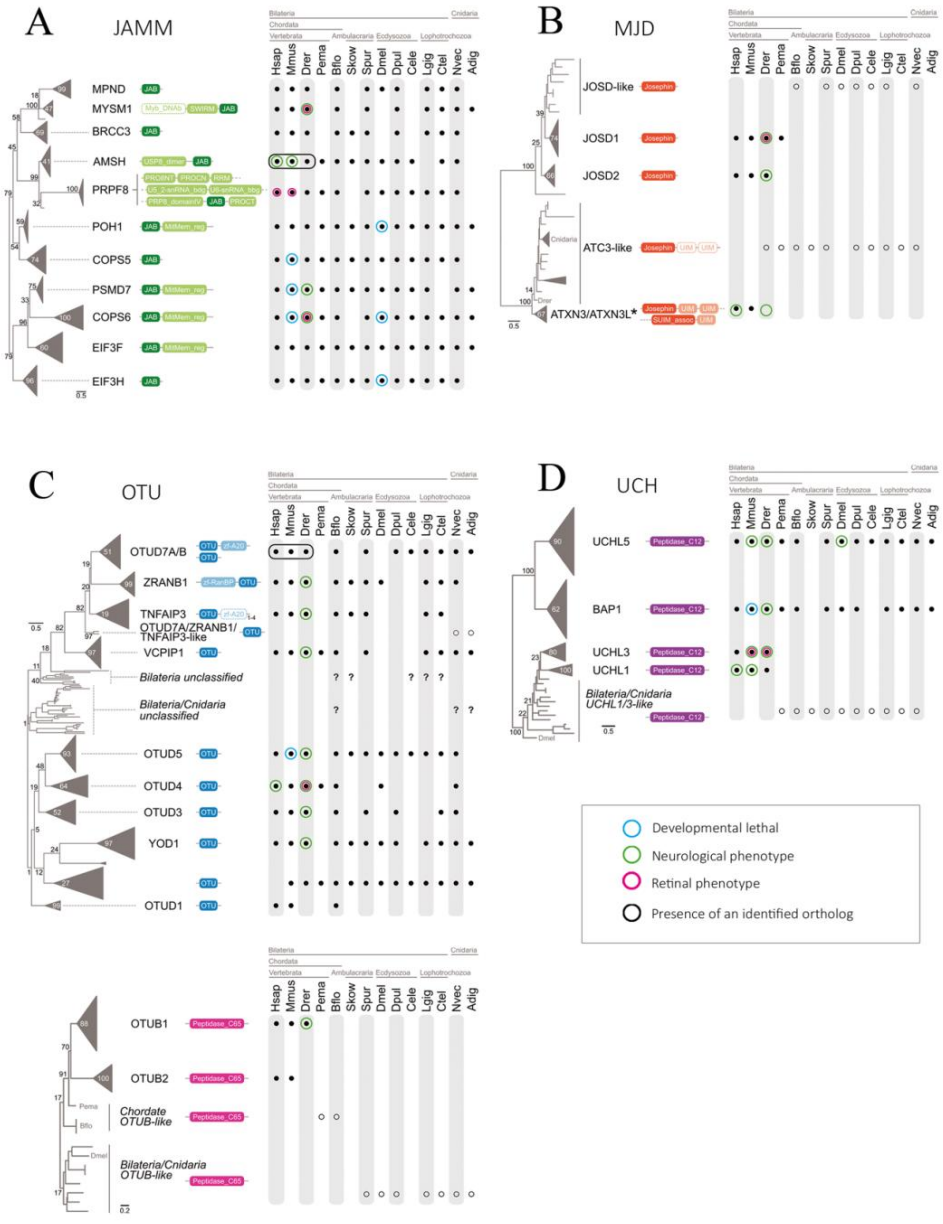
A
JAMM
MPND
MYSM1
BRCC3
AMSH
PRPF8
POH1
COPS5
PSMD7
COPS6
EIF3F
EIF3H
B
MJD
JOSD-like
JOSD1
JOSD2
ATC3-like
ATXN3/ATXN3L*
C
OTU
OTUD7A/B
ZRANB1
TNFAIP3
OTUD7A/ZRANB1/
TNFAIP3-like
VCPIP1
Bilateria unclassified
Bilateria/Cnidaria
unclassified
OTUD5
OTUD4
OTUD3
YOD1
OTUD1
OTUB1
OTUB2
Chordate
OTUB-like
Bilateria/Cnidaria
OTUB-like
D
UCH
UCHL5
BAP1
UCHL3
UCHL1
Bilateria/Cnidaria
UCHL1/3-like
Hsap
Mmus
Drer
Pema
Bflo
Skow
Spur
Dmel
Dpul
Cele
Lgig
Ctel
Nvec
Adig
Developmental lethal
Neurological phenotype
Retinal phenotype
Presence of an identified ortholog

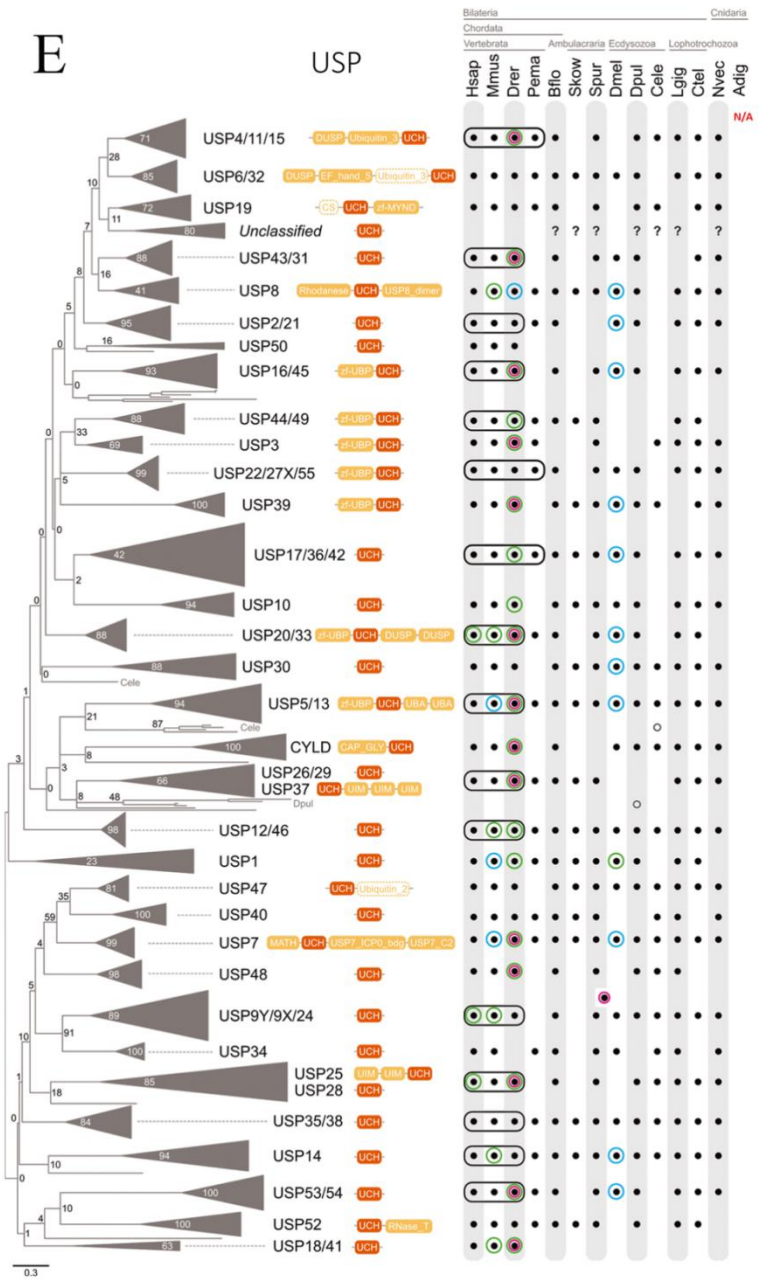
E
USP
Bilateria
Cnidaria
Chordata
Vertebrata
Ambulacraria
Ecdysozoa
Lophotrochozoa
Hsap
Mmus
Drer
Pema
Bflo
Skow
Spur
Dmel
Dpul
Cele
Lgig
Ctel
Nvec
Adig
N/A
USP4/11/15
USP6/32
USP19
Unclassified
USP43/31
USP8
USP2/21
USP50
USP16/45
USP44/49
USP3
USP22/27X/55
USP39
USP17/36/42
USP10
USP20/33
USP30
USP5/13
CYLD
USP26/29
USP37
USP12/46
USP1
USP47
USP40
USP7
USP48
USP9Y/9X/24
USP34
USP25
USP28
USP35/38
USP14
USP53/54
USP52
USP18/41
0.3

Figure 16. Phylogenetic analysis of DUB genes and Neuronal/Retinal Phenotype. Protein sequences from the catalytic region of each enzyme group were queried in complete genome sequences of 14 animal taxa and aligned. The protein domain architectures including the catalytic and accessory domain motifs are represented next to each dub member (A, JAMM; B, MJD; C, OTU; D, UCH; and E, USP). Black dots indicate presence of the ortholog; whereas white dots indicate homologs that cannot be confidently assigned to a dub type (see results). Question marks represent statistically supported clades of uncharacterized dubs. DUB sequences that are highly similar and cluster closely together appear collapsed under a common name. In general, invertebrates have a single representative member of the collapsed branch, whereas vertebrate genomes show one member of each paralog (species circled in black). *Acropora digitifera* USP homologs were excluded from the analysis as they impaired the resolution of the USP phylogeny. Genes reported to produce an abnormal neuronal phenotype when mutated are circled in magenta, whilst genes producing abnormal eye or retinal phenotype are circled in green. Genes whose mutation is lethal during developmental stages are circled in blue. A schematic summary of the DUB mRNA localization in the mouse retina (from ISH) is also presented next to the corresponding family. The intensity of the colour indicates hybridization signal intensity. Retinal layers appear indicated as in Figure **14**.

Notably, the phylogenetic distribution of OTU DUBs reveals two different groups that appeared at the origin of eukaryotes: OTUs with peptidase C65 domains (OTUB1 and OTUB2 in animals) and those with OTU domain [22] (Figure 16 D). Given that 1) these two catalytic domains diverged long before the origin of metazoans, 2) OTUB1/B2 protein domain architectures are clearly different from the other OTUs, 3) OTUB homologs are present in all metazoan clades, and 4) this split does not occur in any other family of DUBs, a new classification might be in order to acknowledge a new subfamily of DUBs.

The JAMM family has clear sequence assignment in all the analyzed animals, even though some species have secondarily lost some DUB members, e.g. *Acropora* (cnidarian), *C. elegans* (nematode), *Drosophila* (insect) *Saccoglossus*

(hemichordate), and *Petromyzon* (sea lamprey, an early-branching vertebrate). These species also show specific gene loss for other DUB families, pointing to a divergent evolution in their lineages. On the other hand, a clear expansion within each DUB family has occurred in the vertebrate lineage (Figure 16 and Figure 17). When these duplicated members have rapidly diverged, the DUB protein sequences are in separate branches, but the common ancestry becomes evident since there a single ancestral ortholog is present in the rest of clades (white dots). This is the case within the UCH (UCHL1 and UCHL3) and MJD families (JOSD1 and JOSD2).

When the duplicated sequences have diverged but still branch closely together in the phylogenetic tree, the vertebrate paralogs have been collapsed into a single branch for easy phylogenetic comparison (indicated by black circles in Figure 16). This is particularly evident for USPs, where we can identify a single ancestral sequence in all clades, although several members are present in vertebrates (e.g. USP4/11/15; USP22/27X/51; USP17/36/42). The *ATXN3* gene deserves specific mention, since its close paralog, *ATXN3L*, is a retroposon, that is, a gene generated by a very late retrotransposition event within the primate lineage.

The DUB gene expansion in animal phylogeny is visually summarized in the heat map of Figure 17. Colour intensity reflects the number of genes per genome. Finally, it becomes evident that a burst of gene expansion within all DUB families was at the basis of the vertebrate lineage. Nonetheless, the innovation in the protein architectures, with the acquisition of new domains accompanying the DUB catalytic domains**,** pre-dates the origin of vertebrates in all the analyzed families–as vertebrate-like domain arrangements are often identified in the other animal clades. In fact, extensive phylogenetic analyses

of the Ub and SUMO signalling pathway proteins showed that: 1) very early on the explosion of eukaryotes, and intrinsic to the origin of multicellularity, all the DUB families present in animals already showed composite domain architectures, and 2) animal-specific domain arrangements were already present in their unicellular ancestors [22].

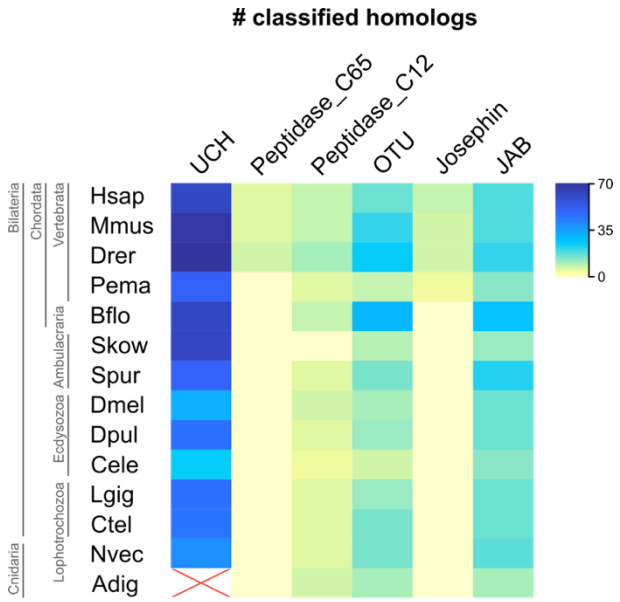

Figure 17. Counts of classified DUB homologs. Heatmap representing the number of classified genes in each analyzed genome. Increasing intensity reflects increasing number of genes. Only orthologs marked with black dots in Figure 16 are considered. *Acropora digitifera* USP homologs, excluded from the phylogenetic classification, are marked as not analyzed (red cross).

2.2. PHENOTYPIC ANALYSIS OF DUBS THROUGH SPECIES

Since the aim of the present work was to study DUB expression in the retina as a means to suggest relevant genes for hereditary visual disorders and/or potential genes important for retinal development, an extensive bibliography search was performed to compare the reported phenotypes of several animal

models (*Drosophila*, zebrafish, mouse) and human diseases, associated to gene mutations, knockouts or knockdowns of DUBs. Early developmental lethality, neuronal phenotype (during developmental stages, but also neurodegeneration) and retinal alterations were noted when available (Figure 16 A, B, C, D and E). For a detailed phenotypic trait list, see Annex I, S2 Table and references therein. In general, when the mutation or knockdown of a particular gene produces a relevant phenotype in one of the analyzed taxa, it usually replicates or provides a similar alteration in the other analyzed organisms. In the cases of neuronal phenotype, there is an accompanying alteration in the eye (the optic vesicle is an evagination of the neural tube, and the retina forms part of the central nervous system). However, most phenotypic assessment in the eye describes only gross alterations, but a detailed retinal study has not yet been reported for most animal models.

3. TRANSCRIPTOMIC ANALYSIS OF DUBS DURING RETINAL DEVELOPMENT

One of our aims was to determine how DUBs are involved in photoreceptor development. As no previous data was available at that moment on the expression of these enzymes in the mouse retina, a first approach was to perform expression analyses (see section 1 of the present chapter) on P60 adult mouse retinas. This age resulted adequate as a first approach and to define the working frame in a young though completely functional retina; however, it gave no insights into the relevance of these enzymes during the development of this sensory organ.

Thus, further time points were required to properly assess the developmental variations of the DUBs expression and consequently, evaluate whether any of them could be involved in the development of the mouse retina. To this end, we performed *in silico* comparative analyses using high throughput RNA-sequencing data.

3.1. RNA-SEQUENCING ANALYSIS

The RNA-sequencing from different stages of mouse wild type (WT) and knockout (KO) retinas; as well as on different human retina developmental stages was performed in Dr. Anand Swaroop's group, who kindly shared the raw data with us. For mouse WT retinas, RNA-seq data was available at stages Embryonic 11 (E11), E12, E14, E16, post-natal 0 (P0), P2, P4, P6, P10, P14 and P21. Data from P2 and P21 stages of mouse *Crx* -/- and *Nrl* -/- knockout retinas was also available; as it was from flow-sorted mouse photoreceptors at P0, P2, P4, P10, P14 and P21, separated into Rod-like cells and in Cone-like cells. Regarding the human retina, RNA-seq data was available for day 52 post-fertilization (D52), D53, D57 (two different samples: D57.1 and D57.2), D67 (two different samples: D67.1 and D67.2), D70, D80, D87, D94 (two different samples: D94.1 and D94.2), D105, D107, D115, D125, D132 and D136.

We performed a comprehensive analysis and comparison of DUB expression levels using these transcriptomic data. Results for the expression levels of all known DUBs in the retina are summarized in **Figure 18** as a Heatmap representing the average log2 of FPKM (Fragments per Kilobase of exon per Milion reads) values, were dark blue indicates very low expression, while dark

red indicates high expression of a particular gene at a particular developmental stage.

Figure 18. Expression heatmap of deubiquitinating enzyme genes in several human and mouse developmental stages. WT- wild type mouse retinas; **CRX**- mouse CRX knockout (KO) retina; **NRL**- mouse NRL KO retinas. For mouse WT retinas, the data presented correspond to Embryonic 11 (E11), E12, E14, E16, post-natal 0 (P0), P2, P4, P6, P10, P14 and P21 stages. Rod-like and Cone-like data correspond to flow-sorted photoreceptors from stages P0, P2, P4, P10, P14 and P21. For human retina, data correspond to day 52 post-fertilization (D52), D53, D57 (two different samples: D57.1 and D57.2), D67 (two different samples: D67.1 and D67.2), D70, D80, D87, D94 (two different samples: D94.1 and D94.2), D105, D107, D115, D125, D132 and D136 (details in the text).

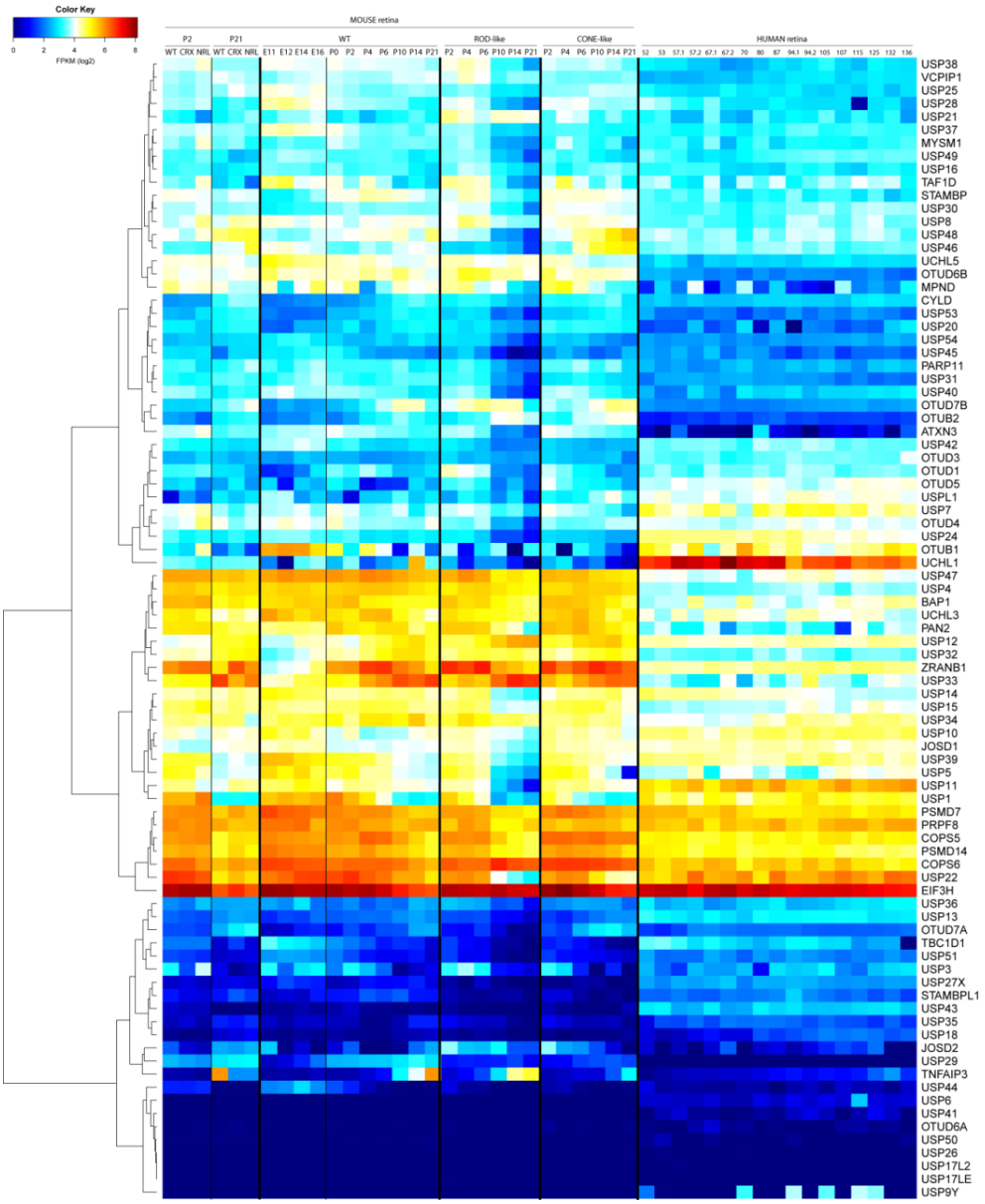
Color Key
0 2 4 6 8
FPKM (log2)
MOUSE retina
P2
P21
WT
ROD-like
CONE-like
HUMAN retina
WT CRX NRL WT CRX NRL E11 E12 E14 E16 P0 P2 P4 P6 P10 P14 P21 P2 P4 P6 P10 P14 P21 P2 P4 P6 P10 P14 P21
52 53 57.1 57.2 67.1 67.2 70 80 87 94.1 94.2 105 107 115 125 132 136
USP38
VCPIP1
USP25
USP28
USP21
USP37
MYSM1
USP49
USP16
TAF1D
STAMBP
USP30
USP8
USP48
USP46
UCHL5
OTUD6B
MPND
CYLD
USP53
USP20
USP54
USP45
PARP11
USP31
USP40
OTUD7B
OTUB2
ATXN3
USP42
OTUD3
OTUD1
OTUD5
USPL1
USP7
OTUD4
USP24
OTUB1
UCHL1
USP47
USP4
BAP1
UCHL3
PAN2
USP12
USP32
ZRANB1
USP33
USP14
USP15
USP34
USP10
JOSD1
USP39
USP5
USP11
USP1
PSMD7
PRPF8
COPS5
PSMD14
COPS6
USP22
EIF3H
USP36
USP13
OTUD7A
TBC1D1
USP51
USP3
USP27X
STAMBPL1
USP43
USP35
USP18
JOSD2
USP29
TNFAIP3
USP44
USP6
USP41
OTUD6A
USP50
USP26
USP17L2
USP17LE
USP9Y

A throughout analysis was performed to select which DUB genes could be good candidates to participate in retinal development. This RNA-seq data was analysed together with 1) chromatine immunoprecipitation sequencing (ChIP-seq) data on adult retinas; 2) RNA-seq expression data on other mouse tissues; and 3) detailed reads of RNA-seq data on P28 in flow-sorted rods and cones. These additional datasets on DUB genes were also kindly provided by Dr. Anand Swaroop.

ChIP-seq was performed on DNA from adult mouse retina, cross-linked and immunoprecipitated with antibodies against either CRX or NRL, in order to determine target gene promoters where CRX and NRL were bound. On the other hand, RNA-seq data of mouse tissues provided clues on the spatial pattern and tissular specificity of DUB gene expression (data not shown): for instance, a broadly expressed gene might have a more general role than a gene expressed only in the central nervous system (CNS).

All these data was contrasted with previously published bibliography on DUB genes as well as with the retinal and neuronal phenotypes described in section 2.2 of the present chapter.

Overall, a total of 12 genes were pre-selected as possible candidates to be involved in developmental decisions in the retina. In fact, one of the main criteria for including a gene on this list was differential expression between cones and rods. The prioritized gene list is shown in Table 11 .

To narrow down the list for further assays, we made a second selection with the five most interesting DUB genes, indicated in gray in Table 11: *Josd1, Otud7b, Usp22, Usp46 and Usp48*. All data applied for selection of these last 5 DUBs is summarized in Figure 19.

Table 11. DATA Summary of the 12 pre-selected genes as possible candidates to contribute in retinal development.

DUB	RNA-seq on total RETINA[a]	ChIP-seq[b]	RNA-seq on TISSUES[c]	PHENOTYPE[d]	BIBLIOGRAPHY
JOSD1	**Decrease** during development in whole retina and in rods, but **not in cones.**	CRX	**Adrenal Gland,** Cerebellum, **Spleen,** Thymus	3dpf: funny eyes shape, abnormal retinotectal projection **(ZF)**	Almost no bibliography.
OTUD7B	**Low expression** throughout development with a small increase from P10. Continuously expressed in rods.	-	Testis	-	**NFκB** signaling. **Oncogene**: via deubiquitination of **EGFR**
PAN2 (USP52)	Highly expressed in the retina. Shut down in rods at P21, but maintenance in cones.	CRX	**Cerebellum**, **CNS**, Testis, Cortical Plate, **Frontal Cortex**, Limb, Liver, Placenta, Testis, Urinary Bladder	-	**mRNA Deadenylation.**
USP10	Decrease in rods from P10, but not in cones.	CRX NRL	Cerebellum, **CNS**, **Cortical Plate**, Female Gonad, **Frontal Cortex**, Limb	CNS necrosis (**ZF**)	**DNA damage.** **CANCER:** Adrenal tumours, tumour-associated marker in grastrocarcinoma, p53 regulation. **NFκB** signaling.
USP11	Stricking shut down in rods and not in cones.	-	**Cerebellum**, **CNS**, Cortical Plate, **Frontal Cortex**, Gonadal Fat Pad, Kidney, Large Intestine, **Placenta**, Testis	-	**Transport to the Golgi** and **Protein folding**. **NF-kappa-B.** **DNA repair** after –double-stranded DNA breaks. **Possibly related to X-linked retinal disorders.**[71]
USP14	Stable expression in retina, with a slight shut down only in rods.	-	Cerebellum, CNS, Cortical Plate, Frontal Cortex, Liver, Placenta, Testis	(**Neuronal**) slower adults, early death (**D**). Reduced USP14 levels → tremors, **abnormal brain**	**Parkinson.** **Oncogene:** breast, hepatocellular carcinoma, lung adenocarcinoma.

				morphology, altered synaptic transmission and increased apoptosis (**H**).	**Lowers apoptosis.**
USP15	Stable expression in retina, with a slight shut down only in rods.	NRL	Adrenal Gland, Cerebellum, **CNS**, Colon, Cortical Plate, Heart, Kidney, Large Intestine, **Limb**, **Testis**	2dpf: **small eyes**, and 4dpf: **unshaped eyes (ZF).**	**Interferon** signaling. **Mitophagy.** **Oncogene** through TGFβ.
USP20	Very low levels of expression in whole retina, with a slightly shut down in rods from P10.	-	Kidney, Thymus	Earlier adult death (**D**). 3dpf: **small eyes** (**ZF**).	**NFκB** signaling. **β2** adrenergic receptor recycling. **Tyroid** hormone activation.
USP22	Highly expressed throughout development with a shut down in rods from P10.	CRX	Testis	(**Neuronal**) slower adults, early death (**D**). -/- Homozygotes are embryonic lethal (**M**).	**ONCOGEN**: liver, colon, lung, gastric, nasopharyngeal, pancreas (Via histone and p53 regulation).
USP39	Slight shut down both in retina and rods from P10, but not in cones.	CRX	CNS, **Limb**, **Testis**	Larval death (**D**). 2dpf: **small eyes** (**ZF**).	**Cancer:** promotes cell proliferation.
USP46	Low expression in rods and strong shut down in rods, but high expression in postnatal cones.	-	Adrenal Gland, Colon, Duodenum, **Female Gonad**, Kidney, Mammal Gland, Spleen, **Subcutaneous Adipose**, **Thymus**	-	**Neurotransmission circuits** involved in behaviour.
USP48	Strong difference between rods (low) and cones (high) expression.	CRX	Cerebellum, CNS; **Placenta**	3dpf: **small eyes** (**ZF**).	Almost no bibliography.

[a]**RNA-seq on total retina** summarizes the expression features observed in the RNA-seq expression data. [b]**ChIP-Seq "CRX" and "NRL"** in each file indicate that the gene promoter was targeted by CRX or NRL, respectively in ChIP assays. [c]**RNA-seq on tissues** present those tissues in which the DUB gene is mainly expressed; in bold, those tissues which a higher expression is presented. [d]**Phenotype** includes information from section 2.2. Phenotypic analysis of DUBs through species in this chapter. **D**: *Drosophila melanogaster*; **H**: Human; **M**: Mouse; **ZF**: Zebrafish. Gray rows mark those DUB genes selected for further analysis.

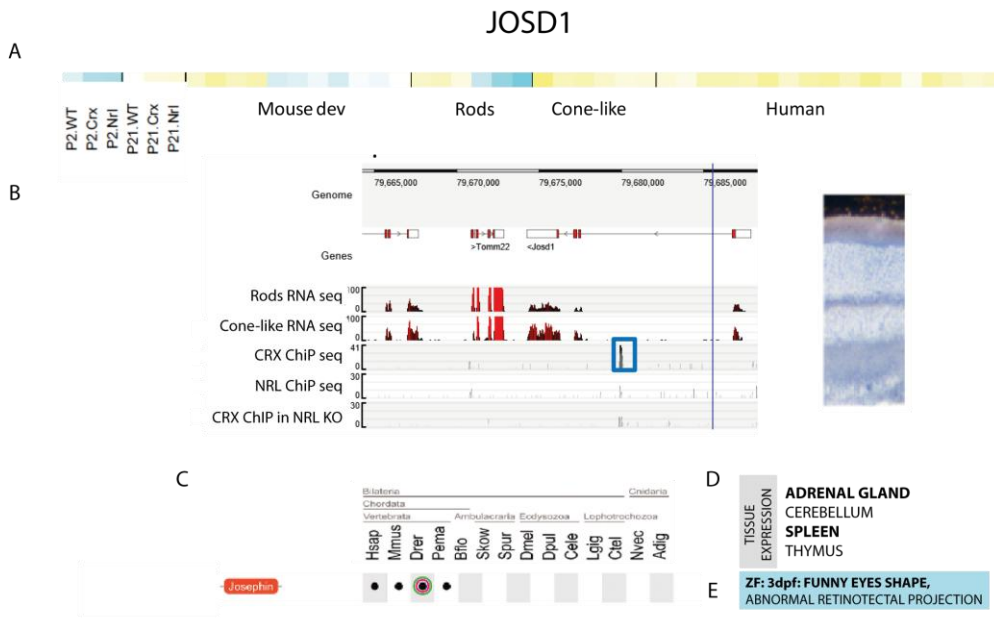
JOSD1
A
P2.WT
P2.Crx
P2.Nrl
P21.WT
P21.Crx
P21.Nrl
Mouse dev
Rods
Cone-like
Human
B
Genome
79,665,000
79,670,000
79,675,000
79,680,000
79,685,000
Genes
>Tomm22
<Josd1
Rods RNA seq
Cone-like RNA seq
CRX ChiP seq
NRL ChiP seq
CRX ChIP in NRL KO
C
Bilateria
Cnidaria
Chordata
Vertebrata
Ambulacraria
Ecdysozoa
Lophotrochozoa
Hsap
Mmus
Drer
Pema
Bfio
Skow
Spur
Dmel
Dpul
Cele
Lgig
Ctel
Nvec
Adig
Josephin
D
TISSUE EXPRESSION
ADRENAL GLAND
CEREBELLUM
SPLEEN
THYMUS
E
ZF: 3dpf: FUNNY EYES SHAPE,
ABNORMAL RETINOTECTAL PROJECTION

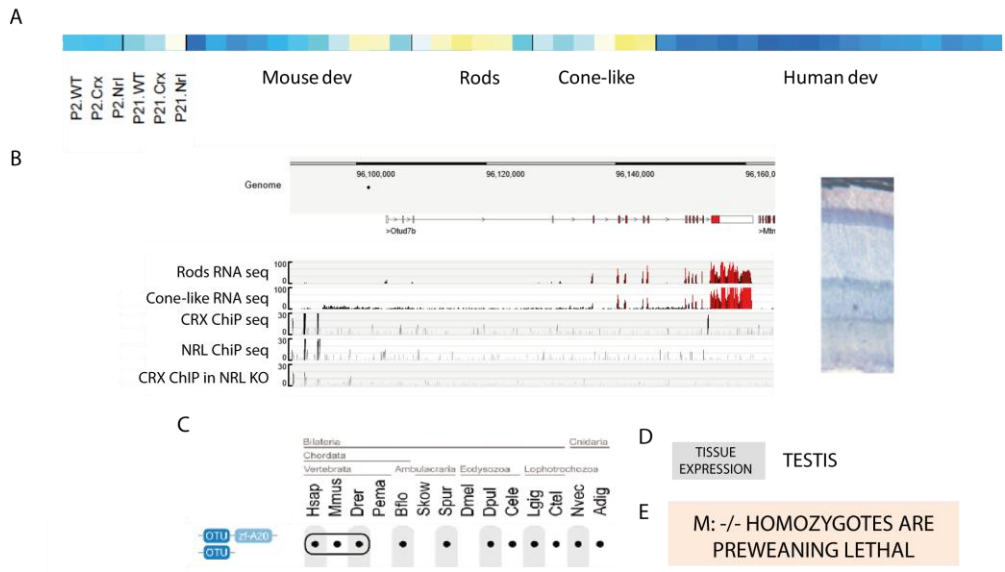
OTUD7B
A
P2.WT
P2.Crx
P2.Nrl
P21.WT
P21.Crx
P21.Nrl
Mouse dev
Rods
Cone-like
Human dev
B
Genome
96,100,000
96,120,000
96,140,000
>Otud7b
Rods RNA seq
Cone-like RNA seq
CRX ChiP seq
NRL ChiP seq
CRX ChIP in NRL KO
C
Bilateria
Cnidaria
Chordata
Vertebrata
Ambulacraria
Ecdysozoa
Lophotrochozoa
Hsap
Mmus
Drer
Pema
Bfio
Skow
Spur
Dmel
Dpul
Cele
Lgig
Ctel
Nvec
Adig
OTU
zf-A20
OTU
D
TISSUE EXPRESSION
TESTIS
E
M: -/- HOMOZYGOTES ARE
PREWEANING LETHAL

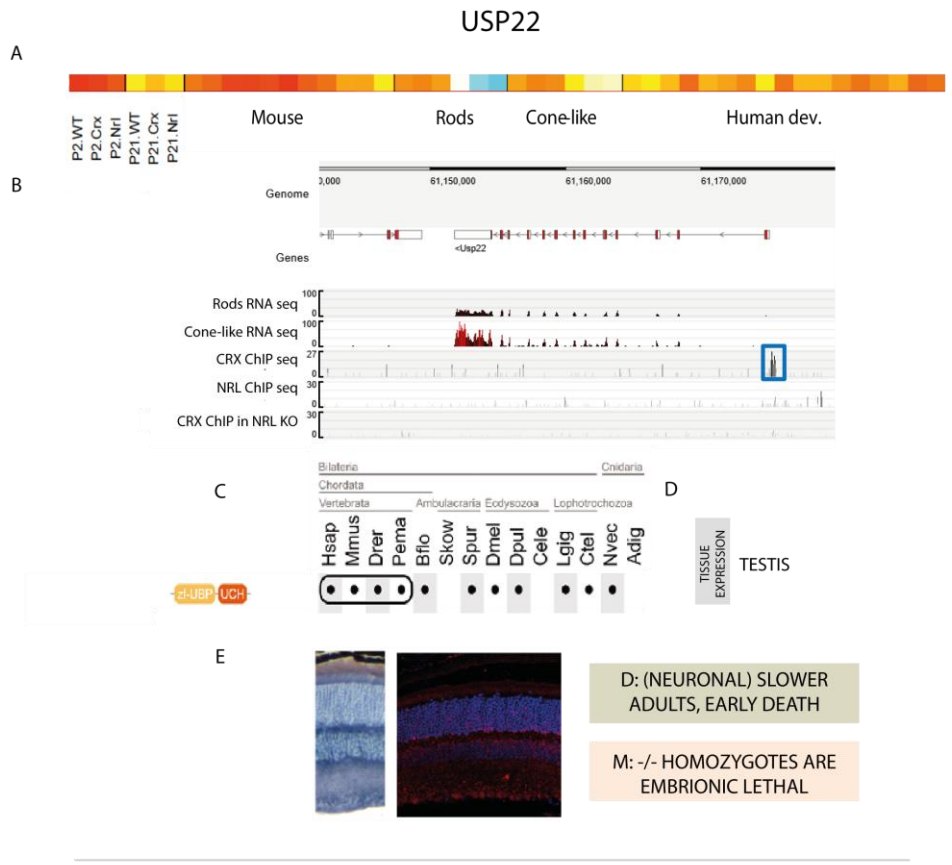
USP22
A
P2.WT
P2.Crx
P2.Nrl
P21.WT
P21.Crx
P21.Nrl
Mouse
Rods
Cone-like
Human dev.
B
Genome
61,150,000
61,160,000
61,170,000
Genes
Usp22
Rods RNA seq
Cone-like RNA seq
CRX ChIP seq
NRL ChIP seq
CRX ChIP in NRL KO
C
Bilateria
Cnidaria
Chordata
Vertebrata
Ambulacraria
Eodysozoa
Lophotrochozoa
Hsap
Mmus
Drer
Pema
Bflo
Skow
Spur
Dmel
Dpul
Cele
Lgig
Ctel
Nvec
Adig
ct-UBP
UCH
D
TISSUE EXPRESSION
TESTIS
E
D: (NEURONAL) SLOWER ADULTS, EARLY DEATH
M: -/- HOMOZYGOTES ARE EMBRIONIC LETHAL

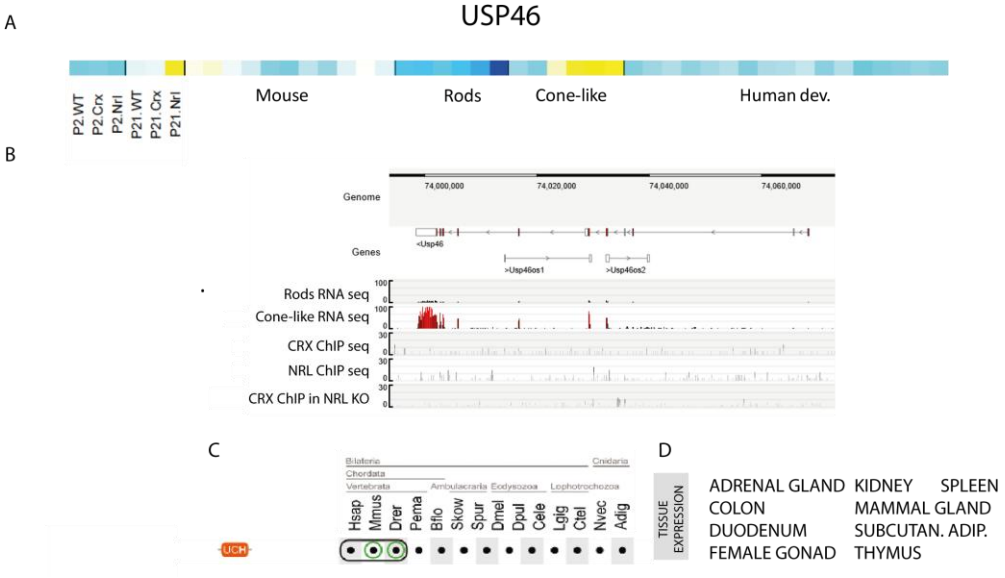
USP46
A
P2.WT
P2.Crx
P2.Nrl
P21.WT
P21.Crx
P21.Nrl
Mouse
Rods
Cone-like
Human dev.
B
Genome
74,000,000
74,020,000
74,040,000
74,060,000
Genes
Usp46
Usp46os1
Usp46os2
Rods RNA seq
Cone-like RNA seq
CRX ChIP seq
NRL ChIP seq
CRX ChIP in NRL KO
C
Bilateria
Cnidaria
Chordata
Vertebrata
Ambulacraria
Eodysozoa
Lophotrochozoa
Hsap
Mmus
Drer
Pema
Bflo
Skow
Spur
Dmel
Dpul
Cele
Lgig
Ctel
Nvec
Adig
UCH
D
TISSUE EXPRESSION
ADRENAL GLAND
KIDNEY
SPLEEN
COLON
MAMMAL GLAND
DUODENUM
SUBCUTAN. ADIP.
FEMALE GONAD
THYMUS

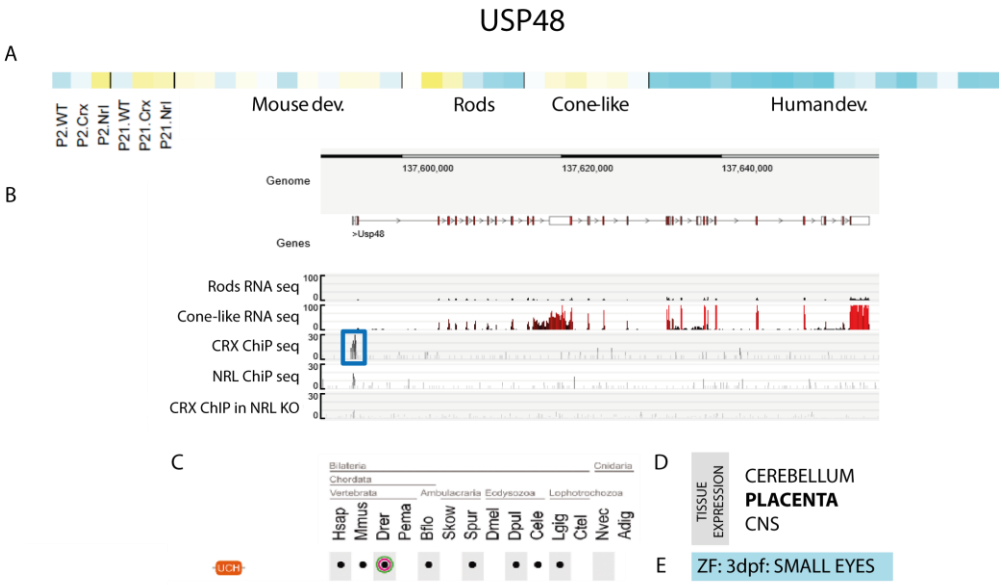

Figure 19. Criteria considered for the selection of the 5 most interesting DUBs for silencing: Josd1, Otud7b, Usp22, Usp46 and Usp48. A. Transcriptome results for each selected gene. Blue squares indicate low expression; Red, high expression; intermediate expressions are colored in white (see Results Chapter 1). **B**. RNA sequence reads for flow-sorted Rods and Cone-like cells; CRX immunoprecipitated P28 WT mouse retinas; NRL immunoprecipitated P28 WT mouse retinas; and for CRX immunoprecipitated Nrl -/- mouse retinas. **C**. Conservation analysis results (see Results Chapter 1). **D**. Tissue expression of each gene, according to RNA sequencing experiments from Dr. Anand Swaroop's laboratory. **E**. Described phenotypes in knockout and knockdown animals. **M**: Mouse; **D**: Drosophila melanogaster; **ZF**: zebrafish.

3.2. IMMUNOHISTOCHEMISTRY ASSAYS FOR RNA-SEQ DATA VALIDATION

Fluorescent immunohistochemistry was performed to evaluate the different patterns of expression of the five selected DUBs in three different stages: P4, P10 and P21. Results in Figure 20 show that JOSD1, USP22 and USP46 are detected ubiquitously in the retina of the three analyzed developmental stages, even at P4 stage, where retinas are still immature and have merely two rows of nuclear layers – being the outer layer considerably thicker.

However, in the case of OTUD7B and USP48 expression, proteins are only detected at P10 and P21. The expression pattern of OTUD7B is clearly consistent with the RNA-seq data, since RNA values increase through all the developmental stages analyzed.

Figure 20. Fluorescent immunohistochemistry on retinal sections of several DUB candidate genes at stages P4, P10 and P21. DUBs are immunodetected in red, whereas nuclei counter-staining with **DAPI** is shown in blue. Details in Annex I, S4 fig. **RPE**- retinal pigmented epithelium; **PhR**- photoreceptor cell layer; **ONL**- outer nuclear layer; **OPL**- Outer plexiform layer; **INL**- inner nuclear layer; **IPL**- inner plexiform layer; **GCL**- ganglion cell layer.

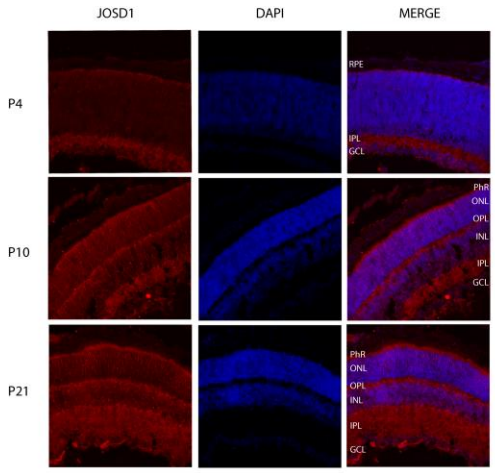
JOSD1
DAPI
MERGE
P4
P10
P21
RPE
IPL
GCL
PhR
ONL
OPL
INL

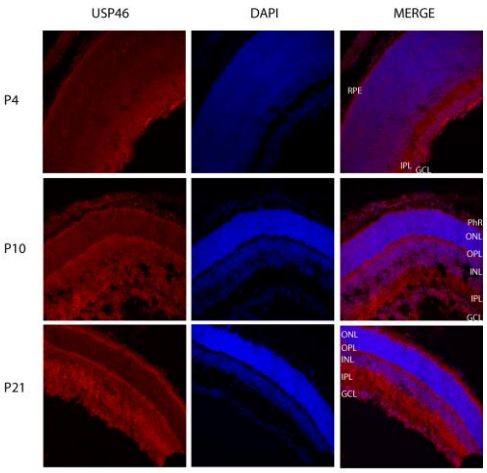
USP46
DAPI
MERGE
P4
P10
P21
RPE
IPL
GCL
PhR
ONL
OPL
INL

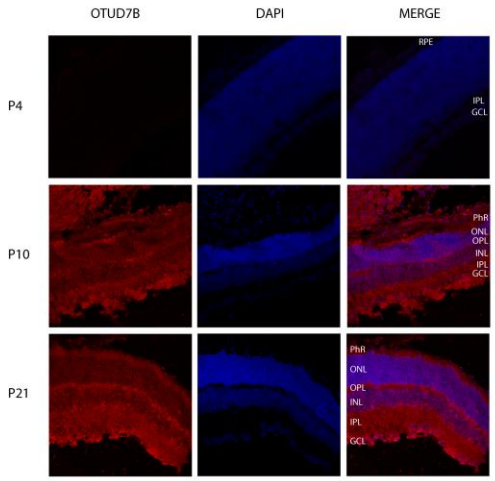
OTUD7B
DAPI
MERGE
P4
P10
P21
RPE
IPL
GCL
PhR
ONL
OPL
INL

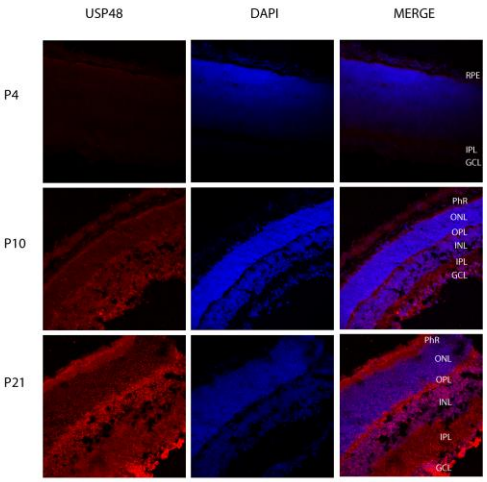
USP48
DAPI
MERGE
P4
P10
P21
RPE
IPL
GCL
PhR
ONL
OPL
INL

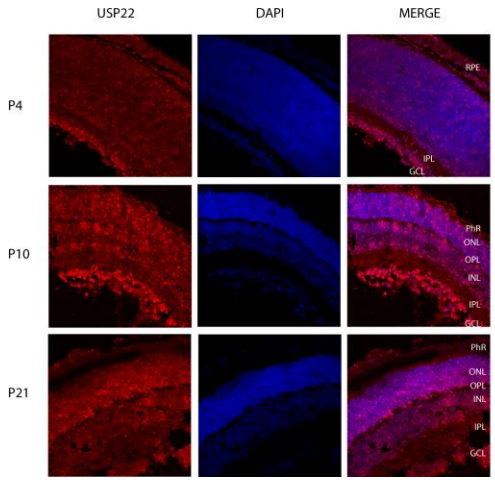
USP22
DAPI
MERGE
P4
P10
P21
RPE
IPL
GCL
PhR
ONL
OPL
INL

3.3. *IN VIVO* DNA ELECTROPORATION IN THE MOUSE RETINA

To functionally assess the role of the selected DUBs, an *in vivo* silencing experiment was performed in murine retinas. These experiments are very time consuming, therefore we selected three out of the five candidates: JOSD1, USP46 and USP48, which were those showing a higher IHC fluorescent signal in the photoreceptor layer throughout all the analyzed stages.

In order to silence the selected genes, two shRNA constructs against murine JOSD1 or USP46 were jointly injected and electroporated into the subretinal space of P1 mice. For USP48, two siRNA were used instead, as no commercial shRNA constructs were available. Also and for each gene, either the two shRNA plasmids or siRNA molecules were injected together with a reporter EGFP-expression construct (Green Fluorescent Protein cloned downstream to a constitutive Ubiquitin promoter) to detect positively electroporated cells. Retinas were dissected from mice at P10 and P21 stages, fixed and sectioned for analysis. A total of 22 retinas were electroporated. However, only 5 resulted GFP-positive: two retinas injected with anti-JOSD1 shRNAs; two injected with anti-USP48 siRNAs; and another one injected with anti-USP46 shRNAs.

Fluorescent IHC on sections was performed to identify possible morphological aberrations in the retinal structure caused by the silencing effects of the electroporated shRNA. Antibodies against JOSD1 and USP46 were respectively used to detect changes in protein expression and localization; while a GFP antibody was used to detect and increase the signal of GFP-positive cells, as a means to detect positively electroporated cells.

Finally, PNA (Peanut Aglutinin) was used to label cone photoreceptors and DAPI, to counter-stain cell nuclei.

No morphological differences were observed in the GFP-positive retinas silenced for either JOSD1 or USP46 when compared to non-electroporated control (CTRL) retinas (Figure 21 A). Nonetheless, note that in USP46 silenced retinas, retinal rosettes were observed (Figure 21 B). Commonly, these rosettes - round clumps in the centre of the image- are formed by the aberrant invagination of the PhR layer during development and excess growth. However, we should not consider them as a consequence of the silencing of any particular gene, as they are also caused by the microinjection procedure *per se*, irrespective of the gene. Figure 21 B shows the images of IHC using antibodies against β-3-Tubulin (β3TUB), a common marker of the GCL.

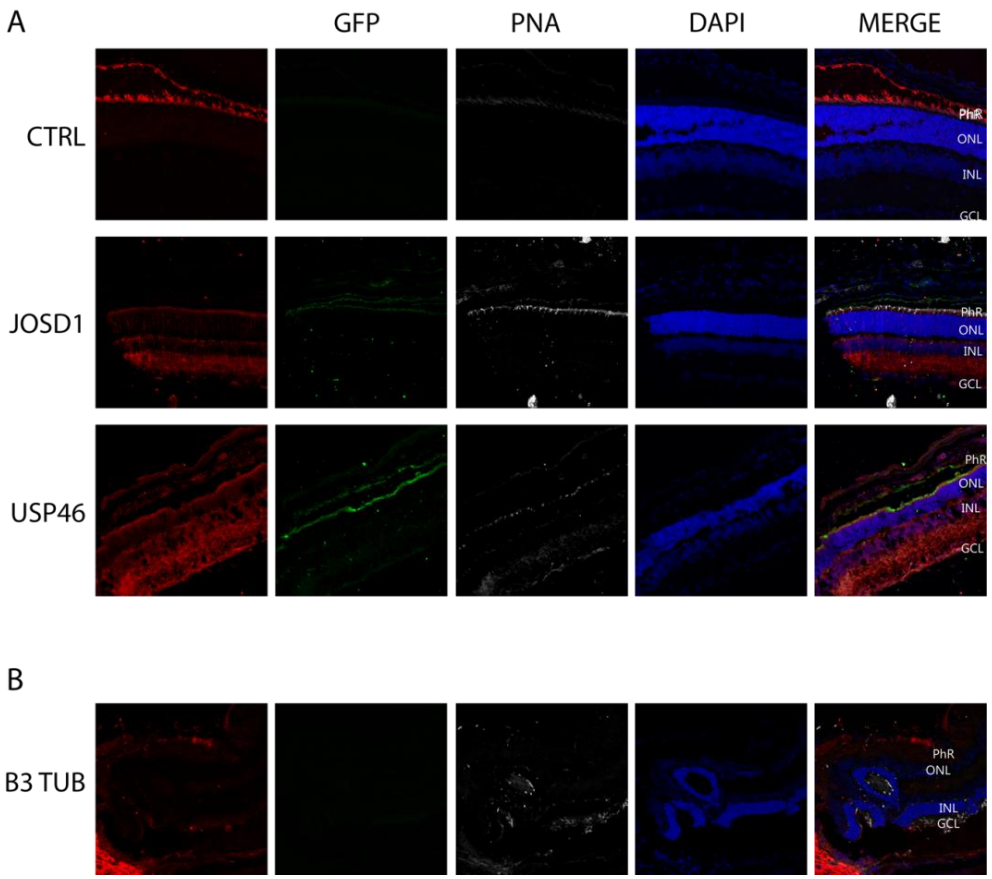

Figure 21. Fluorescent IHC of electroporated mice retinas. A. CTRL- IHC against rhodopsin performed on a WT P21 non-electroporated retina; **JOSD1**- P21 electroporated retina with shRNA against JOSD1; **USP46**- P21 electroporated retina with shRNA against USP46. **B. β3-TUB**- IHC against B3-tubulin (GCL marker) in a P21 electroporated retina with shRNA against USP46. **GFP**- IHC against the green fluorescent protein (GFP), as a reporter of electroporated cells in green. **PNA**- IHC against peanut agglutinin (PNA) to label cone cells (in gray). **DAPI** labels cell nuclei (in blue). **PhR**- Photoreceptors; **ONL**- outer nuclear layer; **INL**- inner nuclear layer; **GCL**- ganglion cell layer.

Notably, retinas injected with USP48 shRNAs showed severe morphological retinal alterations, with a prominent PhR overgrowth (Figure 22 B) and

rosettes also affecting the INL (Figure 22 C). Figure 21 A, B and C are images obtained from sections of the same retina.

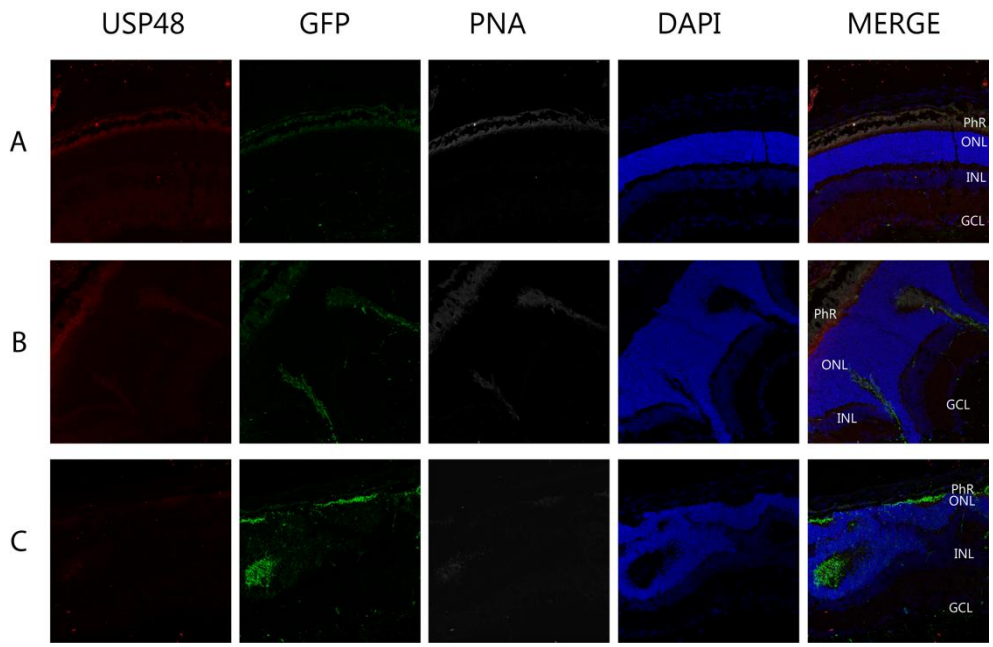

Figure 22. Fluorescent IHC in retinas electroporated with siRNA against *USP48*. **A**, **B** and **C** correspond to different parts of the same retinal section, showing three different morphologies: **A**. Expected mouse retinal morphology, undistinguishable from a wild-type retina in this region; **B**. Increased thickness of the outer nuclear layer (ONL) and deformed retinal layering; **C**. Rosettes of the inner nuclear layer (INL) formed by cells expressing photoreceptor cell markers (which are usually restricted at the PhR layer).

3.4. AON DESIGN FOR INTRAVITREAL INJECTION IN THE MOUSE RETINA

As previously mentioned, the electroporation experiments rendered very low electroporation efficiency, resulting in a small amount of retinas that could be analyzed. The results obtained in the knockdown of *Usp48* were very

promising and thus, further replicates needed to be performed. Given the low efficiency obtained in the siRNA subretinal electroporation, we decided to perform intravitreal injections with a more stable molecule, namely AONs (Antisense Oligonucleotides).

AONs are small RNA modified molecules that are used in genetic therapy approaches[72,73] and that can enter the cells without external factors. They are designed to bind complementarily to mRNA transcripts and either alter splicing outcomes, or drive targeted cleavage of the mRNA, efficiently causing a knockdown of gene expression (Figure 23). Moreover, the use of vitreal injection minimizes both, retinal damage due to the technical procedure, and animal manipulation. Once more, we decided to target *Josd1*, *Otud7b* and *Usp48* with two independent AONs.

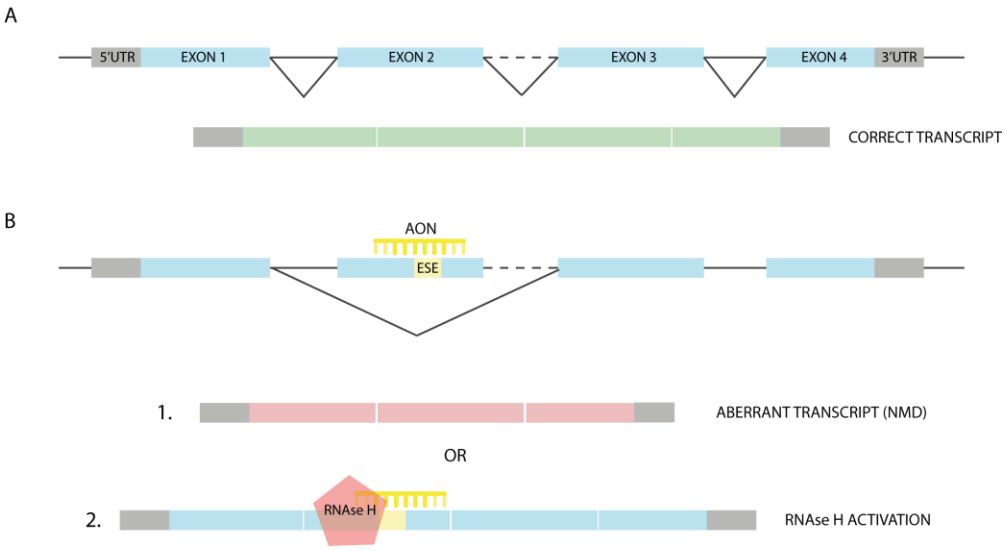

Figure 23. AON mechanism of action. A. Common splicing. **B.** AON are RNA antisense oligonucleotides designed to target Exonic Splicing Enhancer sites (ESEs) that can either cause exon skipping (B1) or RNAse H activation (B2), in both cases producing transcript degradation. (Esquerdo, M; 2017)

Therefore, AONs were designed following previous reports[74] and Dr. Alejandro Garanto-Iglesias kind advice. Briefly, AONs were unique 20 bp RNA antisense oligonucleotides sequences, designed 1) on open secondary structures (calculated using Mfold web service: *http://unafold.rna.albany.edu/?q=mfold/RNA-Folding-Form*); 2) coincident with Exonic Splicing Enhancer sites (ESEs; calculated in: *http://rulai.cshl.edu/cgi-bin/tools/ESE3/esefinder.cgi?process=home*). Free energy of the AON and of its interaction with the target sequence was calculated to find the most stable binding these two sequences (calculated in the web server: *http://rna.urmc.rochester.edu/RNAstructureWeb/Servers/Predict1/Predict1.html*).

A part from the aforementioned targeted genes, two further AON were designed against *Crx*, to be used as a positive control. At the present moment, tests on the efficiency of the AONs are being performed in 661W cells. The best fitted AON per each of the genes will be used for *in vivo* vitreal injection in P0 mice and possible morphological aberration will be analyzed via fluorescent immunohistochemistry.

CHAPTER 2. ESTABLISHMENT OF A CELL SYSTEM FOR ASSAYING THE ACTIVITY OF RETINAL TRANSCRIPTION FACTORS.

1. DESIGN OF THE ASSAY

1.1. RATIONALE

The main objective of this work was to determine how deubiquitinating enzyme genes participate in the regulation of retinal development or retinal cell fate. As aforementioned, the retina is a tissue with a complex architecture and thus, an intricate genetic and functional regulation is bound to be deployed during development. In this context, post-translational modifications, e.g. ubiquitination, may play an important role in a finely tuned gene regulation. To study these implications, we aimed to establish a cell culture system that allowed us to characterize the function of the DUBs on retinal promoters.

Note that the whole set of deubiquitinating enzymes sums up to 90 genes in the mouse genome and that we intended to evaluate their contribution to the regulation of specific retinal promoters; therefore, a high-throughput assay had to be performed. We then considered the selection of a suitable system for testing the relevance of DUBs: a) in vertebrates, with a set of DUB genes similar to humans (for instance mouse or zebrafish), a high-throughput knockdown study would entail a large economic and time effort; b) in invertebrates, such as *Drosophila* or planarians, a knockdown assay would be feasible in terms of the required time, but both the limited amount of DUB genes present in their genomes and their retinal structure differ significantly from the number of DUBs and the retina structure found in humans or

mouse. Therefore, we opted for a high-throughput assay in a mammalian cell culture system where we could control the parameters.

Since our goal was to study the role of DUBs in the retina, we also took into account that: i) primary cultures of neuronal cells, particularly highly specialized cells such as photoreceptors, is not an easy task; and ii) genetic manipulation of DUB gene expression (either over-expression of silencing) requires transfection, which is very difficult to achieve at a high percentage in neuronal cells; therefore, we decided to recreate a retina-like cell environment in an easy to maintain and transfectable cultured cell line. To recreate a retina-like cell milieu, we designed a cell system based in the cotransfection of two elements: 1) the use of retinal specific gene promoters, such as those of S opsin or Rhodopsin, regulated by 2) one or several retinal transcription factors (TF) (which were produced by expression constructs). For easy assessment of changes in the activity of these retinal promoters, they were cloned into a *pGL3-promoter* vector (Promega), which contains the firefly luciferase gene as a reporter gene downstream to the cloning site. The luciferase gene produces a protein that emits light at 560 nm, which can be detected with a luminometre. Then, if the co-transfected TF bound the promoter, it would regulate (trans-activate or repress) the activity of the downstream luciferase gene; and thus, we would be able to indirectly quantify the activity of the corresponding transcription factor by determining changes in the amount of the luciferase produced.

In brief, the TFs included in our study were CRX, NR2E3, NRL and NR1D1, all of them previously described as cojointly playing a key role in determining the photoreceptor fate. The selected promoters used to drive the expression of luciferase were those of *S opsin*, *M opsin* and *Rhodopsin*. We

planned to use several combinations of promoters and TFs in different transfection conditions, thereby mimicking a basic retinal genetic context.

Finally, we addressed our main question: Do DUBs participate in relevant retinal cell developmental decisions, such as those in determining rod and cone fates? To answer this question we planned to knockdown one by one all the DUB genes in a high-throughput experiment, using the described system. To perform the knockdown of endogenous DUBs we resourced to several silencing approaches (siRNA, shRNA or the Gapmer® technology). We surmised that in our cell system, were any DUB involved in the regulation of certain retinal promoters due to the regulation of the post-translational modification of TFs, we could observe and quantify changes in the luciferase values (Figure 24)

.

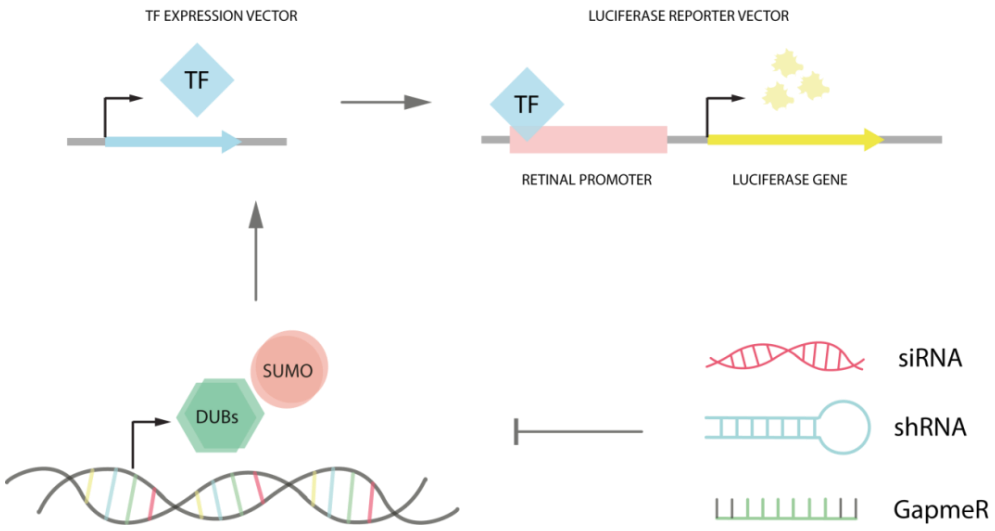

Figure 24. Diagram of the devised cell culture system. To assess the possible regulation of retinal promoters by deubiquitinating enzymes or SUMO pathway genes, HEK293 cells were co-transfected with constructs for expression of 1) a particular retina-specific transcription factor (TF) and 2) a reporter luciferase gene regulated by specific retinal promoter genes. The activity of the TF –due to Ub or SUMO post-translational modifications– on the retinal promoter can be assessed through the quantification of the luciferase expression, using a luminometer. Based on this, three different silencing methods, siRNA, shRNA or GAPMERs were used to downregulate SUMO pathway and DUB genes. Luciferase quantification was used to determine possible changes in the regulation of the retinal promoters. (Esquerdo, M.; 2017).

1.2. SELECTION OF THE CELL LINE AND LIPOFECTION SYSTEM

To determine which cell line was the most suitable to attain our aims, Real Time PCR (RT qPCR) in several mammalian cell lines was performed. The basal expression levels of the genes whose promoters we intended to use as well as the genes encoding the TFs we planned to include in our study were assessed. Our cell line selection included: 1) the mouse precursor of cones 661W, 2) the rat transformed ganglion RGC5, 3) the human retinoblastoma

Y-79, 4) the MIO-M1 human Müller cells, 5) HEK293 (Human Embryonic Kidney), and 6) HEK293T (Human Embryonic Kidney transformed with SV40 virus T antigen). Note that the last two cell lines are not retinal-derived types, however, they were included as they were previously used in other retinal transcription factor studies[44,75]. In addition, wild type P60 mouse retinas were used as a reference for expression levels. The relative expression of the genes is plotted in Figure 25, expressed as the $\log_{10}$ after normalization to the housekeeping gene Glyceraldehyde-3-phosphate dehydrogenase (GAPDH).

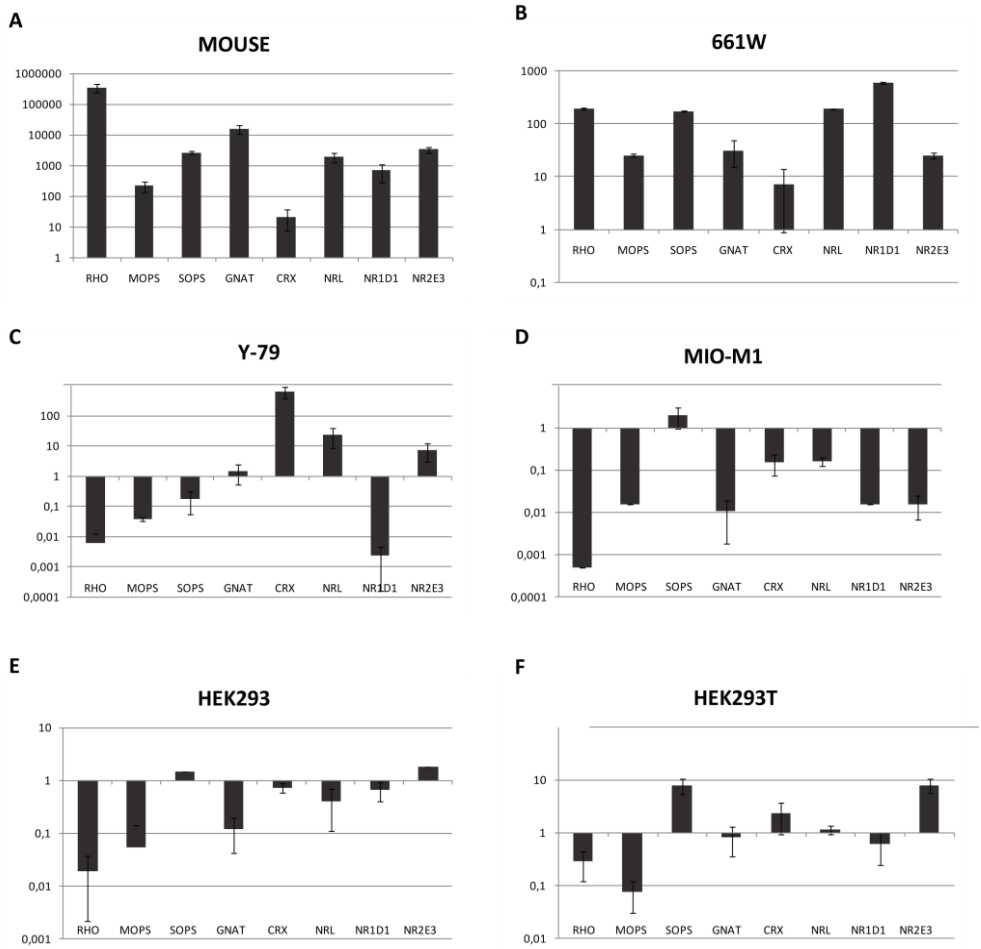

Figure 25. Real Time RT-PCR in several cultured cell lines. Real time RT-PCR (RT-qPCR) was performed in several cell lines to assess the basal mRNA levels of the genes to be used in the transfections in our cell system. mRNA levels of Rhodopsin (RHO), M and S opsin (MOPS and SOPS), GNAT and the transcription factors CRX, NRL, NR1D1 and NR2E3 were tested in: mouse adult retina (mouse), 661W cone precursor cells, Y79 retinoblastoma cells, MIO-M1 human Müller cells, human embryonic kidney cells (HEK293) and in HEK293 transformed with SV40 virus t antigen (HEK293T) cells. Values are expressed as the log10 normalized to the expression levels of GAPDH (a housekeeping gene).

The criterion we favoured to select any cell line for further assays considered that cells had to present a combination of both, a relative gene expression that allowed a quantifiable genetic manipulation as well as ensured proper control of the transfection system. Thus, low levels of expression of retinal genes were positively evaluated, in general. Observing RT qPCR results, 661W cells were those with a closer pattern of expression to that obtained in the mouse retina (Figure 25 A and B), but endogenous gene expression levels were too high to control the expression of transfected genes. Something similar happened with the Y-79 cell line, which showed low levels of the retinal genes, but high levels of the transcription factors (Figure 25 C). In conclusion, mouse 661W and human Y-79 cell lines were discarded for this assay. Human MIO-M1, HEK293T and HEK293 cells were the most interesting candidates since they all presented low levels of the analyzed genes (Figure 25 D, E and F), particularly MIO-M1 and HEK293.

To determine which cell line was more suitable for our technical requirements, different transfections with pEGFP reporter vector and several commercial liposome-based transfection reagents were performed to select the brand (liposomal composition) with higher transfection efficiency in our conditions (Figure 26). Tested cationic liposomes included *FUGENE HD Transfection Reagent* (Roche), *Lipofectamine 2000* (Invitrogen), *Metafectene Pro* (Biontex), *TransFast Transfection Reagent* (Promega) and *TransIT-Neural* (Mirus).

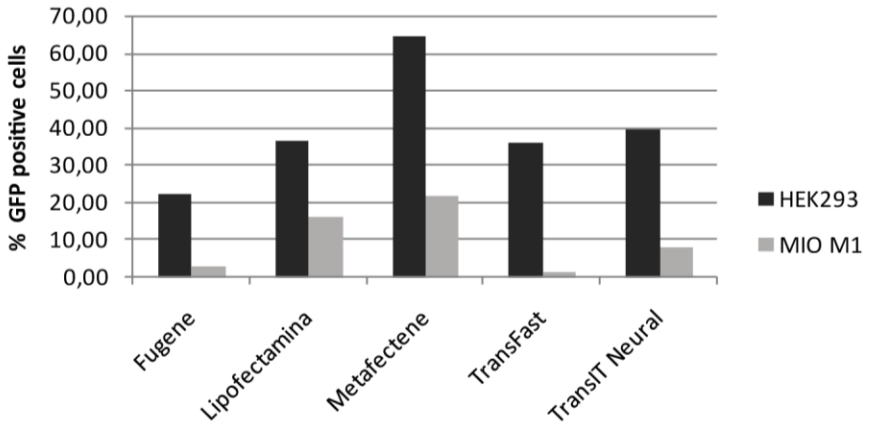

Figure 26. Lipofection efficiency of several liposome reagents in two cell lines. Five different transfection commercial liposomes were tested on HEK293 and MIO-M1 cells for efficiency in transfecting a pEGFP reporter vector, following manufacturer's instructions. The percentage of GFP-positive cells was used to determine which combination of liposomes/cell line rendered the best transfection efficiency.

Finally, HEK293 was chosen as the best cell line for the requirements of our cell culture assay. These cells had a genetic context that allowed us to easily manipulate and control transfection conditions, and showed good transfection efficiency, especially when using *Metafectene Pro* (Biontex) liposomes.

1.3. LIPOFECTION CONDITIONS

Another technical point to address was the determination of the amount of DNA required in transfections, particularly since several constructs had to be co-transfected in the same assay. Previous work carried by Cheng *et al.* (2004)[75] and Peng *et al.* (2005)[44] presented very different ratios of promoters:TFs (0.3 μg:1 μg; and 2 μg:50-200 ng, respectively). Therefore,

several transfections with different DNA ratios were carried out to establish the best combination in our hands (Table 4 in Materials and Methods).

These tests were performed prior to the RT qPCR results on cell lines. We first performed transfections on HEK293T cells using the ratios reported in Cheng and Peng articles. This preliminary test was performed using the Rhodopsin promoter and the transcription factor CRX. However, despite it was a previously described system, several problems emerged when validating and reproducing luciferase results (not shown).

1.4. PROOF OF PRINCIPLE

Eventually, after determining that MIO-M1 and HEK293 were the most suitable cell lines, the promoter activity in response to the transfected TFs was evaluated in both cell types. For this experiment, 0.3 μg of the promoter and 0.5 μg of the TF expression constructs were used, following the protocol established by a former PhD student of our lab (Dr. Pomares, as specified in her DEA, *Diploma d'Estudis Avançats*). In the case of HEK293, *Rhodopsin, S opsin, M opsin* and *Gnat* promoters were tested alone or in co-transfection with either CRX or CRX plus NR2E3. For the assay in MIO-M1 cells, the *Rhodopsin* promoter was tested either alone, co-transfected with CRX, or with CRX plus NR2E3. Results are expressed as luciferase values normalized using β-galactosidase (Figure 27).

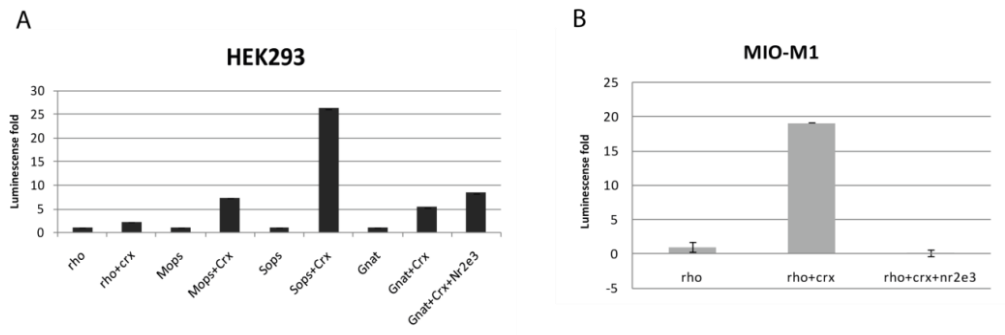

Figure 27. Evaluation of promoter activity in response to co-transfection of retinal transcription factors. The *Rhodopsin* (RHO), *M opsin* (MOPS) and *Gnat* promoters were cloned upstream of a luciferase reporter gene. The regulation of each promoter by the co-transfected transcription factors CRX and NR2E3 was assessed by measuring luciferase activity variations. Registered luminescence was normalized to β-galactosidase control vector activity. Results are plotted as fold values of each promoter activity transfected alone, which was considered arbitrarily as 1.

In HEK293 cells a high activation of the *S opsin* promoter by CRX was observed, being more moderate for the *M opsin* and *Gnat* promoters, and barely detectable for the *Rhodopsin* promoter (Figure 27 A). On the other hand, activation of the *Rhodopsin* promoter by CRX was clearly observed in MIO-M1 cells, whereas the addition of NR2E3 to CRX caused a severe repression (Figure 27 B).

Rhodopsin promoter activation by CRX and repression by the combination of CRX and NR2E3 observed in the MIO-M1 cell line is similar to what has been previously described to in the events leading to rod determination during the development of the mouse retina. On the other hand, activation of the S opsin promoter with no activation of the Rhodopsin promoter when co-transfected with CRX is equivalent to the regulation of the default cone pathway also described in the development of the mouse retina. For these

reasons, a transfection system using MIO-M1 was deemed as a possible rod model; while the system using HEK293 might serve as a cone model. Nonetheless, due to their lower transfection efficiency results, MIO-M1 cells were discarded as a first option, and HEK293 was selected as the cell line to perform our high-throughput DUB silencing assays.

In summary, in our conditions HEK293 cells were chosen to be co-transfected with the S opsin promoter and CRX (as TF), as our best basal cell system to assay the possible effect of DUB genes knockdown in the control of retinal promoters by retina-specific TFs. Furthermore, our results allowed us to establish a cell culture model that somehow mimicked some of the conditions of a developmental retinal cell in which CRX activates the *S opsin* but does not activate the *Rhodopsin* gene. On the plus, HEK293 cells are easy to work with and manipulate, and they usually render reproducible results that can be statistically analyzed.

2. ASSESSMENT OF DUB SILENCING IN OUR CELLULAR SYSTEM

After establishing the transfection parameters in HEK293 cells, the next step was to perform high-throughput silencing assays using the established cell system. These assays were considered as a first screening step to identify possible DUB enzymes as candidates for the regulation of the S opsin promoter in the development of photoreceptors. We used two different high-throughput approaches, based on a short hairpin RNA (shRNA) library and a small interfering RNA (siRNA) collection to selectively knockdown

one by a one a large selection of deubiquitinating enzymes and SUMO pathway genes.

2.1. shRNA-MEDIATED SILENCING

The use of shRNA-expression plasmids is a common RNA interference-silencing method. It is characterized by relatively low degradation and turnover rates and thus, it represents an optimum system when working with cell culture as well as in *in vivo* approaches. Considering these characteristics, shRNA-mediated knockdown was one of the mechanisms we selected to interfere with the endogenous DUB expression in our system, and detect the subsequent effect on the transactivation/repression of photoreceptor-specific promoters. A high-throughput knockdown study was performed at the CIC-Biogune (Bilbao) facilities (Dr. E. Berra), since a large shRNA library against all human genes was available. We made a selection of interesting ubiquitin and SUMO pathway genes to be silenced.

A total of 43 genes were selected for this study, 27 belonging to the SUMO pathway and 16 to the DUB family (Table 12). All SUMO pathway genes were included on the list whilst DUBs were selected depending on their mRNA expression pattern in the retinal layers, as observed in the *in situ* hybridization results– namely, we picked those genes that showed expression in the photoreceptor layer and had a neat hybridization signal (see section 1.2 in Results – Chapter 1).

When available, a maximum of three different shRNAs against several regions were used per gene. Also, two different controls for the silencing procedure were used: one shRNA against a random non-complementary sequence, shSIMA, as a negative control; plus several shRNAs against *CRX*,

as a positive control. In the case of *CRX*, five different shRNAs were used, and since they were not cloned into the same vector as the rest of the shRNA library, a second random non-complementary shRNA had to be added as a control, named shSCRAMBLE. Moreover, the pcDNA empty vector was used as a transfection negative control. All transfections were performed including the S opsin promoter-luciferase together with CRX (as TF) expression constructs.

Table 12. Human SUMO pathway and DUB genes silenced using a high-throughput shRNA library.

SUMO GENES				DUBs	
SUBSTRATES	**E3 LIGASES**		**PROTEASES**	*JOSD2*	*UCHL1*
SUMO1	*PIAS1*	*HDAC7*	*DESI1*	*ATXN3*	*UCHL3*
SUMO2	*PIAS2*	*MUL1*	*DESI2*	*BAP1*	*USP12*
SUMO3	*PIAS3*	*RASD2*	*SENP1*	*STAMPB*	*USP11*
E1 LIGASES	*PIAS4*	*TOPORS*	*SENP2*	*USP9X*	*TNFAIP3*
SAE1	*RANBP2*	*TLS*	*SENP3*	*USP25*	*USP47*
SAE2	*CBX4*	*TRAF-7*	*SENP5*	*USP45*	*PRPF8*
E2 LIGASE	*MMS21*	*USPL1*	*SENP6*	*USP54*	*OTUD7B*
UBC9	*HDAC4*		*SENP7*		

Previous to performing the complete high-throughput study, *CRX* was silenced on its own as a proof of sensitivity for the luciferase system. A striking statistically significant decrease in luciferase levels was observed when silencing *CRX* (shCRX compared to shSCRAMBLE; p-value <0,0001). Besides, this decrease was more evident with time, as it was higher after 72 h than 48 h post-transfection. (Figure 28)

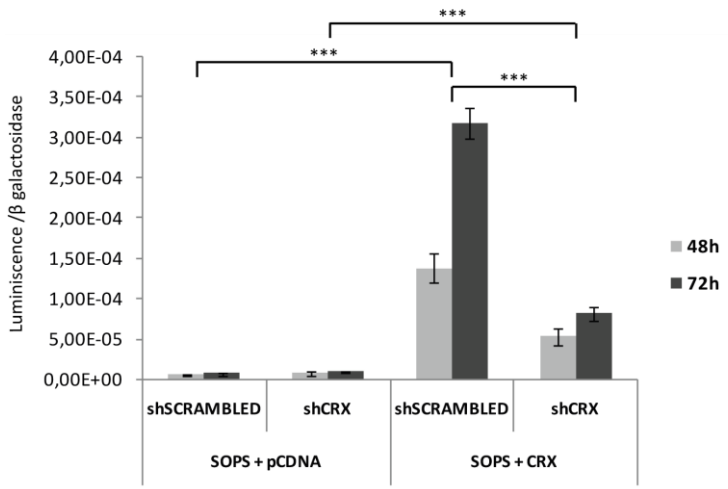

Figure 28. Effects of *CRX* silencing by shRNA on the S opsin retinal promoter at 48 and 72h post-transfection. HEK293 cells were transfected with the reporter luciferase gene controlled by the mouse *S opsin* promoter, which was activated by the cotransfected transcription factor CRX. The pcDNA empty vector was used as a negative control for the activation of the S opsin promoter. *CRX* was silenced using 5 different shRNA jointly; shSCRAMBLED, an shRNA against a random sequence, was used as a negative control for the silencing method. Samples were obtained and luciferase was mesured and normalized to β-galactosidase activity 48 and 72 hours post transfection. Mean values of luciferase activity are plotted showing the SD (standard deviation) for all analyzed conditions. The activation of the *S opsin* promoter by CRX was statistically significant (p-value <0,0001; ***) at both timepoints; as it was the silencing efect of the shRNA against CRX.

Four different independent high-throughput silencing replicate experiments were performed, each one containing three technical replicates per silenced gene. Per gene, two to three different shRNAs against different coding regions were assayed in the same well to improve silencing. Mean values of luciferase normalized to β-galactosidase activities for the four experimental replicates are plotted in Figure 29. After performing statistic analysis by the Dunnett's test, no significant differences were observed between the silencing among all the genes and the control. However, some genes such as

UBC9, *PIAS2*, *PIAS3*, *SENP1*, *SENP3*, *DESI1*, *TRAF7*, *USP11* and *PRPF8*, showed a clear trend in their variation, when compared to the control.

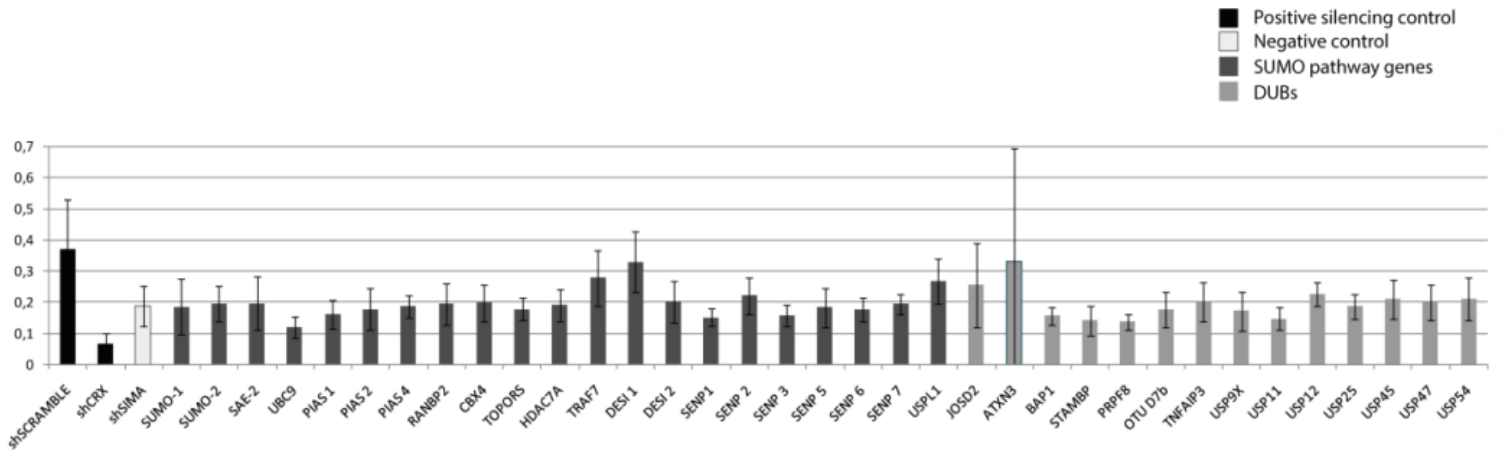

Figure 29. High-throughput shRNA screening of the SUMO pathway and DUB genes using the transactivation of the S opsin promoter as a reporter. HEK293 cells were transfected with the reporter luciferase gene controlled by the mouse *S opsin* promoter, which was activated by the cotransfected transcription factor CRX. The shRNA screening was performed by knocking down the SUMO pathway genes and selected DUB genes. Luciferase values are represented after normalization with β-galactosidase activity. The results of the shRNA positive control against CRX (in black), the two shRNA negative controls, one for the vector expressing shRNA against *CRX* (shSCRAMBLE) and the SIMA vector constructs (shSIMA) (in white), and the specific shRNAs against the SUMO pathway (dark gray) and DUB (light gray) genes are also shown. This is a plot assay of four independent replicates. No reproducible/statistically significant results could be obtained after applying Dunnett's test.

Concerning the fact that no statistical differences were observed, it is worth noting that shSIMA results were not consistent with those obtained with the other negative control, shSCRAMBLE, when they should be quite similar. In fact, shSIMA luciferase values were lower than the observed in the alternative negative control, which suggested a silencing context effect of this vector upon the *S opsin* promoter (even when no shRNA was expressed). This observation made it difficult to assess statistical differences between the effect of DUB gene silencing and the shSIMA negative control. For this reason, and as an attempt to clarify these results, another knockdown assay was performed focusing our efforts on the genes that presented some suggestive trend when compared to the control.

At the University of Barcelona, a deconvolution assay was performed, transfecting separately each of the shRNAs that targeted a particular gene (three different shRNAs were jointly tested per most genes in the high-throughput screening). Three replicates of the experiment were performed, each of them containing three independent replicates. In the case of *SENP3*, *DESI1* and *USPL1* only a single shRNA construct was available and so, for these cases the deconvolution experiment was a replicate of the high-throughput test. Experimental conditions and controls were the same as those used in the high-throughput assay. As an experimental reference, the transfection of all the shRNA per gene in a single well was also used.

The folds of luciferase mean values of the three experiments, normalized to β-galactosidase, compared to the shSIMA control are plotted in Figure 30. Unfortunately, this deconvolution assay did not help to shed light on the previously obtained results. Nearly in all cases, each individual shRNA showed the opposite behaviour that the one obtained when using the three

shRNA of each gene together; e.g. most of the genes showed a repression of the S opsin promoter when using all shRNA together, but each shRNA showed activation of the promoter when transfected separately. This behaviour was observed in all genes except for *TRAF7*. Light gray bars indicate that shRNA luciferase values show a consistent behaviour –either an increase or a decrease– as those obtained in the high-throughput experiment; whereas black bars indicate that the result was opposite. It is worth mentioning that when transfecting all shRNA together, results were reproducible from the high-throughput assay, except for *DESI1*.

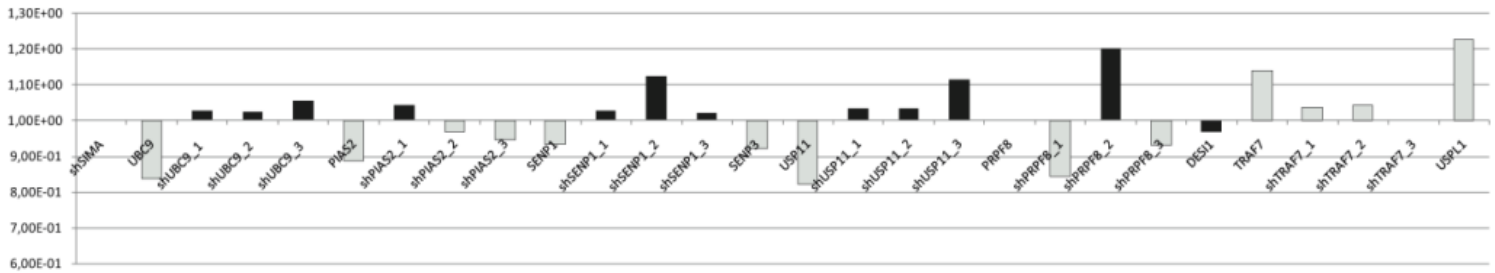

Figure 30. shRNA deconvolution of selected genes. The genes that showed some differential behaviour from the scrambled control on the high-throughput screening were selected for deconvolution. Each of the 2-3 shRNA constructs per gene were transfected either together or separately (indicated with a lower dash and a number). Three replicates of the experiment were performed, each of them containing three independent replicates. Mean luciferase values were normalized to β-galactosidase values, and the fold values (increase or decrease in expression) compared to shRNA control (shSIMA) are plotted for each gene. Values that correlate with the luciferase values obtained in the high-throughput screening are indicated in gray, whereas those values that are not consistent are depicted in black.

Since the technical difficulties did not allow obtaining consistent results and shSIMA was the only negative control available and could not be substituted (another vector would have probably produced statistically significance in at least a few number of genes), no further experiments could be performed using the shRNA library.

2.2. siRNA-MEDIATED SILENCING

Despite the shRNA results were rather disappointing because of they did not show any statistical significance, we still intended to elucidate whether any of the deubiquitinating enzyme genes were responsible or else, had a plausible relationship with the regulation of photoreceptor development. Therefore, to complement data obtained from the shRNA knockdown assay and to evaluate the efficacy and consistency of other silencing methods, transfection with small interfering RNA (siRNA) was also performed in our cell system. It is worth mentioning that siRNA is introduced as a small double stranded RNA molecule, and it is a transient silencing method, less stable within cells than shRNA, but also commonly used in cell culture and in *in vivo* assays. In our experiments, two different siRNA targeting different regions per gene against a total of 35 USP family genes, were tested. All of them were kindly provided by Dr. Jose Antonio Rodríguez Pérez at Universidad del País Vasco (Table 13).

Table 13. List of siRNA against USP genes used in the siRNA high-throughput screening.

USP 1	*USP 8*	*USP 15*	*USP 25*	*USP 36*
USP 2	*USP 9*	*USP 16*	*USP 29*	*USP 37*
USP 3	*USP 10*	*USP 18*	*USP 30*	*USP 42*
USP 4	*USP 11*	*USP 19*	*USP 31*	*USP 44*
USP 5	*USP 12*	*USP 20*	*USP 32*	*USP 46*
USP 6	*USP 13*	*USP 22*	*USP 33*	*USP 47*
USP 7	*USP 14*	*USP 24*	*USP 34*	*CYLD*

Similarly to the assays using shRNA, in these knockdown assays HEK293 cells were co-transfected with the *S opsin* promoter, CRX as a TF, and the siRNAs corresponding to each DUB that targeted the expression of the endogenous genes. A random siRNA-sequence, siSCRAMBLE, was used as a negative control. No *CRX* silencing control was performed; instead *GAPDH* silencing was used as a positive control.

As a proof-of-principle, before attempting the high-throughput test, we first tested the efficiency of siRNA gene silencing in the endogenous expression of *USP5* and *USP19* in HEK293 cells. These two genes were selected since they were highly and lowly expressed in the mouse retina, respectively (see results of section 1.1 from Results – Chapter 1). The effect on the mRNA levels was assessed by specific RT qPCRs. Relative expressions were normalized to *β2-Microglobulin* (Figure 31).

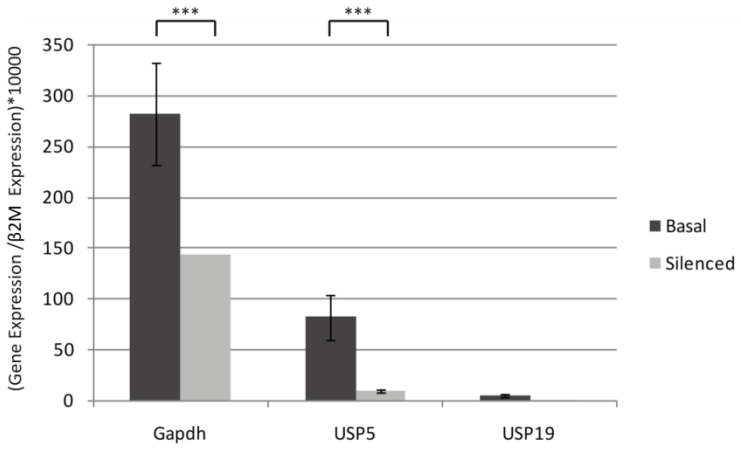

Figure 31. mRNA expression levels before (basal) and after (silenced) silencing by siRNA against USP5 and USP19. USP5 and USP19 endogenous genes were silenced in HEK293 cells using siRNA. real time qPCR was performed to assess the knockdown effect in these genes. siRNAs against *Gapdh* were used as a positive control. mRNA expression levels for each gene, were normalized to β2-microglobuline (β2M). The knockdown of these two genes rendered significant statistical differences when comparing to untreated cells (p-value <0,001; ***).

A knockdown effect of 50% was observed for *GAPDH* expression, which was used as a control; and a very effective knockdown (down to 10% of the basal expression) was detected for *USP5*. However, the basal expression of *USP19* was barely detectable in HEK293 cells and therefore, the knockdown effect could not be reliably assessed.

Once the efficiency of gene knockdown using siRNAs had been validated, we finally got to perform the high-throughput siRNA silencing assay. Again, as in the case of the shRNA assay, four independent experiments were conducted, each of them including three replicates per sample (Figure 32). Unfortunately, the four different experiments did not render any reproducible or plausible results, for high levels of variability between

experiments were observed. To illustrate this striking variability, the values obtained in each experiment have been plotted in Figure 32. Luciferase values were normalized to β-galactosidase values in each independent experiment.

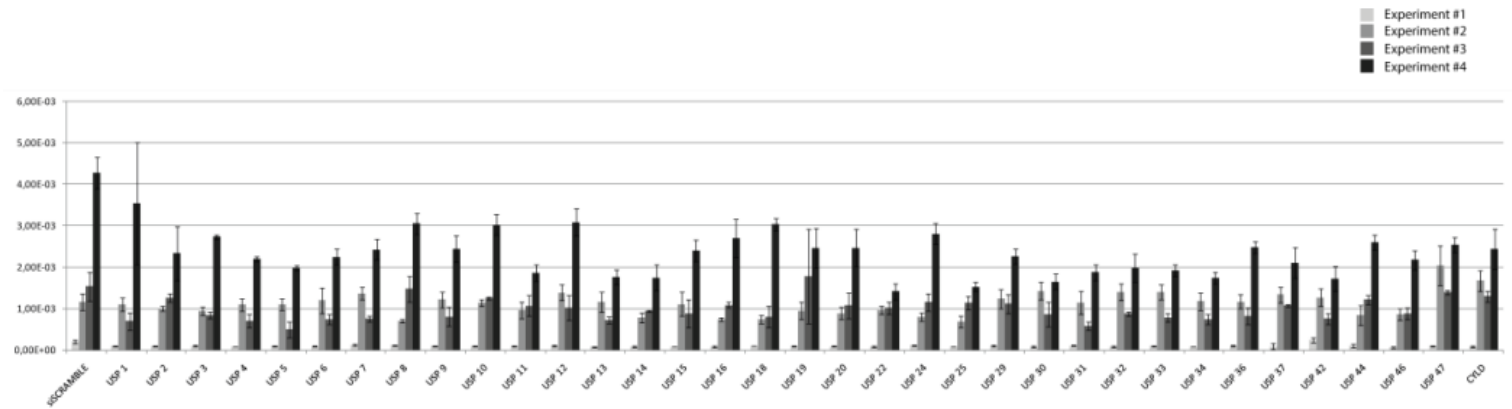

Figure 32. Effects of DUBs' siRNA silencing in a high-throughput screening. HEK293 cells were co-transfected with the S *opsin* promoter cloned upstream of a luciferase gene, the CRX transcription factor and 2 different siRNA per USP gene to be silenced. siSCRAMBLE random sequence was used as a negative control. Four different experiments were performed (#1-#4), each of them including three separate replicates, which produced highly variable and inconsistent results.

Given this unusual variability, no statistical analysis could be performed and so, we had to look at the results in a different manner. In an attempt to make sense of the results, only those values from the two closest experiments were considered, that is, the two central values (experiments #2 and #3) in Figure 33. When taking into account only these values, the knockdown of *USP18* rendered statistically significant differences; while *USP1*, *USP3*, *USP46* and *USP47* showed a suggestive trend (though not yet significant). Mean luciferase values of these two experiments normalized to β-galactosidase values are plotted in Figure 33.

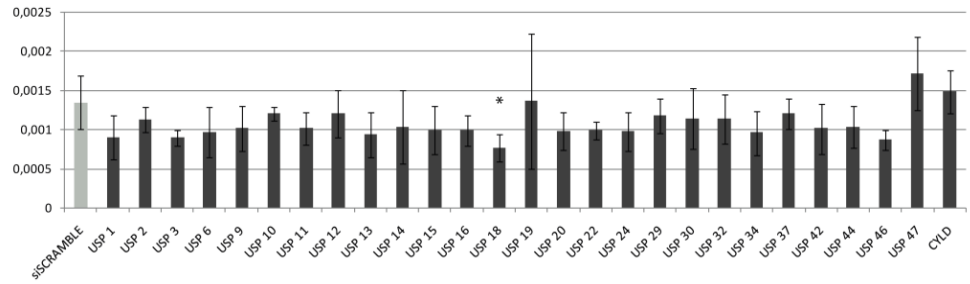

Figure 33. Statistical comparison of the two closest mean values obtained in the high-throughput siRNA screening. Dunnett's statistical test resulted in *USP18* being statistically differing from the shSCRAMBLE control.

Since some DUBs showed suggestive changes in luciferase expression after siRNA-mediated knockdown, we decided to confirm the assays in a smaller scale. The siRNA-mediated knockdown of *USP1*, *USP3*, *USP18*, *USP46* and *USP47* by siRNA were analyzed again, checking the effect on the regulation of the *S opsin* promoter by CRX. No clear reproducible results were obtained (Figure 34 A). Since one of the possible effects of DUBs is the edition and rescue of ubiquitinated proteins targeted for proteasome degradation, we

checked whether the knockdown of these specific DUBs by siRNA could alter the protein stability of CRX. Therefore, we checked CRX levels on siRNA transfected cell lysates (Figure 34 B). We could detect a significant reduction in the CRX protein levels when silencing *USP18* (Figure 34 C); which is consistent with the reduction of luciferase values in the siRNA silencing screening.

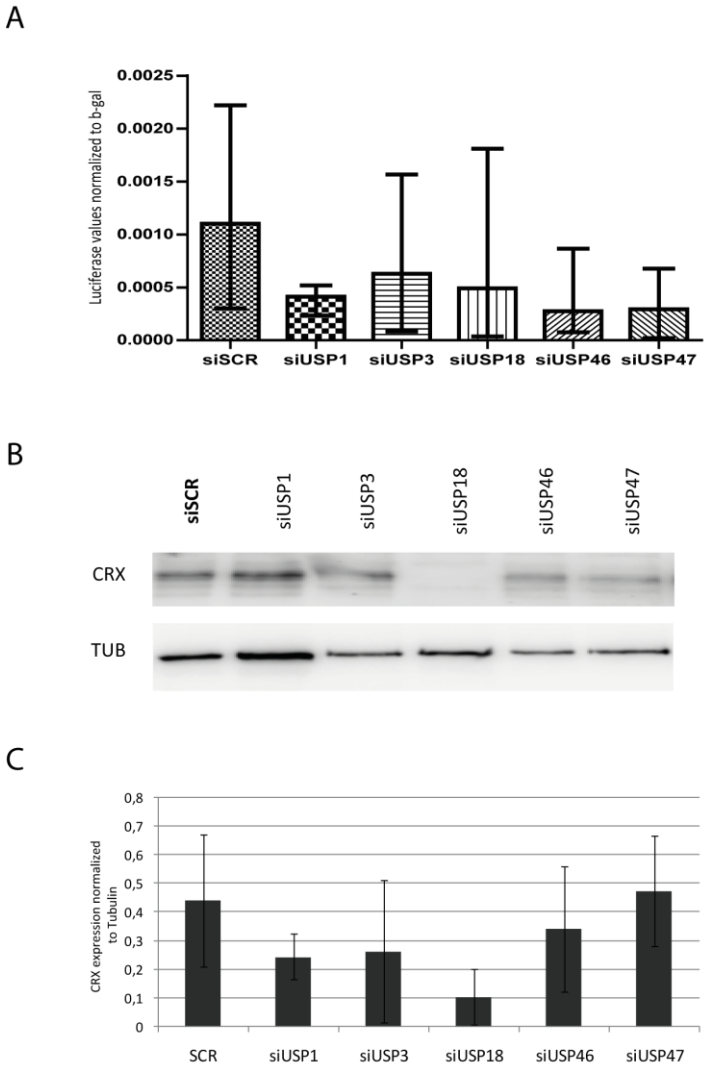

Figure 34. CRX protein stability and transactivation activity in knockdown assays of cells transfected with siRNAs against specific DUBs. A. Luciferase values after silencing 5 deubiquitinating enzyme genes (*USP1*, *USP3*, *USP18*, *USP46* and *USP48*) on HEK293 cells co-transfected with the constructs for CRX TF and the *S opsin* promoter driving the expression of the luciferase reporter gene. siSCR is the negative control siRNA against a random scramble sequence. **B**. Immunodetection of CRX and tubulin (TUB) (normalization control) by Western blot. **C**. CRX quantification normalized to tubulin after four independent replicates.

These experiments showed that the knockdown of *USP18* affected CRX protein levels. Therefore, the regulation of CRX by USP18 appeared as a good starting point to further investigate the involvement of this DUB in retinal development. Despite this promising result, later transcriptome analysis by high-throughput RNA-sequencing (section 3.1 in Results – Chapter 1) of different retinal developmental stages barely detected any *Usp18* retinal expression levels throughout all the stages and species (mouse and human) analyzed. Unfortunately, the endogenous expression of *USP18* in HEK293 cells did not correlate with its level of expression in retinal cells. If expression of *USP18* and *CRX* apparently did not coincide during development, any possibility of physiological relevance for the regulation of CRX (a key retinal-specific TF) via USP18 would be extremely low. Therefore, we decided not to pursue this seemingly spurious interaction.

Up to then, all silencing methods evaluated triggered several technical difficulties that could not be overcome. On one hand, shRNAs seemed to shed promising results but the unique negative control interfered with the luciferase reads, and made it impossible to find statistical differences. On the other hand, siRNA experiments rendered extremely variable results between independent experiments. In addition, the statistically differences found in CRX levels after *USP18* knockdown did not seem to bear physiological relevance. For this reason, alternative methodologies needed to be approached in order to elucidate the role of DUB genes in the regulation of retinal development.

2.3. GAPMER®-MEDIATED SILENCING

Simultaneously to using siRNA and shRNA, a new gene knockdown technology was also tested, namely, Gapmers®. Gapmers® (from heretofore, Gapmers) are synthetic antisense DNA oligonucleotide probes flanked by two 2'-O modified RNA regions. When they target a particular mRNA molecule by sequence complementarity, the cell detects an mRNA-DNA double strand hybrid, thereby inducing RNAse H activity, which results in cleavage of the mRNA strand of the hybrid and ensures the expression knockdown of the target gene. Their application ranges from *in vitro* cell cultures to *in vivo* assays, making them a good tool for gene functional analyses (Figure 35). Thereby, if the shRNA/siRNA assays resulted with a good DUB candidate; the silencing effects would have been tested in *in vivo* retinal explants.

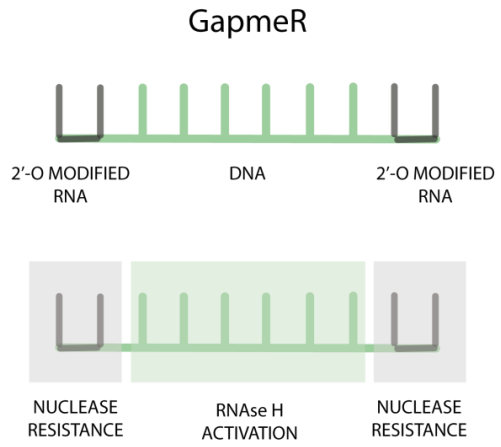

Figure 35. Gapmer® structure and mechanism of action. GAPMERS are DNA oligonucleotides flanked by 2'-O modified RNA nucleotides. these two modified ends confer this synthetic small RNA-DNA molecule with a resistance against endogenous cell nucleases and thus, a longer half-life of the molecule. besides, when the binding to the target mRNA-sequence occurs, a DNA-RNA double strand hybrid is formed that activates RNAse H. RNAse H activity cleaves the RNA strand within the hybrid, resulting in effective silencing of the target gene.

To test the efficiency of this new system, we performed control assays by attempting Gapmer-mediated silencing of well-known retinal genes *CRX*, *NR2E3* and *PIAS3* in our HEK293 cell system. CRX and NR2E3 are known modulators of photoreceptor cell promoters – CRX is an activator of the *S opsin* gene and other cone-related genes; while NR2E3 is an activator of rod-specific genes. Concerning PIAS3, it is the SUMO E3 ligase responsible for SUMOylating NR2E3 thereby switching its function from activator of rod-specific genes to repressor of cone-specific genes. While the relationship between NR2E3 and PIAS3 has been previously addressed; it is yet unclear whether PIAS3 somehow interacts with or modulates the function CRX.

On one hand, *CRX* and *PIAS3* were separately silenced in our *S opsin* promoter – CRX system (Figure 36 A); and on the other, *NR2E3* and *PIAS3* were silenced in the same transfection system together with NR2E3 as an extra mediating TF (Figure 36 B). In all cases, three different Gapmers against three different regions per gene were used in a single condition. A random sequence Gapmer, Ctrl NegA, was used as a silencing negative control. The assay was performed in three separate experiments, each of them containing three independent samples. Cells were harvested and luciferase activity was measured 48h post-transfection.

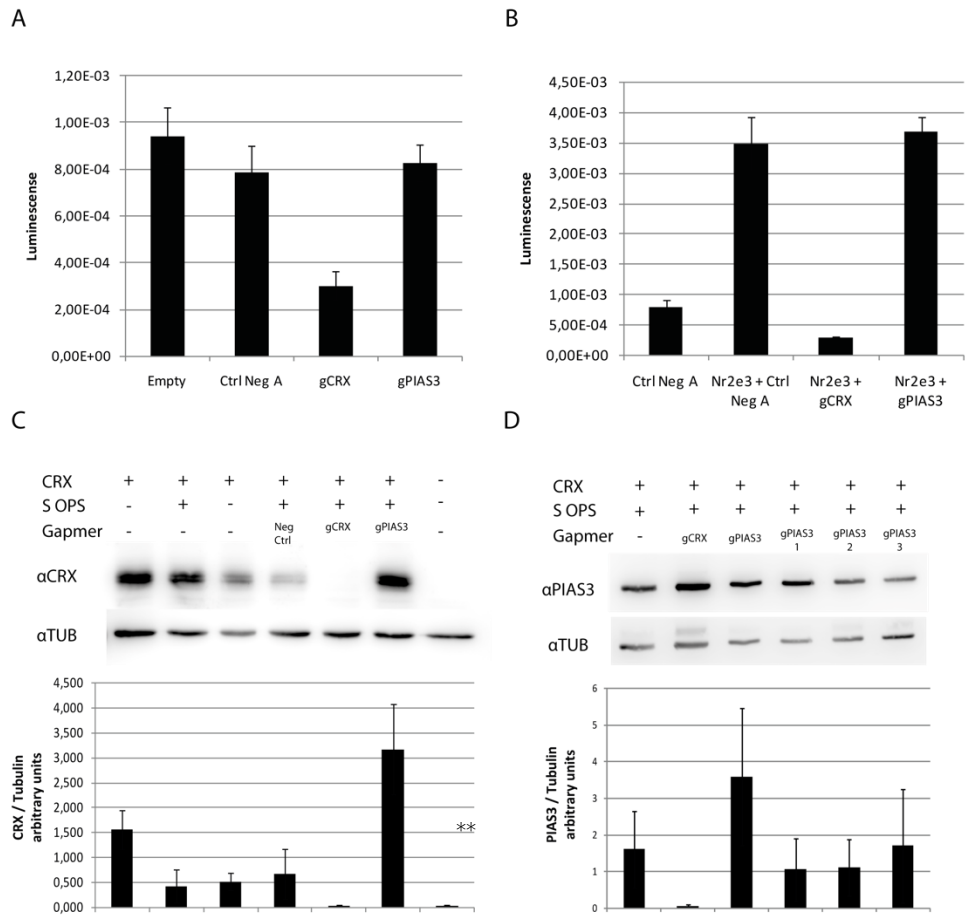

Figure 36. Gene silencing assays using Gapmers. A. Non-denatured cell lysates were used to perform luciferase assays and test transcription factor activity on the *S opsin* promoter, as well as the gene silencing efficiency of Gapmers against *CRX* or *PIAS3* compared to two different controls: empty (non-transfected cells) and a random sequence Gapmer, control NegA. **B.** Silencing of *NR2E3* in the same cell system, which was also co-transfected with NR2E3 retinal TF. A random sequence Gapmer, Control NegA, was used as a silencing negative control. **C.** Western blot immunodetection against CRX allowed us to assess the silencing efficiency of the Gapmers against CRX. This quantification is shown below. Each histogram bar corresponds to the upper Western blot lane. **D.** Validation of the silencing efficiency of the Gapmer against *PIAS3* using Western blot immunodetection against PIAS3. No decrease in *PIAS3* endogenous protein levels could be observed when using the three designed Gapmers, both together or separately. CRX protein quantification normalized to tubulin is also shown below. Each histogram bar corresponds to the upper Western blot lane.

As revealed by the quantification of the luciferase activity, the *S opsin* promoter was almost completely silenced when *CRX* was silenced, as expected. However, the silencing of *PIAS3* did not affect the activation of the promoter (Figure 36 A). As seen in Figure 36 B, the *S opsin* promoter activity was increased when NR2E3 was co-transfected and expressed together with CRX. However, the sole presence of NR2E3 was not sufficient to activate the promoter in the absence of CRX (Nr2e3 + gCRX in Figure 36 B). In this part of the experiment, the knockdown of *PIAS3* had, again, no effect on the activation of the *S opsin* promoter by CRX co-expressed with NR2E3.

Further validation of the gene knockdown was performed by Western blot, using antibodies against CRX (Figure 36 C) and PIAS3 (Figure 36 D); in both cases, tubulin was used as a loading control. According to our results, the gene silencing efficiency was much higher for the Gapmer against CRX than that for PIAS3, since the endogenous CRX levels were more diminished compared to those of the controls. After applying t-Student test analysis, no statistical differences could be detected in the reduction of CRX or PIAS3 protein levels when compared to the controls (p-value >0,05). In the case of CRX, no protein band was detected whatsoever in the immunodetection when silencing it with Gapmers; therefore, further experimental replicates need to be performed, to increase the sample number and be able to reach statistical differences.

When assessing CRX protein levels by Western blot (Figure 36 C), a statistically significant increase was found when using Gapmers against PIAS3 (p-value <0.01). Nonetheless, this increase in CRX protein levels

caused by the absence of PIAS3 might have been a technical artefact, for Gapmers against PIAS3 were proved to be ineffective, as previously mentioned (Figure 36 D).

When planning this approach, we first intended to test the silencing efficiency of Gapmers in a cell culture environment and afterwards, in an *in vivo* approach using mouse retinal explants. Once the efficiency was tested, the reasonable step was to silence any candidate DUB that we might have identified in our cell culture system assay. However, as no solid candidate gene was obtained at this point, no further experiments with Gapmers were performed.

CHAPTER 3. UNVEILING CRX POST-TRANSLATIONAL MODIFICATIONS.

1. EVIDENCES IN FAVOUR OF POST-TRANSLATIONAL MODIFICATIONS OF CRX

While validating the silencing efficiency of the Gapmers technology, two extremely close bands of CRX were detected (using an anti-CRX protein antibody, data not shown). Since we intended to immunodetect over-expressed CRX in transfected cultured cells, or even the endogenous CRX basal protein expression in HEK293, we did not expect several protein isoforms; thus, the finding was suggestive and warranted further consideration. To determine whether the double CRX band was due to any technical artefact, we immunodetected endogenous levels of CRX on mouse 661W, human MIO-M1, Y-79, HEK293 and HEK293T cells; together with mouse P30 and P60 retinal extracts (Figure 37).

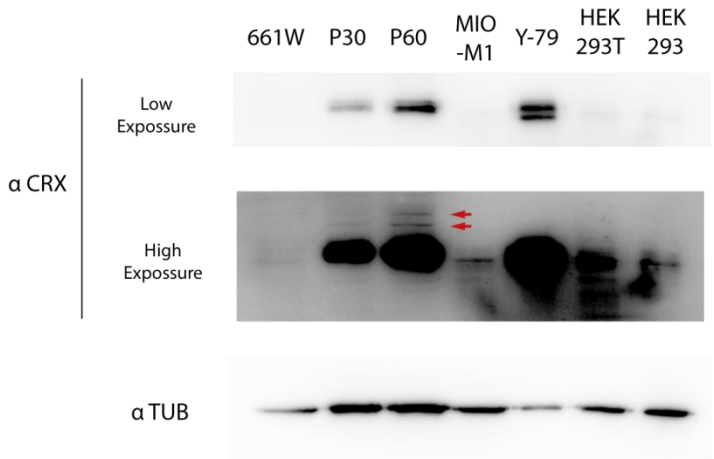

Figure 37. CRX expression in several mouse and human cell types as well as in the mouse retina. Endogenous CRX protein levels were immunodetected on adult mouse retina and on several cell types: mouse 661W cone precursor cells, human Y79 retinoblastoma cells, human MIO-M1 (derived from Müller cells), as well as human embryonic kidney cells (HEK293) and HEK293 cells transformed with the SV40 virus T antigen (HEK293T) cells. High and low exposure times were performed to detect faint intensity bands. Western blot against tubulin was used as a loading control.

In the low exposure immunodetection results, an upper mirror band was observed in both mouse P30 and P60 retinas; while a clear double band appeared in human Y-79 cells. Expression in the rest of type cells was too low to be assessed. However, in a higher exposure picture, CRX was detected in all cells, which all presented the mentioned mirror band, except for 661W cells, where the protein was not detected. Furthermore, in P30 and P60 retinas two faint, additional higher molecular weight bands were observed above the previously detected ones.

The two bands observed in the P30 and P60 stages correspond to the two mouse isoforms of CRX already reported, with a calculated molecular weight (MW) of 32.38 kDa and 34.98 kDa. Nonetheless, there is one single isoform

reported in humans, with an approximate molecular weight of 32.27 kDa. Therefore, the two bands detected in the HEK293 and HEK293T human cell lines probably corresponded to post-translationally modified forms of the protein. Relevant to this argument is the fact that CRX constructs transfected in HEK293 cells, also result in two immunodetected separate bands, regardless of the fact that the construction was expressing a single isoform as a cDNA sequence, and that no alternative splicing could be plausibly envisioned. The fact that CRX is post-translationally modified also *in vivo* was supported by the fainter higher molecular weight bands detected on retinal samples, which could be explained by modification with ubiquitin moieties or other post-translational modifications.

Concerning the two endogenous CRX-detected bands observed in cultured Y-79 human retinoblastoma cells, they might be explained as an abnormal transcription or alternative splicing event derived from their cluttered kariotype, which includes hypertriploidy with dicentric chromosomes and chromosomal breaks.

2. DETERMINATION OF SUMO AND/OR UBIQUITIN MODIFICATIONS OF CRX

From the above mentioned results, a possible post-translational modification of CRX via a small peptide-conjugation was suspected. To determine which type of pos-translational modification was tagging CRX, we designed immunoprecipitation assays. At first, and in order to determine whether the conjugation of a SUMO moiety was the possible post-translational modification of CRX, we performed an immunoprecipitation assay. In this

experiment, HEK293 cells were transfected with either 1) CRX, 2) CRX and HA-SUMO1, 3) CRX and HA-SUMO2, or 4) HA-SUMO2 alone. CRX was tagged with an XPRESS epitope; while SUMO constructs were tagged with an HA epitope, which was also used to immunoprecipitate SUMO from cellular lysates. Subsequently, samples were separated by electrophoresis, and immunoblotted against the XPRESS epitope to detect CRX in the immunoprecipitation outputs. As seen in Figure 38, no CRX band was detected in the outputs from the immunoprecipitation against SUMO-HA; thus, the post-translational modification observed in CRX was not due to the addition of a SUMO moiety.

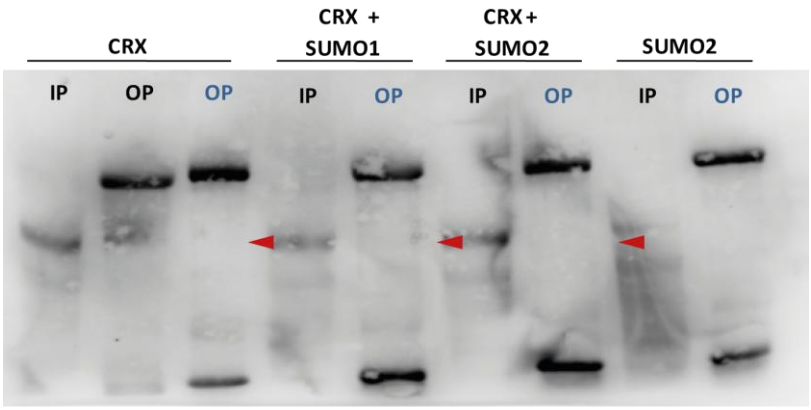

Figure 38. Co-Immunoprecipitation assays showed that CRX was not SUMOylated in cultured cells. HEK293 cells were transfected with constructs to express: 1) CRX, 2) CRX and SUMO1, 3) CRX and SUMO2 or 4) SUMO2. Immunoprecipitation was performed using antibodies against the HA-tag (which in this assay, it could bind SUMO and SUMO-conjugated proteins). The immunoblot was performed using an anti-XPRESS antibody to detect CRX. **IP**: input lysates containing total protein; **OP**: final eluted output from the immunoprecipitation. Red arrows indicate the position were the immunoprecipitated CRX band should appear if eluted in the immunoprecipitation. No band can be observed in any of the cases, indicating that CRX is not conjugated to SUMO moieties. **COIP**: Co - Immunoprecipitation; **WB**: immunodetection by Western Blot.

Simultaneously to the SUMO immunoprecipitation, we set up several immunoprecipitation assays to detect possible interactions with ubiquitin moieties. As in the case of SUMO, HEK293 cells were transfected with CRX and HA-ubiquitin or with HA-ubiquitin alone. To enrich the lysate in ubiquitinated proteins, a new condition was created adding MG132 to cells, to inhibit proteasomal degradation. An HA-antibody was used to immunoprecipitate ubiquitinated proteins, and subsequently, samples were immunoblotted against CRX. As a control, an immunoprecipitation test was also performed against CRX. In this case, a clear CRX band was detected in the outputs of both immunoprecipitations, demonstrating that CRX is post-translationally modified with ubiquitin (Figure 39).

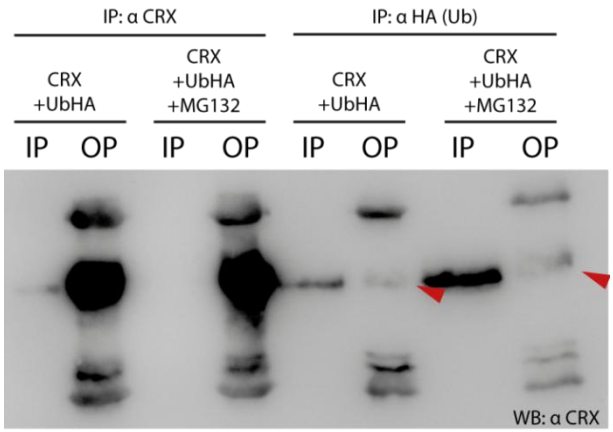

Figure 39. Co-Immunoprecipitation assays show that CRX is ubiquitinated in cultured cells. HEK293 cells were transfected with CRX (XPRESS tag) and ubiquitin (HA tag) with or without the proteasomal inhibitor MG132. Co-immunoprecipitation was performed simultaneously against CRX (positive control) and against HA (the later to immunoprecipitate Ub and Ub-conjugated proteins). Immunoblot detection was performed against CRX. Input (**IP**) lysates containing total protein, and the final eluted output (**OP**) after the immunoprecipitation were electrophoresed. The red arrows indicate the presence of the co-immunoprecipitated CRX in the outputs of lysates immunoprecipitated against ubiquitin (HA), thus indicating that CRX was ubiquitinated. **WB**: Western Blot immunodetection. **IP: α-X**: immunoprecipitation against X.

3. CRX MASS-SPECTOMETRY

To further investigate CRX ubiquitination sites and possible ubiquitin machinery linked to it, immunoprecipitation of CRX and consequent mass spectrometry assays were performed. Different independent approaches were carried out. In the first experiment, CRX was immunoprecipitated from HEK293 cells transfected with both CRX and HA-Ubiquitin constructs. In the second immunoprecipitation assay, P60 wild type mouse retinas were analyzed. No ubiquitinated peptides could be detected in any of the subsequent mass spectrometry assays, probably due to technical sample limitations.

To improve the sample quality, a third experiment was performed. HEK293 cells were transfected again together with CRX and HA-ubiquitin constructs, plus MG132, in order to inhibit proteasomal degradation and favour ubiquitinated protein forms; besides, siRNA against *USP18* was also co-transfected. At that moment, our working hypothesis was that USP18 (catalytically active) could rescue and increase the amounts of the key transcription factor CRX. However, no CRX ubiquitinated peptides were detected in this third experiment. Raw mass spectrometry data on CRX immunoprecipitation from adult WT mouse retina lysates can be found in the Annex II of the present work. CRX does appear in the list but no ubiquitinated peptides could be assigned to CRX.

Moreover, mass spectrometry was also performed to detect possible CRX interactors. As CRX is a transcription factor, most of the peptides found corresponded to transcriptional and translational protein complexes (Figure 40). From all the rest of interactors, both in cell culture and in retina, it is worth mentioning that deubiquitinating enzyme OTUB1 was detected in a

relatively high number of peptide counts; and also was OTUD6B. The finding of these two DUB enzymes in the immunoprecipitation of CRX turned them into good candidates for CRX regulation; besides, note that no peptide corresponding to USP18 was detected. Future work will consider on the function of OTUB1 and OTUD6B in CRX post-translational regulation.

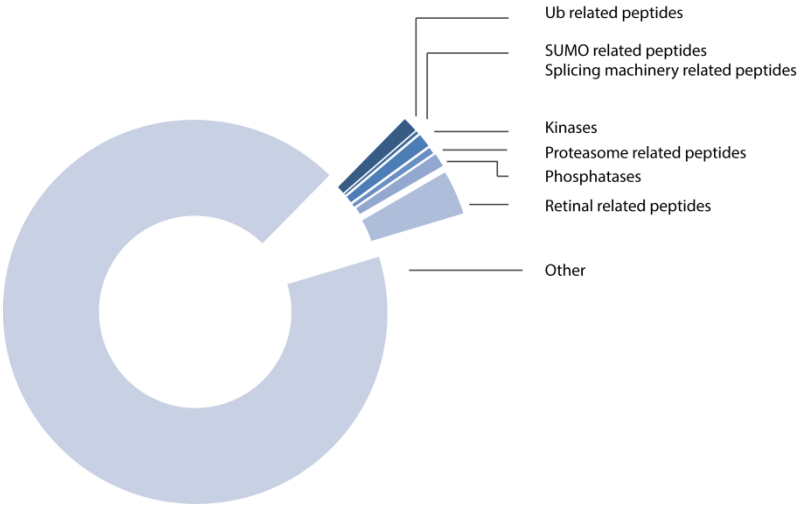

Figure 40. CRX-interacting proteins according to a mass spectrometry assay in mouse retina. Note that 1,3% of the total peptides corresponded to ubiquitin (Ub) related peptides, being either ligases, ubiquitin chains and deubiquitinating enzymes OTUB1 and OTUD6B.

Finally, we could demonstrate via co-immunoprecipitation assays that CRX was post-translationally modified by at least one ubiquitin moiety. Experiments with transfected HEK293 cells transfected with CRX and treated with proteasomal inhibitor MG132, showed that one of the roles of CRX ubiquitination is to determine its protein fate to proteasomal degradation. Furthermore, mass spectrometry experiments showed that CRX

immunoprecipitated with ubiquitin system machinery, including deubiquitinating enzymes OTUB1 and OTUD6B.

Future experiments need to be performed to determine the ligases and DUBs involved in the CRX ubiquitination and to clarify further physiological implication of this protein modification with Ub. With these results, we will be able to establish a new regulation point –due to post-translational modification of the CRX transcription factor– in photoreceptor development learning more about how this biological process occurs and possibly finding new clues for the aetiology of some retinal diseases.

Discussion

1. APPROACHING THE FUNCTION OF DUBS IN THE MOUSE RETINA PHYSIOLOGY AND DEVELOPMENT

The ubiquitin pathway is currently viewed as one of the most dynamic and versatile cell regulatory system in eukaryotes. Perturbations in the ubiquitin pathway are involved in many human disorders, among which cancer and neurodegeneration[76,77] have been extensively reported and investigated. Disruption of the ubiquitin pathway mainly causes accumulation of misfolded proteins or dysfunction of protein homeostasis, leading to cell cycle disruption or cell death. In this context, deubiquitinating enzymes (DUBs) may play a major role due to their ability to regulate the ubiquitin pathway and make it a reversible process. As supported by reports of systematic DUB knockdown in zebrafish embryos and flies[67,68] described in the results section of the present work, disruption of DUB genes has dramatic consequences for the animal taxa analyzed, either during development or in adult stages.

In mammals, several comprehensive surveys of DUBs have been reported resulting in a wide range of DUB structure, localization and function description. A recent review focused on the expression levels of DUBs in human organs and disease phenotypes associated to DUB mutations in humans and animal models[29]. However, despite their importance, detailed expression and functional analysis for most DUBs on particular tissues or organs, such as the retina, is still missing.

One of the main objectives of the present work was to fill this gap and produce a descriptive atlas of DUB expression, delineate an evolutionary and phenotypic landscape of the complete set of DUBs in the adult mouse retina,

and thus provide a reference framework for DUB enzymes in this neuronal tissue.

1.1. DEFINING A LANDSCAPE FOR DUB EXPRESSION IN THE MOUSE RETINA

Before knowing any roles DUBs might play in retina, our starting point was to describe the actual expression of DUBs in the adult mouse retina. Real Time RT-PCR (RT-qPCR), *in situ* hybridization and fluorescent immunohistochemistry experiments were performed to that end, which eventually allowed us to establish a defined DUB expression landscape. Notably, a wide variety of gene expression patterns were observed, pointing to specific retinal functions for each DUB.

First, it is important to understand that when working with such a particular tissue as it is the retina, certain technical aspects had to be taken into account: 1) the amount of tissue obtained per animal is very low and 2) the size and structural complexity of the retina, make it a very delicate working material. Therefore, we had to set up the methodology standards for the Real Time-qPCR and *in situ* hybridization procedures. For the first, three different retinal samples per each biological replicate had to be used, instead of one, to achieve both enough material and technical robustness for performing the RT qPCR. In the case of *in situ* hybridization, a big effort was invested in adapting the protocol to the fragility of the retinal sections. It is also worth noting that approaching RT qPCR as a high-throughput analysis has been largely improved in the last years, however, for *in situ* hybridization we had to consider reducing the number of analyzed genes to get as much information as possible and optimizing the time and effort invested. Moreover, the

number of analyzed DUBs was even narrowed when assaying protein localization, adapting it to the commercially available and functional antibodies.

Taken as a whole, we obtained highly valuable information on the expression of the DUBs in the adult mouse retina yet it represents a first approach. The techniques used allowed us to gain a general overview on the expression pattern of DUB genes in the adult mouse retina; however, other techniques need to be performed to finely define the expression in each one of the seven retinal cell types, as well as their subcellular localization. If these results were available, we would be able to hypothesize and learn more consistently about the role DUBs play in retinal physiology and development. In the following Discussion sections the possible roles of DUB enzymes in the mouse retina will be discussed, considering together information obtained from our results and from previously reported data.

1.1.1. LOW EXPRESSION LEVELS IN GENES INVOLVED IN THE CONTROL OF CELL REPLICATION AND DIVISION

Genes such as *Brcc36, Poh1, Bap1, Otub2,* and *Usp44* showed relatively low mRNA levels according to the RT qPCR results. This was consistent with their previously reported physiological role, since they are recruited to complexes that regulate DNA repair and mitosis checkpoints[56] during replication events; and the adult retina (from P21 onwards) is formed basically by post-mitotic and differentiated cells. The comparison of these results with those obtained in our RNA sequencing (RNA-seq) analyses helped to reinforce the data obtained in the mRNA expression results. In the cases of *Poh1, Bap1* and *Usp44*, a decrease of expression throughout

development was observed, thus supporting their functional role in replicative cells.

For the latter, some considerations must be also taken into account: the levels of expression of *Poh1* were considerably higher in the RNA-seq results than those observed in the RT qPCR. Both techniques are useful to quantify RNA levels and similar results are expected; therefore, these disparities might be due to technical differences in the corresponding protocols. Concerning *Otub2*, the expression in RNA-seq was indeed low, but a slight increase during development was observed; which indicate that it might not really be involved in the regulation of mitosis or the response to DNA damage during replication. *Brcc36* RNA-seq data was not processed. In any case, further experiments need to be performed to validate the physiological relevance of these hypotheses.

1.1.2. VARIABLE EXPRESSION LEVELS IN GENES INVOLVED IN NEURONAL PHYSIOLOGY

As the retina is a neural tissue, it is conceivable that some DUB genes have a general neural function and are as important for the retina as they are for the rest of the nervous system. Indeed these might be the case for *Otub1*, *Usp22* and *Usp33*, which are highly expressed in the retina, and have been previously described to be differentially expressed in the human brain[29]. Something similar occurs with *Uchl1*, *Atxn3* and *Usp6*, with differential expression in the human brain and high levels of expression in our RT qPCR results (although this is not so apparent in the RNA-seq data). Note that *Uchl1, Otub1* and *Atxn3* have been related to neurodegenerative diseases in human[78,79], namely Parkinson's disease (*Uchl1* and *Otub1*) and cerebellar ataxia (*Atxn3*), whose symptoms also include vision degeneration.

On the other hand, some genes are lowly expressed in the retina but have been described to be differentially expressed in the human brain, like *Mysm1*, *Usp26*, *Usp29*, *Usp35* or *Usp51*; suggesting a specific role in the CNS which does not include the retinal tissue. It is worth noting however, that a slight malfunction of a barely expressed gene might have functional implications for the retina, since high oxidative stress and protein turnover rates make the retina a very sensitive tissue, with a lower threshold to disease compared to other tissues.

1.1.3. LAYER-SPECIFIC EXPRESSION AND RETINAL FUNCTION

In situ hybridization and fluorescent immunohistochemistry showed that most DUBs are globally expressed, although a handful of them are differentially expressed in specific retinal layers. For instance, *Usp45*, *Usp53* and *Usp54* did show retinal layer specificity, as they were mainly expressed in the photoreceptors (PhR inner segment, ONL and OPL), suggesting a specific role for these genes in these highly specialized neurons and underscoring their role as potential candidates for visual disorders. The low expression of these genes observed in the RT qPCR might be explained by their expression being restricted to this layer, since photoreceptor cells represent a small percentage of the entire retina.

Complementary to the mRNA localization revealed by *in situ* hybridization, fluorescent immunohistochemical localizations also pointed to specific functions for some DUBs: e.g. OTUD4, which is highly localized in axons; TNFAIP3, highly expressed in the photoreceptor outer segment and GCL; and USP22, whose localization is mainly nuclear and perinuclear. These results again suggest that these genes may be good candidates for particular retinal phenotypes. On the other hand, they might also play a more general

role in the cellular physiology, since *Tnfaip3* and *Otud4* knockdown in zebrafish resulted in severe developmental alterations[68], and *Usp22* causes pup death in homozygous mice. Moreover, *Otud4* is mutated together with *Rnf216* in cerebellar ataxia and hypogonadotropic hypogonadism (Gordon Holmes syndrome)[70].

Not only, the localization patterns differ between some genes, but also a wide range of DUB expression levels was detected by Real Time qPCR, even between evolutionary close genes. Thus *Otud7a*, *Tnfaip3* and *Zranb1* showed low, medium and high levels of mRNA expression respectively; or the close *Usp31* and *Usp43* show medium and very low expression levels respectively. This variety of levels and patterns of expression in the mouse retina strongly suggest that DUBs have either substrate specificity, cell type specificity or might be required for differential requirements in the different retinal layers, and argue against DUB functional redundancy, as proposed after DUB knockout early experiments in yeast.

1.2. UNVEILING POSSIBLE ROLES FOR DUBS IN RETINAL DEVELOPMENT

As previously mentioned, the data obtained from RT qPCR, *in situ* hybridization and IHC in P60 mice retinas were a good starting point to define DUB gene and protein expression in adult mice retina. However, once these data was obtained and analyzed, further question aroused mainly about how this expression might vary during retinal development. Learning more about these variations, would help us understand which DUB genes might be important at which developmental stages. We could have approached this

question measuring RNA levels of the different developmental stages via RT qPCR, however, this would have supposed a major investment in time, cost and effort. Moreover, investing in a high-throughput RNA-sequencing was, at that moment, beyond our economic limits; fortunately, we were able to use Dr. Swaroop's data for our analysis.

As in the case of RT qPCR, RNA-Seq data revealed a wide variety of expression patterns: some DUB genes were only expressed at early embryonic stages while others were expressed throughout the development and adult stages, or not expressed at all. Some DUB genes showed activation in the transcription only from birth, and others showed differences when comparing rod and cone development, overall pointing to their possible involvement in the regulation of retinal development. Below, we discuss this variation and their possible implications in the physiology of the developing retina.

1.2.1. TRANSCRIPTOMIC ANALYSIS SHOWED A WIDE RANGE OF DUB EXPRESSION PATTERNS DURING RETINAL DEVELOPEMENT

RNA-seq analysis showed clear variations in the expression levels of DUB genes during mouse retinal development. For instance, *Usp37* or *Josd3* (*Traf1d*), highly expressed in embryonic stages but whose expression was shut down after birth; or *Zranb1* or *Usp32*, whose expression was extremely low at embryonic stages but clearly increased around and after birth date.

A possible explanation for these differences in gene expression is that *Usp37* and *Josd3* function might be important for the differentiation of certain cell types; thus, when those cells are finally differentiated, the action of these genes are no longer needed and consequently their expression levels drop. In

this context, the most feasible scenario is that they participate in the differentiation of cells like ganglion, horizontal or amacrine cells, which fully differentiate in mouse embryonic stages. Concerning *Zranb1* and *Usp32*, their increase from birth might be explained by two different possibilities: 1) either they are important for differentiation of rods, which peak by P2; or 2) they are rod-specific genes and thus, as the number of rods increases, their expression levels consequently increase.

Note that the cellular heterogeneity found in the retina makes it difficult to determine which gene is important for any particular cell type. Most RNA-seq data and RT qPCR data have been generated from total retinas, and consequently, genes expressed in most abundant cell types are overrepresented. Despite large efforts in recent years, the isolation and culture of precise retinal cell types has still to overcome technical difficulties, since these cells are very fragile and sensitive to environmental changes. However, the research group of Dr. Swaroop has long-standing expertise in isolating rod- and cone-like photoreceptors and they could approach differential transcriptomic analyses, making lists of genes that might be important for each type of cell.

Besides, genes such as *Usp14*, *Usp10*, *Josd1*, *Usp22* or *Usp39* switch off their expression in rods from P6, even though their expression is constant over time in cones. Therefore, these genes might be important for the maintenance of early photoreceptor fate, and when rods are finally differentiated, they might be no longer needed while cones might still express photoreceptor default pathway genes over time. Of note, becoming a cone is the default pathway, and the differentiation of rods needs active transcription of differential proteins. Another interesting case is *Usp48*, which is barely

expressed in rods at any of the analyzed stages, but its expression is always present in cone cells; defining a role in cone photoreceptor cells maintenance.

Usp11 presents a remarkable expression pattern during development. Considering the whole retina, its expression lowers slightly at final developmental stages, coincidentally with an expression switch-off observed in rods. Thus, the decrease observed in the total retina might be a consequence of the increase in the relative amount of rod cells in the retina rather than a general decrease of its expression in all cell types. As previously mentioned, the techniques used so far do not allow more precision to solve this issue.

Whether deubiquitinating enzymes participate together with specific TFs in key steps of the retinal development is still unclear and further experiments need to be performed. However, the RNA-seq results and the previous report of SUMO participating in NRL and NR2E3 modulation[46,47], together with knockout and knockdown models in zebrafish[68] and mice suggest the implication of DUBs in this tightly controlled regulatory network.

1.2.2. VALIDATING TRANSCRIPTOMIC ANALYSIS DATA PERFORMING *IN VIVO* EXPERIMENTS

To determine functional implication of selected DUB genes in the developing retina, we decided to directly assess this question in an *in vivo* experiment using mice. We could have also used cultured cells or retinal explants, but working directly with functional tissue would give us a completely physiologic framework; which we thought it was the best context

to analyze gene function. For this reason, we opted to silence genes via subretinal electroporation in P1 mice using shRNA and siRNA constructs.

The results obtained from the mouse subretinal electroporation experiments, although preliminary, showed no retinal affectation when knocking down *Josd1* and *Otud7b* genes; however, retinal rosettes were observed when silencing *Usp48*. This observed phenotype was interesting, since rosettes originate from the invagination of the distal retina and they are mostly due to cell overgrowth, and appear when retinal damage has occurred.

We wanted to prove these rosettes were generated due to the action of the siRNA used against *Usp48* and not due to damage caused during injection. However, we had obtained a very low cell electroporation efficiency in the retina when proceeding with subretinal microinjections. For this reason, we analyzed the possibility of using alternative methods, such as the vitreal injection. siRNA are not stable enough as to be injected vitreally and thus, we had to find further silencing methods.

Therefore, we designed new assays using a novel silencing method, the AONs (Antisense OligoNucleotides). With this, we aimed to obtain an increased transfection efficiency and a higher sample number to analyze and statistically support possible phenotypic aberrations.

Despite we have not yet performed these assays, we are optimistic about the results we might get because we have evidences in favour of a possible involvement of *Usp48* in retinal development since it shows: 1) a differential expression pattern in cone and rod development, with a shut down in rods at postnatal stages; 2) an strong ChIP seq peak with CRX (which means that the retinal-specific CRX TF binds to the *Usp48* promoter; 3) an altered

retinal phenotype when silenced in zebrafish; and 4) no previous functional or physiological role. For want of stronger evidences, we currently hypothesize that *Usp48* in maintenance of cone physiology.

2. GENERATING A CELL CULTURE SYSTEM TO SIMULATE RETINAL PHYSIOLOGICAL CONDITIONS

As mentioned, SUMO modifications have already been associated to the regulation of retinal transcription factors, such as NR2E3 and NRL. The SUMOylated fraction of these two TFs targets different retinal promoters and exerts the opposite function than the non-tagged fraction[46]. Considering that ubiquitin is structurally and functionally very close to SUMO, we hypothesized that ubiquitin –and the whole set of enzymes of the cycle, including deubiquitinating enzymes– similarly participated in the regulation of retinal promoters. Therefore, one of the main objectives of this thesis was to identify DUBs that might regulate key retinal genes via the regulation of the transactivation activity of retinal-specific transcription factors. We reasoned that the effect of post-translational modifications (such as ubiquitin) on TFs would be best checked by their transcriptional effect on the target promoters, and that this effect could be dissected and statistically evaluated if we used a reporter measurable gene (such as luciferase) to detect changes in transcriptional activity, and an in vitro cell system amenable to control conditions and parameters.

Moreover, considering the relatively large number of DUB genes described in the mouse and human genome (close to one hundredth), if we were to analyze all of them we would have to resort to high-throughput experimental approaches. The use of any animal model for high-throughput studies would

have implied a great investment of unavailable economical and temporal resources; thus, cell culture came out as the best of options. This rationale prompted us to generate a cell culture system easy to transfect, in which to "simulate" a retinal-like background to test the retinal TF activation upon a target promoter driving the expression of a reporter gene.

2.1. ESTABLISHMENT OF A RETINAL-LIKE CELL SYSTEM

The cell system we devised was based on the transfection of a retinal-specific promoter cloned upstream of the reporter luciferase gene, so that when the cotransfected the luciferase reporter together with retinal transcription factor constructs, variations on luciferase activity could be measured. If this basic system worked out, later on we could test the effect of DUBs' knockdown using RNA silencing methodologies. We surmised that most variations in the luciferase activity would be small and hard to be detected, thus, it was important to control as many variables as possible. For this reason, a thorough set up was planned in which cells, liposomes (our transfection vector of choice), retinal promoters and transcription factors were to be tested, in order to obtain the most optimized system.

Previous reports on luciferase activity experiments using retinal promoters had been already performed[44,75], and were taken as reference. Despite HEK293T were the cultured cells used in those seminal articles, retina-derived cultured cells appeared as the most physiological approach for the planned study. Therefore, the expression levels of retinal relevant genes were tested in 661W cone precursor cells, retinoblastoma Y79 cells, human precursor Müller MIO-M1 cells; together with HEK293 and HEK293T.

However, analysis experiments showed HEK293 as the best suitable cell lines; apart from that, they are also easy to handle and genetically manipulate.

Concerning the combination of retinal promoters and TFs, several tests were made taking into account previous works[75,44]. However, after assaying several transfection combinations, luciferase measurements for each condition were mostly highly variable and non reproducible. Finally, the combination of CRX (as the TF) and the *S opsin* promoter rendered the more reproducible results, which correlated with the physiological activity of CRX in the retina, where CRX activates the *S opsin* promoter.

Thus, our basic working in vitro system was: 1) HEK293 cells transfected with 2) the *S opsin* promoter (driving the expression of luciferase) 3) activated by CRX, a trans-activation activity that was quantified as an increase/decrease of luciferase activity. Once the system was set up, DUB and SUMO metabolism genes would be silenced using an exhaustive shRNA plasmid library, and changes on the luciferase activity reads would reflect activation/inactivation of the *S opsin* promoter due to the regulation of the CRX TF via conjugation of ubiquitin or SUMO.

2.2. shRNA-MEDIATED SILENCING OF DUBS AND SUMO GENES IN A RETINAL-LIKE CONTEXT

To perform the knockdown high-throughput assay, a selected shRNA library was used. Constructs against DUBs and SUMO pathway genes were used in the established transfection system. Unfortunately, after performing four experimental replicates no statistical differences could be observed after

silencing the selected genes. The levels of luciferase activity were rather "wild" and variable between replicates.

Looking closely to the results, the vector used as a control for the shRNA library, unexpectedly favoured some luciferase activity on its own. As previously mentioned, the negative control had to be cloned in the same vector as the rest of the tested shRNAs. We could not avoid using this control if using the high-throughput shRNA library. Even though we could not obtain statistically significant results in our attempts, it is feasible that if we could have changed the vectors for expression of the shRNAs to other vectors that did not interfere with our system, we could have identified some candidate while using the shRNA screening in our cell system. As it was, this is merely hypothetical.

Although these results were somewhat discouraging, deconvolution experiments were performed to determine if more consistent results could be obtained when using single shRNA constructs per condition. Again, not only no statistically differences were obtained, but also no consistency in the activation/inactivation of the *S opsin* promoter was observed. For instance, in some cases the luciferase activation obtained for a single transfected shRNA against a particular gene was the opposite to that observed when the three constructs for the same gene were transfected together.

We concluded that either the system was intrinsically too variable to measure any retinal TF activity with some consistency, or the expression from the shRNA constructs was drifty and therefore, extremely sensitive to environmental parameters that we were not controlling. In most cases, more intra- than inter-variability was detected and consequently, no further experiments were carried out using shRNA constructs.

2.3. siRNA-MEDIATED SILENCING OF DUBS IN A RETINAL-LIKE CONTEXT

To test another silencing method and possibly obtain more consistent results than those from the shRNA high-throughput silencing, siRNAs were assessed in our transfection system. siRNAs were available for 35 USP genes, and high-throughput silencing experiment was again performed.

In this case, the four experimental replicates performed rendered highly variable results, not within each experiment, but rather between the independent replicates. Therefore, the statistical analysis was incongruous as the standard deviation between experiments achieved maximum values. To sort out this high variability issue, only the values of luciferase activity from the two closest experiments results were considered. Dunnett's statistical test showed that *USP18* was the only tested USP with statistically significative differences compared to the control and the rest of DUBs. Therefore, we considered it a good candidate to contribute to the regulation of the *S opsin* promoter by CRX.

Several experiments were performed to assess the effects of USP18 upon CRX protein stability and ability to transactivate the *S opsin* promoter. The reduction of CRX protein levels when *USP18* was silenced was apparent. This was a very interesting result, as it meant that somehow USP18 was participating on the regulation of protein levels of CRX. However, the results of RNA-seq in physiological conditions in the developing retina, in the adult retina in mouse and human, as well as in cone and rods did not support that *USP18* was expressed in the retina. Therefore, the results obtained regarding the control of USP18 upon CRX protein stability were biochemically sound

(Figure 41) but unfortunately, did not seem to bear any real physiological sense in the retina.

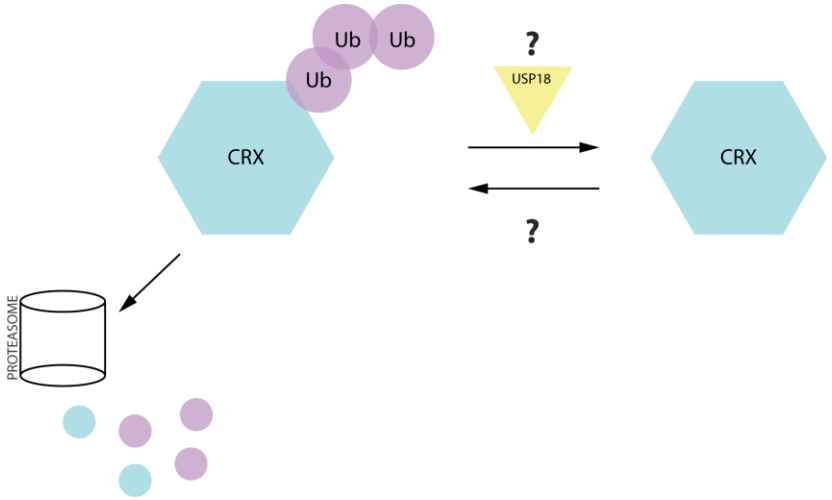

Figure 41. Hipothesis on USP18 regulation of ubiquitinated CRX. Our results obtained from transfections in HEK293 cells showed a clear relationship between CRX protein half-live and USP18. We hipothesised that most probably, USP18 rescues ubiquitinated CRX from proteasomal degradation. Unfortunatelly, retinal transcriptome analyze demonstrated that USP18 is not expressed in the mouse or human retina and therefore, this hypothesis did not bear any physiological sense.

2.4. ANALYSIS AND IMPROVEMENTS ON THE ESTABLISHED CELLULAR SYSTEM

In general, the cell system we designed had a good theoretical basis, since the bibliography supported: on the one hand, the study of retinal promoters via luciferase activation by retinal TFs[44,75], and on the other hand, the assay of knockdown methods in cell culture models had been widely proven. However, we detected several weak points throughout the procedures to study DUB function in the regulation of retinal promoters.

One main problem was the variability observed in the luciferase activity measurements, both in the initial experiments for deciding which combination of retinal promoter and TFs to be used; and later on, in the silencing experiments. This variability was eliminated or not disruptive in those cases were there was a strong transactivating effect of the TF upon the promoter, as was the case of CRX and the *S opsin* promoter. Nonetheless, when looking closer to the possibly small variations caused by the silencing of DUB genes, the results were not solid enough.

The possible causes for these non-conclusive results might have been that: 1) the whole devised cell system to study retinal gene regulation via DUBs was quite an indirect approach, which accumulated many control points that could fail; 2) the luciferase activity measurements might not be sensitive enough to detect faint changes; or 3) the silencing efficiency of shRNAs and siRNAs were not evaluated for each of the corresponding molecules on its own since a high-throughput screening was approached, which might have implied that effective silencing might not have been optimal for all the siRNA analyzed.

One must take into account, after all, that the system intended to evaluate the role any deubiquitinating enzyme might play on the regulation of a small proportion of CRX molecules. Thus, the knockdown of part of the active DUB protein might affect merely a small fraction of the ubiquitinated CRX molecules in the pool of CRX, and therefore, have a very slight effect on the promoter regulation, which need strongly unbiased and repetitive results to be detectable and statistically significant. On top of that, the detection system, with so many components, might not be sensitive enough to faint changes, so that no differences can be assessed when comparing to controls.

On the other hand, we should rationally consider the possibility that there is no such relationship between DUB enzymes, CRX transactivation activity and the *S opsin* promoter regulation. However, we must conclude that the present work does not provide enough scientific evidence to assure such affirmation. Therefore, our first hypothesis still stands up for evaluation, and further experiments should be performed using other functional approaches.

3. STUDY OF CRX POST-TRANSLATIONAL MODIFICATIONS

While working on USP18-dependent regulation of CRX protein stability, two different but close molecular weight bands were observed when performing Western blotting against CRX. To discard technical artefacts, more immunodetection assays were performed in several types of cells and mouse retinal samples. In all cases, the two bands were observed, and even two further upper bands were also detected in retina samples. Mice have only one single CRX mRNA isoform described, hence, a single protein should be translated and these observed bands ought to correspond to post-translational modifications of CRX. Furthermore, cultured cells were transfected with one construct containing a single cDNA isoform. Yet, two bands were again detected reinforcing the post-translational modification hypothesis.

Previous experience indicated that most possibly, this pattern of bands might correspond to post-translational modification with ubiquitin or ubiquitin-like peptides. Therefore, cell culture transfections including either CRX and HA-ubiquitin, or CRX and SUMO1 or SUMO2 constructs were undertaken. Subsequent immunoprecipitations against Ub or SUMO demonstrated that there was a fraction of CRX peptides that were indeed ubiquitinated while none were SUMOylated in our conditions.

Moreover, inhibition of proteasomal activity with MG132 treatment demonstrated that CRX was degraded via proteasome, meaning that ubiquitination tags CRX and targets this TF to proteasomal degradation. Concerning the interaction of DUBs with CRX, OTUB1 and OTUD6B were detected in the Mass Spectrometry experiments using whole retina

lysates; pointing them as possible regulators of the ubiquitination cycle of CRX (Figure 42). Were this regulation to occur, the hypotheses on how this control might work include: 1) that the two enzymes work to modulate CRX function via ubiquitin (Figure 42 A); 2) that the two enzymes modulate other proteins' function that might be working together in a complex with CRX (Figure 42 B); 3) that the two enzymes rescue CRX from proteasomal degradation (Figure 42 C). Of course, it might well be that both enzymes work together to fulfil a specific function, but most probably each of them might be exhorting only one. Overall, both enzymes might well be involved in CRX protein stability and function.

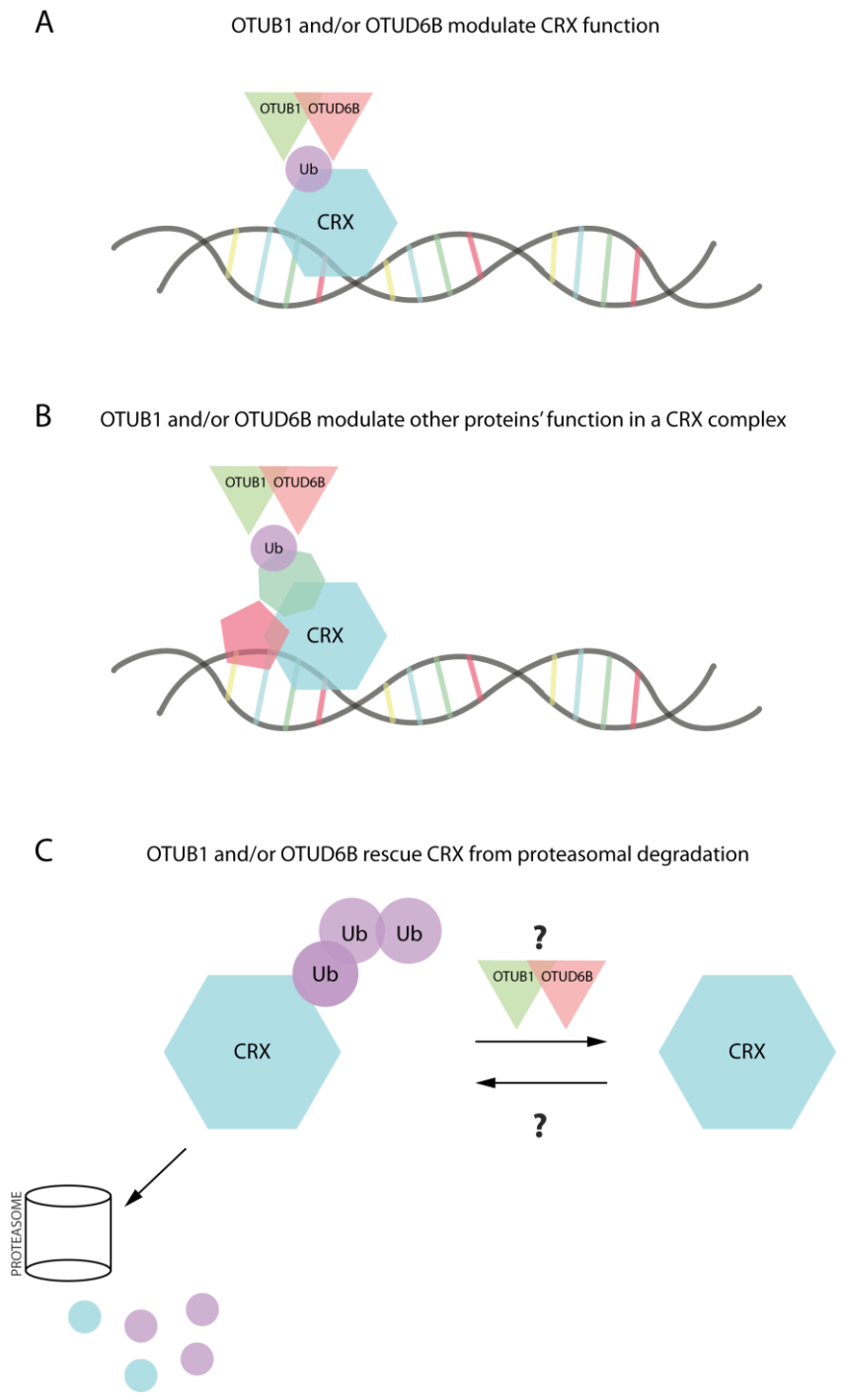

Figure 42. Model on a possible role of OTUB1 and OTUD6B in the CRX ubiquitination regulation. (Esquerdo, M; 2017)

While OTUB1 has been linked to cancer proliferation prognosis and very little is known about OTUD6B, none of them have been related to retinal function. As previously mentioned, OTUB1 contains other functional domains within its sequence and therefore, its function among CRX might not be related to its deubiquitinating activity. Overall, although the regulation of CRX protein is still unclear, we have provided some evidences that ubiquitination might be one of the mechanisms to regulate this TF activity or protein stability. Our results are intriguing enough to demand further work to unveil the exact mechanisms of interaction between CRX and these two DUB enzymes, the ligases involved in the reciprocal process of ubiquitination and the possible consequences of their interactions.

Conclusions

1. From the analysis of the involvement of deubiquitinating enzymes (DUBs) in the mouse retina:

I. The deubiquitinating enzymes (DUBs) present a wide range of expression in the adult WT mouse retina. This diversity is widespread among all 5 DUB families analyzed.

II. The analyzed DUBs present different mRNA expression pattern in the layers of the adult WT mouse retina. Most DUBs present a consistent mRNA expression in the photoreceptor layer (PhR), outer nuclear (ONL) and outer plexiform layers (OPL); while presence is the ganglion cell layer (GCL) is more variable.

III. The analyzed DUBs present a protein localization that correlates with that observed in mRNA localization experiments.

IV. Sequence and functional conservation analysis of DUBs through phylogenetic and phenotypic studies showed that a burst of gene expansion within all DUB families was at the basis of the vertebrate lineage.

V. The mutation or knockdown of a particular DUB gene that produces a relevant phenotype in one of the analyzed taxa, it usually replicates or provides a similar alteration in other analyzed organisms. In the cases of neuronal phenotype, there is an accompanying alteration in the eye.

VI. Transcriptomic analysis of DUBs' mRNA expression in the retina during development showed that DUB genes present differential expression patterns throughout retinal development in mouse and human. Some of the genes also presented differences of mRNA expression between the development of cones and rods.

VII. *Josd1*, *Otud7b*, *Usp22*, *Usp46* and *Usp48* were selected as good candidates for regulating mouse photoreceptor development

VIII. Preliminary analysis of the functional role of selected DUBs in mouse retinal development, via *in vivo* gene retinal electroporation, showed silencing of Usp48 caused retinal malformations by P21. Further experiments need to be performed to statistically validate these results.

2. From the design of an in-vitro retinal-like cell system to study the role of DUB enzymes on the regulation of retinal promoters:

I. A cell culture system was established to study the possible regulatory role of DUBs upon retinal promoters. In this system HEK293 cells were selected to be co-transfected with 1) the *S opsin* promoter cloned upstream of a luciferase gene, and 2) CRX, acting as an activating transcription factor.

II. High-throughput silencing of DUBs in the devised cellular system with shRNAs and siRNAs did not render consistent or reproducible results. Some of the analyzed genes seemed to act upon the *S opsin* promoter – CRX system (a tendency not yet statistically significant). Further experiments need to be performed to confirm these tendencies.

III. USP18 seemed to participate in the regulation of CRX half-life. Nonetheless, RNA-seq data barely detected any reliable expression of *USP18* in any developmental stage of the mouse and human retina. Therefore, the possible physiological relevance for the regulation of CRX via USP18 in the retina is extremely low.

IV. Gapmers® showed to be an efficient but rather expensive silencing technology.

3. From the identification of CRX post-translational modifications, particularly ubiquitination.

I. CRX is not post-translationally modified by SUMO 1 or SUMO2 in transfected human HEK293 cells.

II. CRX is post-translationally modified by ubiquitination in transfected human HEK293 cells.

III. Treatment of cells with the MG132 inhibitor showed that CRX ubiquitination is associated to its proteasomal degradation. Further experiments need to be performed to assess further roles of CRX ubiquitination.

IV. Immunoprecipitation experiments followed by mass spectrometry assays showed that CRX binds the deubiquitinating enzymes OTUB1 and OTUD6B. Future experiments need to be performed to determine the ligases and DUBs involved in the CRX ubiquitination.

Bibliography

. Swaroop, A., Kim, D. & Forrest, D. Transcriptional regulation of photoreceptor development and homeostasis in the mammalian retina. *Nat. Rev. Neurosci.* **11,** 563–76 (2010).

2. Wong, R. O. . & Godinho, L. in *The Visual Neurosciences* (ed. MIT Press) 77–93 (L.M. Chalupa, J.S. Werner (Eds.), 2003). at <http://nawrot.psych.ndsu.nodak.edu/Courses/Psych718.06/Readings/tvn_chap_006.pdf>

3. Reese, B. E. Development of the retina and optic pathway. *Vision Res.* **51,** 613–32 (2011).

4. Szél, A., Röhlich, P., Mieziewska, K., Aguirre, G. & van Veen, T. Spatial and temporal differences between the expression of short- and middle-wave sensitive cone pigments in the mouse retina: a developmental study. *J. Comp. Neurol.* **331,** 564–77 (1993).

5. Carter-Dawson, L. D. & LaVail, M. M. Rods and cones in the mouse retina. I. Structural analysis using light and electron microscopy. *J. Comp. Neurol.* **188,** 245–62 (1979).

6. Roorda, A. & Williams, D. R. The arrangement of the three cone classes in the living human eye. *Nature* **397,** 520–2 (1999).

7. Hendrickson, A. *et al.* Rod photoreceptor differentiation in fetal and infant human retina. *Exp. Eye Res.* **87,** 415–26 (2008).

8. Swaroop, A., Kim, D. & Forrest, D. Transcriptional regulation of photoreceptor development and homeostasis in the mammalian retina. *Nat. Rev. Neurosci.* **11,** 563–76 (2010).

9. Carter-Dawson, L. D. & LaVail, M. M. Rods and cones in the mouse retina. II. Autoradiographic analysis of cell generation using tritiated thymidine. *J. Comp. Neurol.* **188,** 263–72 (1979).

10. Huang, L. *et al.* Molecular genetics of cone-rod dystrophy in Chinese patients: New data from 61 probands and mutation overview of 163 probands. *Exp. Eye Res.* **146,** 252–258 (2016).

11. Arcot Sadagopan, K., Battista, R., Keep, R. B., Capasso, J. E. & Levin, A. V. Autosomal-dominant Leber Congenital Amaurosis Caused by a

Heterozygous CRX Mutation in a Father and Son. *Ophthalmic Genet.* **36,** 156–159 (2015).

12. Corton, M. *et al.* Identification of the Photoreceptor Transcriptional Co-Repressor SAMD11 as Novel Cause of Autosomal Recessive Retinitis Pigmentosa. *Sci. Rep.* **6,** 35370 (2016).

13. Haider, N. B. *et al.* Mutation of a nuclear receptor gene, NR2E3, causes enhanced S cone syndrome, a disorder of retinal cell fate. *Nat. Genet.* **24,** 127–131 (2000).

14. Newman, H. *et al.* Homozygosity for a Recessive Loss-of-Function Mutation of the *NRL* Gene Is Associated With a Variant of Enhanced S-Cone Syndrome. *Investig. Opthalmology Vis. Sci.* **57,** 5361 (2016).

15. Gerber, S. *et al.* The photoreceptor cell-specific nuclear receptor gene (PNR) accounts for retinitis pigmentosa in the Crypto-Jews from Portugal (Marranos), survivors from the Spanish Inquisition. *Hum. Genet.* **107,** 276–84 (2000).

16. Qin, Y. *et al.* Identification of a novel NRL mutation in a Chinese family with retinitis pigmentosa by whole-exome sequencing. *Eye* (2017). doi:10.1038/eye.2016.327

17. Xu, G. & Jaffrey, S. R. Proteomic Identification of Protein Ubiquitination Events. doi:10.1080/02648725.2013.801232

18. Marfany, G. & Denuc, A. To ubiquitinate or to deubiquitinate: it all depends on the partners. *Biochem. Soc. Trans.* **36,** 833–8 (2008).

19. Breitschopf, K., Bengal, E., Ziv, T., Admon, A. & Ciechanover, A. A novel site for ubiquitination: the N-terminal residue, and not internal lysines of MyoD, is essential for conjugation and degradation of the protein. *EMBO J.* **17,** 5964–73 (1998).

20. Cadwell, K. & Coscoy, L. Ubiquitination on nonlysine residues by a viral E3 ubiquitin ligase. *Science* **309,** 127–30 (2005).

21. Husnjak, K. & Dikic, I. Ubiquitin-Binding Proteins: Decoders of Ubiquitin-Mediated Cellular Functions. *Annu. Rev. Biochem.* **81,** 291–322 (2012).

22. Grau-Bové, X., Sebé-Pedrós, A. & Ruiz-Trillo, I. The eukaryotic ancestor had a complex ubiquitin signaling system of archaeal origin. *Mol. Biol. Evol.* **32,** 726–39 (2015).

23. Akutsu, M., Dikic, I. & Bremm, A. Ubiquitin chain diversity at a glance. *J. Cell Sci.* **129,** 875–880 (2016).

24. Meyer, H.-J. & Rape, M. Enhanced protein degradation by branched ubiquitin chains. *Cell* **157,** 910–21 (2014).

25. Clague, M. J. & Urbé, S. Ubiquitin: same molecule, different degradation pathways. *Cell* **143,** 682–5 (2010).

26. Gatti, M. *et al.* RNF168 promotes noncanonical K27 ubiquitination to signal DNA damage. *Cell Rep.* **10,** 226–38 (2015).

27. Komander, D., Clague, M. J. & Urbé, S. Breaking the chains: structure and function of the deubiquitinases. *Nat. Rev. Mol. Cell Biol.* **10,** 550–63 (2009).

28. Nijman, S. M. B. *et al.* A genomic and functional inventory of deubiquitinating enzymes. *Cell* **123,** 773–86 (2005).

29. Clague, M. J. *et al.* Deubiquitylases from genes to organism. *Physiol. Rev.* **93,** 1289–315 (2013).

30. Amerik, A. Y. & Hochstrasser, M. Mechanism and function of deubiquitinating enzymes. *Biochim. Biophys. Acta* **1695,** 189–207 (2004).

31. Makarova, K. A novel superfamily of predicted cysteine proteases from eukaryotes, viruses and Chlamydia pneumoniae. *Trends Biochem. Sci.* **25,** 50–52 (2000).

32. Sun, X.-X., Challagundla, K. B. & Dai, M.-S. Positive regulation of p53 stability and activity by the deubiquitinating enzyme Otubain 1. *EMBO J.* **31,** 576–92 (2012).

33. Tran, H., Hamada, F., Schwarz-Romond, T. & Bienz, M. Trabid, a new positive regulator of Wnt-induced transcription with preference for binding and cleaving K63-linked ubiquitin chains. *Genes Dev.* **22,** 528–42 (2008).

34. Wang, G., Sawai, N., Kotliarova, S., Kanazawa, I. & Nukina, N. Ataxin-3, the MJD1 gene product, interacts with the two human homologs of yeast DNA repair protein RAD23, HHR23A and HHR23B. *Hum. Mol. Genet.* **9,** 1795–803 (2000).

35. Abdul Rehman, S. A. *et al.* MINDY-1 Is a Member of an Evolutionarily Conserved and Structurally Distinct New Family of Deubiquitinating Enzymes. *Mol. Cell* **63,** 146–155 (2016).

36. Heideker, J. & Wertz, I. E. DUBs, the regulation of cell identity and disease. *Biochem. J.* **465,** (2015).

37. Kirkin, V. & Dikic, I. Role of ubiquitin- and Ubl-binding proteins in cell signaling. *Curr. Opin. Cell Biol.* **19,** 199–205 (2007).

38. Hochstrasser, M. Origin and function of ubiquitin-like proteins. *Nature* **458,** 422–9 (2009).

39. Bohren, K. M., Nadkarni, V., Song, J. H., Gabbay, K. H. & Owerbach, D. A M55V polymorphism in a novel SUMO gene (SUMO-4) differentially activates heat shock transcription factors and is associated with susceptibility to type I diabetes mellitus. *J. Biol. Chem.* **279,** 27233–8 (2004).

40. Owerbach, D., McKay, E. M., Yeh, E. T. H., Gabbay, K. H. & Bohren, K. M. A proline-90 residue unique to SUMO-4 prevents maturation and sumoylation. *Biochem. Biophys. Res. Commun.* **337,** 517–20 (2005).

41. Wilkinson, K. A. & Henley, J. M. Mechanisms, regulation and consequences of protein SUMOylation. *Biochem. J.* **428,** 133–45 (2010).

42. Wilkinson, K. A. & Henley, J. M. Mechanisms, regulation and consequences of protein SUMOylation. *Biochem. J.* **428,** 133–45 (2010).

43. Hay, R. T. SUMO. *Mol. Cell* **18,** 1–12 (2005).

44. Peng, G.-H., Ahmad, O., Ahmad, F., Liu, J. & Chen, S. The photoreceptor-specific nuclear receptor Nr2e3 interacts with Crx and exerts opposing effects on the transcription of rod versus cone genes. *Hum. Mol. Genet.* **14,** 747–64 (2005).

45. Hennig, A. K., Peng, G.-H. & Chen, S. Regulation of photoreceptor gene expression by Crx-associated transcription factor network. *Brain Res.* **1192,** 114–33 (2008).

46. Onishi, A. *et al.* NIH Public Access. **61,** 234–246 (2010).

47. Roger, J. E., Nellissery, J., Kim, D. S. & Swaroop, A. Sumoylation of bZIP transcription factor NRL modulates target gene expression during photoreceptor differentiation. *J. Biol. Chem.* **285,** 25637–44 (2010).

48. Schob, C. *et al.* Mutations in TOPORS: a rare cause of autosomal dominant retinitis pigmentosa in continental Europe? *Ophthalmic Genet.* **30,** 96–8 (2009).

49. Bowne, S. J. *et al.* Mutations in the TOPORS gene cause 1% of autosomal dominant retinitis pigmentosa. *Mol. Vis.* **14,** 922–7 (2008).

50. de Sousa Dias, M. *et al.* Detection of novel mutations that cause autosomal dominant retinitis pigmentosa in candidate genes by long-range PCR amplification and next-generation sequencing. *Mol. Vis.* **19,** 654–64 (2013).

51. Hugosson, T. *et al.* Phenotype associated with mutation in the recently identified autosomal dominant retinitis pigmentosa KLHL7 gene. *Arch. Ophthalmol.* **128,** 772–8 (2010).

52. Wen, Y. *et al.* Phenotypic characterization of 3 families with autosomal dominant retinitis pigmentosa due to mutations in KLHL7. *Arch. Ophthalmol.* **129,** 1475–82 (2011).

53. Campello, L., Esteve-Rudd, J., Cuenca, N. & Martín-Nieto, J. The ubiquitin-proteasome system in retinal health and disease. *Mol. Neurobiol.* **47,** 790–810 (2013).

54. Sowa, M. E., Bennett, E. J., Gygi, S. P. & Harper, J. W. Defining the human deubiquitinating enzyme interaction landscape. *Cell* **138,** 389–403 (2009).

55. Clague, M. J., Coulson, J. M. & Urbé, S. Cellular functions of the DUBs. *J. Cell Sci.* **125,** 277–86 (2012).

56. Nishi, R. *et al.* Systematic characterization of deubiquitylating enzymes for roles in maintaining genome integrity. *Nat. Cell Biol.* **16,** 1016–26, 1–8 (2014).

57. Finn, R. D. *et al.* Pfam: the protein families database. *Nucleic Acids Res.* **42,** D222-30 (2014).

58. Katoh, K. & Standley, D. M. MAFFT multiple sequence alignment software version 7: improvements in performance and usability. *Mol. Biol. Evol.* **30,** 772–80 (2013).

59. Darriba, D., Taboada, G. L., Doallo, R. & Posada, D. ProtTest 3: fast selection of best-fit models of protein evolution. *Bioinformatics* **27,** 1164–5 (2011).

60. Stamatakis, A. RAxML version 8: a tool for phylogenetic analysis and post-analysis of large phylogenies. *Bioinformatics* **30,** 1312–3 (2014).

61. Roger, J. E. *et al.* OTX2 loss causes rod differentiation defect in CRX-associated congenital blindness. *J. Clin. Invest.* **124,** 631–643 (2014).

62. ENCODE Project Consortium, I. *et al.* An integrated encyclopedia of DNA elements in the human genome. *Nature* **489,** 57–74 (2012).

63. Matsuda, T. & Cepko, C. L. Electroporation and RNA interference in the rodent retina in vivo and in vitro. *Proc. Natl. Acad. Sci. U. S. A.* **101,** 16–22 (2004).

64. Komander, D. The emerging complexity of protein ubiquitination. *Biochem. Soc. Trans.* **37,** 937–53 (2009).

65. Graziotto, J. J. *et al.* Three gene-targeted mouse models of RNA splicing factor RP show late-onset RPE and retinal degeneration. *Invest. Ophthalmol. Vis. Sci.* **52,** 190–8 (2011).

66. Abad-Morales, V., Domènech, E. B., Garanto, A. & Marfany, G. mRNA expression analysis of the SUMO pathway genes in the adult mouse retina. *Biol. Open* (2015). doi:10.1242/bio.201410645

67. Tsou, W.-L. *et al.* Systematic analysis of the physiological importance of deubiquitinating enzymes. *PLoS One* **7,** e43112 (2012).

68. Tse, W. K. F. *et al.* Genome-wide loss-of-function analysis of deubiquitylating enzymes for zebrafish development. *BMC Genomics* **10,** 637 (2009).

69. Strunnikova, N. V *et al.* Transcriptome analysis and molecular signature of human retinal pigment epithelium. *Hum. Mol. Genet.* **19,** 2468–86 (2010).

70. Margolin, D. H. *et al.* Ataxia, dementia, and hypogonadotropism caused by disordered ubiquitination. *N. Engl. J. Med.* **368,** 1992–2003 (2013).

71. Swanson, D. A., Freund, C. L., Ploder, L., McInnes, R. R. & Valle, D. A ubiquitin C-terminal hydrolase gene on the proximal short arm of the X chromosome: implications for X-linked retinal disorders. *Hum. Mol. Genet.* **5,** 533–8 (1996).

72. Slijkerman, R. W. *et al.* Antisense Oligonucleotide-based Splice Correction for USH2A-associated Retinal Degeneration Caused by a Frequent Deep-intronic Mutation. *89 Off. J. Am. Soc. Gene Cell Ther.* (2016). doi:10.1038/mtna.2016.89

73. Garanto, A. *et al. In vitro* and *in vivo* rescue of aberrant splicing in *CEP290* -associated LCA by antisense oligonucleotide delivery. *Hum. Mol. Genet.* **25,** ddw118 (2016).

74. Niks, E. H. & Aartsma-Rus, A. Exon skipping: a first in class strategy for Duchenne muscular dystrophy. *Expert Opin. Biol. Ther.* **17,** 225–236 (2017).

75. Cheng, H. *et al.* Photoreceptor-specific nuclear receptor NR2E3 functions as a transcriptional activator in rod photoreceptors. *Hum. Mol. Genet.* **13,** 1563–75 (2004).

76. Dantuma, N. P. & Bott, L. C. The ubiquitin-proteasome system in neurodegenerative diseases: precipitating factor, yet part of the solution. *Front. Mol. Neurosci.* **7,** 70 (2014).

77. Hussain, S., Zhang, Y. & Galardy, P. J. DUBs and cancer: the role of deubiquitinating enzymes as oncogenes, non-oncogenes and tumor suppressors. *Cell Cycle* **8,** 1688–97 (2009).

78. Puschmann, A. Monogenic Parkinson's disease and parkinsonism: clinical phenotypes and frequencies of known mutations. *Parkinsonism Relat. Disord.* **19,** 407–15 (2013).

79. Ristic, G., Tsou, W.-L. & Todi, S. V. An optimal ubiquitin-proteasome pathway in the nervous system: the role of deubiquitinating enzymes. *Front. Mol. Neurosci.* **7,** 72 (2014).

80. Tse, W. K. F. *et al.* Genome-wide loss-of-function analysis of deubiquitylating enzymes for zebrafish development. *BMC Genomics* **10,** 637 (2009).

81. Ishii, N. *et al.* Loss of neurons in the hippocampus and cerebral cortex of AMSH-deficient mice. *Mol. Cell. Biol.* **21,** 8626–37 (2001).

82. Homan, C. C. *et al.* Mutations in USP9X are associated with X-linked intellectual disability and disrupt neuronal cell migration and growth. *Am. J. Hum. Genet.* **94,** 470–8 (2014).

83. Schwickart, M. *et al.* Deubiquitinase USP9X stabilizes MCL1 and promotes tumour cell survival. *Nature* **463,** 103–7 (2010).

84. Adorno, M. *et al.* Usp16 contributes to somatic stem-cell defects in Down's syndrome. *Nature* **501,** 380–4 (2013).

85. Bingol, B. *et al.* The mitochondrial deubiquitinase USP30 opposes parkin-mediated mitophagy. *Nature* **510,** 370–5 (2014).

86. Yuasa-Kawada, J., Kinoshita-Kawada, M., Wu, G., Rao, Y. & Wu, J. Y. Midline crossing and Slit responsiveness of commissural axons require USP33. *Nat. Neurosci.* **12,** 1087–1089 (2009).

87. Tomida, S. *et al.* Usp46 is a quantitative trait gene regulating mouse immobile behavior in the tail suspension and forced swimming tests. *Nat. Genet.* **41,** 688–695 (2009).

Annex I

ARTICLE #1

TITLE

"Expression atlas of the deubiquitinating enzymes in the adult mouse retina, their evolutionary diversification and phenotypic roles."

AUTHORS

Mariona Esquerdo, Xavier Grau-Bové, Alejandro Garanto, Vasileios Toulis, Sílvia Garcia-Monclús, Erica Millo, Mª José López-Iniesta, Víctor Abad-Morales, Iñaki Ruiz-Trillo, Gemma Marfany

REFERENCE

PLoS One. 2016 Mar 2;11(3):e0150364. doi: 10.1371/journal.pone.0150364. eCollection 2016.

ABSTRACT

Ubiquitination is a relevant cell regulatory mechanism that determines protein fate and function. Most data has focused on the role of ubiquitin as a tag molecule to target substrates to proteasome degradation, and on its impact in the control of cell cycle, protein homeostasis and cancer. Only recently, systematic assays have pointed to the relevance of the ubiquitin pathway in the development and differentiation of tissues and organs, and its implication in hereditary diseases. Moreover, although the activity and composition of ubiquitin ligases has been largely addressed, the role of the deubiquitinating enzymes (DUBs) in specific tissues, such as the retina, remains poorly known. In this work, we performed a systematic analysis of

the transcriptional levels of DUB genes in the adult mouse retina by RT qPCR and analyzed the expression pattern by *in situ* hybridization and fluorescent immunohistochemistry, thus providing a unique spatial reference map of retinal DUB expression. To provide a wider view of possible DUB roles in the retina, we aimed to relate the evolutionary landscape and gene expansions within the DUBs families with the reported phenotypes in the eye and other neural tissues. Overall, our results constitute a reference framework for further characterization of the DUB roles in the retina and suggest new candidates for inherited retinal disorders.

CONTRIBUTION TO THE WORK

Although I have performed most of the work of this article, several other people in Dr. Marfany's group have contributed to some figures, as well as Xavier Grau-Bové from Dr. Ruiz-Trillo's group. My personal contribution has been: a) the Real Time qPCR for all DUB genes (Figure 13; Article Figure 1); b) *in situ* hybridization of all OTU family members and several genes from the JAMM, UCH and USP families (Figure 14; Article Figure 2); c) immunohistochemistry for all analyzed genes (Figure 15; Article Figure 3); d) bibliographic analysis of retinal and neuronal phenotypes in mutant animal models and in human: phenotypes in Figure 16 (article Figure 4) and article Supplementary Table 2).

PLOS ONE

RESEARCH ARTICLE

Expression Atlas of the Deubiquitinating Enzymes in the Adult Mouse Retina, Their Evolutionary Diversification and Phenotypic Roles

Mariona Esquerdo[1], Xavier Grau-Bové[1,2], Alejandro Garanto[1¤a], Vasileios Toulis[1], Sílvia Garcia-Monclús[1¤b], Erica Millo[1], Ma José López-Iniesta[1,3], Víctor Abad-Morales[1], Iñaki Ruiz-Trillo[1,2,4], Gemma Marfany[1,3,5]*

1 Departament de Genètica, Facultat de Biologia, Universitat de Barcelona, Barcelona, Spain, **2** Institut de Biologia Evolutiva (CSIC- Universitat Pompeu Fabra), Barcelona, Spain, **3** Centro de Investigación Biomédica en Red de Enfermedades Raras (CIBERER), Instituto de Salud Carlos III, Barcelona, Spain, **4** Institució Catalana de Recerca i Estudis Avançats (ICREA), Barcelona, Spain, **5** Institut de Biomedicina de la Universitat de Barcelona (IBUB), Barcelona, Spain

¤a Current address: Radboud University Medical Center, Radboud Institute for Molecular Life Sciences, Department of Human Genetics, Nijmegen, The Netherlands
¤b Current address: Sarcoma research group, Molecular Oncology Lab, Bellvitge Biomedical Research Institute (IDIBELL), L'Hospitalet de Llobregat, Barcelona, Spain
* gmarfany@ub.edu

Citation: Esquerdo M, Grau-Bové X, Garanto A, Toulis V, Garcia-Monclús S, Millo E, et al. (2016) Expression Atlas of the Deubiquitinating Enzymes in the Adult Mouse Retina, Their Evolutionary Diversification and Phenotypic Roles. PLoS ONE 11 (3): e0150364. doi:10.1371/journal.pone.0150364

Editor: Alfred S Lewin, University of Florida, UNITED STATES

Received: November 10, 2015

Accepted: February 12, 2016

Published: March 2, 2016

Data Availability Statement: All relevant data are within the paper and its Supporting Information files.

Funding: This study was supported by grants BFU2010-15656 (MICINN) and SAF2013-49069-C2-1-R (MINECO) to G.M., and 2014SGR-0932 (Generalitat de Catalunya) grant (BFU-2011-23434) from Ministerio de Economía y Competitividad (MINECO) and co-funded by the Fondo Europeo de Desarrollo regional (FEDER) to I.R-T. The funders had no role in study design, data collection and analysis, decision to publish, or preparation of the manuscript.

Abstract

Ubiquitination is a relevant cell regulatory mechanism to determine protein fate and function. Most data has focused on the role of ubiquitin as a tag molecule to target substrates to proteasome degradation, and on its impact in the control of cell cycle, protein homeostasis and cancer. Only recently, systematic assays have pointed to the relevance of the ubiquitin pathway in the development and differentiation of tissues and organs, and its implication in hereditary diseases. Moreover, although the activity and composition of ubiquitin ligases has been largely addressed, the role of the deubiquitinating enzymes (DUBs) in specific tissues, such as the retina, remains mainly unknown. In this work, we undertook a systematic analysis of the transcriptional levels of DUB genes in the adult mouse retina by RT-qPCR and analyzed the expression pattern by *in situ* hybridization and fluorescent immunohistochemistry, thus providing a unique spatial reference map of retinal DUB expression. We also performed a systematic phylogenetic analysis to understand the origin and the presence/absence of DUB genes in the genomes of diverse animal taxa that represent most of the known animal diversity. The expression landscape obtained supports the potential subfunctionalization of paralogs in those families that expanded in vertebrates. Overall, our results constitute a reference framework for further characterization of the DUB roles in the retina and suggest new candidates for inherited retinal disorders.

Competing Interests: The authors have declared that no competing interests exist.

Introduction

Ubiquitination is a dynamic regulatory mechanism that controls cell processes such as protein quality control (via proteasome degradation), cellular signalling, transcriptional regulation or DNA repair [1–3]. As ubiquitination is reversible, cells deploy a large set of enzymes to conjugate (E1, E2 and E3 ligases) and deconjugate (deubiquitinating enzymes) ubiquitin moieties [4]. The human genome contains several hundreds of ubiquitin ligases, and close to 80 deubiquitinating enzymes (DUBs), indicating that: i) ubiquitination is a highly regulated process, and ii) substrate recognition specificity is inherent to the system.

Most data on the physiological relevance of ubiquitin has focused on its role as the tag molecule to target substrates to proteasome degradation, its role in cell cycle control and cancer, as well as its involvement in the molecular basis of neurodegenerative disorders [5,6]. Besides, a number of high-throughput approaches have focused on finding substrates for either ligases [7] or deubiquitinating enzymes (DUBs) [8]. Nonetheless, most high-throughput studies have been performed *in vitro* using mammalian cell cultures, and only recently, systematic assays in animal models have indicated the relevance of the ubiquitin pathway in the development, differentiation and maintenance of tissues and organs [9,10].

One of the tissues that requires a tight gene and protein regulation is the retina. The retina consists of structured layers of highly specialized neurons in the eye that capture and process light stimuli enabling vision [11]. Such a fine architecture turns retinal differentiation into an extremely complex mechanism that must be accurately regulated [12], and in which ubiquitin and ubiquitination play a relevant role. In fact, mutations in the genes encoding the E3 ligases TOPORS [13–15] and KLHL7 [16,17]; and in PRPF8, which belongs to the JAB1-MPN--MOV34 (JAMM) family of DUBs, are causative of the most prevalent retinal hereditary dystrophy, retinitis pigmentosa (RP). Moreover, protein homeostasis via the ubiquitin-proteasome system is also relevant to other retinal diseases and specific altered protein degradation has been associated to Stargardt's disease, age-related macular degeneration, glaucoma, diabetic retinopathy, and retinal inflammation (reviewed in [18]).

Lately, DUBs are becoming the focus of attention given that their specificity in substrate selection makes them key checkpoints of protein degradation and fate. Moreover, their fewer numbers (compared to E2 and E3 ligases) makes their functional analysis more feasible. An increasing number of reports propose DUBs as pharmacological targets in disease: cancer [19–21] and neurodegenerative diseases [6]. DUBs are classified into five different subfamilies depending on their catalytic domains [22]: Machado-Joseph Disease protein domain proteases (MJD), Ovarian Tumor proteases (OTU), Ubiquitin C-Terminal Hydrolases (UCH) and Ubiquitin-Specific Proteases (USP) are cysteine proteases, whereas JAB1/MPN/MOV34 family proteases (JAMM) are Zn^{2+} metalloproteases; overall adding up to 90 genes in the human genome, of which only 79 are predicted to be functional [1].

A recent review compiled the gathered knowledge of the functional roles of individual DUBs, focusing on their subcellular localization, levels of expression in human tissues, and gene mutation phenotype in human and model organisms [23], yet a comprehensive study on the expression pattern of DUBs in highly specialized tissues, such as the retina, has not been performed. Besides, previous comparisons of DUB mutant phenotypes in different model organisms attempt to directly assign, without a phylogenetic framework, orthology and function between invertebrate and vertebrate genes. Some of these assignments may need revision under robust phylogenetic data, since ubiquitin ligase and protease families have expanded in eukaryotes [24], and subfunctionalization and neofunctionalization are known to occur after gene expansion.

Thus, we here aimed to draw an expression pattern map for DUB genes in the mouse retina, by using RT-qPCR, *in situ* hybridization and immunohistochemistry. We have also applied comparative genomics to infer the basic protein domain architecture within the DUB subfamilies and illustrate their diversification within metazoans. These data combined with the reported phenotypes will help to identify relevant retinal genes and potential new candidates for retinal diseases. Overall, we provide a comprehensive reference framework on DUB function and their roles in neuronal tissues that will be useful for future functional and evolutionary studies.

Material and Methods

Ethics statement

All procedures in mice were performed according to the ARVO statement for the use of animals in ophthalmic and vision research, as well as the regulations of the Animal Care facilities at the Universitat de Barcelona. The protocols and detailed procedures were evaluated and approved by the Animal Research Ethics Committee (CEEA) of the Universitat de Barcelona (our institution), and were submitted and also approved by the Generalitat de Catalunya (local Government), with the official permit numbers DAAM 6562 and 7185.

Animal handling, tissue dissection and preparation of samples

Murine retina samples and eye slides were obtained from 2 month-old C57BL/6J (wild-type) and CD-1 (albino) animals. Animals were euthanized by cervical dislocation. Some retinas were dissected and immediately frozen in liquid nitrogen, while the rest were fixed in 4% paraformaldehyde (PFA) for 2 h at room temperature (RT), washed, cryoprotected overnight in acrylamide at 4°C, embedded in O.C.T. (Tissue-Tek, Sakura Finetech, Torrance, CA), frozen in liquid nitrogen and sectioned at -17°C.

RNA extraction and cDNA synthesis

For each sample, retinas from three different animals were pooled. Therefore, up to 9 animals in three independent replicates were analyzed. Retinas were homogenized using a Polytron PT 1200 E homogenizer (Kinematica, AG, Lucerne, Switzerland). Total RNA was extracted using the High Pure RNA Tissue Kit (Roche Diagnostics, Indianapolis, IN) following the manufacturer's instructions with minor modifications (increasing the DNAse I incubation step). Reverse transcription reactions were carried out using the qScript cDNA Synthesis Kit (Quanta Biosciences) following the manufacturer's protocol.

RT-qPCR

Quantitative reverse transcription PCR (RT-qPCR) was performed using the LightCycler® 480 SYBR Green I Master Mix (Roche Applied Science) and a LightCycler® 480 Multiwell Plate 384. The final reaction volume was 10 μl. Raw data was analyzed with the LightCycler® 480 software using the Advanced Relative Quantification method. *Gapdh* expression was used to normalize the levels of expression. *Rho* and *Cerkl* were considered as reference genes with high and low levels of expression, respectively, in the mouse retina. Three independent samples replicates were analyzed for each gene. Differences in gene expression levels within the same sample and between the samples were directly compared by their Z-score values. The mean and standard deviation of the Z-scores are plotted in Fig 1. The name and sequence of all the primers used for RT-qPCR and *in situ* hybridization are listed in S1 Table.

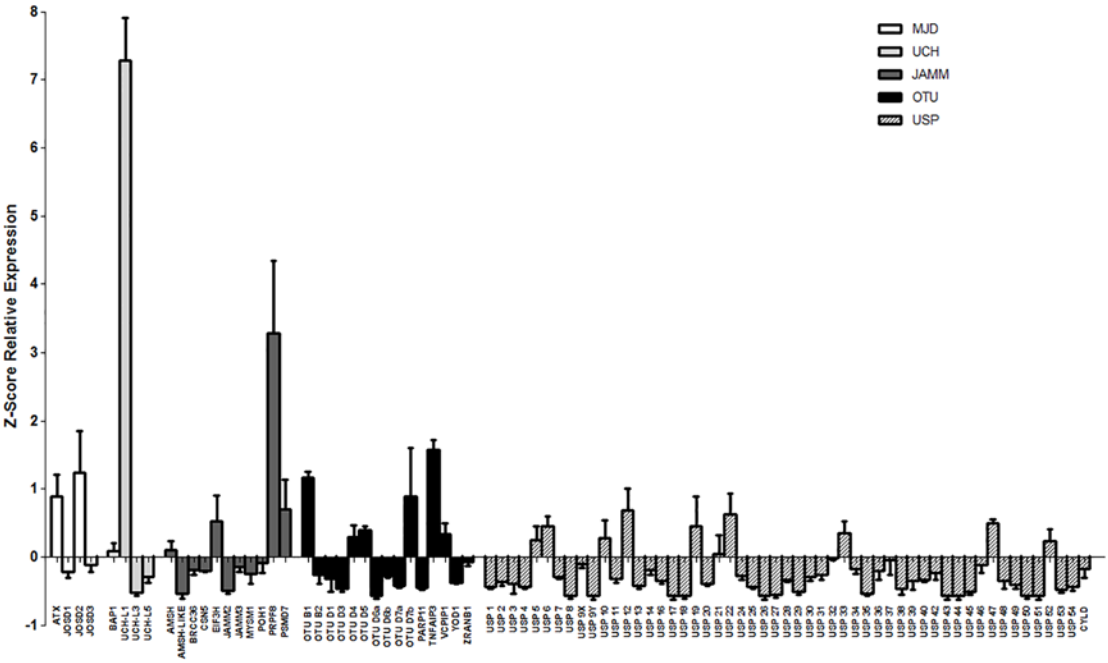

Fig 1. Relative expression levels of the five subfamilies of DUB enzymes. Gene expression values are the average of three independent samples (measured in three replicates), each sample contained retinas from three individuals. The expression levels are obtained as a ratio with *Gapdh* expression (used for normalization) per 10^4. The Z-score has been calculated for the whole set of genes per each sample, and mean and standard deviation has been obtained, so that the results can be directly compared among them. Negative values indicate when genes are expressed below the global mean of the gene expression obtained in the analysis, and positive values when genes are more highly expressed. To simplify the comparison, the graph starts at the negative values, being 0 the mean value of gene expression for the whole set of genes (87 in total) in each sample. **JAMM**- JAB1/MPN/MOV34 motif proteases; **MJD**- Machado-Joseph Disease protein domain proteases; **UCH**- Ubiquitin C-Terminal Hydrolases; **OTU**- Ovarian Tumor proteases; **USP**- Ubiquitin-Specific Proteases.

doi:10.1371/journal.pone.0150364.g001

In situ hybridization

For *in situ* hybridization (ISH), 16–18μm sections were recovered on commercial Superfrost Plus glass slides (Electron Microscopy Sciences, Hatfield, PA), dried 1 h at RT, rinsed three times for 10 min with phosphate-buffered saline (PBS), treated with 2 μg/ml proteinase K for 15 min at 37°C, washed twice for 5 min with PBS, and fixed with 4% PFA. Acetylation with 0.1 M triethanolamine-HCl (pH 8.0) containing first 0.25%, and then 0.5% acetic anhydride, was performed for 5 min each. Hybridization was carried out overnight at 55°C with digoxigenin-labelled riboprobes (2 μg/ml) in 50% formamide, 1 x Denhardt's solution, 10% dextran-sulfate, 0.9 M NaCl, 100 mMTris-HCl (pH 8.0), 5 mM EDTA (pH 8.0), 10 mM NaH_2PO_4, and 1 mg/ml yeast tRNA. For each gene, cDNA fragments generated by RT-PCR of approximately 400-700bp were subcloned into the pGEM-T® Easy Vector (Promega) and sense and antisense riboprobes were generated from the flanking T7 RNApol promoter. The name and sequence of all the primers used for RT-qPCR and *in situ* hybridization are listed in S1 Table.

After hybridization, the slides were washed in 2x SSC for 20 min at 55°C, equilibrated in NTE (0.5 M NaCl, 10 mM Tris-HCl pH 8.0, 5 mM EDTA) at 37°C, and then treated with 10 μg/ml RNase A in NTE at 37°C for 30 min. Subsequently, the sections were washed at 37°C in NTE for 15 min, twice in 2x SSC and 0.2x SSC for 15 min each, equilibrated in Buffer 1 (100 mM Tris-HCl pH 7.5, 150 mM NaCl), and blocked in Blocking Buffer (1% BSA and 0.1% Triton X-100 in buffer 1) for 1 h at RT. An anti-digoxigenin-AP conjugate antibody (1:1000; Roche Diagnostics, Indianapolis, IN) in Blocking Buffer was incubated overnight at 4°C. The sections were then washed twice in Buffer 1 for 15 min, once in Buffer 2 (100 mM Tris-HCl pH

9.5, 150 mM NaCl), and once in Buffer 2 supplemented with 50 mM $MgCl_2$ (5 min each) prior to adding the BM Purple AP Substrate (Roche Diagnostics, Indianapolis, IN). For each gene, antisense and sense ISH staining reactions were processed in parallel. The reaction was stopped in 1x PBS. Sections were cover-slipped with Fluoprep (Biomérieux, France) and photographed using a Leica DFC Camera connected to a Leica DM IL optic microscope (Leica Microsystems, Germany).

Fluorescent immunohistochemistry

For retina immunofluorescence, 16 μm sections were recovered on commercial Superfrost Plus glass slides (Electron Microscopy Sciences, Hatfield, PA), dried 30–45 min at RT, washed 10 min with PBS and blocked for 1 h with Blocking Buffer (2% Sheep Serum and 0.3% Triton X-100, in PBS 1x). Primary antibodies were incubated overnight at 4°C with Blocking Buffer. After incubation, slides were washed with PBS (3 x 10 min) and treated with DAPI (Roche Diagnostics, Indianapolis, IN) (1:300) and with secondary antibodies conjugated to either Alexa Fluor 488 or 561 (Life Technologies, Grand Island, NY) (1:300). After secondary antibody incubation slides were washed again in PBS (3 x 10min). Sections were mounted in Fluoprep and analyzed by confocal microscope (SP2, Leica Microsystems).

Primary antibodies and dilutions used were: 1:50 Rabbit anti-JOSD2 (Aviva Systems Biology); 1:50 Rabbit anti-JOSD3 (Aviva Systems Biology), 1: 50 Rabbit anti-ATXN3 (in house, a gift from Dr. S. Todi); 1:20 Rabbit anti-BAP1 (Abcam); 1:100 Rabbit anti-OTUD4 (Abcam ab106368), 1:100 Rabbit anti-PRPF8 (Abcam ab79237), 1:100 Rabbit anti-TNFAIP3 (Abcam ab74037), 1:100 Rabbit anti-UCHL3 (Abcam ab126703), 1:100 Rabbit anti-USP9X (Abcam ab19879), 1:100 Rabbit anti-USP13 (Abcam ab109264), 1:50 Rabbit anti-USP16 (Abcam ab135509), 1:100 Rabbit anti-USP22 (Abcam ab4812), 1:300 Rabbit anti-USP25 (in house), 1:250 Rabbit anti-USP28 (ABGEN AP2152b).1:500 for Mouse anti-Rhodopsin (Abcam, Cambridge, UK). Antibodies against AMSH (Biorbyt orb101007), JAB1 (Abcam ab12323), OTUB1 (Abcam ab76648), OTUD1 (Abcam ab122481), POH1 (Abcam ab8040), USP5 (Abcam ab154170) and USP45 (Novusbio H00085015) did not produce reproducible results.

Phylogenetic analyses

Protein sequences from each enzyme group were queried in complete genome sequences of 14 animal taxa (*Homo sapiens*, *Mus musculus*, *Danio rerio*, *Petromyzon marinus*, *Branchiostoma floridae*, *Saccoglossus kowalevskii*, *Strongylocentrotus purpuratus*, *Drosophila melanogaster*, *Daphnia pulex*, *Caenorhabditis elegans*, *Lottia gigantea*, *Capitella teleta*, *Nematostella vectensis* and *Acropora digitifera*) using the HMMER 3.1 algorithm. For each analyzed enzyme family (USP, UCH, OTU, MJD and JAMM) we searched all proteins containing the Hidden Markov motifs of their catalytic region as defined in Pfam (UCH/UCH_1, Peptidase_C12, OTU/Peptidase_C65, Josephin and JAB domains, respectively). Protein domain architectures of each retrieved protein were then computed using Pfamscan 1.5 and Pfam 27 database [25] of protein domains.

We aligned the catalytic region of each enzyme family using Mafft 7 L-INS-i [26](optimized for local sequence homology), and inspected each alignment matrix manually. The most suitable evolutionary model for the analyses, selected with ProtTest 3.4 [27], was LG+ Γ. We used RaxML 8.1.1 [28] to infer Maximum Likelihood trees of each family, with 100 bootstrap replicates as statistical supports. Complete sequences, alignments and phylogenies are provided in S1–S3 Files. Manual inspection of the trees allowed us to identify subfamilies, named after their human orthologs, based on their bootstrap support and conservation of protein domain architectures.

Results

Expression level of deubiquitinating enzymes in the mouse retina

A RT-qPCR was performed on mouse neuroretinas to assess the expression levels of the whole set of 87 mouse genes that encode the deubiquitinating enzymes belonging to the five aforementioned families (11 JAMM, 4 MJD, 15 OTU, 4 UCH, and 53 USP genes). Two reference genes, *Rhodopsin* and *Cerkl*, were included in the analysis due to their previously reported high and low levels of expression in the mouse retina, respectively [29]. The relative expression levels have been normalized to the expression of *Gapdh*, and the Z-score was calculated for the whole set of genes per each sample, so that they could be directly compared among them and between different samples. The results (mean and standard deviation of the Z-scores per each gene) are plotted in Fig 1, ordered by DUB family. A Z-score of zero indicates the mean value of expression for all the DUBs analyzed in the retina. Thus, genes with positive values have an expression above the mean, whereas genes with negative values show less expression than the mean (e.g. most USP genes).

The results showed that *Prpf8* was the highest expressed gene from the JAMM subfamily, followed by *Eif3h* and *Psmd7*. Both *Atxn3* and *Josd2* rendered the highest expression levels within the MJD subfamily. Concerning the OTU subfamily, *Otub1* and *Tnfaip3* produced the higher expression levels, followed by *Otud7b*, *Vcpip1*, *Otud4* and *Otud5*; whereas the levels of *Otud6a* were considered as negligible. *Uchl1* was the most highly expressed gene from the UCH family (and also with respect to all DUB genes), while *Uchl3* and *Uchl5* are lowly expressed in the retina. Finally, the genes from the large USP subfamily showed the lowest level of expression among all the DUB genes. Some USPs (20%) were highly expressed and showed positive Z-scores (*Usp5*, *Usp6*, *Usp10*, *Usp12*, *Usp19*, *Usp21*, *Usp22*, *Usp33*, *Usp47* and *Usp52)* whereas 25% of the USPs showed lower levels than the mean (*Usp8*, *Usp9Y*, *Usp17*, *Usp18*, *Usp26*, *Usp27*, *Usp29*, *Usp35*, *Usp43*, *Usp44*, *Usp45*,*Usp50*, and *Usp51*) (Fig 1).

Expression map of the DUBs in the mouse retina

Once the expression levels of all the DUB family members were assessed, we characterized and compared their expression pattern within the different layers of the mouse retina. We first decided to detect gene expression by mRNA localization using *in situ* hybridization (ISH) and then performed fluorescent immunohistochemistry of selected proteins.

For ISH, antisense (AS) riboprobes against a large group of DUBs were used on mouse retinal cryosections (Fig 2). As negative controls, the corresponding sense riboprobes (S) of each gene were generated and hybridized in parallel using the same conditions (see S1 Fig). The staining time was adjusted for each set of antisense/sense riboprobes so that a maximum signal was obtained in the antisense retinal sections with minimum background in the sense counterparts (for instance, *Prpf8* and *Tnfaip3* in situs stained in much less time than *Uchl5*, *Usp8* and *Usp18*, which required half a day). *Rhodopsin* was used as a positive control because of the reported high expression in the retina and its well-known localization in the inner segment of the photoreceptors. The large USP subfamily contains 57 members in the mouse genome but only a set of genes was considered for ISH. Representative ISH results are displayed in Fig 2. Our selection criteria included genes with relevant ocular phenotypes in systematic knockdown analyses of DUBs in *Drosophila* [9] and zebrafish [30].

Most DUBs are expressed ubiquitously throughout the layers of the murine retina, which would be compatible with a general role in the neuronal cell metabolism and regulation and thus, not restricted to particular retinal neurons. Nonetheless, specific patterns of expression were detected for particular DUBs. For instance, a strong hybridization signal in the plexiform

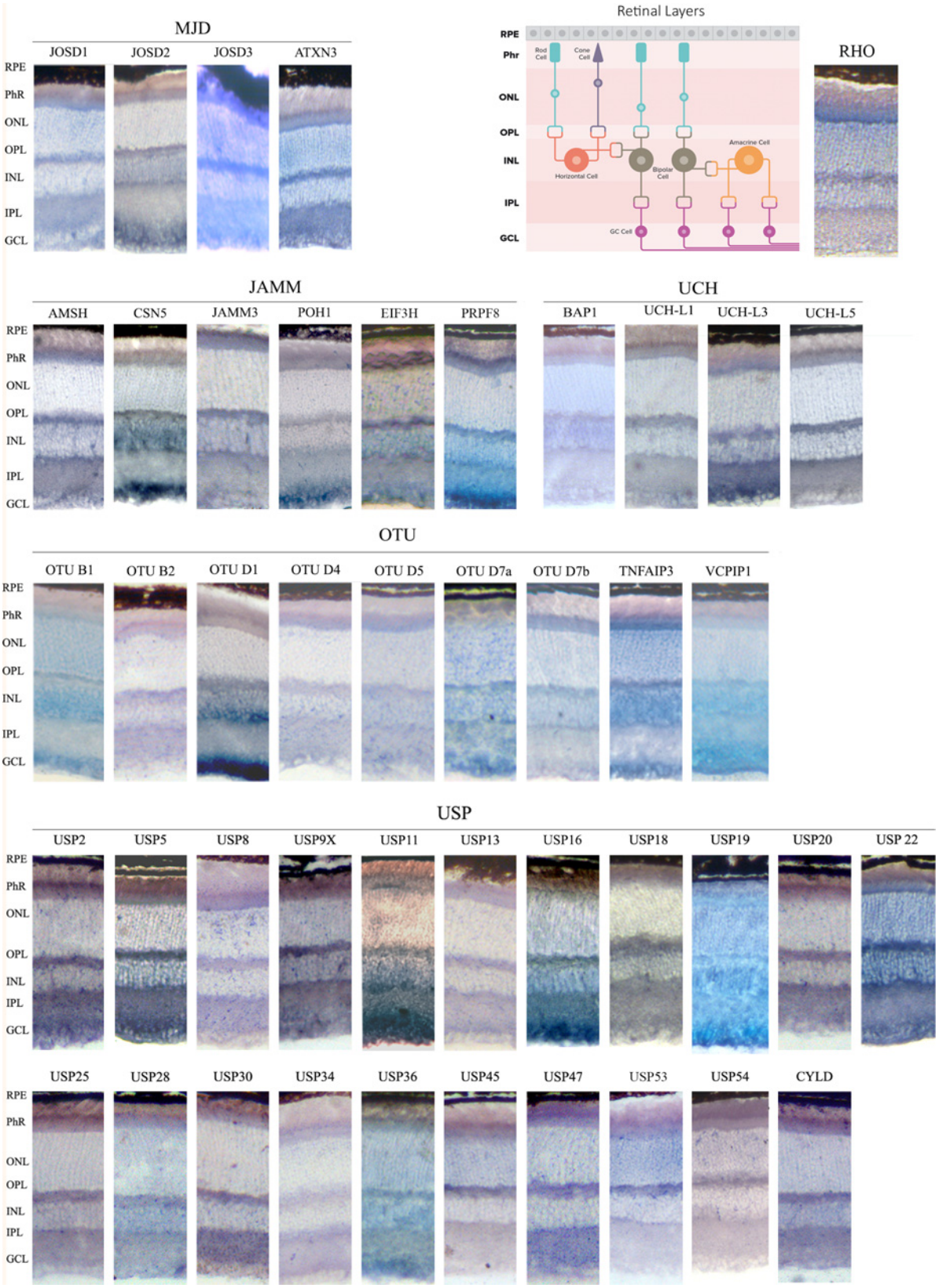
MJD
JOSD1
JOSD2
JOSD3
ATXN3
RPE
PhR
ONL
OPL
INL
IPL
GCL
Retinal Layers
Rod Cell
Cone Cell
Horizontal Cell
Bipolar Cell
Amacrine Cell
GC Cell
RHO
JAMM
AMSH
CSN5
JAMM3
POH1
EIF3H
PRPF8
UCH
BAP1
UCH-L1
UCH-L3
UCH-L5
OTU
OTU B1
OTU B2
OTU D1
OTU D4
OTU D5
OTU D7a
OTU D7b
TNFAIP3
VCPIP1
USP
USP2
USP5
USP8
USP9X
USP11
USP13
USP16
USP18
USP19
USP20
USP 22
USP25
USP28
USP30
USP34
USP36
USP45
USP47
USP53
USP54
CYLD

Fig 2. *In situ* hybridization of genes encoding DUB enzymes on retinal cryosections. Sections from wild-type C57BL/6J mouse retinas were hybridized using digoxigenin-labelled antisense riboprobes. Their corresponding sense riboprobes (negative controls) stained for the same length of time (lower panels in each row) are in the S1 Fig. The antisense *Rhodopsin* probe, which strongly labels the inner photoreceptor segment, was used as a positive control for the assay. **RPE**- Retinal pigmented epithelium; **Phr**- Photoreceptor cell layer; **ONL**- Outer nuclear layer; **OPL**. Outer plexiform layer; **INL**- Inner nuclear layer, **IPL**- Inner plexiform layer; **GCL**- Ganglion cell layer.

doi:10.1371/journal.pone.0150364.g002

layers was observed for *Uchl3*, *Uchl5*, *Usp2*, *Usp9X*, including in some cases the inner segment of the photoreceptor layer, as detected for *Amsh*, *Josd3*, *Atxn3* and *Usp47*. Some DUBs appear to be highly expressed in the GCL (*Csn5*, *Poh1*, *Prpf8*, *Josd2*, *Otud1*, *Vcpip1*, *Usp11*, *Usp5* and *Usp19*) in contrast to the pattern generated by *Usp8*, *Usp13*, *Usp30*, *Usp45* and *Usp54*, which yielded virtually no mRNA localization signal in the ganglion cells.

Several DUB genes of the USP family (*Usp5*, *Usp13*, *Usp19* and *Usp34*) were previously reported to be differentially expressed in the Retinal Pigmented Epithelium (RPE) by transcriptome analysis [31]. To assess their specific pattern of expression, and given that pigmented cells mask positive hybridization signals, we also performed ISH on albino retinas from CD-1 mice (S2 Fig). Although these four genes are expressed in this non-neuronal layer, their expression is not restricted to the RPE. In fact, *Usp5* and *Usp19* are very highly expressed throughout the retina (Fig 2). Comparison of the retinal expression pattern for these four genes did not show any detectable difference between C57BL/6J (wild-type black) and CD-1 (albino) mice strains.

Several genes, namely *Amsh-like*, *Brcc36*, *Jamm2*, *Mysm1* and *Psmd7* (JAMM group) and *Otud3*, *Yod1*, *Zranb1* (OTU group), did not render reproducible and reliable ISHs, even though several riboprobes spanning different gene regions were used. In most cases (e.g. *Amsh-like*, *Brcc36*, *Jamm2*, *Mysm1*, and *Otud3*) we obtained very low levels of expression and the signal was too faint to be distinguished from the negative control (sense riboprobe), or the sense and antisense riboprobes both produced signals of similar intensity. The ISH results of these genes are not included here.

Taking the ISH results together, we drew an atlas of expression for DUBs in the retina of adult mouse. In general, all analyzed genes except *Otud1* are expressed in the photoreceptors, and their mRNAs are localized in a wide range of intensities in the inner segment (perinuclearly) and the outer plexiform layer. Among layers, the GCL showed the most different pattern of gene expression. Notably, some DUBs, such as *Usp45*, *Usp53* and *Usp54*, are only detected in photoreceptors (PhR -inner segments, ONL (photoreceptor nuclei and perinuclei) and OPL (photoreceptor synapsis), whereas nearly no hybridization could be detected in the rest of retinal layers, which would suggest specific roles for these DUBs in this highly specialized photosensitive cells.

These ISH results prompted us to confirm and define more accurately protein localization within the retinal cell layers by fluorescent immunohistochemistry, since in cells with a highly specialized morphology, mRNA and protein localization might be different (e.g. the mRNA of rhodopsin is localized in the ribosome-rich photoreceptor inner segment whereas the protein is highly abundant in the membranous disks of the outer segment). We selected a group of DUBs for immunohistochemistry based on: i) particular ISH patterns, ii) relevance for eye phenotype in animal models, iii) putative functional diversification in phylogenetically closely related enzymes (see next section), and iv) antibody commercial availability and affinity. We selected 21 DUBs (the list of genes is detailed in the Material and Methods), of which 14 immunodetections rendered a reproducible and reliable signal (Fig 3 and S3 Fig).

Overall, the immunodetection confirms the ISH results since protein is detected in the same retinal cells than mRNA (Fig 3). Comparing RT-qPCR to ISH and immunohistochemistry results, high levels of retinal expression correlated with a ubiquitous expression pattern.

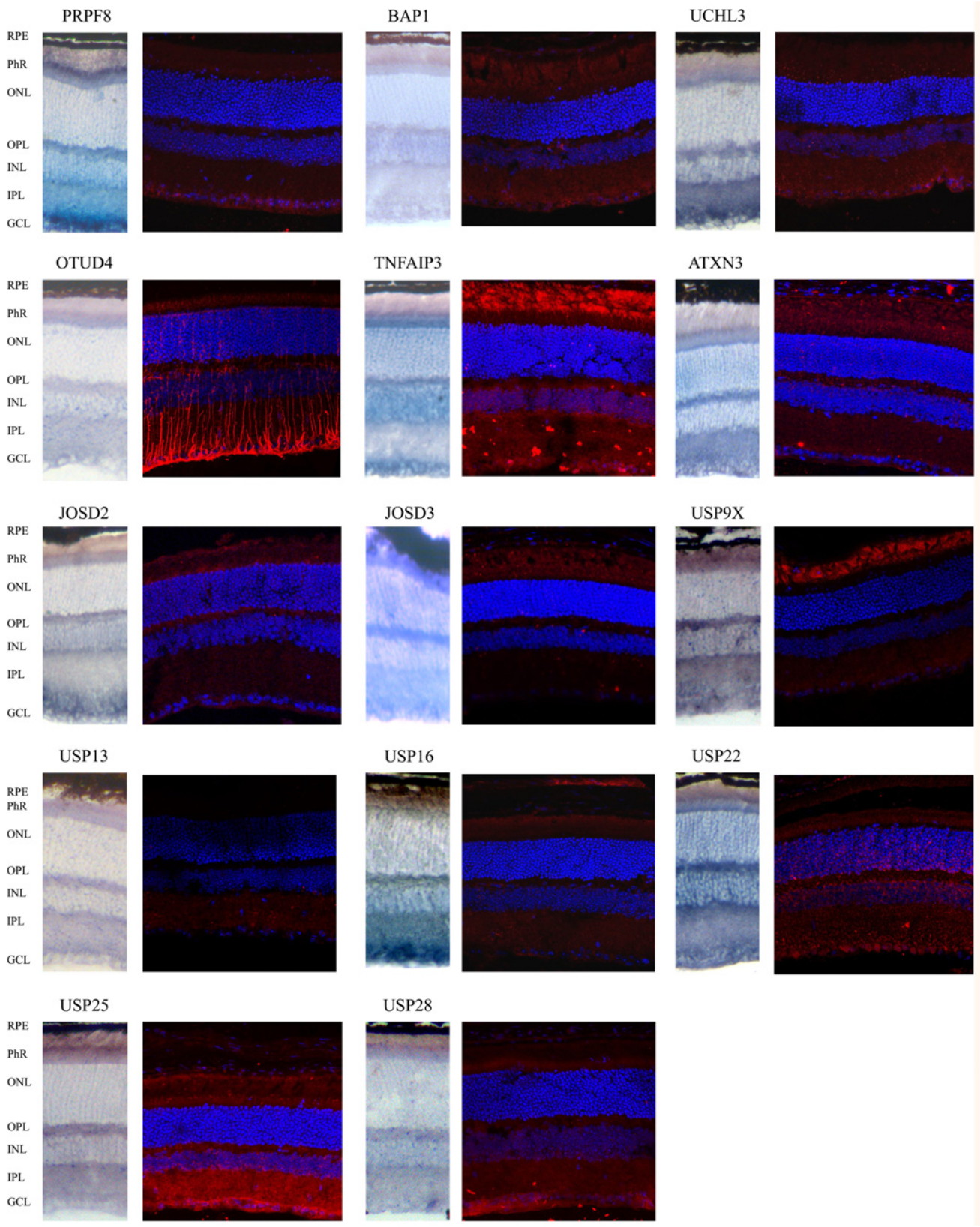
PRPF8
BAP1
UCHL3
OTUD4
TNFAIP3
ATXN3
JOSD2
JOSD3
USP9X
USP13
USP16
USP22
USP25
USP28
RPE
PhR
ONL
OPL
INL
IPL
GCL

Fig 3. Comparison of mRNA and protein immunodetection of selected DUBs in mouse retinal cryosections. Most analyzed genes render a consistent expression pattern when comparing mRNA and protein localization in the wild type mouse retina. The merge immunohistochemistry show DUBs immunodetected in red, and nuclei counter-staining with DAPI (in blue). Details in S3 Fig. **RPE**- Retinal pigmented epithelium; **Phr**- Photoreceptor cell layer; **ONL**- Outer nuclear layer; **OPL**. Outer plexiform layer; **INL**- Inner nuclear layer, **IPL**- Inner plexiform layer; **GCL**- Ganglion cell layer.

doi:10.1371/journal.pone.0150364.g003

Besides, some protein locations are worth mentioning as indicative of distinct functions in specific cellular compartments. For instance, OTUD4 is strongly detected in the axonal processes of bipolar and other retinal cells, supporting its involvement in neurodegeneration in human [32]. USP25 is mainly detected in the inner plexiform and ganglion cell layer; while USP9X and TNFAIP3 are particularly detected (but not exclusively) at the outer photoreceptor segment. Besides, USP22 is localized in the nucleus of ganglion cells, and perinuclearly in the rest of retinal neurons. For details, merge and separate immunodetection images, see S3 Fig.

DUB phylogenetic analysis, protein domain architecture and neuronal phenotypes

To provide a rational framework for gene expression patterns in extended families, it is crucial to have an understanding of the origin and phylogenetic closeness between the different DUB genes. Therefore, we performed a bioinformatic survey of DUB protein sequences across animal taxa. A recent phylogenetic analysis of the ubiquitin system across eukaryotes already showed that a massive expansion of ubiquitin ligases and proteases, which involves innovation and incorporation of new protein domains, occurred at the origin of animal multicellularity [24]. This was likely associated with the diversity of proteins and protein roles in different cell types. We here provide a comprehensive picture of the DUB families during the diversification of metazoans, related to previously described neuronal function, with an emphasis on eye and retinal phenotype.

Completely sequenced genomes from 14 species (from cnidarians to vertebrates) were queried with the catalytic region of each enzyme family (as defined in Pfam) in search of orthologs. Phylogenetic trees were generated using the retrieved sequences, and the statistical support for each node is also indicated (Fig 4A, 4B, 4C, 4D and 4E). For the sake of clarity, protein nomenclature is according to human DUBs. Highly similar sequences that expanded recently (during the pre-vertebrate/vertebrate expansion) and clustered together appear collapsed. The presence of an identified ortholog in each species/clade is represented with a black dot. Vertebrate species that present all the paralogs in a collapsed branch are circled in black. White dots mark the presence of homologs that could not be confidently assigned to a characterized DUB type, either because they are sister-group to various known DUB paralogs (and therefore represent the pre-duplication homolog), or because statistical support is too low to confidently cluster them with a specific ortholog. Question marks represent statistically supported clades that cannot be assigned to any known DUB (or group of paralogous DUBs). Protein motifs (as defined in Pfam) including the catalytic domain are drawn next to each branch to illustrate the diversity/conservation in protein architecture within each family. For detailed and complete phylogenetic trees, see S3 File.

Notably, the phylogenetic distribution of OTU DUBs reveals two different groups that appeared at the origin of eukaryotes OTUs with peptidase C65 domains (OTUB1 and OTUB2 in animals) and those with OTU domain [24] (Fig 4D). Given that i) these two catalytic domains diverged long before the origin of metazoans, ii) OTUB1/B2 protein domain architectures are clearly different from the other OTUs, iii) OTUB homologs are present in all metazoan clades, and iv) this split does not occur in any other family of DUBs, a new classification might be in order to acknowledge a new subfamily of DUBs.

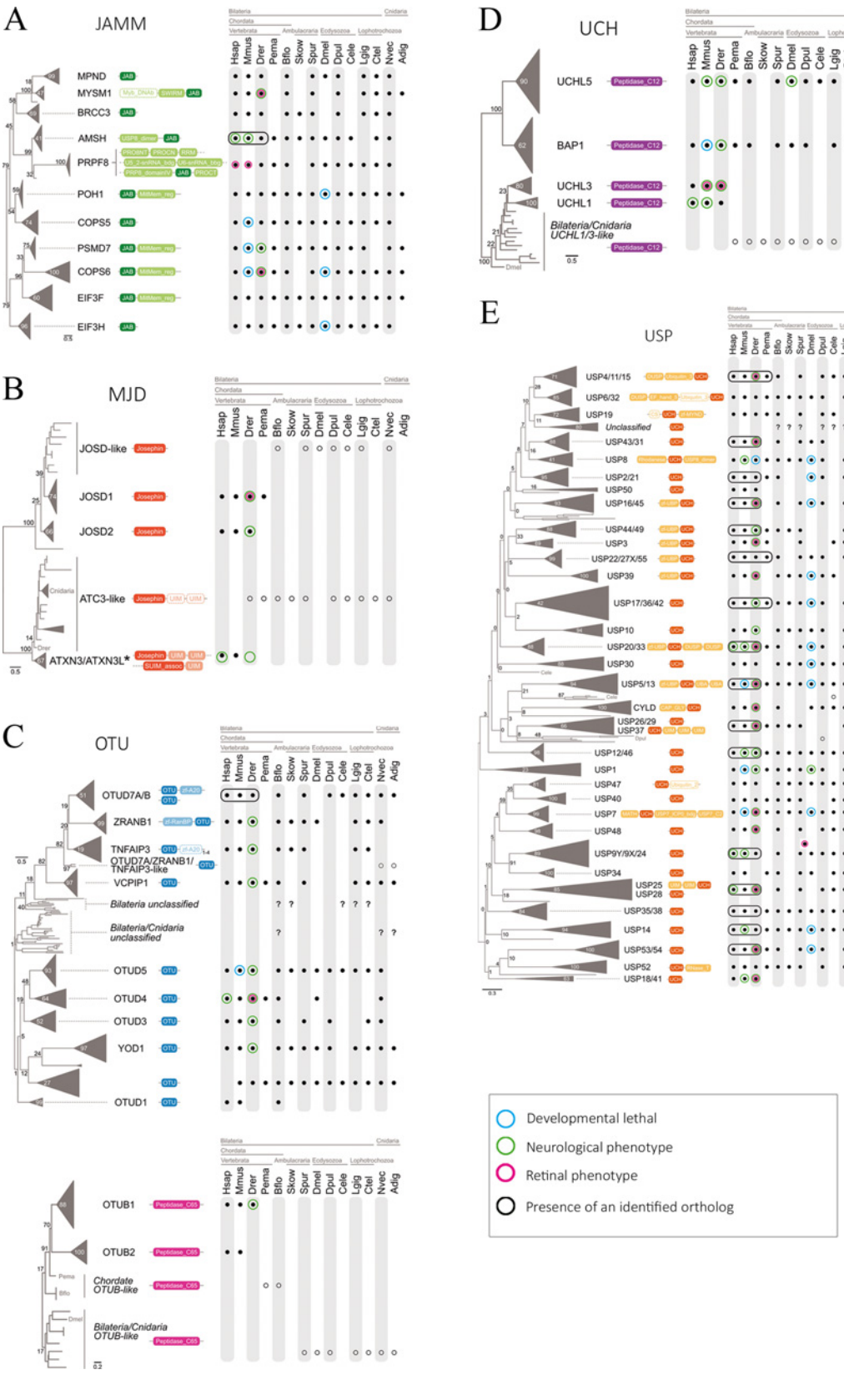
A
JAMM
MPND
MYSM1
BRCC3
AMSH
PRPF8
POH1
COPS5
PSMD7
COPS6
EIF3F
EIF3H
B
MJD
JOSD-like
JOSD1
JOSD2
ATC3-like
ATXN3/ATXN3L*
C
OTU
OTUD7A/B
ZRANB1
TNFAIP3
OTUD7A/ZRANB1/TNFAIP3-like
VCPIP1
Bilateria unclassified
Bilateria/Cnidaria unclassified
OTUD5
OTUD4
OTUD3
YOD1
OTUD1
OTUB1
OTUB2
Chordate OTUB-like
Bilateria/Cnidaria OTUB-like
D
UCH
UCHL5
BAP1
UCHL3
UCHL1
Bilateria/Cnidaria UCHL1/3-like
E
USP
USP4/11/15
USP6/32
USP19
Unclassified
USP43/31
USP8
USP2/21
USP50
USP16/45
USP44/49
USP3
USP22/27X/55
USP39
USP17/36/42
USP10
USP20/33
USP30
USP5/13
CYLD
USP26/29
USP37
USP12/46
USP1
USP47
USP40
USP7
USP48
USP9Y/9X/24
USP34
USP25
USP28
USP35/38
USP14
USP53/54
USP52
USP18/41
Hsap Mmus Drer Pema Bflo Skow Spur Dmel Dpul Cele Lgig Ctel Nvec Adig
Developmental lethal
Neurological phenotype
Retinal phenotype
Presence of an identified ortholog

Fig 4. Phylogenetic analysis of DUB genes and neuronal/retinal phenotype. Protein sequences from the catalytic region of each enzyme group were queried in complete genome sequences of 14 animal taxa and aligned. The protein domain architectures including the catalytic and accessory domain motifs are represented next to each DUB member (A, JAMM; B, MJD; C, OTU; D, UCH; and D, USP). Black dots indicate presence of the ortholog, whereas white dots indicate homologs that cannot be confidently assigned to a DUB type (see Results). Question marks represent statistically supported clades of uncharacterized DUBs. DUB sequences that are highly similar and cluster closely together appear collapsed under a common name. In general, invertebrates have a single representative member of the collapsed branch, whereas vertebrate genomes show one member of each paralog (species circled in black). *Acropora digitifera* USP homologs were excluded from the analysis as they impaired the resolution of the USP phylogeny. Genes reported to produce an abnormal neuronal phenotype when mutated are circled in magenta, whilst genes producing abnormal eye or retinal phenotype are circled in green. Genes whose mutation is lethal during developmental stages are circled in blue. An schematic summary of the DUB mRNA localization in the mouse retina (from ISH) is also presented next to the corresponding family. The intensity of the color indicates hybridization signal intensity. Retinal layers appear indicated as in Fig 2.

doi:10.1371/journal.pone.0150364.g004

The JAMM family has clear sequence assignment in all the analyzed animals, even though some species have secondarily lost some DUB members, e.g. *Acropora* (cnidarian), *C. elegans* (nematode), *Drosophila* (insect) *Saccoglossus* (hemichordate), and *Petromyzon* (sea lamprey, an early-branching vertebrate). These species also show specific gene loss for other DUB families, pointing to a divergent evolution in their lineages.

On the other hand, a clear expansion within each DUB family has occurred in the vertebrate lineage (Figs 4 and 5). When these duplicated members have rapidly diverged, the DUB protein sequences are in separate branches, but the common ancestry becomes evident since a single ancestral ortholog is present in the rest of clades (white dots in Fig 4). This is the case within the UCH (UCHL1 and UCHL3) and MJD families (JOSD1 and JOSD2). When the duplicated sequences have diverged but still branch closely together in the phylogenetic tree, the vertebrate paralogs have been collapsed into a single branch (black circles in Fig 4). This is particularly evident for USPs, where we can identify a single ancestral sequence in all invertebrate clades whereas several members are present in vertebrates (e.g. USP4/11/15. . .). Note that in the case of USP 18/41, a duplication event occurred only in the case of humans; as it is a single-species case, we have not included any black box on the figure. The *ATXN3* gene deserves specific mention, since its close paralog, *ATXN3L*, is a retrogene, that is, a gene generated by a very late retrotransposition event within the primate lineage.

The DUB gene expansion in animal phylogeny is visually summarized in the heat map of Fig 5. Color intensity reflects the number of genes per genome. It becomes evident that a burst of gene expansion within all DUB families was at the basis of the vertebrate lineage. Nonetheless, the innovation in the protein architectures with the acquisition of new domains accompanying the DUB catalytic signatures, pre-dates the origin of vertebrates in all the analyzed families, as vertebrate-like domain arrangements are often identified in other animal clades.

To complement our DUB expression study in the retina and in order to suggest relevant genes for hereditary visual disorders, we have compared the reported DUB mutant phenotypes of several animal models and human diseases, and viewed them under our new phylogenetic framework. We have specifically searched for early developmental lethality, neuronal phenotype and retinal alterations when available (Fig 4A, 4B, 4C, 4D and 4E). In the cases of neuronal phenotype, there is an accompanying alteration in the eye. However, most phenotypic assessment in the eye report only gross alterations, but a detailed retinal study has not yet been described for most animal models. For a detailed phenotypic trait list, see S2 Table and references therein.

In general, we observe that families with ancestral genes that have not been expanded in vertebrates (particularly the JAMMs) have a ubiquitous expression profile in the retina, suggesting a basic cell function. Moreover, mutations of these real orthologs produce consistent phenotypes through the analyzed taxa, arguing in favor of functional and evolutionary conservation. In contrast, for close paralog DUB genes arisen by duplication events in the vertebrate lineage,

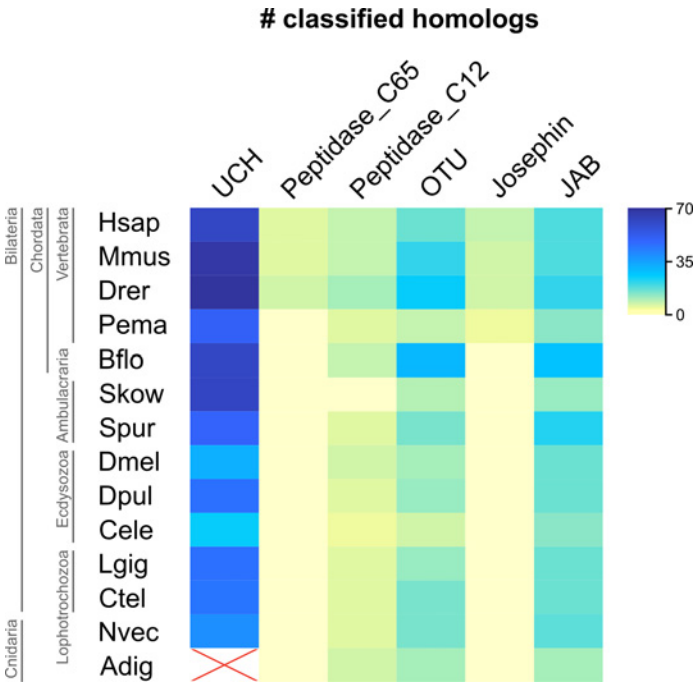

Fig 5. Counts of classified DUB homologs. Heatmap representing the number of classified genes in each analyzed genome. Increasing intensity reflects increasing number of genes. Only orthologs marked with black dots in Fig 4 are considered. *Acropora digitifera* USP homologs, excluded from the phylogenetic classification, are marked as not analyzed (NA).

doi:10.1371/journal.pone.0150364.g005

different patterns of retinal gene expression are often observed. A good example is OTUD7A/B (with one ancestral gene in most animals, and expanded in vertebrates), where OTUD7A is more highly expressed in the GCL and plexiform layers, whereas OTUD7B is more expressed in the photoreceptors. Similarly, UCHL3 and UCHL1 (both specific to vertebrates and associated to neuronal phenotypes) are expressed differently. Notably, UCHL3 (detected in the GCL and photoreceptors by ISH and immunodetection) produces eye specific retinal alterations, supporting subfunctionalization of these two paralogs. Other examples are included in the discussion.

Discussion

The ubiquitin-proteasome system (UPS) is currently viewed as one of the most dynamic and versatile cell regulators in eukaryotes. Perturbations of this system are known to be at the basis of many human disorders, particularly cancer and neurodegeneration [5,33]. Due to their ability to deconjugate ubiquitin, DUBs play a major regulatory role in the UPS. The disruption of DUB genes has dramatic consequences for the animal taxa analyzed, either during development or in adult stages, as shown by reports of the systematic DUB knockdown in zebrafish embryos and flies [9,30].

In mammals, several comprehensive surveys of DUBs have been reported resulting in: *in silico* inventories of the DUBs in the human genome [22,34]; identification of protein interactors by cell-based proteomics analysis [8]; studies of subcellular localization [1]; functional involvement in maintaining genome integrity in cells [35]. A recent review reported the expression levels of DUBs in human organs and the disease phenotypes associated to DUB mutations in humans and animal models [23]. Despite their importance, detailed expression and functional

analysis for most DUBs on particular tissues or organs, such as the retina, is still missing. We here aimed to fill this gap and produced a descriptive landscape of the expression of the complete set of DUBs in the mouse retina by combining mRNA and protein localization. We have also delineated a detailed evolutionary history of the different DUB families using phylogenetic analysis. We compared their protein domain architectures, and considered the neuronal and retinal phenotypes associated to each gene mutation/knockdown. We thus provide a reference framework for researchers interested in this visual tissue, either in physiological or in disease conditions, and suggest new avenues of research in DUBs as excellent candidates for retinal/visual hereditary disorders.

Differential levels of DUB gene expression in the adult mouse retina

Some genes that are barely expressed in the mouse retina (e.g. *Brcc36*, *Poh1*, *Bap1*, *Otub2*, and *Usp44*) are reported to be induced in replicative cells instead, being recruited to DNA damage sites where they regulate DNA repair and mitosis checkpoints [35]. These results are consistent with the fact that the adult retina is mostly formed by differentiated cells.

Among the genes highly expressed in the adult retina, *Uchl1*, *Atxn3*, *Otub1*, *Usp6*, *Usp22* and *Usp33* are also highly expressed in the brain [23]. In fact, *Uchl1*, *Otub1* and *Atxn3* are involved in neurodegenerative diseases in human, namely Parkinson's disease and cerebellar ataxia [6,36], thus indicating a relevant role in neurodegeneration. Our ISH results showed ubiquitous mRNA localization through all the retinal layers for these three genes, supporting a possible basal function in the retina. On the other hand, other DUB genes that are highly expressed in the brain [23], such as *Mysm1*, *Usp26*, *Usp29*, *Usp35* and *Usp51*, were barely expressed in the adult mouse retina; and genes that showed very low levels of expression when analyzed by qPCR within this work such as *Usp2*, *Usp25*, *Usp45*, *Usp53* and *Usp54* rendered eye phenotype when knocked-down in zebrafish [30]. Note that we performed RT-qPCR in whole adult neuroretinas at P60, and the role of these genes during development might be more relevant than in the adult stage. It is also worth noting that *Usp45*, *Usp53* and *Usp54* did show layer specificity, as they were mainly expressed in the photoreceptors (PhR inner segment, ONL and OPL), suggesting a specific role for these genes in photoreceptors and underscoring their role as potential candidates for visual disorders.

Immunohistochemical localizations also point to specific functions for some DUBs, e.g. OTUD4 is highly localized in axons; TNFAIP3 is highly expressed in the photoreceptor outer segment and GCL, and USP22 protein localization is mainly nuclear and perinuclear, thus suggesting that these genes may be good candidates for particular retinal phenotypes.

Phenotypic comparison of DUB mutants and gene expression profiles under the new evolutionary framework

Animal models have been generated by gene disruption (mouse) or knockdown (*Drosophila*, zebrafish) for some DUBs. When the DUB function is extremely relevant for cell cycle or cell differentiation, a lethal/early and extensive neuronal phenotype is consistently apparent in different organisms, as it is the case for most JAMMs and several USPs (see Fig 4 and S2 Table). In vertebrates, when some mutants show neuronal/brain affectation, a retinal/eye phenotype is also one of the accompanying phenotypic traits (examples are found in all the families). In fact, multiple vertebrate USP genes are present in paralogs (probably arising from the several rounds of genome duplication at the base of their linage), whereas their invertebrate relatives have a single homolog (black boxes in Fig 4). Therefore, it is not surprising that most USP knockdowns are lethal in *Drosophila* (where only a single member is present), whereas in vertebrates, the mutant phenotype mostly affect specific tissues, probably related to the larger

panoply of USP members and a higher functional diversification. For instance, in zebrafish the knockdown of *Usp33* (whose close relative homolog is *Usp20*) alters the nervous system development including the eye [9], which is consistent with a reported subcellular localization associated to microtubules and centrosomes; whereas the knockdown of the only member USP20/33 in *Drosophila* is lethal. Something very similar occurs with the knockdown of *Usp53* (whose close relative homolog is *Usp54*), which affects brain and eye development in zebrafish, whereas the knockdown of the single USP53/54 member is lethal in *Drosophila* (Fig 4B and S2 Table). For all the DUB families, orthologs share both high sequence similarities and consistent mutant phenotypes in vertebrates; overall, pointing to their functional conservation and supporting mouse and zebrafish models for assessing DUB roles in the human retina.

The knockdown phenotypes in different species are sometimes partially overlapping between neuronal and retinal alterations, probably due to subfunctionalization of different paralogs due to duplication events. For instance, *Usp5* and *Usp13* (encoding enzymes that expanded and diverged in the vertebrate lineage, and sharing 59.5% amino acid identities in human) showed a distinct pattern of expression in the mouse retina, with *Usp5* being highly expressed in the GCL in contrast to *Usp13*, which is barely expressed in this layer and the protein is mostly localized in the inner plexiform layer, thus indicating different roles despite sequence similarity. The knockdown of any of them severely alters zebrafish embryonic development and causes neurodegeneration (even though only the *Usp5* knockdown showed a clear eye phenotype), whereas in *Drosophila* the disruption of the single member *Usp5/13* alters eye development by increasing photoreceptor apoptosis, thus recapitulating neurodegeneration and retinal phenotype. Similarly, the close paralogs *Usp16* and *Usp45* have a contrasting expression pattern, with the former in GCL and plexiform layers, and the latter restricted to the photoreceptor cell layer, supporting again subfunctionalization or neofunctionalization of the vertebrate paralogs. Of note, the knockdown of Usp45 in zebrafish shows reduced eyes. Interestingly, *fat facets* (the ortholog of *Usp9X*, involved in endocytosis in the Notch pathway) limits the number of photoreceptors in *Drosophila* [37], while the human homolog *USP9X* has been involved in neurodegeneration, mental retardation, epilepsy and autism, as well as in cancer [38], but not yet in visual disorders. Nonetheless, the strong immunodetection in the outer segment of photoreceptors would indicate that it is also a good candidate for retinal dystrophies.

Finally, the only DUB-related gene that has been directly involved in human inherited retinal degeneration and causative of autosomal dominant Retinitis Pigmentosa is *PRPF8*, the JAMM-family member with the highest level of expression in the retina. Notably, PRPF8 (which is not properly a DUB since it is catalytically inactive) forms part of the splicing machinery [39]. Even though *PRPF8* is a housekeeping gene, its haploinsufficiency might cause a shift in the splicing patterns, which in turn alters the highly sensitive photoreceptors and triggers their apoptosis. Knock-in mice bearing human missense mutations also display retinal degeneration, thus strengthening the significance of this JAMM-gene in the retina [40].

Conclusions

In summary, our results show that data on the expression of the deubiquitinating enzyme gene family cannot be directly extrapolated between tissues or organs since cell requirements might be completely different, particularly in highly specialized and structured tissues, such as the retina. Therefore, in large families of seemingly redundant enzymes (such as DUBs) the integration of systematic expression maps together with a robust phylogenetic analysis and available phenotypic information provides an insightful reference framework for further functional characterization. This framework may be helpful for researchers working in the ubiquitin-

related field as well as for those working in the molecular bases of neurological and retinal disorders.

Supporting Information

S1 Fig. *In situ* hybridization of genes encoding DUB enzymes on mouse retina cryosections, with the comparison between antisense and sense riboprobes.
(PDF)

S2 Fig. *In situ* hybridization of genes encoding DUB enzymes on CD-1 (albino) mouse retina cryosections.
(PDF)

S3 Fig. Fluorescent immunohistochemistry of selected DUBs.
(PDF)

S1 File. Zip file containing the DUB catalytic domain sequences (per family) used for the phylogenetic analysis in FASTA format.
(ZIP)

S2 File. Zip file containing the sequence alignments obtained per each DUB family.
(ZIP)

S3 File. Zip file containing the complete phylogenetic trees with their corresponding bootstraps.
(ZIP)

S1 Table. Sequences of the primer pairs used in the reverse transcriptase Real Time qPCR and *in situ* hybridization.
(PDF)

S2 Table. Mutant neuronal and retinal phenotypes in different animal models and human listed per DUB family and gene.
(PDF)

Acknowledgments

We are grateful to D. Vystavělová and N. Peña-Auladell for technical support. We are also indebted to Dr. C. Arenas for advice on data statistical analysis. This study was supported by grants BFU2010-15656 (MICINN) and SAF2013-49069-C2-1-R (MINECO) to G.M., and 2014SGR-0932 (Generalitat de Catalunya) grant (BFU-2011-23434) from Ministerio de Economía y Competitividad (MINECO) and co-funded by the Fondo Europeo de Desarrollo regional (FEDER) to I.R-T. The funders had no role in study design, data collection and analysis, decision to publish, or preparation of the manuscript.

Author Contributions

Conceived and designed the experiments: AG GM. Performed the experiments: ME XG-B AG VT SG-M EM MJL-I VA-M. Analyzed the data: ME XG-B AG VT SG-M EM MJL-I VA-M IR-T GM. Contributed reagents/materials/analysis tools: GM XG-B IR-T. Wrote the paper: ME GM. Revised the final text: GM ME XG-B AG VT SG-M EM MJL-I VA-M IR-T.

References

1. Clague MJ, Coulson JM, Urbé S. Cellular functions of the DUBs. J Cell Sci. 2012; 125: 277–86. doi: 10.1242/jcs.090985 PMID: 22357969
2. Duncan LM, Piper S, Dodd RB, Saville MK, Sanderson CM, Luzio JP, et al. Lysine-63-linked ubiquitination is required for endolysosomal degradation of class I molecules. EMBO J. 2006; 25: 1635–1645. doi: 10.1038/sj.emboj.7601056 PMID: 16601694
3. Hunter T. The Age of Crosstalk: Phosphorylation, Ubiquitination, and Beyond. Mol Cell. 2007; 28: 730–738. doi: 10.1016/j.molcel.2007.11.019 PMID: 18082598
4. Clague MJ, Urbé S. Ubiquitin: same molecule, different degradation pathways. Cell. 2010; 143: 682–5. doi: 10.1016/j.cell.2010.11.012 PMID: 21111229
5. Dantuma NP, Bott LC. The ubiquitin-proteasome system in neurodegenerative diseases: precipitating factor, yet part of the solution. Front Mol Neurosci. 2014; 7: 70. doi: 10.3389/fnmol.2014.00070 PMID: 25132814
6. Ristic G, Tsou W-L, Todi S V. An optimal ubiquitin-proteasome pathway in the nervous system: the role of deubiquitinating enzymes. Front Mol Neurosci. 2014; 7: 72. doi: 10.3389/fnmol.2014.00072 PMID: 25191222
7. Kim TY, Siesser PF, Rossman KL, Goldfarb D, Mackinnon K, Yan F, et al. Substrate Trapping Proteomics Reveals Targets of the βTrCP2/FBXW11 Ubiquitin Ligase. Mol Cell Biol. 2014; doi: 10.1128/MCB.00857-14
8. Sowa ME, Bennett EJ, Gygi SP, Harper JW. Defining the human deubiquitinating enzyme interaction landscape. Cell. 2009; 138: 389–403. doi: 10.1016/j.cell.2009.04.042 PMID: 19615732
9. Tsou W-L, Sheedlo MJ, Morrow ME, Blount JR, McGregor KM, Das C, et al. Systematic analysis of the physiological importance of deubiquitinating enzymes. PLoS One. 2012; 7: e43112. doi: 10.1371/journal.pone.0043112 PMID: 22937016
10. Kang N, Won M, Rhee M, Ro H. Siah ubiquitin ligases modulate nodal signaling during zebrafish embryonic development. Mol Cells. 2014; 37: 389–98. doi: 10.14348/molcells.2014.0032 PMID: 24823357
11. Hoon M, Okawa H, Della Santina L, Wong ROL. Functional architecture of the retina: Development and disease. Prog Retin Eye Res. 2014; 42C: 44–84. doi: 10.1016/j.preteyeres.2014.06.003
12. Swaroop A, Kim D, Forrest D. Transcriptional regulation of photoreceptor development and homeostasis in the mammalian retina. Nat Rev Neurosci. 2010; 11: 563–76. doi: 10.1038/nrn2880 PMID: 20648062
13. Schob C, Orth U, Gal A, Kindler S, Chakarova CF, Bhattacharya SS, et al. Mutations in TOPORS: a rare cause of autosomal dominant retinitis pigmentosa in continental Europe? Ophthalmic Genet. 2009; 30: 96–8. doi: 10.1080/13816810802695543 PMID: 19373681
14. Bowne SJ, Sullivan LS, Gire AI, Birch DG, Hughbanks-Wheaton D, Heckenlively JR, et al. Mutations in the TOPORS gene cause 1% of autosomal dominant retinitis pigmentosa. Mol Vis. 2008; 14: 922–7. Available: http://www.pubmedcentral.nih.gov/articlerender.fcgi?artid=2391085&tool=pmcentrez&rendertype=abstract PMID: 18509552
15. De Sousa Dias M, Hernan I, Pascual B, Borràs E, Mañé B, Gamundi MJ, et al. Detection of novel mutations that cause autosomal dominant retinitis pigmentosa in candidate genes by long-range PCR amplification and next-generation sequencing. Mol Vis. 2013; 19: 654–64. Available: http://www.pubmedcentral.nih.gov/articlerender.fcgi?artid=3611935&tool=pmcentrez&rendertype=abstract PMID: 23559859
16. Hugosson T, Friedman JS, Ponjavic V, Abrahamson M, Swaroop A, Andréasson S. Phenotype associated with mutation in the recently identified autosomal dominant retinitis pigmentosa KLHL7 gene. Arch Ophthalmol. 2010; 128: 772–8. doi: 10.1001/archophthalmol.2010.98 PMID: 20547956
17. Wen Y, Locke KG, Klein M, Bowne SJ, Sullivan LS, Ray JW, et al. Phenotypic characterization of 3 families with autosomal dominant retinitis pigmentosa due to mutations in KLHL7. Arch Ophthalmol. 2011; 129: 1475–82. doi: 10.1001/archophthalmol.2011.307 PMID: 22084217
18. Campello L, Esteve-Rudd J, Cuenca N, Martín-Nieto J. The ubiquitin-proteasome system in retinal health and disease. Mol Neurobiol. 2013; 47: 790–810. doi: 10.1007/s12035-012-8391-5 PMID: 23339020
19. Ramatenki V, Potlapally SR, Dumpati RK, Vadija R, Vuruputuri U. Homology modeling and virtual screening of ubiquitin conjugation enzyme E2A for designing a novel selective antagonist against cancer. J Recept Signal Transduct Res. 2014; 1–14. doi: 10.3109/10799893.2014.969375
20. Crosas B. Deubiquitinating enzyme inhibitors and their potential in cancer therapy. Curr Cancer Drug Targets. 2014; 14: 506–16. Available: http://www.ncbi.nlm.nih.gov/pubmed/25088039 PMID: 25088039

21. D'Arcy P, Brnjic S, Olofsson MH, Fryknäs M, Lindsten K, De Cesare M, et al. Inhibition of proteasome deubiquitinating activity as a new cancer therapy. Nat Med. 2011; 17: 1636–40. doi: 10.1038/nm.2536 PMID: 22057347

22. Nijman SMB, Luna-Vargas MP a, Velds A, Brummelkamp TR, Dirac AMG, Sixma TK, et al. A genomic and functional inventory of deubiquitinating enzymes. Cell. 2005; 123: 773–86. doi: 10.1016/j.cell.2005.11.007 PMID: 16325574

23. Clague MJ, Barsukov I, Coulson JM, Liu H, Rigden DJ, Urbé S. Deubiquitylases from genes to organism. Physiol Rev. 2013; 93: 1289–315. doi: 10.1152/physrev.00002.2013 PMID: 23899565

24. Grau-Bové X, Sebé-Pedrós A, Ruiz-Trillo I. The eukaryotic ancestor had a complex ubiquitin signaling system of archaeal origin. Mol Biol Evol. 2015; 32: 726–39. doi: 10.1093/molbev/msu334 PMID: 25525215

25. Finn RD, Bateman A, Clements J, Coggill P, Eberhardt RY, Eddy SR, et al. Pfam: the protein families database. Nucleic Acids Res. 2014; 42: D222–30. doi: 10.1093/nar/gkt1223 PMID: 24288371

26. Katoh K, Standley DM. MAFFT multiple sequence alignment software version 7: improvements in performance and usability. Mol Biol Evol. 2013; 30: 772–80. doi: 10.1093/molbev/mst010 PMID: 23329690

27. Darriba D, Taboada GL, Doallo R, Posada D. ProtTest 3: fast selection of best-fit models of protein evolution. Bioinformatics. 2011; 27: 1164–5. doi: 10.1093/bioinformatics/btr088 PMID: 21335321

28. Stamatakis A. RAxML version 8: a tool for phylogenetic analysis and post-analysis of large phylogenies. Bioinformatics. 2014; 30: 1312–3. doi: 10.1093/bioinformatics/btu033 PMID: 24451623

29. Abad-Morales V, Domènech EB, Garanto A, Marfany G. mRNA expression analysis of the SUMO pathway genes in the adult mouse retina. Biol Open. 2015; doi: 10.1242/bio.201410645

30. Tse WKF, Eisenhaber B, Ho SHK, Ng Q, Eisenhaber F, Jiang Y-J. Genome-wide loss-of-function analysis of deubiquitylating enzymes for zebrafish development. BMC Genomics. 2009; 10: 637. doi: 10.1186/1471-2164-10-637 PMID: 20040115

31. Strunnikova N V, Maminishkis a, Barb JJ, Wang F, Zhi C, Sergeev Y, et al. Transcriptome analysis and molecular signature of human retinal pigment epithelium. Hum Mol Genet. 2010; 19: 2468–86. doi: 10.1093/hmg/ddq129 PMID: 20360305

32. Margolin DH, Kousi M, Chan Y-M, Lim ET, Schmahmann JD, Hadjivassiliou M, et al. Ataxia, dementia, and hypogonadotropism caused by disordered ubiquitination. N Engl J Med. 2013; 368: 1992–2003. doi: 10.1056/NEJMoa1215993 PMID: 23656588

33. Hussain S, Zhang Y, Galardy PJ. DUBs and cancer: the role of deubiquitinating enzymes as oncogenes, non-oncogenes and tumor suppressors. Cell Cycle. 2009; 8: 1688–97. Available: http://www.ncbi.nlm.nih.gov/pubmed/19448430 PMID: 19448430

34. Komander D, Clague MJ, Urbé S. Breaking the chains: structure and function of the deubiquitinases. Nat Rev Mol Cell Biol. 2009; 10: 550–63. doi: 10.1038/nrm2731 PMID: 19626045

35. Nishi R, Wijnhoven P, le Sage C, Tjeertes J, Galanty Y, Forment J V, et al. Systematic characterization of deubiquitylating enzymes for roles in maintaining genome integrity. Nat Cell Biol. Nature Publishing Group; 2014; 16: 1016–26, 1–8. doi: 10.1038/ncb3028 PMID: 25194926

36. Puschmann A. Monogenic Parkinson's disease and parkinsonism: clinical phenotypes and frequencies of known mutations. Parkinsonism Relat Disord. 2013; 19: 407–15. doi: 10.1016/j.parkreldis.2013.01.020 PMID: 23462481

37. Cadavid AL, Ginzel A, Fischer JA. The function of the Drosophila fat facets deubiquitinating enzyme in limiting photoreceptor cell number is intimately associated with endocytosis. Development. 2000; 127: 1727–36. Available: http://www.ncbi.nlm.nih.gov/pubmed/10725248 PMID: 10725248

38. Murtaza M, Jolly LA, Gecz J, Wood SA. La FAM fatale: USP9X in development and disease. Cell Mol Life Sci. 2015; doi: 10.1007/s00018-015-1851-0

39. Pena V, Liu S, Bujnicki JM, Lührmann R, Wahl MC. Structure of a multipartite protein-protein interaction domain in splicing factor prp8 and its link to retinitis pigmentosa. Mol Cell. 2007; 25: 615–24. doi: 10.1016/j.molcel.2007.01.023 PMID: 17317632

40. Graziotto JJ, Farkas MH, Bujakowska K, Deramaudt BM, Zhang Q, Nandrot EF, et al. Three gene-targeted mouse models of RNA splicing factor RP show late-onset RPE and retinal degeneration. Invest Ophthalmol Vis Sci. 2011; 52: 190–8. doi: 10.1167/iovs.10-5194 PMID: 20811066

SUPPLEMENTARY FIGURE 1

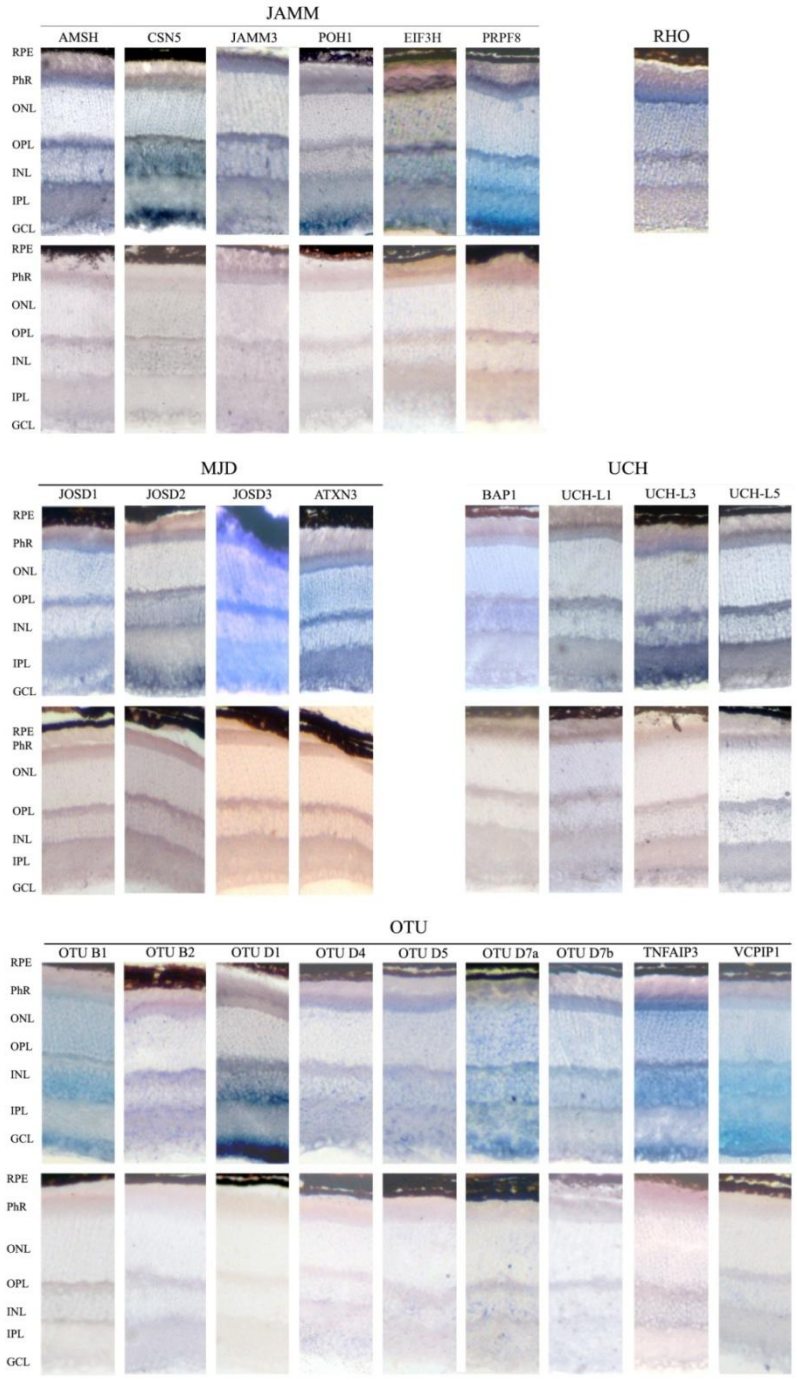

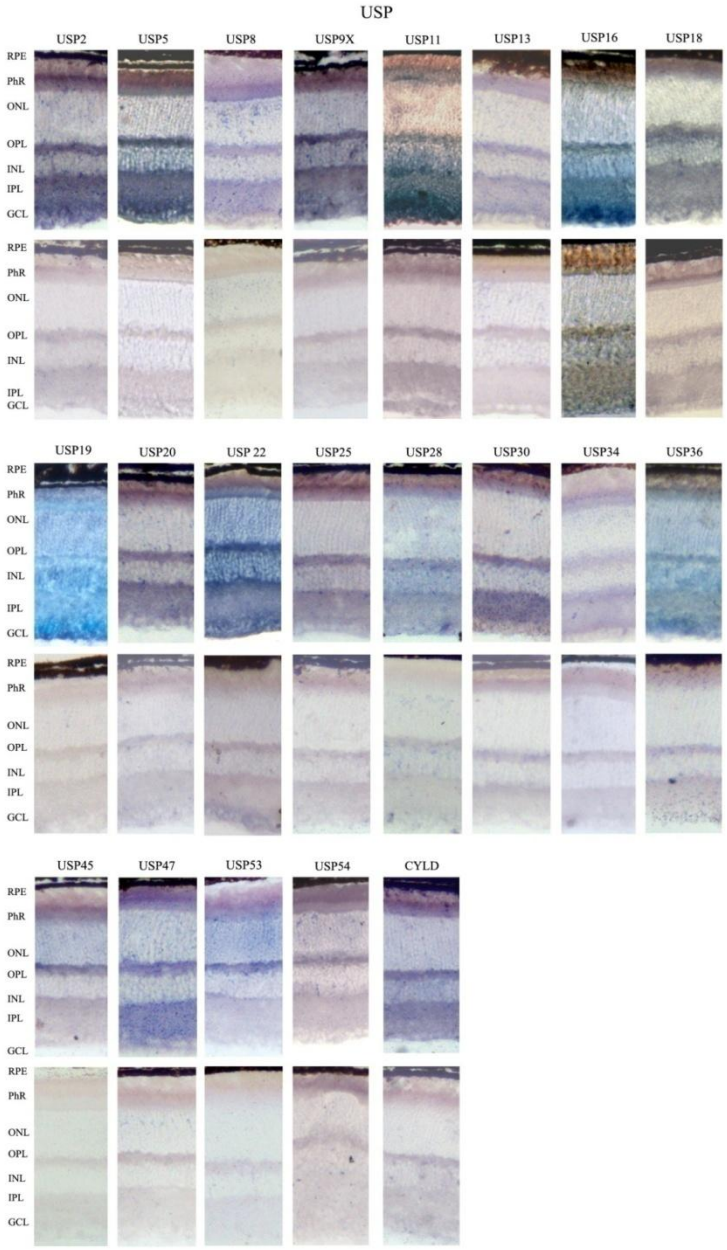

S1 Fig. ***In situ*** **hybridization of genes encoding DUB enzymes on mouse retina cryosections, with the comparison between antisense and sense riboprobes.**

SUPPLEMENTARY FIGURE 2

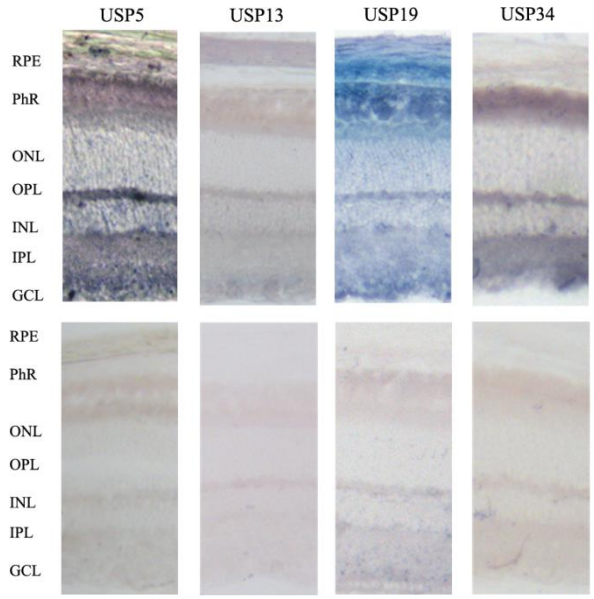

Supplementary Figure 2. *In situ* hybridization of genes encoding DUB enzymes on CD-1 (albino) mouse retina cryosections, using digoxigenin-labelled antisense riboprobes (top panels in each row) and their corresponding sense riboprobes (negative controls) stained for the same length of time (lower panels in each row). **RPE**- Retinal pigmented epithelium; **Phr**- Photoreceptor cell layer; **ONL**- Outer nuclear layer; **OPL**. Outer plexiform layer; **INL**- Inner nuclear layer, **IPL**- Inner plexiform layer; **GCL**- Ganglion cell layer.

SUPPLEMENTARY FIGURE 3

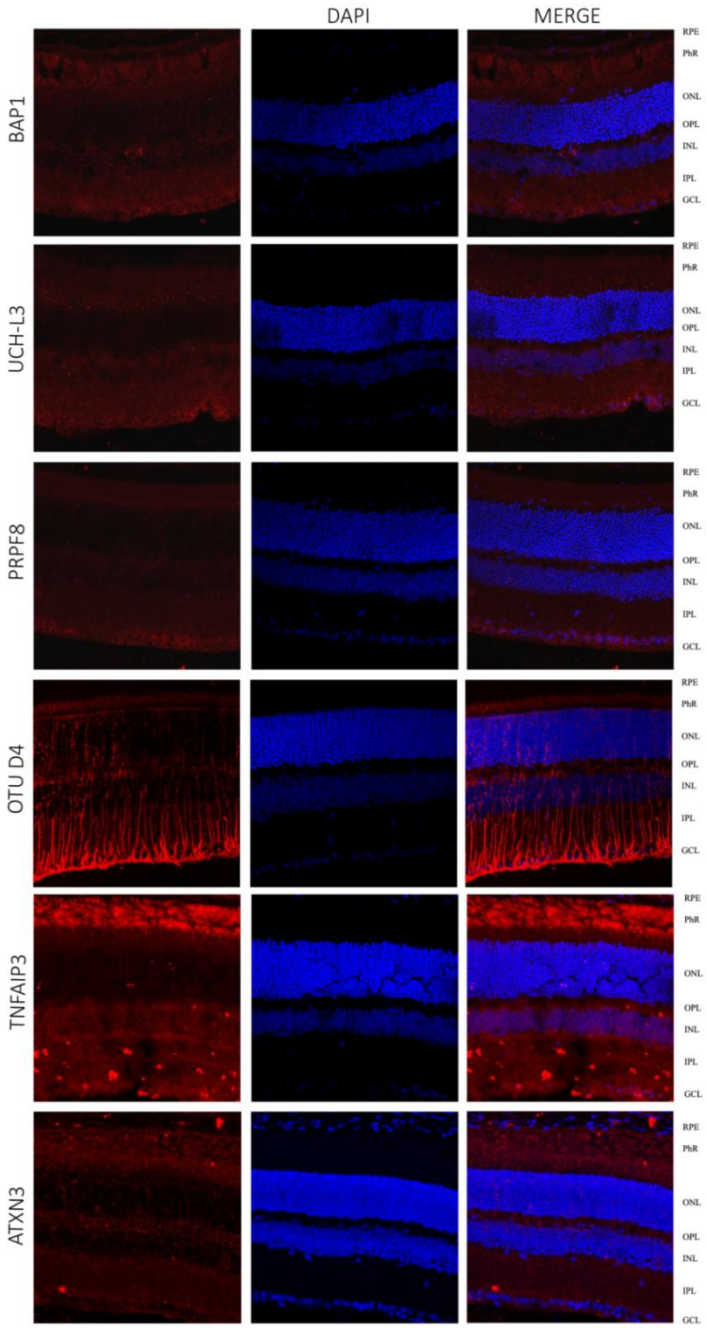

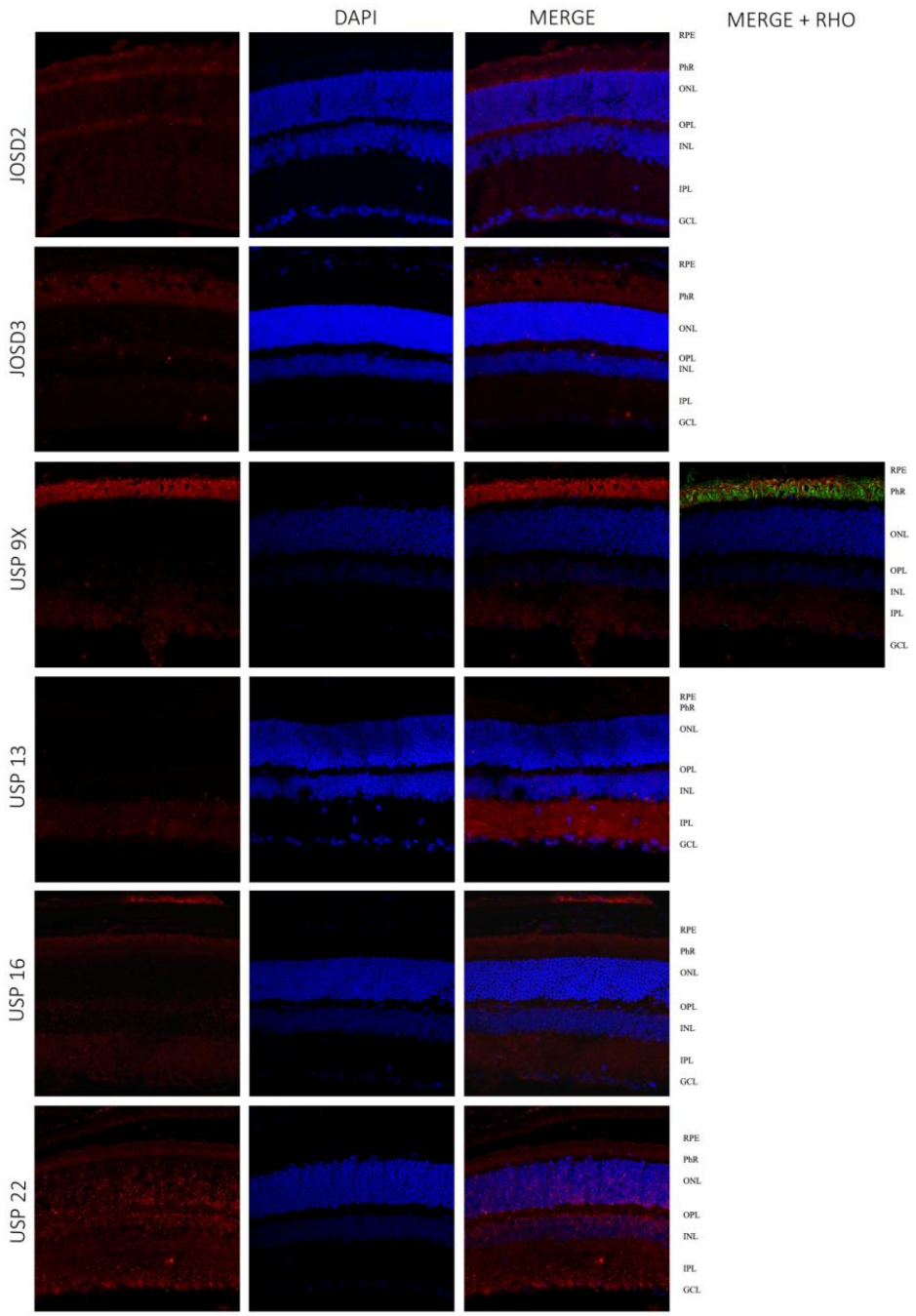
DAPI
MERGE
MERGE + RHO
JOSD2
JOSD3
USP 9X
USP 13
USP 16
USP 22
RPE
PhR
ONL
OPL
INL
IPL
GCL

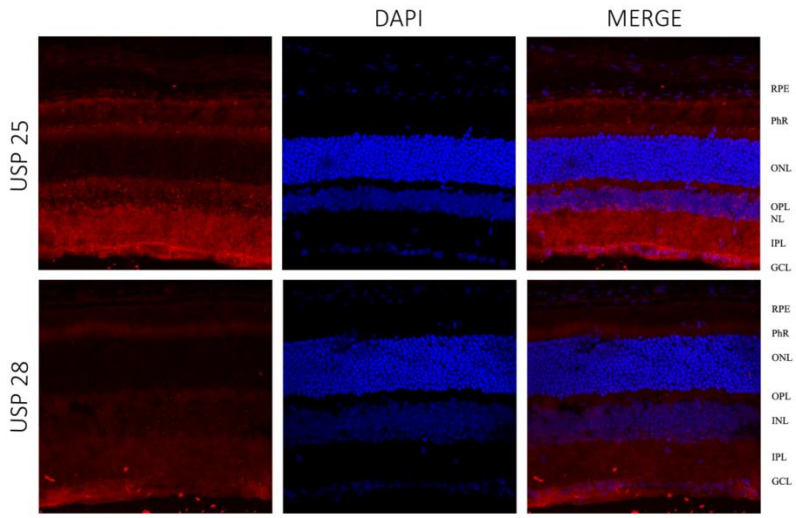

Supplementary Fig 4. Fluorescent immunohistochemistry of selected genes on retinal cryosections, using antibodies against a selection of DUB proteins. The figure shows the immunodetection of the indicated DUBs (in red), DAPI counter-staining of the nuclei (in blue) and the merged channels. In USP9X, the extra image shows its co-localization with Rhodopsin in the outer photoreceptor segment, where phototransduction occurs. **RPE**- Retinal pigmented epithelium; **Phr**- Photoreceptor cell layer; **ONL**- Outer nuclear layer; **OPL**. Outer plexiform layer; **INL**- Inner nuclear layer, **IPL**- Inner plexiform layer; **GCL**- Ganglion cell layer.

SUPPLEMENTARY FILES

S1 FILE - Zip file containing the dub catalytic domain sequences (per family) used for the phylogenetic analysis in fasta format.

S2 FILE - Zip file containing the sequence alignments obtained per each DUB family.

S3 FILE - Zip file containing the complete phylogenetic trees with their corresponding bootstraps.

SUPPLEMENTARY TABLE 1

		Real Time qPCR			*In Situ Hybridization*	
Family	**Gene**	**Orientation**	**Sequence (5'-3')**	**Gene**	**Orientation**	**Sequence (5'-3')**
	Gapdh*	Fw	tgacaatgaatacggctacagcaa			
		Rv	tactccttggaggccatgtagg			
	Rho	Fw	gcccttctccaacgtcacag	***Rho****	Fw	gcccttctccaacgtcacag
		Rv	gcagcttcttgtgctgtacgg		Rv	gcagcttcttgtgctgtacgg
JAMM	***Amsh***	Fw	attgttcaagagttcgggaagg	***Amsh***	Fw	caccgagactacaaatcagctatc
		Rv	gggggccacatctacacaagg		Rv	gggggccacatctacacaagg
	Amsh-like	Fw	gctgctatgcctgaccatacaga	***Amsh-like***	Fw	gagaacccagaggcccggacta
		Rv	gacctgaagtaacggcgtggggtg		Rv	gacctgaagtaacggcgtggggtg
	Brcc36	Fw	gcggcgttctgacaagagaaagg	***Brcc36***	Fw	aacacaaagactggccgggta
		Rv	ataccagccaacaactctcatggg		Rv	cgatgcaggaaccaaagcag
	Csn5	Fw	ttccgggagtggtatggcccag	***Csn5***	Fw	ttccgggagtggtatggcccag
		Rv	cgccgccaggatttctttcttgttg		Rv	gtgtactaacatcaatcccggag
	Eif3h	Fw	catgtttgaagaagtgccgattg	***Eif3h***	Fw	NP
		Rv	gtgcttatccgccacagctgac		Rv	NP
	Jamm2	Fw	cctgcctgaatgctgtaaagattg	***Jamm2***	Fw	cctgcctgaatgctgtaaagattg
		Rv	agtaagatggctgccagaattctgt		Rv	tcctctcttacttctcctctgtg
	Jamm3	Fw	cctgttcctcgaggcctgt	***Jamm3***	Fw	tccatggcagctcccgagtct
		Rv	tcaatgtcctgcaagcaaggagggta		Rv	ctcctccaacagcagttcttcc
	Mysm1	Fw	tgtctctgctctgtgccaactg	***Mysm1***	Fw	NP
		Rv	cacctctcctgctgagaaacca		Rv	NP
	Poh1	Fw	acatgtggatgtcttatgacttca	***Poh1***	Fw	caatgctaatatgatggtcttgg
		Rv	gcgccactgacagctctctacgt		Rv	gccactgacagctctctacg
	Prpf8	Fw	gcgtggaattacccctctgc	***Prpf8***	Fw	NP
		Rv	cacccgctgcttcgttactg		Rv	NP
	Psmd7	Fw		***Psmd7***	Fw	NP
		Rv		***Amsh***	Rv	NP
MJD	***Atxn***	Fw	gccctgtggagctatcctcaat	***Atxn***	Fw	gccctgtggagctatcctcaat
		Rv	actccccttctgccattctc		Rv	gagggcactctgctctttcaga
	Josd1	Fw	ccatggtctctgcaggtctga	***Josd1***	Fw	ccatagtttgggacagagttggg
		Rv	tgctcaggattaacatgcaagc		Rv	tgctcaggattaacatgcaagc
	Josd2	Fw	gtgcgaggtgctattggtggt	***Josd2***	Fw	gccgacgaaatctgcaagag
		Rv	gcagcagatcagcttgtgttca		Rv	gcagcagatcagcttgtgttca
	Josd3	Fw	gaacaccaccttaaggaatgcttg	***Josd3***	Fw	ggcatcggatagagctggagat
		Rv	gtatttgtgcctccgactgtca		Rv	gtatttgtgcctccgactgtca

OTU	***Otub1***	Fw	agcaggtggacaagcagacctc	***Otub1***	Fw	agcaggtggacaagcagacctc
		Rv	cagtcgcaggtagaccacaagg		Rv	cctctgtacatgtctagcgcc
	Otub2	Fw	gccacttaccttgccttgctgc	***Otub2***	Fw	acattctatccattcttcgggatca
		Rv	acagggtggtcccatggttatc		Rv	agaagtcagctcggttcctgatg
	Otud1	Fw	catggggcagatgctgaatgtg	***Otud1***	Fw	agaagctagccctgtacctgg
		Rv	ggcccagatagtggatcatgg		Rv	ggcccagatagtggatcatgg
	Otud3	Fw	gatgcggaggagaaccatga	***Otud3***	Fw	tccacatcgcctaccgctac
		Rv	tgccttcatttctgccctga		Rv	tgccttcatttctgccctga
	Otud4	Fw	cctgttcccgtgtatcctcaga	***Otud4***	Fw	cctgttcccgtgtatcctcaga
		Rv	catcggtgcaaggacagtcac		Rv	tccaaaggcaaatccaattctcc
	Otud5	Fw	ctgagcaccctgaactgcat	***Otud5***	Fw	gcctaccgtcatttaagccagg
		Rv	tgaaggaggtttggcaagagcta		Rv	tgaaggaggtttggcaagagcta
	Otud6a	Fw	cgagatggagcagaggcacaa	***Otud6a***	Fw	NP
		Rv	gctgtaaccgaatccacactgc		Rv	NP
	Otud6b	Fw	ccgggaagaaaggatagcagagg	***Otud6b***	Fw	NP
		Rv	ggctgccaatatttgagcaagtt		Rv	NP
	Otud7a	Fw	tctgacggattcggaacacaag	***Otud7a***	Fw	cttgcacagccagagtctcc
		Rv	tggctaaccgggcattgtcg		Rv	ggcgacgctcccgacgc
	Otud7b	Fw	atgatccagcgttaccttgcag	***Otud7b***	Fw	gggcctgatgcacagcaagg
		Rv	ccctccattcatgatcttcctc		Rv	ccctccattcatgatcttcctc
	Parp11	Fw	tgctatccccatccagctttg	***Parp11***	Fw	NP
		Rv	tgcttcccaatttgagtgactg		Rv	NP
	Tnfaip3	Fw	ataatggattctgtgagcgttgc	***Tnfaip3***	Fw	tttgagcttgttcagcacgaatac
		Rv	gaaggcaggcttggcactttc		Rv	gaaggcaggcttggcactttc
	Vcpip1	Fw	atggggtgtgcctcaggaccttatt	***Vcip1***	Fw	gaaacgaagggaccgaagaatc
		Rv	ctgcaaacttctgtctcctccaa		Rv	tgctgctgaaagtgctgctta
	Yod1	Fw	cagcgtaacttccctgatccaga	***Yod1***	Fw	gaaggaccgaggccgagtc
		Rv	cttcatcagctaattccagtgcttg		Rv	cgggtagccaacgaggattc
	Zranb1	Fw	tcccagacctaataacattgaagca	***Zranb1***	Fw	ggtggaagtagtcctttgatatg
		Rv	ctccatcgagctctgtcttgctc		Rv	ctccatcgagctctgtcttgctc
UCH	***Bap1***	Fw	tcctgggagtgggagtgacat	***Bap1***	Fw	ctgcttcctgagcattgaggag
		Rv	ctgcttcctgagcattgaggag		Rv	gctgtgactcttgagatttgtg
	Uch-l1	Fw	gattaaccccgagatgctgaac	***Uch-l1***	Fw	cgcttcgccgacgtgctagg
		Rv	ggatggcactgagcccagag		Rv	gcccatcgagctcgtacaga
	Uch-l3	Fw	tatgcgcgcagtgttactcctctt	***Uch-l3***	Fw	tatgcgcgcagtgttactcctctt
		Rv	tcgttccacaggcattgctgat		Rv	ggcatcctctaacaacgtctcatc
	Uch-l5	Fw	agatgtgattcgacaagtgcacaa	***Uch-l5***	Fw	ggggtcttcaccgagctcat
		Rv	agatgtgattcgacaagtgcacaa		Rv	agatgtgattcgacaagtgcacaa
USP	***Usp1***	Fw	ggacaccattcaccgacaatag	***Usp1***	Fw	NP
		Rv	aacgcctgtttggtcactggat		Rv	NP

Usp2	Fw	acctgaagcgattctcagaatc	***Usp2***	Fw	gatggtctccacaatgaggtg
	Rv	ctctcaagtccaggtctctta		Rv	ctctcaagtccaggtctctta
Usp3	Fw	ccgctggttccatttcaatgac	***Usp3***	Fw	NP
	Rv	ctggcctgacgctccacataa		Rv	NP
Usp4	Fw	tggtgaggacgatcagggaga	***Usp4***	Fw	NP
	Rv	aggagttcacgaggctgaagg		Rv	NP
Usp5	Fw	cacccatgctggacgaatccg	***Usp5***	Fw	cggatgagcccaaaggtagcct
	Rv	gccccgctgtttcccgtatag		Rv	gccccgctgtttcccgtatag
Usp6	Fw	cggaagtatctggagctgagc	***Usp6***	Fw	NP
	Rv	cagtccatctttcggcccttc		Rv	NP
Usp7	Fw	gatgatgacgtggtatccaggtg	***Usp7***	Fw	NP
	Rv	catataggcatttgtgcagtgtc		Rv	NP
Usp8	Fw	caacgagcacctggatgacc	***Usp8***	Fw	tatttggaggatcaggaccagc
	Rv	acgatgatggactcgttgagc		Rv	acgatgatggactcgttgagc
Usp9X	Fw	ttaaaaggaaatggacctgggc	***Usp9X***	Fw	tcaagaatgcagtcttcgatca
	Rv	gctttgcactggaggagacc		Rv	gctttgcactggaggagacc
Usp9Y	Fw	gtggacttgggctatggaatgg	***Usp9Y***	Fw	NP
	Rv	gtactggaggagaccagttgc		Rv	NP
Usp10	Fw	atgcccaggacttgtgacagc	***Usp10***	Fw	NP
	Rv	cctggcatcgcctcctagtg		Rv	NP
Usp11	Fw	gcctggcagaaccataaacgac	***Usp11***	Fw	NP
	Rv	cattgccacaatcagggcacac		Rv	NP
Usp12	Fw	accagcttcaccggtacacga	***Usp12***	Fw	NP
	Rv	ctgtcagggttggtcgcatct		Rv	NP
Usp13	Fw	cactggactggatcttcagcc	***Usp13***	Fw	tgatgaaccagttgatagaccc
	Rv	gcctcagacacgatgttggca		Rv	gcctcagacacgatgttggca
Usp14	Fw	atggaattgccatgtggattgac	***Usp14***	Fw	NP
	Rv	gggcatctttgagttcaggcac		Rv	NP
Usp15	Fw	cgcgcagtcacttaaggagca	***Usp15***	Fw	NP
	Rv	ccatcagtgtgtaccagctgac		Rv	NP
Usp16	Fw	agcacttgcgggagaagtgga	***Usp16***	Fw	NP
	Rv	ggccatccaaatccttctggtta		Rv	NP
Usp17L8	Fw	ctgccaatgacaagcccagtc	***Usp17L8***	Fw	NP
	Rv	cagggctgcattcaggtagca		Rv	NP
Usp18	Fw	acgcaggagtccctgatttgc	***Usp18***	Fw	NP
	Rv	cagaggctttgcgtccttatcaa		Rv	NP
Usp19	Fw	cctggctctggtgtggcgga	***Usp19***	Fw	NP
	Rv	cagcagagcctggatcttcagc		Rv	NP
Usp20	Fw	cggcatgaggtgatgtactcct	***Usp20***	Fw	tggctggccttcatcgtgg
	Rv	cagggacgtgcactccttgg		Rv	cagggacgtgcactccttgg

Usp21	Fw	ccgagtgggagccaagatacc	***Usp21***	Fw	NP
	Rv	cctgggaggcaaaggtcgtaa		Rv	NP
Usp22	Fw	tctaccccattctggcccttg	***Usp22***	Fw	NP
	Rv	ttcgcaggcagtctgtgagag		Rv	NP
Usp24	Fw	gtgtgcccagacaggatgctc	***Usp24***	Fw	NP
	Rv	ggttctcctcccactcctgg		Rv	NP
Usp25	Fw	agagcagccatcaagaagtgac	***Usp25***	Fw	ccaccgggagagccggtggat
	Rv	atcttcaagatcatgtgacgcct		Rv	atcttcaagatcatgtgacgcct
Usp26	Fw	cgcaaggtggatccaacaaagt	***Usp26***	Fw	NP
	Rv	tagtggcctccattgggactg		Rv	NP
Usp27X	Fw	tctggacttgcctggctcttg	***Usp27X***	Fw	NP
	Rv	agtggtgatgcctgggatgtg		Rv	NP
Usp28	Fw	catgaggagtactccaggctct	***Usp28***	Fw	catgaggagtactccaggctct
	Rv	catgctgaaggcgagggtcac		Rv	acaccaggtaggacaatgcttc
Usp29	Fw	ccagcgcagaagtgaacaagg	***Usp29***	Fw	NP
	Rv	ttctctgctttgccgcctctg		Rv	NP
Usp30	Fw	ctgccacagtgcctctgcat	***Usp30***	Fw	actggaagtctcagcaccct
	Rv	aactgcacgtgctcgtgcc		Rv	aactgcacgtgctcgtgcc
Usp31	Fw	ctgacagagccagcgtcacct	***Usp31***	Fw	NP
	Rv	acgtgcttgccatccactctg		Rv	NP
Usp32	Fw	caccgactctgcctacattctt	***Usp32***	Fw	NP
	Rv	ctcgtgtccgccatcttcttg		Rv	NP
Usp33	Fw	tcctccgacctccagttgttc	***Usp33***	Fw	NP
	Rv	gtgtcctcagaactacaaagagc		Rv	NP
Usp34	Fw	atggcaggtttgacgactgt	***Usp34***	Fw	tgacgaaggagcaactcctgt
	Rv	tcggattcatcttcagctagtg		Rv	tcggattcatcttcagctagtg
Usp35	Fw	catggtggcctctctggtcaa	***Usp35***	Fw	NP
	Rv	agcccgggaaccgaaacacc		Rv	NP
Usp36	Fw	gcatcgacacgctcctccca	***Usp36***	Fw	gcatcgacacgctcctccca
	Rv	gcaccctcaccctccgagc		Rv	ctcttcatcctgctgtggctc
Usp37	Fw	agaggtgctggcagctgtgtt	***Usp37***	Fw	NP
	Rv	gtgtccggactgctggttgg		Rv	NP
Usp38	Fw	cagcttcgttacccagtgctca	***Usp38***	Fw	NP
	Rv	gacaaaggcagctgttgctgga		Rv	NP
Usp39	Fw	caagccgtccacaagaacacc	***Usp39***	Fw	NP
	Rv	tgatgaagcacgtggatcctg		Rv	NP
Usp40	Fw	ctgaggacacagctacgcatc	***Usp40***	Fw	NP
	Rv	tcaaggagccagcagtccatc		Rv	NP
Usp41	Fw		***Usp41***	Fw	NP
	Rv			Rv	NP

Usp42	Fw	acaacgtcgacttcccccagt	***Usp42***	Fw	NP
	Rv	tctgaggactcggccccatag		Rv	NP
Usp43	Fw	gactcgggagcctcaacaaca	***Usp43***	Fw	NP
	Rv	tggtgaagacaggagagtcgg		Rv	NP
Usp44	Fw	gagcccagttccccgtacag	***Usp44***	Fw	NP
	Rv	agcatggcaaacggtgagacc		Rv	NP
Usp45	Fw	agcctcactgacggcagcg	***Usp45***	Fw	agcctcactgacggcagcg
	Rv	aggctgcttggaagcgatc		Rv	gacaggactggactgagcat
Usp46	Fw	accgggtggtcttccctctg	***Usp46***	Fw	NP
	Rv	aacgaccacagcaaccaggtc		Rv	NP
Usp47	Fw	gtccatgtcacagcttgccatc	***Usp47***	Fw	gagagtacagagttaaagtgtgcc
	Rv	gctttccaacacaagctcctgg		Rv	gctttccaacacaagctcctgg
Usp48	Fw	gcagcagcaggatgcacaaga	***Usp48***	Fw	NP
	Rv	ctgctgcacaacattccgaaca		Rv	NP
Usp49	Fw	caggagcctggagctcattca	***Usp49***	Fw	NP
	Rv	cccacttcccagaccacatga		Rv	NP
Usp50	Fw	actttggagatctggatggtgg	***Usp50***	Fw	NP
	Rv	tcactgactcgggtgtcatcaa		Rv	NP
Usp51	Fw	gacctgggtagcagtgccaaa	***Usp51***	Fw	NP
	Rv	gaaagcaggccacaatcggtaa		Rv	NP
Usp52	Fw	cggaagtatctggagctgagc	***Usp52***	Fw	NP
	Rv	cagtccatctttcggcccttc		Rv	NP
Usp53	Fw	ggagtccatgcatgacccagg	***Usp53***	Fw	tgaacaactggacgggtagctg
	Rv	tgaacaactggacgggtagctg		Rv	catctgtgagaactgctgggct
Usp54	Fw	cacgtgcaacctgcctagaa	***Usp54***	Fw	gaagagagcactgtcgctgg
	Rv	tccagttcagaggtctcctgc		Rv	tccagttcagaggtctcctgc
Cyld	Fw	tcccaggcagtgccgcatc	***Cyld***	Fw	tcccaggcagtgccgcatc
	Rv	tgcttgatcttcccagctgag		Rv	gaatgttgaagccattctgacc

SUPPLEMENTARY TABLE 2

JAMM								
	D. melanogaster [67]		***D. rerio*** [80]		***M. musculus***		***H. sapiens***	
	Neuronal phenotype	**Retinal phenotype**	**Neuronal phenotype**	**Retinal phenotype**	**Neuronal phenotype**	**Retinal phenotype**	**Neuronal phenotype**	**Retinal phenotype**
AMSH	ND	ND			Loss of neurons in the hippocampus and cerebral cortex [81]		Microcephaly-capillary malformation syndrome (OMIM)	
AMSH-Like								
BRCC36	ND	ND						
CSN5					-/- homozygotes die soon after implantation and exhibit growth-retardation, decrease in cell proliferation, and an increase in cell apoptosis.			
CSN6	Pupal death		1dpf: **cns necrosis**, fused somite; 4dpf: small size and short body, small head, pericardial edema, unconsumed egg yolk with no yolk extension, **shorten notochord length**, dysmorphic axis, underdeveloped tail	4dpf: small eyes	-/- homozygotes are embryonic lethal [29]			
EIF3H	Pan-neural knockdown is							

	developmentally lethal						
JAMM2							
JAMM3							
MYSM1	ND	ND	1dpf: **cns necrosis**, curled tail developed; 3dpf: narrow head; closed otoliths, abnormal yolk shape with short yolk extension, **abnormal notochord shape**, slightly curled tail, ratty caudal fin	3dpf: funny eyes shape			
POH1	Larval death						
PRPF8						Retinal degeneration in heterozygotes, more severe in homozygotes [29]	autosomal dominant retinitis pigmentosa
PSMD7			1dpf: **serious cns necrosis**; 2dpf: small and short body, underdeveloped head, preicardical edema, **shorten notochord**, thin trunk, fused somite, shorten and fatty tail, shorten yolk extension		-/- homozygotes are embryonic lethal [29]		

MJD								
	D. melanogaster		**D. rerio**		**M. musculus**		**H. sapiens**	
	Neuronal phenotype	**Retinal phenotype**	**Neuronal phenotype**	**Retinal phenotype**	**Neuronal phenotype**	**Retinal phenotype**	**Neuronal phenotype**	**Retinal phenotype**
ATX3	**ND**	**ND**	**1dpf: cns necrosis, fused somite; 3dpf: reduced body length, dysmorphic axis development, malformed and shorter tail**				**Neurodegenerative disease SCA3** [79]	
JOSD1	**ND**	**ND**	**1dpf: serious cns necrosis,**	**3dpf: funny**				

			slightly trunk and tail necrosis, fused somite, shorten tail; 3dpf: small head, strange yolk shape, abnormal notochord shape, irregular floorplate, hemorrhage at tail region, fused somite, shorten and curled tail	eyes shape, abnormal retinotectal projection		
JOSD2			1dpf: abnormal head shape, fused somite; 4dpf: small and short body, strange head shape, tectum enlarged, pericardial edema, unconsumed egg yolk, fat and short yolk extension, dysmorphic axis development, abnormal notochord shape, curled tail			
JOSD3	ND	ND	ND	ND		

	OTU							
	D. melanogaster		D. rerio		M. musculus		H. sapiens	
	Neuronal phenotype	Retinal phenotype	Neuronal phenotype	Retinal phenotype	Neuronal phenotype	Retinal phenotype	Neuronal phenotype	Retinal phenotype
OTUB1			1dpf: cns necrosis, fused somite; 2dpf: small and short body, round yolk shape with thin yolk extension, thin trunk, curled tail					
OTUB2	ND	ND	ND	ND				
OTUD1	ND	ND	ND	ND				
OTUD3	ND	ND	1dpf: slightly cns and trunk necrosis, fused					

			somite; 3dpf: serious dysmorphic development of axis and notochord, curled tail			
OTUD4			1dpf: underdeveloped trunk; 3dpf: small and short body, reduced pigementation, cns necrosis, dysmorphic notochord shape, thin trunk, slightly curled tail (Tse)	3dpf: undeveloped eye (Tse). Reduction in size of the optic tecta and cerebellum (Margolin 2013)		Mutated, together with RNF216, in cerebellar ataxia and hypogonadotropic hypogonadism (Gordon Holmes syndrome) [70]
OTUD5			1dpf: cns necrosis, fused somite; 3dpf: reduced pigement, small and short body, pericardial edema, thin and short yolk extension, slightly bent body		Abnormal embryo turning and developmental patterning [29]	
OTUD6a	ND	ND	ND	ND		
OTUD6b						
OTUD7a	ND	ND				
OTUD7b	ND	ND	ND 1dpf: underdeveloped trunk and notochord, fused somite; 3dpf: small and short body, slightly trunk necrosis, fused and curled tail	ND		
PARPF11			1dpf: cns necrosis, fused somite; 4dpf: strange head shape, small and short body, dysmorphic axis shape, thin trunk curled tail, ratty caudal			

			fin			
TNFAIP3	**ND**	**ND**	**1dpf: trunk and tail necrosis; 4dpf: abnormal head shape, pericardial edema, axis and notochord problems, thin trunk, unconsumed egg yolk with no yolk extension, short and curled tail**			
VCPIP1	**ND**	**ND**	**1dpf: underdeveloped trunk and notochord, shorten and fused tail; 4dpf: small and small body, small head, thin trunk, abnormal somite shape, curled and thin tail**	**4dpf: small eyes**		
YOD1			**No early phenotype; 3dpf: short and edema body, pericardial edema, unconsumed egg yolk with fat and shorten yolk extension, underdeveloped liver and gut, abnormal axis and notochord shape, fused somite, short and curled tail**			
ZRANB1	**Pharate adult and young adult death (Sokol)**		**1dpf:fused somite, curled tail developed; 3dpf: shorten body length, abnormal notochord shape, no yolk extension, curled tail**			

UCH								
	D. melanogaster		D. rerio		M. musculus		H. sapiens	
	Neuronal phenotype	Retinal phenotype	Neuronal phenotype	Retinal phenotype	Neuronal phenotype	Retinal phenotype	Neuronal phenotype	Retinal phenotype
BAP1			1dpf: serious cns and trunk necrosis, fused somite; 4dpf: hemorrhage in head, unconsumed egg yolk, abnormal notochord shape, curled tail		-/- homozygotes are embryonic lethal(Clague)			
UCHL1	ND	ND			Gracile axonal dystrophy [79]		Linked to PD and other diseases [79]Childhood-Onset Neurodegeneration With Optic Atrophy: Progressive visual loss due to optic atrophy at around age 5 years, followed by spasticity, cerebellar ataxia, peripheral neuropathy, and myokymia, consistent with systemic neurodegeneration and deficits at the neuromuscular junction (OMIM)	
UCHL3			1dpf: slightly trunk necrosis, fused somite; 3dpf: small and short body, pericardial edema, fat and short yolk extension, abnormal notochord shape, curled and malformed tail	3dpf: reduced eye pigment	Learning and working memory deficits [79]	Retinal degeneration [79]		

UCHL5	**Pupal and pharate adult death (FUNC: NEUROGENESIS)**	**1dpf: cns necrosis, abnormal head shape, fused somite; 4dpf: thick looking jaw, enlarged otolith, pericardial edema, thin yolk extension, slightly body bent and curled tail, ratty caudal fin**	**Prenatal lethality, severely abnormal brain development [29]**	

USP								
	D. melanogaster		**D. rerio**		**M. musculus**		**H. sapiens**	
	Neuronal phenotype	**Retinal phenotype**	**Neuronal phenotype**	**Retinal phenotype**	**Neuronal phenotype**	**Retinal phenotype**	**Neuronal phenotype**	**Retinal phenotype**
USP 1	**(Neuronal) Slower Adults**		**No early phenotype; 3dpf: abnormal notochord development, body bent, thin trunk and curved tail**		**Elevated perinatal lethality, male infertility. Fancony anemia [29]**			
USP 2	**Pan-neuronal knockdown leads to reduced locomotion and earlier adult death [79]**							**Upregulated in high-grade gliomas [79]**
USP 3	**ND**	**ND**	**1dpf: serious cns necrosis, fused somite; 2dpf: small and short body, underdeveloped head, reduced pigmentation, enlarged tectum, thin trunk, body bent, abnormal notochord development, curled and fused tail**	**2pdf: underdeveloped eyes**				

USP 4	**ND**	**ND**	**ND** **1dpf: cns necrosis; 2dpf: small and short body, small head, unconsumed yolk with thin extension, notochord problem, curled tail**	**ND** **2dpf: small eyes**		
USP 5	**Pupal death(Sokol)**		**1dpf: slightly cns necrosis, undeveloped trunk, fused tail; 2dpf: small and short body, abnormal head shape, percardial edema, dysmorphic axis shape, shorten notochord, trunk and tail necrosis, short and curled tail**	**2dpf: underdeveloped small eyes**	**-/- homozygotes are embryonic lethal** [29]	
USP 6	**ND**	**ND**	**ND**	**ND**		
USP 7	**Pharate adult death**		**1dpf: slightly cns damage; 2dpf: small and short body, small head, reduced pigment, "bud" on head, abnormal notochord development, fused tail, ratty caudal fin, ; 3dpf: close otoliths, slightly percardial edema, unconsumed yolk in pear shape**	**2dpf: small eyes**	**-/- homozygotes are embryonic lethal(Clague). Brain specific knockdown causes brain malformation and neonatal lethality, due at least in part to p53-dependent mechanisms.** [79]	
USP 8	**Larval death**		**1dpf: serious cns and truck necrosis, fused somite; 3dpf: small body, slightly cns necrosis, percardial edema, abnormal**		**Brain development deficiencies in brain targeted knockout (Hausp fl/fl nes-Cre) mice**	

			notochord development, fused somite, curled tail with ratty caudal fin			
USP 9X			ND	ND	reduction in axonal length and arborisation, decrease in neuronal migration [82]	Involved in neuronal fate specification and NMJ function.(Sokol?) patients with multiple myeloma overexpressing USP9X have a poor prognosis [83]
USP 9Y	ND	ND	ND	ND		
USP 10			1dpf: cns necrosis, fused somite; 2dpf: small and short body, reduced pigment, thin trunk, body bent ventrically, curled tail, ratty caudal fin			
USP 11	ND	ND				
USP 12	ND	ND	1dpf: cns and tail necrosis; 4dpf: slightly edema body, pericardial edema, unconsumed yolk, abnormal yolk shape with thin yolk extension, dysmorphic notochord and axis shape, curled tail			
USP 13	ND	ND	1dpf: cns necrosis, fused somite; 2dpf:			

			small and short body, reduced pigment, thin trunk, dysmorphic notochord shape, pericardial edema, slightly curled tail			
USP 14	(Neuronal)Slower adults, early death (Sokol)				Mutations in intron leads to redyced USP14 leves. Tremors, abnormal brain morphology, altered synaptic transmission and increased apoptosis. [29]	
USP 15	ND	ND	1dpf: cns necrosis, fused somite; 2dpf: underdeveloped head and trunk, axis and notochord problems, pericardial edema, fused somite, short and slightly curled tail; 4dpf: unshaped head; body edema, round shape unconsumed yolk, underdeveloped liver and gut, tail slightly necrosis	2dpf: small eyes 4dpf: unshaped eyes		
USP 16	ND	ND			reduces the self-renewal of hematopoietic stem cells and the expansion of mammary epithelial cells, neuroprogenitors, and fibroblasts [84]	overexpression of USP16 reduces the expansion of normal fibroblasts and postnatal neural progenitors, whereas downregulation of USP16 partially rescues the

						proliferation defects of Down syndrome [84]
USP 17	ND	ND	ND	ND		
USP 18	ND	ND	1dpf: cns and tail necrosis, fused somite; 2dpf: underdeveloped trunk, tail necrosis; 3dpf: small and short body, small head, thin trunk, shorten notochord length, serious pericardial edema, unconsumed yolk with short yolk extensionshorten, short and curved tail	3dpf: small eyes	Tremors, seizures, abnormal nervous system, death [29]	
USP 19	ND	ND	1dpf: slightly cns necrosis, fused somite; 2dpf: small and short body, reduced pigement, small head, shorten notochord length, pericardial edema, short and curled tail with slightly necrosis (with "buds"),	2dpf: small eyes		
USP 20	Earlier adulth death		1dpf: cns necrosis, fused somite; 2dpf: small and short body, reduced pigment, "buds" on the pericardial and yolk area, tail necrosis; 3dpf: small head, precardial edema,	3dpf: small eyes		

			"buds" (necrosis) on the precardical area, unconsumed yolk with short extension, curled tail with slightly necrosis at the end			
USP 21	ND	ND	1dpf: mild necrosis throughout the body; 3dpf: underdeveloped head, small head, abnormal axis and notochord development, trunk necrosis, pericardial edema, roundly and unconsumed yolk with no yolk extension, no tail	3dpf: small eyes		
USP 22		Axonal projection of photoreceptor cells [79]	No early phenotype at 1dpf; 2dpf: inflated brain		-/- homozygotes are embryonic lethal [29]	
USP 24	ND	ND	1dpf: body necrosis, fused somite; 2dpf: small and short body, cns necrosis became more seriously, abnormal notochord development, thin trunk, fat and short yolk extension, curled short tail with necrosis	2dpf: abnormal eyes		May be involved in PD susceptibility [79]
USP 25	ND	ND	1dpf: cns and tail necrosis; 2dpf: small and short body, unshaped head, cns necrosis, bulging	2dpf: unshaped eyes		Overexpressed in Down Syndrome brains [79]

			forebrain, thin trunk, fused somite, tail necrosis			
USP 26	ND	ND	ND	ND		
USP 27	ND	ND	ND	ND		
USP 28	ND	ND	ND 1dpf: head damage, fused somite; 2dpf: serious cns necrosis, reduced pigment, notochord and axis underdevelopment, thin trunk, shorten and curved tail	ND		
USP 29	ND	ND	ND	ND		
USP 30	Knockdown of Usp30 in dopaminergic neurons protects flies against paraquat toxicity in vivo, ameliorating defects in dopamine levels, motor function, and organismal survival. [85]					
USP 31	ND	ND				
USP 32						
USP 33	ND	ND	1dpf: cns necrosis; 3dpf: small and short	3dpf: small eyes	in cultured mouse embryonic	Regulates axonal pathfinding during

			body, small head, notochord development problem, curled tail		commissural axons and was required for growth cone collapse in response to Slit exposure [86]	development [79] (AQUI??))
USP 34	Pan neuronal knockdown is developmentaly lethal [79]					
USP 35			ND	ND		
USP 36	Larval death		1dpf: slightly cns necrosis; 3dpf: small and short body, reduced pigment, very thin trunk, pericardial edema, funny yolk shape with fat yolk extension, curled tail			
USP 37	ND	ND	1dpf: cns necrosis; 3dpf: small and short body, small head, tectum enlargement, pericardial edema, round yolk shape, thin trunk, notochord problem, shorten and slightly curled tail	3dpf: small eyes		
USP 38	ND	ND				
USP 39	Larval death		1dpf: cns and tail necrosis, 2dpf: small and short body, small head, slightly pericardial edema, dysmorphic notochord development, fused	2dpf: small eyes		

			somite, curled tail			
USP 40	ND	ND				May be involved in PD susceptibility [79]
USP 41	ND	ND	ND	ND		
USP 42	ND	ND	1dpf: slightly cns necrosis, fused somite; 3dpf: inflated hindbrain, slightly pericardial edema and body bent			
USP 43			1dpf: slightly cns necrosis, fused somite; 2dpf: small and short body, reduced pigment, small head, bulging forebrain, pericardial edema, curled tail	2dpf: small eyes		
USP 44	ND	ND	1dpf: abnormal development, cns and tail necrosis, fused somite; 3dpf: very small and short body, underdeveloped head and trunk, shorten notochord length, axis development problem, serious pericardial edema, unconsumed round yolk with short yolk extension, short and curled tail			
USP 45	Pupal, pharate adult and young adult death		1dpf: cns necrosis; 2dpf: reduced pigment, a bit smaller head, close otolith distance,	2dpf: reduced eyes		

			slightly pericardial edema, thin yolk extension			
USP 46					role in the GABAergic neurotransmission [87]	
USP 47						
USP 48	ND	ND	No early phenotype; 3dpf: small and short body, reduced pigement, small head, pericardial edema, body bent, slightly tail necrosis	3dpf: small eyes		
USP 49	ND	ND	ND	ND		
USP 50	ND	ND	ND	ND		
USP 51	ND	ND	ND	ND		
USP 52			ND	ND		
USP 53	ND	ND	No early phenotype at 1dpf; 3dpf: small and short body, reduced pigment, small head, inflated brain, notochord problem, curled tail	3dpf: small eyes		
USP 54	Pharate adult and young adult death					
CYLD			1dpf: cns necrosis; 2dpf: small and short body, strange head shape, thinner mid/hidbrain	1dpf: small eyes (Cyldb)		

	boundary, midbrain enlargement, round yolk shape with thin extension, slightly axis and notochord problem, curled tail **1dpf: cns necrosis, trunk necrosis; 2dpf: small and short body, small head, necrosis spread through the body, pericardial edema, thin trunk, notochord problem, body bent**		

Annex II

Table 14. Mass spectrometry results from CRX-immunoprecipitated adult WT mouse retina.

Accession	Description	Proteins	Unique Peptides	Peptides	AAs	MW [kDa]
P09651	Heterogeneous nuclear ribonucleoprotein A1 OS=Homo sapiens GN=HNRNPA1 PE=1 SV=5 - [ROA1_HUMAN]	1	22	26	372	38,7
P22626	Heterogeneous nuclear ribonucleoproteins A2/B1 OS=Homo sapiens GN=HNRNPA2B1 PE=1 SV=2 - [ROA2_HUMAN]	1	19	22	353	37,4
P13645	Keratin, type I cytoskeletal 10 OS=Homo sapiens GN=KRT10 PE=1 SV=6 - [K1C10_HUMAN]	1	33	37	584	58,8
P35908	Keratin, type II cytoskeletal 2 epidermal OS=Homo sapiens GN=KRT2 PE=1 SV=2 - [K22E_HUMAN]	1	28	37	639	65,4
P04264	Keratin, type II cytoskeletal 1 OS=Homo sapiens GN=KRT1 PE=1 SV=6 - [K2C1_HUMAN]	1	32	35	644	66,0
P35527	Keratin, type I cytoskeletal 9 OS=Homo sapiens GN=KRT9 PE=1 SV=3 - [K1C9_HUMAN]	1	27	28	623	62,0
P02769	SWISS-PROT:P02769 (Bos taurus) Bovine serum albumin precursor	1	29	29	607	69,2
P31942	Heterogeneous nuclear ribonucleoprotein H3 OS=Homo sapiens GN=HNRNPH3 PE=1 SV=2 - [HNRH3_HUMAN]	1	13	13	346	36,9
Q15717	ELAV-like protein 1 OS=Homo sapiens GN=ELAVL1 PE=1 SV=2 - [ELAV1_HUMAN]	1	12	12	326	36,1
P12004	Proliferating cell nuclear antigen OS=Homo sapiens GN=PCNA PE=1 SV=1 - [PCNA_HUMAN]	1	14	14	261	28,8
P13647	Keratin, type II cytoskeletal 5 OS=Homo sapiens GN=KRT5 PE=1 SV=3 - [K2C5_HUMAN]	1	12	23	590	62,3
P02538	Keratin, type II cytoskeletal 6A OS=Homo sapiens GN=KRT6A PE=1 SV=3 - [K2C6A_HUMAN]	2	11	24	564	60,0
P02533	Keratin, type I cytoskeletal 14 OS=Homo sapiens GN=KRT14 PE=1 SV=4 - [K1C14_HUMAN]	1	8	21	472	51,5
P07195	L-lactate dehydrogenase B chain OS=Homo sapiens GN=LDHB PE=1 SV=2 - [LDHB_HUMAN]	1	14	15	334	36,6
P51991	Heterogeneous nuclear ribonucleoprotein A3 OS=Homo sapiens GN=HNRNPA3 PE=1 SV=2 - [ROA3_HUMAN]	1	16	18	378	39,6
P08779	Keratin, type I cytoskeletal 16 OS=Homo sapiens GN=KRT16 PE=1 SV=4 - [K1C16_HUMAN]	1	8	21	47	51,2

					3	
Q99623	Prohibitin-2 OS=Homo sapiens GN=PHB2 PE=1 SV=2 - [PHB2_HUMAN]	1	16	16	299	33,3
P63244	Guanine nucleotide-binding protein subunit beta-2-like 1 OS=Homo sapiens GN=GNB2L1 PE=1 SV=3 - [GBLP_HUMAN]	1	16	16	317	35,1
P00338	L-lactate dehydrogenase A chain OS=Homo sapiens GN=LDHA PE=1 SV=2 - [LDHA_HUMAN]	1	14	15	332	36,7
Q9P015	39S ribosomal protein L15, mitochondrial OS=Homo sapiens GN=MRPL15 PE=1 SV=1 - [RM15_HUMAN]	1	16	16	296	33,4
P46777	60S ribosomal protein L5 OS=Homo sapiens GN=RPL5 PE=1 SV=3 - [RL5_HUMAN]	1	12	12	297	34,3
P07437	Tubulin beta chain OS=Homo sapiens GN=TUBB PE=1 SV=2 - [TBB5_HUMAN]	1	4	13	444	49,6
P61247	40S ribosomal protein S3a OS=Homo sapiens GN=RPS3A PE=1 SV=2 - [RS3A_HUMAN]	1	16	16	264	29,9
Q13151	Heterogeneous nuclear ribonucleoprotein A0 OS=Homo sapiens GN=HNRNPA0 PE=1 SV=1 - [ROA0_HUMAN]	1	9	10	305	30,8
P61978	Heterogeneous nuclear ribonucleoprotein K OS=Homo sapiens GN=HNRNPK PE=1 SV=1 - [HNRPK_HUMAN]	1	12	12	463	50,9
P06576	ATP synthase subunit beta, mitochondrial OS=Homo sapiens GN=ATP5B PE=1 SV=3 - [ATPB_HUMAN]	1	11	11	529	56,5
P68371	Tubulin beta-4B chain OS=Homo sapiens GN=TUBB4B PE=1 SV=1 - [TBB4B_HUMAN]	1	4	13	445	49,8
P21796	Voltage-dependent anion-selective channel protein 1 OS=Homo sapiens GN=VDAC1 PE=1 SV=2 - [VDAC1_HUMAN]	1	13	14	283	30,8
O75569	Interferon-inducible double-stranded RNA-dependent protein kinase activator A OS=Homo sapiens GN=PRKRA PE=1 SV=1 - [PRKRA_HUMAN]	1	12	12	313	34,4
Q9BYD6	39S ribosomal protein L1, mitochondrial OS=Homo sapiens GN=MRPL1 PE=1 SV=2 - [RM01_HUMAN]	1	12	12	325	36,9
P60891	Ribose-phosphate pyrophosphokinase 1 OS=Homo sapiens GN=PRPS1 PE=1 SV=2 - [PRPS1_HUMAN]	1	3	10	318	34,8
P11908	Ribose-phosphate pyrophosphokinase 2 OS=Homo sapiens GN=PRPS2 PE=1 SV=2 - [PRPS2_HUMAN]	1	2	9	318	34,7
P62873	Guanine nucleotide-binding protein G(I)/G(S)/G(T) subunit beta-1 OS=Homo sapiens GN=GNB1 PE=1 SV=3 - [GBB1_HUMAN]	1	5	12	340	37,4
O60506	Heterogeneous nuclear ribonucleoprotein Q OS=Homo sapiens GN=SYNCRIP PE=1 SV=2 - [HNRPQ_HUMAN]	1	13	13	62	69,6

					3	
P11940	Polyadenylate-binding protein 1 OS=Homo sapiens GN=PABPC1 PE=1 SV=2 - [PABP1_HUMAN]	1	6	11	636	70,6
P19387	DNA-directed RNA polymerase II subunit RPB3 OS=Homo sapiens GN=POLR2C PE=1 SV=2 - [RPB3_HUMAN]	1	8	8	275	31,4
P02662	SWISS-PROT:P02662 Alpha-S1-casein - Bos taurus (Bovine).	1	5	5	199	23,0
P35637	RNA-binding protein FUS OS=Homo sapiens GN=FUS PE=1 SV=1 - [FUS_HUMAN]	1	6	6	526	53,4
P62879	Guanine nucleotide-binding protein G(I)/G(S)/G(T) subunit beta-2 OS=Homo sapiens GN=GNB2 PE=1 SV=3 - [GBB2_HUMAN]	1	3	9	340	37,3
Q01081	Splicing factor U2AF 35 kDa subunit OS=Homo sapiens GN=U2AF1 PE=1 SV=3 - [U2AF1_HUMAN]	1	7	7	240	27,9
P31943	Heterogeneous nuclear ribonucleoprotein H OS=Homo sapiens GN=HNRNPH1 PE=1 SV=4 - [HNRH1_HUMAN]	1	6	8	449	49,2
ENSEMBL:ENSBTAP00000024466	(Bos taurus) 44 kDa protein	1	8	8	401	43,9
ENSEMBL:ENSBTAP00000016242	(Bos taurus) similar to alpha-tubulin I isoform 1	2	8	8	451	50,1
Q9UNP9	Peptidyl-prolyl cis-trans isomerase E OS=Homo sapiens GN=PPIE PE=1 SV=1 - [PPIE_HUMAN]	1	9	9	301	33,4
P00761 SWISS-PROT:P00761	Trypsin - Sus scrofa (Pig). - [TRYP_PIG]	1	6	6	231	24,4
O14979	Heterogeneous nuclear ribonucleoprotein D-like OS=Homo sapiens GN=HNRNPDL PE=1 SV=3 - [HNRDL_HUMAN]	1	8	10	420	46,4
Q13765	Nascent polypeptide-associated complex subunit alpha OS=Homo sapiens GN=NACA PE=1 SV=1 - [NACA_HUMAN]	2	6	6	215	23,4
Q99729	Heterogeneous nuclear ribonucleoprotein A/B OS=Homo sapiens GN=HNRNPAB PE=1 SV=2 - [ROAA_HUMAN]	1	8	9	332	36,2
Q9H9J2	39S ribosomal protein L44, mitochondrial OS=Homo sapiens GN=MRPL44 PE=1 SV=1 - [RM44_HUMAN]	1	11	11	332	37,5
Q15014	Mortality factor 4-like protein 2 OS=Homo sapiens GN=MORF4L2 PE=1 SV=1 - [MO4L2_HUMAN]	1	9	9	288	32,3
Q96AG4	Leucine-rich repeat-containing protein 59 OS=Homo sapiens GN=LRRC59 PE=1 SV=1 - [LRC59_HUMAN]	1	10	10	307	34,9
P07910	Heterogeneous nuclear ribonucleoproteins C1/C2 OS=Homo sapiens GN=HNRNPC PE=1 SV=4 - [HNRPC_HUMAN]	1	8	8	30	33,6

					6	
P38159	RNA-binding motif protein, X chromosome OS=Homo sapiens GN=RBMX PE=1 SV=3 - [RBMX_HUMAN]	1	10	10	3 9 1	42,3
Q01844	RNA-binding protein EWS OS=Homo sapiens GN=EWSR1 PE=1 SV=1 - [EWS_HUMAN]	1	6	6	6 5 6	68,4
Q13310	Polyadenylate-binding protein 4 OS=Homo sapiens GN=PABPC4 PE=1 SV=1 - [PABP4_HUMAN]	1	3	8	6 4 4	70,7
P14866	Heterogeneous nuclear ribonucleoprotein L OS=Homo sapiens GN=HNRNPL PE=1 SV=2 - [HNRPL_HUMAN]	1	9	9	5 8 9	64,1
Q15181	Inorganic pyrophosphatase OS=Homo sapiens GN=PPA1 PE=1 SV=2 - [IPYR_HUMAN]	1	5	6	2 8 9	32,6
Q14103	Heterogeneous nuclear ribonucleoprotein D0 OS=Homo sapiens GN=HNRNPD PE=1 SV=1 - [HNRPD_HUMAN]	1	6	8	3 5 5	38,4
P13804	Electron transfer flavoprotein subunit alpha, mitochondrial OS=Homo sapiens GN=ETFA PE=1 SV=1 - [ETFA_HUMAN]	1	7	7	3 3 3	35,1
Q07021	Complement component 1 Q subcomponent-binding protein, mitochondrial OS=Homo sapiens GN=C1QBP PE=1 SV=1 - [C1QBP_HUMAN]	1	5	5	2 8 2	31,3
Q9HAV0	Guanine nucleotide-binding protein subunit beta-4 OS=Homo sapiens GN=GNB4 PE=1 SV=3 - [GBB4_HUMAN]	1	4	8	3 4 0	37,5
P09493	Tropomyosin alpha-1 chain OS=Homo sapiens GN=TPM1 PE=1 SV=2 - [TPM1_HUMAN]	1	3	7	2 8 4	32,7
Q9BRJ2	39S ribosomal protein L45, mitochondrial OS=Homo sapiens GN=MRPL45 PE=1 SV=2 - [RM45_HUMAN]	1	8	8	3 0 6	35,3
P43307	Translocon-associated protein subunit alpha OS=Homo sapiens GN=SSR1 PE=1 SV=3 - [SSRA_HUMAN]	1	4	4	2 8 6	32,2
P67936	Tropomyosin alpha-4 chain OS=Homo sapiens GN=TPM4 PE=1 SV=3 - [TPM4_HUMAN]	1	3	6	2 4 8	28,5
P68104	Elongation factor 1-alpha 1 OS=Homo sapiens GN=EEF1A1 PE=1 SV=1 - [EF1A1_HUMAN]	2	8	8	4 6 2	50,1
Q9GZS3	WD repeat-containing protein 61 OS=Homo sapiens GN=WDR61 PE=1 SV=1 - [WDR61_HUMAN]	1	6	6	3 0 5	33,6
P06753	Tropomyosin alpha-3 chain OS=Homo sapiens GN=TPM3 PE=1 SV=2 - [TPM3_HUMAN]	1	2	6	2 8 5	32,9
Q9BQ75	Protein CMSS1 OS=Homo sapiens GN=CMSS1 PE=1 SV=2 - [CMS1_HUMAN]	1	6	6	2 7 9	31,9
P60709	Actin, cytoplasmic 1 OS=Homo sapiens GN=ACTB PE=1 SV=1 - [ACTB_HUMAN]	2	8	8	3 7	41,7

					5	
P62753	40S ribosomal protein S6 OS=Homo sapiens GN=RPS6 PE=1 SV=1 - [RS6_HUMAN]	1	5	5	249	28,7
P23396	40S ribosomal protein S3 OS=Homo sapiens GN=RPS3 PE=1 SV=2 - [RS3_HUMAN]	1	6	6	243	26,7
Q13243	Serine/arginine-rich splicing factor 5 OS=Homo sapiens GN=SRSF5 PE=1 SV=1 - [SRSF5_HUMAN]	1	6	6	272	31,2
P09001	39S ribosomal protein L3, mitochondrial OS=Homo sapiens GN=MRPL3 PE=1 SV=1 - [RM03_HUMAN]	1	8	8	348	38,6
P45880	Voltage-dependent anion-selective channel protein 2 OS=Homo sapiens GN=VDAC2 PE=1 SV=2 - [VDAC2_HUMAN]	1	7	8	294	31,5
O95983	Methyl-CpG-binding domain protein 3 OS=Homo sapiens GN=MBD3 PE=1 SV=1 - [MBD3_HUMAN]	1	5	5	291	32,8
P52597	Heterogeneous nuclear ribonucleoprotein F OS=Homo sapiens GN=HNRNPF PE=1 SV=3 - [HNRPF_HUMAN]	1	2	4	415	45,6
P05388	60S acidic ribosomal protein P0 OS=Homo sapiens GN=RPLP0 PE=1 SV=1 - [RLA0_HUMAN]	1	5	5	317	34,3
P15880	40S ribosomal protein S2 OS=Homo sapiens GN=RPS2 PE=1 SV=2 - [RS2_HUMAN]	1	5	5	293	31,3
Q01085	Nucleolysin TIAR OS=Homo sapiens GN=TIAL1 PE=1 SV=1 - [TIAR_HUMAN]	1	4	6	375	41,6
Q9UNQ2	Probable dimethyladenosine transferase OS=Homo sapiens GN=DIMT1 PE=1 SV=1 - [DIM1_HUMAN]	1	7	7	313	35,2
Q8WXX5	DnaJ homolog subfamily C member 9 OS=Homo sapiens GN=DNAJC9 PE=1 SV=1 - [DNJC9_HUMAN]	1	5	5	260	29,9
O00743	Serine/threonine-protein phosphatase 6 catalytic subunit OS=Homo sapiens GN=PPP6C PE=1 SV=1 - [PPP6_HUMAN]	1	5	5	305	35,1
P31483	Nucleolysin TIA-1 isoform p40 OS=Homo sapiens GN=TIA1 PE=1 SV=3 - [TIA1_HUMAN]	1	3	5	386	42,9
O14579	Coatomer subunit epsilon OS=Homo sapiens GN=COPE PE=1 SV=3 - [COPE_HUMAN]	1	3	3	308	34,5
Q00403	Transcription initiation factor IIB OS=Homo sapiens GN=GTF2B PE=1 SV=1 - [TF2B_HUMAN]	1	3	3	316	34,8
Q9Y314	Nitric oxide synthase-interacting protein OS=Homo sapiens GN=NOSIP PE=1 SV=1 - [NOSIP_HUMAN]	1	6	6	301	33,2
P19623	Spermidine synthase OS=Homo sapiens GN=SRM PE=1 SV=1 - [SPEE_HUMAN]	1	5	5	30	33,8

					2	
Q9H2U2	Inorganic pyrophosphatase 2, mitochondrial OS=Homo sapiens GN=PPA2 PE=1 SV=2 - [IPYR2_HUMAN]	1	3	4	33 4	37,9
O43186	Cone-rod homeobox protein OS=Homo sapiens GN=CRX PE=1 SV=1 - [CRX_HUMAN]	1	5	5	29 9	32,2
P50402	Emerin OS=Homo sapiens GN=EMD PE=1 SV=1 - [EMD_HUMAN]	1	5	5	25 4	29,0
Q6ZN17	Protein lin-28 homolog B OS=Homo sapiens GN=LIN28B PE=1 SV=1 - [LN28B_HUMAN]	1	5	5	25 0	27,1
Q07955	Serine/arginine-rich splicing factor 1 OS=Homo sapiens GN=SRSF1 PE=1 SV=2 - [SRSF1_HUMAN]	1	4	4	24 8	27,7
Q6UXN9	WD repeat-containing protein 82 OS=Homo sapiens GN=WDR82 PE=1 SV=1 - [WDR82_HUMAN]	1	7	7	31 3	35,1
Q7L5D6	Golgi to ER traffic protein 4 homolog OS=Homo sapiens GN=GET4 PE=1 SV=1 - [GET4_HUMAN]	1	2	2	32 7	36,5
Q16629	Serine/arginine-rich splicing factor 7 OS=Homo sapiens GN=SRSF7 PE=1 SV=1 - [SRSF7_HUMAN]	1	6	6	23 8	27,4
Q9H9B4	Sideroflexin-1 OS=Homo sapiens GN=SFXN1 PE=1 SV=4 - [SFXN1_HUMAN]	1	4	4	32 2	35,6
Q96C36	Pyrroline-5-carboxylate reductase 2 OS=Homo sapiens GN=PYCR2 PE=1 SV=1 - [P5CR2_HUMAN]	1	3	4	32 0	33,6
Q15006	ER membrane protein complex subunit 2 OS=Homo sapiens GN=EMC2 PE=1 SV=1 - [EMC2_HUMAN]	1	3	3	29 7	34,8
Q9H4A6	Golgi phosphoprotein 3 OS=Homo sapiens GN=GOLPH3 PE=1 SV=1 - [GOLP3_HUMAN]	1	2	2	29 8	33,8
O14893	Gem-associated protein 2 OS=Homo sapiens GN=GEMIN2 PE=1 SV=1 - [GEMI2_HUMAN]	1	3	3	28 0	31,6
P16403	Histone H1.2 OS=Homo sapiens GN=HIST1H1C PE=1 SV=2 - [H12_HUMAN]	3	5	5	21 3	21,4
Q96B26	Exosome complex component RRP43 OS=Homo sapiens GN=EXOSC8 PE=1 SV=1 - [EXOS8_HUMAN]	1	4	4	27 6	30,0
Q9BYD3	39S ribosomal protein L4, mitochondrial OS=Homo sapiens GN=MRPL4 PE=1 SV=1 - [RM04_HUMAN]	1	5	5	31 1	34,9
P36542	ATP synthase subunit gamma, mitochondrial OS=Homo sapiens GN=ATP5C1 PE=1 SV=1 - [ATPG_HUMAN]	1	5	5	29 8	33,0
P08758	Annexin A5 OS=Homo sapiens GN=ANXA5 PE=1 SV=2 - [ANXA5_HUMAN]	1	4	4	32	35,9

					0	
P62995	Transformer-2 protein homolog beta OS=Homo sapiens GN=TRA2B PE=1 SV=1 - [TRA2B_HUMAN]	1	3	3	288	33,6
O00165	HCLS1-associated protein X-1 OS=Homo sapiens GN=HAX1 PE=1 SV=2 - [HAX1_HUMAN]	1	4	4	279	31,6
Q13595	Transformer-2 protein homolog alpha OS=Homo sapiens GN=TRA2A PE=1 SV=1 - [TRA2A_HUMAN]	1	4	4	282	32,7
P00387	NADH-cytochrome b5 reductase 3 OS=Homo sapiens GN=CYB5R3 PE=1 SV=3 - [NB5R3_HUMAN]	1	4	4	301	34,2
Q8WXF0	Serine/arginine-rich splicing factor 12 OS=Homo sapiens GN=SRSF12 PE=2 SV=1 - [SRS12_HUMAN]	1	1	3	261	30,5
P02663	SWISS-PROT:P02663 Alpha-S2-casein [Contains: Casocidin-1 - Bos taurus (Bovine).	1	4	4	207	24,3
P60510	Serine/threonine-protein phosphatase 4 catalytic subunit OS=Homo sapiens GN=PPP4C PE=1 SV=1 - [PP4C_HUMAN]	1	3	3	307	35,1
Q16795	NADH dehydrogenase [ubiquinone] 1 alpha subcomplex subunit 9, mitochondrial OS=Homo sapiens GN=NDUFA9 PE=1 SV=2 - [NDUA9_HUMAN]	1	2	2	377	42,5
P0CG48	Polyubiquitin-C OS=Homo sapiens GN=UBC PE=1 SV=3 - [UBC_HUMAN]	4	3	3	685	77,0
O75494	Serine/arginine-rich splicing factor 10 OS=Homo sapiens GN=SRSF10 PE=1 SV=1 - [SRS10_HUMAN]	1	2	4	262	31,3
Q92734	Protein TFG OS=Homo sapiens GN=TFG PE=1 SV=2 - [TFG_HUMAN]	1	4	4	400	43,4
P09012	U1 small nuclear ribonucleoprotein A OS=Homo sapiens GN=SNRPA PE=1 SV=3 - [SNRPA_HUMAN]	1	5	5	282	31,3
P05141	ADP/ATP translocase 2 OS=Homo sapiens GN=SLC25A5 PE=1 SV=7 - [ADT2_HUMAN]	2	3	3	298	32,8
P62701	40S ribosomal protein S4, X isoform OS=Homo sapiens GN=RPS4X PE=1 SV=2 - [RS4X_HUMAN]	1	2	2	263	29,6
Q9HA64	Ketosamine-3-kinase OS=Homo sapiens GN=FN3KRP PE=1 SV=2 - [KT3K_HUMAN]	1	3	3	309	34,4
Q86V81	THO complex subunit 4 OS=Homo sapiens GN=ALYREF PE=1 SV=3 - [THOC4_HUMAN]	1	3	3	257	26,9
Q9UNE7	E3 ubiquitin-protein ligase CHIP OS=Homo sapiens GN=STUB1 PE=1 SV=2 - [CHIP_HUMAN]	1	4	4	303	34,8
P26599	Polypyrimidine tract-binding protein 1 OS=Homo sapiens GN=PTBP1 PE=1 SV=1 - [PTBP1_HUMAN]	1	2	2	53	57,2

					1	
Q1RMN8	TREMBL:Q1RMN8 (Bos taurus) Similar to Immunoglobulin lambda-like polypeptide 1	1	2	2	2 3 4	24,5
P10768	S-formylglutathione hydrolase OS=Homo sapiens GN=ESD PE=1 SV=2 - [ESTD_HUMAN]	1	2	2	2 8 2	31,4
Q96DH6	RNA-binding protein Musashi homolog 2 OS=Homo sapiens GN=MSI2 PE=1 SV=1 - [MSI2H_HUMAN]	1	3	3	3 2 8	35,2
P08107	Heat shock 70 kDa protein 1A/1B OS=Homo sapiens GN=HSPA1A PE=1 SV=5 - [HSP71_HUMAN]	2	3	3	6 4 1	70,0
Q9NUD5	Zinc finger CCHC domain-containing protein 3 OS=Homo sapiens GN=ZCCHC3 PE=1 SV=1 - [ZCHC3_HUMAN]	1	3	3	4 0 4	43,6
P67809	Nuclease-sensitive element-binding protein 1 OS=Homo sapiens GN=YBX1 PE=1 SV=3 - [YBOX1_HUMAN]	1	2	2	3 2 4	35,9
Q02878	60S ribosomal protein L6 OS=Homo sapiens GN=RPL6 PE=1 SV=3 - [RL6_HUMAN]	1	2	2	2 8 8	32,7
P19338	Nucleolin OS=Homo sapiens GN=NCL PE=1 SV=3 - [NUCL_HUMAN]	1	2	2	7 1 0	76,6
O00487	26S proteasome non-ATPase regulatory subunit 14 OS=Homo sapiens GN=PSMD14 PE=1 SV=1 - [PSDE_HUMAN]	1	2	2	3 1 0	34,6
Q01130	Serine/arginine-rich splicing factor 2 OS=Homo sapiens GN=SRSF2 PE=1 SV=4 - [SRSF2_HUMAN]	1	2	2	2 2 1	25,5
P48739	Phosphatidylinositol transfer protein beta isoform OS=Homo sapiens GN=PITPNB PE=1 SV=2 - [PIPNB_HUMAN]	1	3	3	2 7 1	31,5
P32322	Pyrroline-5-carboxylate reductase 1, mitochondrial OS=Homo sapiens GN=PYCR1 PE=1 SV=2 - [P5CR1_HUMAN]	1	2	3	3 1 9	33,3
Q96FW1	Ubiquitin thioesterase OTUB1 OS=Homo sapiens GN=OTUB1 PE=1 SV=2 - [OTUB1_HUMAN]	1	3	3	2 7 1	31,3
Q9BVG4	Protein PBDC1 OS=Homo sapiens GN=PBDC1 PE=1 SV=1 - [PBDC1_HUMAN]	1	2	2	2 3 3	26,0
O95926	Pre-mRNA-splicing factor SYF2 OS=Homo sapiens GN=SYF2 PE=1 SV=1 - [SYF2_HUMAN]	1	3	3	2 4 3	28,7
A6NDG6	Phosphoglycolate phosphatase OS=Homo sapiens GN=PGP PE=1 SV=1 - [PGP_HUMAN]	1	2	2	3 2 1	34,0
Q9UKM9	RNA-binding protein Raly OS=Homo sapiens GN=RALY PE=1 SV=1 - [RALY_HUMAN]	1	2	2	3 0 6	32,4
P54920	Alpha-soluble NSF attachment protein OS=Homo sapiens GN=NAPA PE=1 SV=3 - [SNAA_HUMAN]	1	2	2	2 9	33,2

					5	
Q14576	ELAV-like protein 3 OS=Homo sapiens GN=ELAVL3 PE=1 SV=3 - [ELAV3_HUMAN]	1	2	2	3 6 7	39,5
P48059	LIM and senescent cell antigen-like-containing domain protein 1 OS=Homo sapiens GN=LIMS1 PE=1 SV=4 - [LIMS1_HUMAN]	1	2	2	3 2 5	37,2
Q96HS1	Serine/threonine-protein phosphatase PGAM5, mitochondrial OS=Homo sapiens GN=PGAM5 PE=1 SV=2 - [PGAM5_HUMAN]	1	2	2	2 8 9	32,0
P26367	Paired box protein Pax-6 OS=Homo sapiens GN=PAX6 PE=1 SV=2 - [PAX6_HUMAN]	1	2	2	4 2 2	46,7
Q13148	TAR DNA-binding protein 43 OS=Homo sapiens GN=TARDBP PE=1 SV=1 - [TADBP_HUMAN]	1	4	4	4 1 4	44,7
P02668	SWISS-PROT:P02668 Kappa-casein [Contains: Casoxin C; Casoxin 6; Casoxin A; Casoxin B; Casoplatelin] - Bos taurus (Bovine).	1	2	2	1 6 9	19,0
O00425	Insulin-like growth factor 2 mRNA-binding protein 3 OS=Homo sapiens GN=IGF2BP3 PE=1 SV=2 - [IF2B3_HUMAN]	2	2	2	5 7 9	63,7
Q16836	Hydroxyacyl-coenzyme A dehydrogenase, mitochondrial OS=Homo sapiens GN=HADH PE=1 SV=3 - [HCDH_HUMAN]	1	2	2	3 1 4	34,3
P12763	SWISS-PROT:P12763 (Bos taurus) Alpha-2-HS-glycoprotein precursor	1	2	2	3 5 9	38,4
P47914	60S ribosomal protein L29 OS=Homo sapiens GN=RPL29 PE=1 SV=2 - [RL29_HUMAN]	1	2	2	1 5 9	17,7
P35548	Homeobox protein MSX-2 OS=Homo sapiens GN=MSX2 PE=1 SV=3 - [MSX2_HUMAN]	1	2	2	2 6 7	28,9
P62424	60S ribosomal protein L7a OS=Homo sapiens GN=RPL7A PE=1 SV=2 - [RL7A_HUMAN]	1	2	2	2 6 6	30,0
P62258	14-3-3 protein epsilon OS=Homo sapiens GN=YWHAE PE=1 SV=1 - [1433E_HUMAN]	1	2	2	2 5 5	29,2
P14923	Junction plakoglobin OS=Homo sapiens GN=JUP PE=1 SV=3 - [PLAK_HUMAN]	1	2	2	7 4 5	81,7